

2006

# Empirical validations of the daylighting/window shading/solar gains models in building energy simulation programs

Peter Gregory Loutzenhiser  
*Iowa State University*

Follow this and additional works at: <https://lib.dr.iastate.edu/rtd>

 Part of the [Environmental Engineering Commons](#), and the [Mechanical Engineering Commons](#)

## Recommended Citation

Loutzenhiser, Peter Gregory, "Empirical validations of the daylighting/window shading/solar gains models in building energy simulation programs " (2006). *Retrospective Theses and Dissertations*. 1281.  
<https://lib.dr.iastate.edu/rtd/1281>

This Dissertation is brought to you for free and open access by the Iowa State University Capstones, Theses and Dissertations at Iowa State University Digital Repository. It has been accepted for inclusion in Retrospective Theses and Dissertations by an authorized administrator of Iowa State University Digital Repository. For more information, please contact [digirep@iastate.edu](mailto:digirep@iastate.edu).

Empirical validations of the daylighting/window shading/solar gains models in building  
energy simulation programs

by

Peter Gregory Loutzenhiser

A dissertation submitted to the graduate faculty  
in partial fulfillment of the requirements for the degree of

DOCTOR OF PHILOSOPHY

Major: Mechanical Engineering

Program of Study Committee:  
Gregory M. Maxwell (Major Professor)  
Heinrich Manz  
Stephen B. Vardeman  
Howard Shapiro  
Ron Nelson  
Michael Pate

Iowa State University

Ames, Iowa

2006

UMI Number: 3217295

### INFORMATION TO USERS

The quality of this reproduction is dependent upon the quality of the copy submitted. Broken or indistinct print, colored or poor quality illustrations and photographs, print bleed-through, substandard margins, and improper alignment can adversely affect reproduction.

In the unlikely event that the author did not send a complete manuscript and there are missing pages, these will be noted. Also, if unauthorized copyright material had to be removed, a note will indicate the deletion.

**UMI**<sup>®</sup>

---

UMI Microform 3217295

Copyright 2006 by ProQuest Information and Learning Company.

All rights reserved. This microform edition is protected against unauthorized copying under Title 17, United States Code.

ProQuest Information and Learning Company  
300 North Zeeb Road  
P.O. Box 1346  
Ann Arbor, MI 48106-1346

Graduate College  
Iowa State University

This is to certify the doctoral dissertation of  
  
Peter Gregory Loutzenhiser  
  
has met the dissertation requirements of Iowa State University

Signature was redacted for privacy.

~~Major~~ Professor

Signature was redacted for privacy.

For the Major Program

## Table of Contents

<b>List of Figures</b> .....	<b>viii</b>
<b>List of Tables</b> .....	<b>xi</b>
<b>Acknowledgements</b> .....	<b>xiii</b>
<b>Abstract</b> .....	<b>xiv</b>
<b>Chapter 1: Introduction</b> .....	<b>1</b>
1.1. Facility Description.....	2
1.1.1. EMPA Outdoor Test Facility .....	2
1.1.2. Energy Resource Station.....	4
1.2. Background Literature .....	5
1.2.1. Empirical Validations .....	6
1.2.1.1. Methodology .....	6
1.2.1.2. Test Cell Validations.....	8
1.2.1.2. ERS Validations.....	10
1.2.2. Heat Transfer Modeling for the Glazing, Windows, and Shading Devices.....	11
1.2.3. Laboratory Measurements .....	12
1.2.4. Test Facility Measurements .....	12
1.2.5. Fenestration Models.....	13
1.3. Overview of the Research.....	14
1.3.1. EMPA Component.....	14
1.3.2. ERS Component.....	15
1.3.3. Empirical Validation Methodology .....	15
1.3.4. Specific Research Objectives.....	16
1.4. Dissertation Organization .....	16
References.....	18
<b>Chapter 2: Series of experiments for empirical validation of solar gain modeling in building energy simulation codes – Experimental setup, test cell characterization, specifications and uncertainty analysis</b> .....	<b>22</b>
Abstract .....	22
2.1. Introduction.....	23
2.2. Concept of Test Cells with Guarded Zones .....	26
2.3. Thermal Properties of Test Cell Envelope.....	29
2.3.1. Layer and Surface Properties .....	29
2.3.2. Thermal Bridges: Door, Edges, Etc. ....	30
2.3.3. Internal Thermal Mass .....	32
2.3.4. Total Steady-State Thermal Properties .....	32
2.3.5. Sensitivity and Uncertainty of Steady-State Thermal Properties .....	33
2.4. Sensors .....	34
2.5. Air Tightness of the Cell.....	36
2.6. Experiment for Steady-State Cell Characterization.....	36

2.7. Transient Experiment for Cell Characterization.....	39
2.8. Simulation of Transient Experiment.....	40
2.9. Statistical Analysis of Transient Experiment Results.....	44
2.10. Conclusions and Outlook.....	48
Acknowledgements.....	49
References.....	50
<b>Chapter 3: Empirical validation of models to compute solar irradiance on inclined surfaces for building energy simulation.....</b>	<b>52</b>
Abstract.....	52
3.1. Introduction.....	53
3.2. Solar Radiation Models.....	56
3.2.1. Isotropic Sky Model.....	57
3.2.2. Klucher Model.....	58
3.2.3. Hay-Davies Model.....	58
3.2.4. Reindl Model.....	59
3.2.5. Muneer Model.....	59
3.2.6. Perez Model.....	60
2.3. Facility and Measurements.....	61
2.3.1. Test Site and Setup.....	61
3.3.2. Solar Irradiance.....	62
3.3.3. Ground Reflectance.....	65
3.4. Simulations.....	66
3.5. Sensitivity Analysis.....	67
3.5.1. Fitted Effects for N-way Factorials.....	68
3.5.2. Monte Carlo Analysis.....	70
3.5.2.1. Sampling.....	70
3.5.2.2. Analysis of Output.....	71
3.5.3. Estimated Uncertainties.....	71
3.6. Results.....	72
3.7. Discussion and Conclusions.....	79
Acknowledgements.....	81
References.....	81
<b>Chapter 4: An Empirical Validation of Solar Gain Models Found in Building Energy Simulation Programs.....</b>	<b>84</b>
Abstract.....	86
4.1. Introduction.....	86
4.2. Experiment.....	89
4.2.1. Facility.....	90
4.2.2. Glazing Unit.....	90
4.2.2.1. Spectral Optical Properties and Emittances.....	90
4.2.2.3. Thermal Properties.....	93
4.3.1. Inputs.....	97

4.3.2. Modeling.....	97
4.3.2.1. EnergyPlus .....	97
4.3.2.2. DOE-2.1E.....	98
4.3.2.3. ESP-r.....	99
4.3.2.4. TRNSYS-TUD.....	99
4.4. Error and Sensitivity Analyses.....	100
4.4.1. Assessing Uncertainties .....	100
4.4.1.1. Temperature Dependent Properties.....	100
4.4.1.2. Temperature Inputs .....	101
4.4.2. Sensitivity Studies.....	103
4.5. Results.....	103
4.5.1. Cooling Power Comparisons .....	104
4.5.3 Convective Heat Transfer Coefficients.....	108
4.6. Discussion .....	110
Acknowledgements.....	113
Nomenclature.....	114
References.....	116
<b>Chapter 5: An empirical validation of modeling solar gain through a glazing unit with external and internal shading screens.....</b>	<b>119</b>
Abstract.....	119
5.1. Introduction.....	120
5.2. Experiments .....	122
5.2.1. External Shading Screen.....	123
5.2.2. Internal Shading Screen .....	125
5.3. Simulation Modeling .....	127
5.3.1. EnergyPlus .....	128
5.3.2. DOE-2.1E.....	129
5.3.3. TRNSYS-TUD.....	129
5.3.4. ESP-r.....	130
5.4. Sensitivity Study .....	131
5.5. Results.....	133
5.5.1. Cooling Power .....	133
5.5.1.1. External Shading Screen.....	133
5.5.1.2. Internal Shading Screen .....	136
5.5.1.3 Statistical Comparisons.....	137
5.5.2. Transmitted Solar Power.....	139
5.6. Discussion.....	141
5.7. Conclusions.....	143
Acknowledgements.....	144
Nomenclature.....	144
References.....	146

<b>Chapter 6: Empirical validations of solar gain models for a glazing unit with exterior Venetian blinds.....</b>	<b>149</b>
Abstract.....	149
6.1. Introduction.....	149
6.2. Experiment.....	152
6.2.1. Boundary Conditions.....	154
6.2.2. Blind Slat Properties.....	155
6.3. Modeling.....	156
6.4. Sensitivity Analyses.....	157
6.4.1. Fitted Effects for N-way Factorial Analysis.....	157
6.4.2. Monte Carlo Analysis.....	158
6.5. Results.....	158
6.6. Discussion and Conclusions.....	161
Acknowledgements.....	162
Nomenclature.....	163
References.....	164
<b>Chapter 7: Empirical Validation of the Daylighting Algorithms and Associated Interactions Using Various Shading Devices and Windows in Building Energy Simulation Programs.....</b>	<b>167</b>
Abstract.....	167
7.1. Introduction.....	168
7.2. Facility Layout.....	170
7.3. Experiment.....	171
7.3.1. Windows and Shading Devices.....	171
7.3.1.1. Windows.....	172
7.3.1.2. Interior Shading Devices.....	172
7.3.1.3 Exterior Fins.....	173
7.3.2. Lighting and Daylighting Controls.....	174
7.4. Simulations.....	175
7.4.1. EnergyPlus.....	176
7.4.2. DOE-2.1E.....	177
7.5. Uncertainties.....	178
7.5.1. Experimental Uncertainties.....	179
7.5.2. Monte Carlo Analysis.....	179
7.6. Results.....	179
7.6.1. Daylight Illuminance.....	181
7.6.1.1. East Test Rooms.....	181
7.6.1.2. South Test Rooms.....	182
7.6.1.3 West Test Rooms.....	183
7.6.1.4. Statistical Comparisons.....	184
7.6.2. Light Power.....	186
7.6.2.1. East Test Rooms.....	186
7.6.2.2. South Test Rooms.....	187

7.6.2.3 West Test Rooms .....	187
7.6.2.4. Statistical Comparisons.....	188
7.6.3. Reheat Coil Power .....	190
7.6.3.1. East Test Rooms .....	191
7.6.3.2. South Test Rooms .....	192
7.6.3.3. West Test Rooms .....	193
7.6.3.4. Statistical Comparisons.....	194
7.7. Discussion .....	196
7.7.1. Daylight Illuminance .....	196
7.7.2. Light Power.....	197
7.7.3. Reheat Coil Power .....	199
7.8. Conclusions.....	200
Acknowledgements.....	201
Nomenclature.....	202
References.....	203
<b>Chapter 8: Conclusions .....</b>	<b>206</b>
8.1. EMPA Experiments .....	206
8.2. ERS Experiment.....	208
<b>Chapter 9: Recommendation for Future Work .....</b>	<b>210</b>
9.1. Glazing Units .....	210
9.2. Window Shading Devices.....	210
9.3. Daylighting .....	210
<b>Appendix A: Test Cell Transient Characteristic Exercise .....</b>	<b>212</b>
<b>Appendix B: Evaluation of Building Energy Simulation Codes' Irradiance Models.</b>	<b>224</b>
<b>Appendix C: Constant Temperature Experiment with Glazing Only.....</b>	<b>232</b>
<b>Appendix D: Constant Temperature Experiment with Glazing and External Shade</b>	<b>249</b>
<b>Appendix E: Constant Temperature Experiment with Glazing and Interior Shade.</b>	<b>258</b>
<b>Appendix F: Constant Temperature Experiment with Glazing and Exterior Blind..</b>	<b>269</b>
<b>Appendix G: ERS Daylighting Experiment Setup Sheet .....</b>	<b>282</b>

## List of Figures

Figure 1.1. EMPA outdoor test facility.....	3
Figure 1.2. EMPA test cell schematic.....	3
Figure 1.3. The Energy Resource Station. ....	4
Figure 1.4. A floor plan of the Energy Resource Station.....	5
Figure 1.5. Methodology for empirical validation of building energy simulation programs. .....	16
Figure 2.1. Outdoor view (left) of test cells with two removable façade elements (3.4 m × 3.4 m) and indoor view (right) showing HVAC cabinet and extract and supply ducts. .	27
Figure 2.2. Concept of test facility with air conditioning of the cell, guarded zone, energy flows into and out of the test cell and optional external chamber. ....	28
Figure 2.3. Thermally controlled external chamber mounted in front of one of the cells and viewed from outside during (left) and after construction (right). ....	28
Figure 2.4. Computed heat fluxes at the outer surfaces of the test cell at a temperature difference of 1 K between cell air and guarded zone.....	31
Figure 2.5. Computed heat flow lines in a horizontal cross-section of the door. ....	31
Figure 2.6. Infrared picture of the cell door, taken when temperature in the cell was 20 K higher than in the guarded zone, shows thermal bridges at the door frame.....	32
Figure 2.7. Location of temperature sensors on inner (30 sensors) and outer (30 sensors) surface of cell envelope. For air temperature (8 sensors) projections on floor, north and west wall are shown. ....	36
Figure 2.8. Mean air temperature inside cell and outside, mean surface temperatures of all six faces and heating power inside the cell as a function of time during phase B of the steady-state experiment (duration 96 h).....	38
Figure 2.9. Comparison of thermal conductances $H_{GZ}$ and $H_{EW}$ as function of temperature found by simulation (curves) and the steady-state experiment (markers). ....	39
Figure 2.10. Measured pseudo-random internal heating power, cell air temperatures (total eight sensors) and mean surface temperatures of all six outer cell surfaces.....	40
Figure 2.11. Comparison between measured mean cell air temperature and cell air temperature simulated by four different codes. ....	43
Figure 2.12. Experimental uncertainty, uncertainty of simulation results due to uncertainty in input parameters and total uncertainty.....	47
Figure 3.1. Test cells with pyranometers visible in the central part of the picture and green artificial turf installed in front of the test cell. ....	62
Figure 3.2. Pyrheliometer for measuring direct-normal and shaded pyranometer for measuring diffuse horizontal solar irradiance are positioned on the roof of the facility.	62
Figure 3.3a. Measured and calculated global horizontal irradiance for Period 1. ....	64
Figure 3.3b. Measured and calculated global horizontal irradiance for Period 2. ....	64
Figure 3.4. Near direct normal-hemispherical reflectance of the artificial turf. ....	66
Figure 3.5. Flowchart for the sensitivity studies.....	68

Figure 4.1. The external view (left) of the test facility shows sensors for weather data acquisition between the two test frames with glazing; the internal view (right) of the test cell shows supply (bottom) and extract (top) ducts. ....	89
Figure 4.2. Measured transmittance and reflectances of solar protection glazing unit as a function of wavelength. ....	91
Figure 4.3. Measured and computed (Window 5.2) angular dependent visible transmittances and reflectances of the glazing unit (Measurements: University of Basel). ....	93
Figure 4.4. The section shows the mounting of the glazing in the frame (left) and a detailed view of the spacer between the glass sheets (right). ....	94
Figure 4.5. Hotbox apparatus featuring a cold zone (left) and a guarded hot zone (right). The test specimen is mounted between the two zones. ....	94
Figure 4.6. Computed heat flow lines at glazing edge. ....	95
Figure 4.7. Comparisons between measured and computed cooling powers as a function of the hour of the day (averaged over 480 h). ....	105
Figure 4.8. Maximum, mean, and minimum hourly absolute differences between experiment and predicted quantities as a function of hour of the day (calculated over 480 h). ....	106
Figure 4.9. Computed solar gains from the building energy simulation codes as a function of hour of the day for the entire period (averaged over 480 h). ....	108
Figure 4.10. Impact comparisons of convective heat transfer coefficient algorithms on cooling power using EnergyPlus. ....	109
Figure 4.11. Parametric study of the impact of heat transfer coefficients on the mean absolute and mean differences. ....	110
Figure 5.1. Side view of the test facility showing energy flows and cell ventilation system. ....	123
Figure 5.2. Photograph of the external shading screen taken using a microscope. ....	124
Figure 5.3. Transmittance and reflectance of the external shade as a function of wavelength. ....	124
Figure 5.4. External shading screen mounted on the test cell. ....	125
Figure 5.5. Photograph of the internal shading screen taken using a microscope. ....	126
Figure 5.6. Transmittance and reflectance of the interior shade as a function of wavelength. ....	126
Figure 5.7. Internal shading screen mounted in the test cell. ....	127
Figure 5.8. Cooling power comparisons averaged over a given hour of the day for the external shading screen experiment (480 h). ....	134
Figure 5.9. Absolute maximum, mean, and minimum differences between measured and predicted cooling power for the external shading screen at any given hour of the day (480 h). ....	135
Figure 5.10. Cooling power comparisons averaged over a given hour of the day for the internal shading screen experiment (480 h). ....	136
Figure 5.11. Absolute maximum, mean, and average differences between measured and predicted cooling power for the internal shading screen at any given hour of the day (480 h). ....	137

Figure 5.12. Predicted transmitted solar power for a given hour of the day during the external shading screen experiment (480 h). .....	140
Figure 5.13. Predicted transmitted solar power for a given hour of the day during the internal shading screen experiment (480 h). .....	141
Figure 6.1. Venetian blind assembly mounted over the test cell glazing unit. ....	153
Figure 6.2. Airflow and temperature patterns around the blind slats from a CFD analysis. ....	154
Figure 6.3. Blind slat reflectance as a function of wavelength. ....	155
Figure 6.4. Dimensioned blind slats relative to the outer glazing in millimeters. ....	156
Figure 6.5. Measured and prediction cooling power for the horizontally positioned blind experiment averaged for a given hour of the day. ....	159
Figure 6.6. Maximum, minimum, and mean absolute cooling power differences for the horizontally positioned blind experiment for a given hour of the day. ....	159
Figure 6.7. Measured and prediction cooling power for the 45° tilted downward blind experiment averaged for a given hour of the day. ....	160
Figure 6.8. Maximum, minimum, and mean absolute cooling power differences for the 45° tilted downward blind experiment for a given hour of the day. ....	160
Figure 7.1. Facility layout (courtesy of [27]). ....	170
Figure 7.2. Drawing and dimensions in meters of the exterior shades for west test rooms. ....	174
Figure 7.3 Light sensor reference point (the sensor height is 0.7239 m from the floor). ...	175
Figure 7.4. Horizontal and vertical global exterior illuminance. ....	180
Figure 7.5. Reference point illuminance for the east test rooms. ....	182
Figure 7.6. Reference point illuminance for the south test rooms. ....	183
Figure 7.7. Reference point illuminance for the west test rooms. ....	184
Figure 7.8. Light power for the east test rooms. ....	186
Figure 7.9. Light power for the south test rooms. ....	187
Figure 7.10. Light power for the west test rooms. ....	188
Figure 7.11. Room temperature for the south test rooms. ....	191
Figure 7.12. Reheat power for the east test rooms. ....	192

## List of Tables

Table 2.1. Location of EMPA test cells.....	26
Table 2.2. Geometrical parameters of test cell. Areas shown in this table are in contact with internal air. ....	26
Table 2.3. Layer properties: Ceiling, north (incl. door), east and west wall.....	29
Table 2.4. Layer properties: Floor. ....	29
Table 2.5. Layer properties: External Wall.....	29
Table 2.6. Optical properties of cell surfaces. ....	30
Table 2.7. Heat transfer coefficients and thermal conductances of cell to the guarded zone (cell air to outer surface of cell envelope). ....	33
Table 2.8. Heat transfer coefficients and thermal conductances of cell to the outside (cell air to outer surface of cell envelope).....	33
Table 2.9. Sensitivity of thermal conductance to changes of important input parameters. ...	34
Table 2.10. Weather data parameters and equipment. ....	34
Table 2.11. Parameters measured in the test cell, the external chamber and the guarded zone and approximate accuracies according to manufacturer specifications. ....	35
Table 2.12. Steady-state experiment: Time-averaged values and uncertainties for thermal conductance calculations. ....	38
Table 2.13. A summary of the descriptive and comparative statistics.....	47
Table 3.1. Instruments used for measuring solar irradiance. ....	63
Table 3.2a. Solar ground reflectance. ....	66
Table 3.2b. Ineichen et al. (1987) measurements for determining average albedo coefficients over a three-month period. ....	66
Table 3.3. Average factorial impacts ( $\alpha_S > 0$ ).....	69
Table 3.4. Analysis of global vertical façade irradiance in $W/m^2$ ( $\alpha_S > 0$ ) for Period 1. ....	73
Table 3.5. Analysis of global vertical façade irradiance in $W/m^2$ ( $\alpha_S > 0$ ) for Period 2. ....	74
Table 3.6. Analysis of global vertical façade irradiance in $W/m^2$ ( $\alpha_S > 0$ ) for both periods. ....	75
Table 4.1. Properties of individual panes of glass. ....	91
Table 4.2. BISCO simulation boundary conditions. ....	95
Table 4.3. Inputs and results for Equations 4.1 and 4.2.....	96
Table 4.4. Standard deviations of the temperature dependent thermal conductivities. ....	101
Table 4.5. Input temperature uncertainties. ....	102
Table 4.6. Additional uncertainties. ....	102
Table 4.7. Overall uncertainty and 10 most influential input parameters from the factorial analyses in Watts.....	103
Table 4.8. Summary of statistics and comparisons of cooling power. ....	107
Table 5.1. Mean envelope temperatures for test cell construction elements during the experiments. ....	128
Table 5.2. Overall uncertainty and 10 most influential parameters that impacted the cooling power uncertainty in Watts for the external screen experiment. ....	132

Table 5.3. Overall uncertainty and 10 most influential parameters that impacted the cooling power uncertainty in Watts for the internal screen experiment. ....	132
Table 5.4. Statistical and comparative parameters of cooling power for the external shading screen experiment. ....	138
Table 5.5. Statistical and comparative parameters of cooling power for the internal shading screen experiment. ....	139
Table 6.1. Optical properties of the slat surfaces. ....	155
Table 6.2. Overall uncertainty and 10 most influential input parameters from the factorial analyses for the horizontally positioned slat experiment in Watts. ....	157
Table 6.3. Overall uncertainty and 10 most influential input parameters from the factorial analyses for the 45° downward tilted slat experiment in Watts. ....	158
Table 6.4. Summary of statistics and comparisons of cooling power. ....	161
Table 7.1. Test rooms shading and window configurations for the experiment. ....	172
Table 7.2. Test room window properties. ....	172
Table 7.3. Optical properties of the interior shading devices. ....	173
Table 7.4. Maximum and minimum light power and corresponding illuminance. ....	175
Table 7.5. Statistical analysis for the room daylight illuminance at the reference point in Lux. ....	185
Table 7.6. Statistical analysis for the room light power in Watts. ....	189

### **Acknowledgements**

I would like to gratefully acknowledge my parents, Gary and Debbie Loutzenhiser, for their constant love, encouragement, and support, especially in difficult times. I would also like to thank my major professor, Dr. Gregory Maxwell, for his guidance and assistance during both my undergraduate and graduate studies. I would like to recognize my supervisor at EMPA, Dr. Heinrich Manz, for never accepting less than my very best and his constant pursuit towards excellence in this endeavor. I would like to show my appreciation to Dr. Stephen Vardeman and Dr. Max Morris for their gentle guidance and helpfulness with the statistical analyses. I would like to thank my committee members, Dr. Gregory Maxwell, Dr. Heinrich Manz, Dr. Stephen Vardeman, Dr. Howard Shapiro, Dr. Ron Nelson, and Dr. Mike Pate, for accommodating my hectic schedule when back in the United States, particularly Dr. Shapiro and Dr. Manz for traveling from Michigan and Switzerland, respectively, to participate in my final defense.

I would also like to thank the IEA Task 34/Annex 43 Subtask C participants who collaborated on many papers included in this work, namely: Dr. Paul Strachan and Dr. Clemens Felsmann for their excellent contributions.

I would like to gratefully acknowledge the financial support of the Swiss Federal Office of Energy (BFE) for building and testing the experimental facility (Project 17'166) as well as the funding for EMPA participation in IEA Task 34/43 (Project 100'765) and recognize my colleagues at EMPA who assisted in this work, including: B. Binder, R. Blessing, M. Camenzind, S. Carl, M. Christenson, T. Frank, K. Meyer, T. Nussbaumer, and R. Vonbank.

I would also like to acknowledge the financial support from the Iowa Energy Center under Grant 9608 and thank the staff at the Energy Resource Station, including: X. H. Zhou, C. Klaassen, E. Kadic, and D. Perry. I would lastly like to thank S. Shrestha for his hard work on the motorized mini-blinds for the daylighting experiment.

## **Abstract**

The purpose of this research was to evaluate the accuracies of building energy simulation programs when modeling glazing units and windows with and without shading devices and daylighting. Program outputs were compared with data from experiments performed at two research facilities designed for these types of studies.

Six experiments were performed in a test cell located on the Swiss Federal Laboratories for Material Testing and Research (EMPA) campus in Duebendorf, Switzerland. After determining thermophysical properties, the thermal bridges of the test cell were analyzed using three-dimensional heat transfer simulations. The experimental series started with a steady-state and a transient experiment to characterize the cell. A preliminary study was then performed to assess various solar radiation models for tilted surfaces and determine which model performed best. Additional experiments were then run to evaluate solar gain models in building energy simulation programs starting with the simplest case and increasing the complexities of the experiments. These experiments were performed using a solar selective glazing unit without shading, with external and internal diffuse shading screens, and with external Venetian blinds with the blind slats horizontally positioned and tilted 45° downward with the outer slat edge pointed towards the ground. Increasing the complexities of subsequent experiments allowed for careful assessments and diagnoses of the results.

An additional experiment was performed at the Iowa Energy Center's Energy Resource Station (ERS) located on the Des Moines Area Community College campus in Ankeny, Iowa USA. In this study, three different windows in combination with three window shading devices were used to evaluate daylighting performance and associated interactions in six exterior test rooms.

Robust experiment and sensitivity analyses were used to evaluate the impact of experimental uncertainties for the experiments and program inputs for all of the experiments. A set of comprehensive statistical parameters was used to compare results building energy simulation programs with the experiments and a 95% level of significance

was used to determine whether the programs were validated or not. Up to four programs were evaluated in this study for each experiment, including: EnergyPlus, DOE-2.1E, TRNSYS-TUD, and ESP-r.

## Chapter 1: Introduction

The validation of building energy simulation programs is an important component in the development and refinement of models and algorithms implemented in the software. Numerous efforts within the framework of the International Energy Agency's (IEA) Solar Heating and Cooling (SHC) Tasks and Energy Conservation in Building Community Systems Annexes (ECBCS) have dealt with many facets of program validations. Judkoff (1988) discusses the three different types of validation used in building energy simulation software which include: 1) analytical validation (comparing program results to an analytical solution), 2) comparative validation (program-to-program comparisons), and 3) empirical validation (comparing results with an actual experiment). Each of these validation methodologies has its own advantages and disadvantages. For analytical validation, the advantages include: no input uncertainty, exact truth standard, and inexpensive, but the disadvantage is that there are limited numbers of cases for which analytical solutions can be derived. The advantages for the comparative validation are that there are no input uncertainties, not limited to simple cases, quick, and inexpensive. The primary disadvantage to these types of comparisons is that there is no truth standard. This research focuses on the third type of validation—empirical validation. The advantages of empirical validation include: an approximate truth standard within uncertainties in the instrumentation and data acquisition system and no limitations due to the complexity of the cases. The disadvantages are that measurements involve some degree of experimental uncertainty, detailed high quality measurements are very expensive and time-consuming, and there are a limited number of data sites where this is economically practical.

Empirical validations can be performed at various levels including structure, systems and equipment, and whole building, which combines and integrates the first two levels of empirical validation into an additional level. The specific focus of this research was to measure and compare output in the building energy simulation software the impact of glazing units, windows, window shading devices, daylighting controls, and load interactions, examining all levels of empirical validation.

## **1.1. Facility Description**

These validations were performed at two facilities equipped with the necessary equipment, data acquisition system, and staff required for this type of endeavor. The facilities are the Swiss Federal Laboratories for Material Testing and Research's (EMPA) outdoor test facility and the Iowa Energy Center's Energy Resource Station (ERS).

### **1.1.1. EMPA Outdoor Test Facility**

The EMPA outdoor test facility is located on the EMPA campus in Duebendorf, Switzerland. The latitude and longitude of the facility are at 47.4 degrees north latitude and 8.6 degrees east longitude, respectively. The elevation of the facility is 430 meters above sea level and is in the Central European Standard Time Zone (GMT +1). A photograph of the south side of the test cell is shown in Figure 1.1. The test facility is comprised of two identical test cells, where five of six faces in each cell are adjacent to guarded zones. The external wall of the test cell is oriented 29° west of south. The test cells and guarded zones each have their own air conditioning unit. The temperatures are controlled by heating with an electric heater with a maximum power of 3500 W and cooling with an air/water heat exchanger with a maximum cooling of 5000 W. The heating power is measured directly, while the cooling power is calculated using measured water flow rates, inlet and exit temperatures, and performing an energy balance. A computer with a data acquisition system is located in the guarded zone and shielded from the test cell with an airtight curtain.



Figure 1.1. EMPA outdoor test facility.

The air in the test cell is distributed near the floor by two textile ducts and extracted near the ceiling through metal ducts. Temperatures within the space are measured with 18 double shielding thermocouples, which divide the cell into 18 equal parts. An illustration of the test cell setup is shown in Figure 1.2.

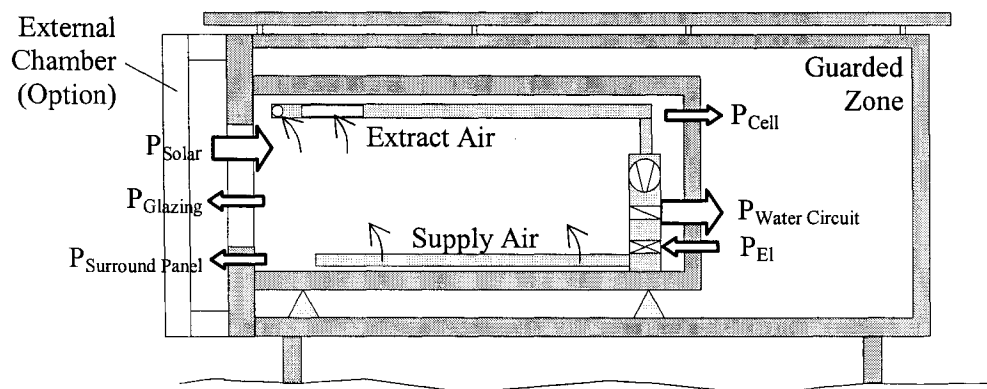


Figure 1.2. EMPA test cell schematic.

### 1.1.2. Energy Resource Station

The ERS is located on the Des Moines Area Community College in Ankeny, Iowa and is operated and owned by the Iowa Energy Center. The latitude and longitude of the facility are  $41.75^\circ$  north latitude and  $93.70^\circ$  west longitude, respectively. The facility is 289 meters above sea level and is in the Central Time Zone (GMT-6) of the United States. Figure 1.3 shows a photograph of the building taken from the east side.

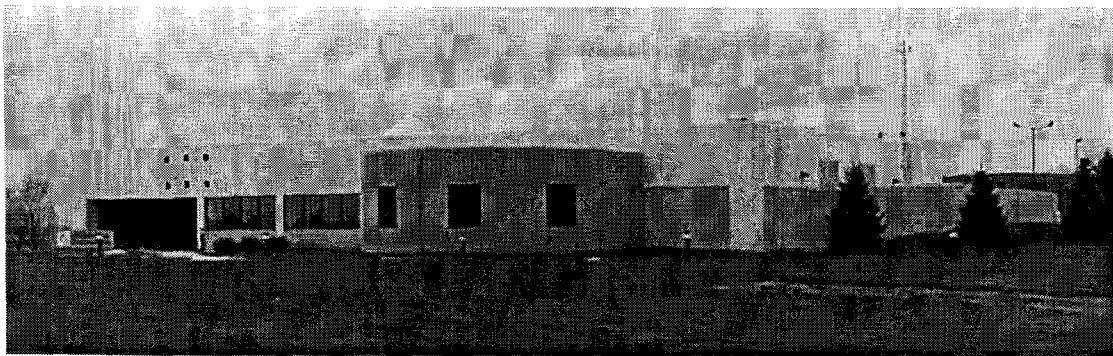


Figure 1.3. The Energy Resource Station.

The building is comprised of eight test rooms, a computer room, offices, two classrooms and other rooms necessary for the support and operation of the facility. A floor plan of the facility is shown in Figure 1.4. The ERS is equipped with three air-handling units, two of which are nearly identical and serve the test rooms. Test rooms designated as A and B Rooms are served by separate air-handling units, while the rest of the facility is controlled by the third air-handling unit. The test rooms are grouped in pairs to provide simultaneous side-by-side testing of different control schemes with “identical” thermal loads. Three of the four pairs of test rooms are located at the perimeter of the building (east, south, and west) while the other pair is located in the interior of the building. The building is situated so that one wall faces true north. Price and Smith (1999) provide a more detailed description of the ERS that documents the specific equipment, construction material, etc.

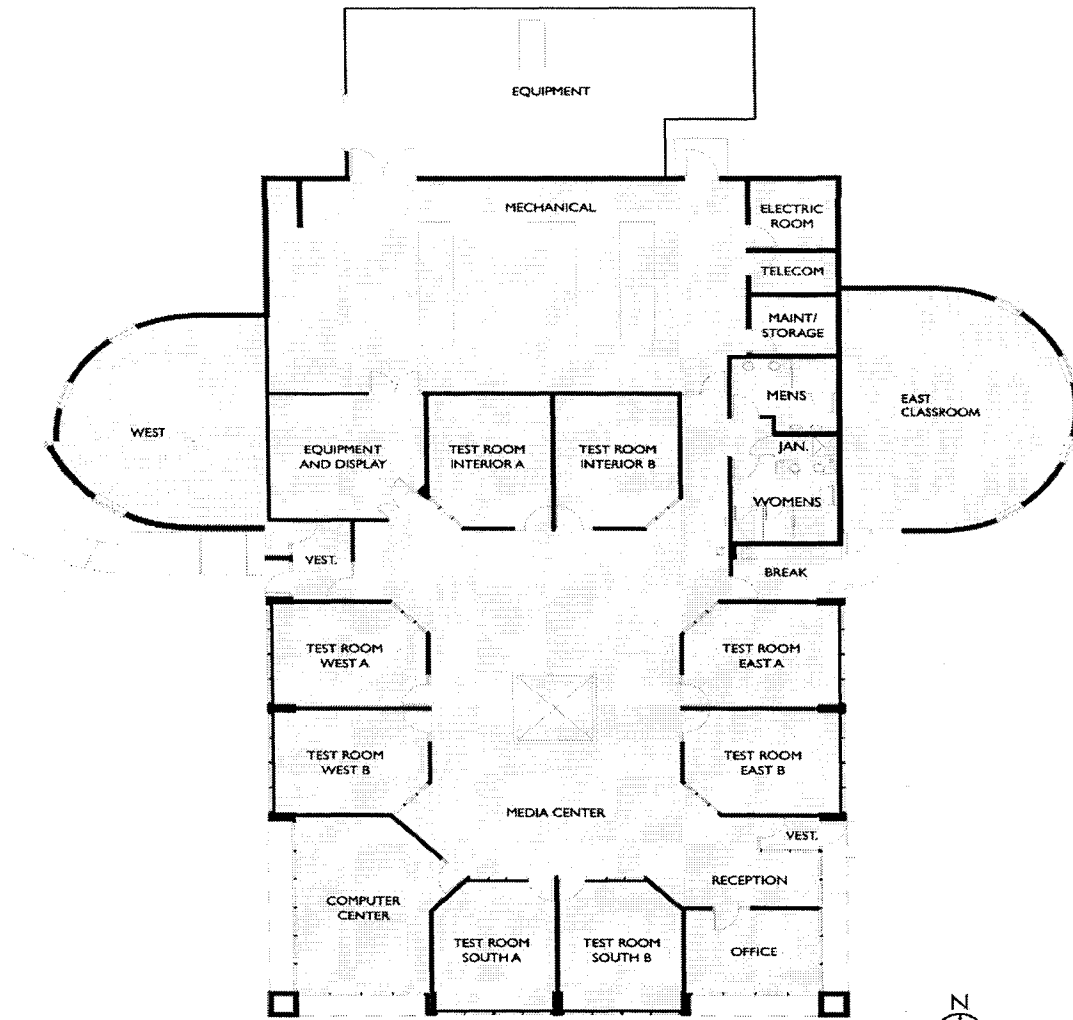


Figure 1.4. A floor plan of the Energy Resource Station.

## 1.2. Background Literature

A considerable amount of research has been done focusing on several topics that intersect with the research being pursued here. The overlapping areas of research can be divided into two general areas: 1) empirical validations of building energy simulation software and 2) heat transfer and daylighting modeling for glazing and windows with/without shading devices.

### 1.2.1. Empirical Validations

Three components of empirical validations will be discussed which include: 1) the methodology behind empirical validation, 2) test cell validations, and 3) ERS validations.

#### 1.2.1.1. Methodology

Empirical validations of building energy simulation software are large undertaking that require extensive planning and a well-instrumented facility. Jensen (1995) describes a methodology for validation used for the PASSYS project, which was formed in 1986 by the Commission of the European Communities with the aim of increasing confidence in passive solar heating systems. When describing the results, Jensen stated that validation is a complicated process that requires rigorous testing of the theory used in the program, implementation in the software, and user interfaces that are typical for expected use. In practice, it is impossible to perform a complete validation of building energy simulation software because there are too many links and possible applications to test all permutations. However, it is possible to increase the confidence in the building energy simulation software by applying well-documented validation methodologies combining the three types of validation techniques. The methodology used in the PASSYS program comprised the following steps and used all three validations techniques.

- A critical evaluation of the theory used in the simulation program to model the different transfer processes, including an investigation of possible alternatives.
- A check of the corresponding source code segments separately and jointly when possible.
- Application of the analytical (for single processes) and intermodel comparisons (for single processes and whole model) elements of the methodology when possible.
- Use of sensitivity analysis for internal consistency and quality assurance checks (for single processes and whole model), and for investigating the overall uncertainty of the program/model predictions due to uncertainty in the input parameters.
- Identification, design, and implementation of empirical validation experiments. These experiments may be at the process level of for the whole model validation. The experimental design includes use of sensitivity analysis to determine the principal factors of the experiment and access the overall uncertainty.

- Application of statistical analysis techniques to determine the acceptability or otherwise of the matched predictions and measured data sets and to help identify possible sources of discrepancy.
- Based on the above-mentioned techniques, recommendations should be given on modifications to the program/model under study.

A set of criteria for a high quality data was defined for the PASSYS program.

- comprehensive
- detailed
- with small uncertainty
- checked and cleaned
- fully documented

The methodology for empirical validations was further refined by Lomas et al. (1997) that agreed upon nine criteria for classifying data sets. The criteria are divided into three subcategories: 1) acceptable data sets, 2) useful data sets, and 3) high quality data sets. The criteria for the “acceptable data sets” are contained in the following list.

1. Structures must not include operating active solar space heating or cooling systems.
2. The weather data must have been collected at the site of the building.
3. The measured building performance data and the weather data must be available at hourly or more frequent intervals.

The criteria for a “useful data sets” include the criteria from the “acceptable data sets” in addition to the following criteria list.

4. All three major elements of the weather, air temperature, wind speed, and the direct and diffuse components of solar radiation must be measured at the site of the building for the whole comparison period.
5. The structure must be unoccupied, it cannot contain passive solar features which cannot be explicitly modeled and each zone in the building must have independent heating and /or cooling plant and controls.
6. Measured infiltration and, where appropriate, inter-zonal air flow rates, must be available for the whole comparison period.

The criteria for “high quality data sets” include the criteria from both the “useful data sets” and the “acceptable data sets” plus the following additional criteria.

7. The structure cannot contain features, or environmental control systems, which cannot be modeled explicitly by any of the programs being validated.

8. The data medium must be of the type which is readily usable, and close liaison with the monitoring institutions must be possible.
9. Data for the sites which have never produced data for model validation work, to data which, due to external errors, has introduced unacceptable uncertainty into previous validation work, must not be included.

The methodology for empirical validations was again further refined in IEA-SHC Task 22 and is described in detail by Palomo Del Barrio and Guyon (2003). The principal aim of empirical validation is to compare actual system behavior that deals with real world complexities with that predicted by a computer model. An important component of empirical validations is to make comparisons between the measured data and the predicted data from the respective computer models. In this framework, the following method for checking model validity was proposed.

- A systematic analysis of the residuals comprising non-stationary patterns detection, mean and standard deviation calculations, and spectral density function analysis.
- A comparison between measurements and simulations that takes into account both the measurement noise and the model input data uncertainties. The agreement between the model and reality is stated to be good when a significant overlap between the simulations and the measurement uncertainty bands. (Last sentence omitted).
- The estimation of the spectral domain of application of the model. It defines the frequency ranges of excitation where no significant differences between the model simulation and measurements are expected.

This framework was implemented in experiments performed at the ETNA building designed by Electricité de France (EDF) (Paloma Del Barrio and Guyon, 2004).

#### **1.2.1.2. Test Cell Validations**

Many empirical validation efforts have been undertaken using test cells. Test cells provide an economical and practical median between the laboratory and full-scale monitoring of buildings (Strachan, 1993) and were used in the PASSYS project for model validation. This project used 12 different well-instrumented test cells that were situated all over Europe that were used for validations (Wouters et al., 1993). The test strategy for the PASSYS involved a one week startup period at a constant temperature, two weeks of constant

minimum power input to the room, two weeks of constant high power, two weeks of moderate constant power, and two weeks with a pseudo-random binary power. From the experiments, the building energy simulation programs predicted a floating temperature in the test cell (Jensen, 1995).

Within the scope of IEA-BCS Annex 21/SHC Task 8, high quality empirical data were gathered from six test cells and used for thermal simulations. Different setups were used for the test rooms to test different facets of the building energy simulation programs. Strategies referred to in the “Methodologies” section were then employed to develop and compare simulation results. The results were from 25 participants were compared by Lomas et al. (1994, 1997).

Validation efforts in the IEA-SHC Task 22 were undertaken to validate building energy simulation software at two different test cells. Two experiments performed in the ETNA facility were designed to compare the energy distribution on the air temperature in the measured at the center of the room. Additional experiments were run in the GENEC test facility, located in France (Commissariat à l’Energie Atomique), in their seven test cells. One of the experiments, used for comparison purposes, was carried out to validate the south wall of the cell that was exposed to climatic conditions and the solar gains through its glazed surfaces; the temperature in the space was allowed to “float”. The other construction elements of the cell (ceiling, floor, east, north, and west walls) were adjacent to guarded zones that were maintained at a constant temperature. There was no infiltration into the test cell and the air was not stirred. A more detailed description of the experiments and the results is provided by Moinard and Guyon (1999).

A similar study was undertaken by Lawrence Berkley National Laboratories (LBNL) to validate DOE-2. Eight buildings were originally constructed to study passive solar heating strategies and later to perform validations. The following four configurations were used for this study.

1. A baseline configuration in which the windows are closed and unshaded, the exterior walls and roof have their original color, and there is not night ventilation.
2. Same as (1) but all the windows except the north window are shaded.
3. Same as (2) but with the roof and exterior walls painted white.

4. Same as (3) but with fan forced ventilation at night.

From these experiments, the measured average air temperature was compared with the simulation results (Meldem and Winkelmann, 1995).

Daylight validations were also performed by the Florida Solar Energy Center (Shrum et al 1996). A trailer contained office sized rooms was used to validate DOE-2.1E with mini-blinds and no window treatment. The tests were performed over an extended period of time and compared with results from a DOE-2.1E model of the facility. The results included daylight interactions but did not simulate other HVAC interactions associated with daylighting.

#### **1.2.1.2. ERS Validations**

The ERS is a building that is uniquely equipped to perform whole building validations in an office-like building configured like in a real system. Therefore the facility has been used for numerous validation studies. A study done by Lee (1999) used the facility configured in three types of heating, ventilation, and air-conditioning (HVAC) systems for validation. These included: 1) variable-air-volume with terminal reheat, 2) constant air-volume with terminal reheat, and 3) four-pipe fan coil units. Experimental measurements were compared with predictions from three different building energy simulation programs and the results were assessed graphically and statistically.

Kuiken (2002) used the facility to evaluate daylighting systems and estimate annual energy saving from a validated DOE-2 model with daylighting and mini-blinds. For the experiments that were run at the ERS, DOE-2 was able to predict the overall energy saving due to daylighting within 11%.

The facility was used in conjunction with IEA-SHC Task 22 to perform three suits of empirical validations. From this research, three IEA reports were generated that dealt with different facets of building configuration and controls.

The first report (Travesi et al, 2001) consisted of validation exercises using three different experiments. The experiments were: 1) a steady-state constant air volume system with low

internal loads, 2) a variable-air-volume system with scheduled internal loads, and 3) a variable-air-volume system with variable internal loads and scheduled system. The second report (Maxwell et al., 2003) validated daylighting systems with diffuse interior window shades and a variable-air-volume system with terminal hydronic reheat. The third report (Maxwell et. al. 2004) validated the performance of air-side economizer controls using a variable-air-volume system with terminal reheat.

### **1.2.2. Heat Transfer Modeling for the Glazing, Windows, and Shading Devices**

Many advances have been made in the last 20 years made when modeling windows. Traditional methods used to model windows in building energy simulation programs are no longer good for approximating hourly performance for a simulation calculation (McCluney 1991). For complicated window glazings, it is recommended that angular-dependent values for the calculation of solar heat gain and visible transmissivity should be used in lieu of traditional shading coefficients and normal (to the window surface) visible transmittance measurements. This angular dependence also impacts the temperature distribution of the windows, which ultimately impacts the overall window thermal transmittance—an important quantity when calculate the heat transfer through windows. DOE-2.1E allows the simulators to use the conventional shading coefficient method to predict solar gain and a solar heat gain method that accounts for angular dependents. In a study performed by Reilly et al. (1995) using Chicago weather conditions in June, calculated solar gain comparisons were made using the shading coefficient method and the solar heat gain method accounting for angular dependence. The shading coefficient method the under-predicted single clear glazing by 35% and over-predicted the double clear glazing by up to 12%.

New methods and improved measuring techniques are being used when calculating the impact of glazing, windows, and window treatments can be divided into laboratory measurements, measurements made in a test facility, and fenestration models.

### **1.2.3. Laboratory Measurements**

Laboratory measurements have proved to be valuable undertakings to arrive at suitable fenestration inputs for building energy simulations software used in empirical validations.

Solar and thermal calorimetric measurements of glazings, windows, and shades offer viable inputs that can be used to simulate one-dimensional heat transfer through fenestration. A study conducted by Wise and Shah (2000) to verify the accuracy of laboratory measurement was done using nine laboratories in the United States testing the same glazing unit; all the laboratories produced a window thermal transmittance that was within two standard deviations of the expected value which provided confidence in the reliability of these measurements. Numerous other studies have produced reliable results for window and shade combinations to quantify solar heat gain factors (SHGF) measuring various shading devices for examining the various permutations of shades, temperatures, and tilt angles (Collins and Harrison, 2001A; Tseng and Goswami, 2001; Fang, 2000) and comparing these results to standard referenced values parameters like those found in ASHRAE Fundamentals (2001). With the popularity of mini-blinds and Venetian blinds in typical office spaces, many of these types of experiments have focused on the various facets of blind configurations, and the impact of the heat transfer properties near the surface (Breitenback et al., 2001; Klem and Kelley, 1996; Collins and Harrison, 2004A; Collins and Harrison, 2001B; Collins and Harrison, 1999; Machin et. al, 1998; Yahoda and Wright, 2004A; De Fang, 2000).

### **1.2.4. Test Facility Measurements**

LBNL has used their Mobile Window Thermal Test (MoWiTT) to test the thermal performance of glazings. MoWiTT was designed to expose fenestration to real weather conditions (Robinson and Littler, 1993). These results were then compared with early versions of Window Software developed by the Windows and Daylight group at LBNL. This facility was also used by Klems (2001) to evaluate electrochromic skylights.

### 1.2.5. Fenestration Models

Because of the limited number of sites to perform calorimetric measurements, models have been created to estimate fenestration properties and associated window treatments. Software like WIS (2004) and Window 5.2 (2003) have been developed to simulate angular dependent properties from glazings and predict solar and visible window properties for multiple glazing systems. Other algorithms within the Standards and Measurements Testing Programme have been validated with measurements (Roos et al, 2000). For shading systems, a simplified model for accounting for the shade when determining the shading coefficient of the window was proposed by McCluney and Mills (1993). Klems (2002) developed a model for windows and the associated shading to inadequacies in measured properties that are currently available. Later research focused on modeling the impact of interior and exterior blinds. Klems and Warner (1997) used measurements from previous experiments to derive a model for interior and between the glazing blinds for clear double glazings. Other studies focusing on other facets with blinds have modeled convective heat transfer effects (Ye et al, 1999), provided a general overview of recent developments in modeling optical and thermal properties (Rosenfeld, et al, 2001), effective longwave radiation properties (Yahoda and Wright, 2004B), solar heat and thermal gain (Collins and Harrison, 2004B), and sensitivity to heat transfer (Collins et al. 2002).

Daylighting models in building energy simulation software have also taken advantage of more robust optical glazing measurements. For a given latitude and longitude and weather data with direct-normal and total irradiation, the DOE-2 building energy simulation program can distinguish between direct and diffuse light entering a bare window. The software can calculate the angle of incidence of the direct light. The daylighting subroutine for the DOE-2.1E building simulations program distinguishes between direct and diffuse light entering the space for the bare window calculation and thus can account for angular dependents (Wilkemann et al, 1985).

### **1.3. Overview of the Research**

This research was done in conjunction with IEA Task 34/Annex 43 Subtask C. Prior to running the experiments, a cohesive set of statistical parameters was developed to assess the performances of the building energy simulation programs. Experiments were then performed to empirically validate building energy simulation software. The experiments were performed in a test cell on the EMPA Campus in Duebendorf, Switzerland and on the Des Moines Area Community College Campus at the ERS. A general overview of the experiments is given in this section as well as an overview of the methodologies employed to validate the software.

#### **1.3.1. EMPA Component**

Six exercises that started simple and increased in complexity were performed in the EMPA test cell and are listed below.

1. Test cell characterization.
2. Evaluation of irradiation models on tilted facades.
3. Glazing only.
4. Glazing with external shading screen.
5. Glazing with internal shading screen.
6. Glazing with external Venetian blinds.

After completion of the cell characterization experiments, subsequent tests used “constant” temperatures within the test cell and the guarded zone. Measured surface temperatures for the test cell construction element surfaces adjacent to the guarded zone were used as boundary conditions for the experiments. The experiments were run during periods when there was no snow on the ground in order to accurately account for ground reflectance. Prior to the experiments with a glazing unit and shading devices, two preliminary experiments were performed for test cell characterization and a three-dimensional heat transfer model of the cell was constructed to simulate the impact of thermal bridges.

### **1.3.2. ERS Component**

One experiment was performed at the ERS to assess the performance of daylighting algorithms in building energy simulation programs. All six of the exterior test rooms were used to evaluate program performances with three different types of windows, interior (mini-blinds and shading screens), and exterior (fins or projectiles) shading devices using a variable-air-volume system with electric reheat coils. The analyses not only included parameters specifically related to daylighting (i.e. reference point daylight illuminances and light powers), but also a comparison of electric coil reheat power for the variable-air-volume boxes.

### **1.3.3. Empirical Validation Methodology**

A consistent methodology was used to compare the performances of each building energy simulation program for all experiments. In order to carefully evaluate each program, experimental uncertainties of parameters were employed to measurements to outputs and detailed sensitivity studies were conducted to quantify how uncertainties in program input parameters propagated through the program and impacted outputs. When the programs were within these overlapping uncertainties evaluated at a 95% significance level, they were considered validated. Figure 1.5 contains a flowchart diagramming the methodology. The specific statistical parameters employed to evaluate the software are described in Chapter 2.

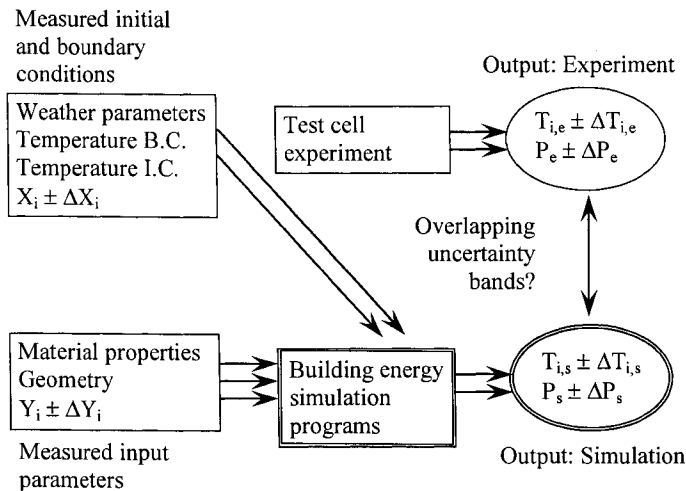


Figure 1.5. Methodology for empirical validation of building energy simulation programs.

### 1.3.4. Specific Research Objectives

There are several objectives to the research presented in this dissertation. The first is to design a set of experiments and to collect quality data which can not only be used by the author, but can also be used by the broader building physics research community. The second is to develop a statistical method which to compare the experimental results with the software output. The third is to provide feedback to code developers as to the accuracy of their models by reporting the results of this research in open literature.

### 1.4. Dissertation Organization

This dissertation was organized by combining journal papers in various stages of the publication process into the next five chapters. Because these papers all address the topic of empirical validation, the introductions for all the papers are very similar in some aspects and different in others. A general overview of the results and recommendations for future work

are provided in the final two chapters. Specification documents were written to provide detailed information about the experiments to the IEA participants and are provided in the appendices.

## References

- ASHRAE, 2001, Handbook of Fundamentals, SI Edition, Atlanta, GA, American Society of Heating Refrigeration and Air Conditioning Engineers
- Beausoleil-Morrison, I., and Strachan, P., On the Significance of Modeling Internal Surface Convection in Dynamic Whole-Building Simulation Programs, ASHRAE Transactions, Vol. 105(2):929-940
- Bisco Version 7.0w, 2004, A computer program to calculate 2D steady-state heat transfer, Physibel, Heirweg 21, B-9990, Maldegem, Belgium
- Breitenbach, J., Lart, S., Längle, I., and Rosenfeld, J.L.J., 2001, Optical and thermal performance of glazing with integral Venetian blinds, Energy and Buildings, 33:433-442
- Collins, M.R., and Harrison, S.J., 1999, Calorimetric Measurement of the Inward-Flowing Fraction of Absorbed Solar Radiation in Venetian Blinds, ASHRAE Transactions, Vol. 105(2): 1022-1030
- Collins, M.R., and Harrison, S.J., 2001A, Test of Measured Solar Heat Gain Variation in a Fenestration and Shade Combination with Respect to Test Specimen Tilt, ASHRAE Transactions, Vol. 107(1): 691-699
- Collins, M.R., and Harrison, S.J., 2001B, The Effects of Calorimeter Tilt on the Inward-Flowing Fraction of Absorbed Solar Radiation in a Venetian Blind, ASHRAE Transactions, Vol. 107(1): 677-683
- Collins, M.R., and Harrison, S.J., 2004A, Calorimetric Analysis of the Solar and Thermal Performance of Windows with Interior Louvered Blinds, ASHRAE Transactions, Vol. 110(1): 474-485
- Collins, M.R., and Harrison, S.J., 2004B, Estimating the Solar Heat and Thermal Gain from a Window with an Interior Venetian Blinds, ASHRAE Transactions, Vol. 110(1): 486-500
- Collins, M.R., Harrison, S.J., Oosthuizen, P.H., and Naylor, D., 2002, Sensitivity Analysis of Heat Transfer from an Irradiated Window and Horizontal Louvered Blind Assembly, ASHRAE Transactions, Vol. 108(1): 503-511
- De Fang, X., 2000, A study of the u-factor of the window with a high-reflectivity Venetian blind, Solar Energy, Vol.68, No. 2:207-214
- DOE-2.1E Software (Version 1.2.0.029), 2002, Building Energy Simulation Code, Lawrence Berkley Laboratories, Berkley, CA, April 9, 2002
- EnergyPlus Software (Version 1.2.1.012), 2004, Building Energy Simulation Code, <http://www.energyplus.gov>
- European Standard EN 6945, 2004, Building components and building elements—Thermal resistance and thermal transmittance—calculation methods, Draft Revision, ISO
- European Standard EN 410, 1998, Glass in building—Determination of luminous and solar characteristics of glazing, European Committee for Standardization, Brussels, Belgium
- Fang, X., 2001, A study of the U-factor of a window with a cloth curtain, Applied Thermal Engineering, Vol. 21:549-558

- Gleser, G.L. 1998, Assessing Uncertainty in Measurement, *Statistical Science*, Vol. 13, No.3:277-290
- Jensen, S.Ø., 1995, Validation of building energy simulation programs: a methodology, *Energy and Buildings*, Vol. 22:133-144
- Judkoff, R.D., 1988, Validation of Building Energy Analysis Simulation Programs at the Solar Energy Research Institute, *Energy and Buildings*, Vol.10:221-239
- Klems, J.H. and Warner, J.L., 1995, Measurement of Bidirectional Optical Properties of Complex Shading Devices, *ASHRAE Transactions*, Vol. 102(1):791-801
- Klems, J.H. and Kelley, G.O., 1996, Calorimetric Measurements of Inward Flowing Fraction for Complex Glazing and Shading Systems, *ASHRAE Transactions*, Vol. 102(1):947-954
- Klems, J.H. and Warner, J.L., 1997, Calorimetric Measurements of Inward Flowing Fraction for Complex Glazing and Shading Systems, *ASHRAE Transactions*, Vol. 103(1): 947-954
- Klems, J.H., 2001, Net energy performance measurements on electrochromic skylights, *Energy and Buildings*, Vol.33:93-102
- Klems, J.H., 2002, Solar Heat Gain Through Fenestration Systems Containing Shading: Summary of Procedures for Estimating Performance from Minimal Data, *ASHRAE Transactions*, Vol. 108(1): 512-524
- Kuiken, T., 2002, Energy Savings with a Commercial Building with Daylighting Controls: Empirical Study and DOE-2 Validation, Master Thesis at Iowa State University, Ames, IA
- Lee, S., 1999 Empirical Validation of Building Energy Simulation Software; DOE-2.1E, HAP, and Trace, PhD Thesis at Iowa State University, Ames, IA
- Lomas, K.J, Eppel, H., Martin, C.J., and Bloomfield, D.P., 1994, Empirical validation of thermal building simulation programs using test room data, Vol. 1 Final Report, International Energy Agency Annex 21/Task 12.
- Lomas, K.J, Eppel, H., Martin, C.J., and Bloomfield, D.P., 1997, Empirical validation of building energy simulation programs, *Energy and Buildings*, Vol. 26:253-275
- Loutzenhiser, P., 2003, Empirical validations of the DOE-2.1E building simulation software for daylighting and economizer controls, Masters Thesis, Iowa State University, Ames, IA
- Machin, A.D., Naylor, Harrison, S.J., and Oosthuizen, P.H., 1998, Experimental Study of Free Convection at an Indoor Glazing Surface with a Venetian Blind, *HVAC&R Research*, Vol.1 No.2:153-166
- Maxwell, G.M., Loutzenhiser, P.G., and Klaassen, C.J., 2003, Daylighting—HVAC Interaction Tests for the Empirical Validation of Building Energy Analysis Tools, Task 22 Subtask D Report, April 2003
- Maxwell, G.M., Loutzenhiser, P.G., and Klaassen, C.J., 2004, Economizer—HVAC Interaction Tests for the Empirical Validation of Building Energy Analysis Tools, Task 22 Subtask D Report, March 2004
- McCluney, R., 1991, Death of the Shading Coefficient?: New Sophisticated Fenestration Systems require New Methods to Determine Their Thermal Performances, *ASHRAE Journal*,(3)1991:36-45

- Mcluney, R., and Mills, L., 1993, Effects of Interior Shade on Window Solar Gain, ASHRAE Transactions, Vol. 99(2): 565-570
- Meldmem, R., and Winklelmann, F., 1995, Comparison of DOE-2 with Measurements in the Pala Test Houses, LBL-37973 UC-1600, July 1995.
- Moinard, S. and Guyon, G., 1999, Empirical Validation of EDF ETNA and Genec Test-Cell Models, A Report of Task 22 Building and Energy Analysis Tools, Project A.3 Empirical Validation
- Palomo Del Barrio, E., Guyon, G., 2003, Theoretical basis for empirical model validation using parameters space analysis tools, Energy and Buildings, Vol. 35:985-996
- Palomo Del Barrio, E., Guyon, G., 2004, "Application of parameter space analysis tools for empirical validation", Energy and Buildings, Vol.36:23-33
- Price, B.A. and Smith, T.F., 2000, Description of the Iowa Energy Center Energy Resource Station: Facility Update III, The University of Iowa, Iowa City, IA
- Reilly, M.S., Windelmann, F.C., Arasteh, D.K., Carroll, W.L., 1995, Modeling Windows in DOE-2.1E, Energy and Building, Vol.22:59-66
- Robinson, P., and Littler, J., 1993, Advanced Glazing: Outdoor Test Room Measurements, Performance Predictions and Building Thermal Simulations, Building and Environment, Vol.28, No.2:145-152
- Roos, A., Polato, P., Van Nijnatten, P.A., Hutchins, M.G., Olive, F., and Anderson, C., 2000, Angular-dependent optical properties of low-e and solar window control windows—simulation versus measurements, Solar Energy, Vol.69(Suppl.), No.1-6:15-26
- Rosenfeld, J.L.J., Platzer, W.J., Van Dijk, W.J., and Maccari, A., 2000, Modeling the optical and thermal properties of complex glazing:overview of recent developments, Solar Energy, Vol. 69(Suppl.):1-13
- Shrum, L. and Parker, D., 1996, DOE-2 Validations: Daylighting Dimming and Energy Savings: The effect of Window Orientation and Blinds, Building Energy Simulation News, Vol. 17 No.1:33-39
- Strachan, P., 1993, Model Validation using the PASSYS Test Cells, Building and Environment, Vol.28, No. 2:153-165
- Travesi, J., Maxwell, G., Klaassen, C., and Holtz, M., 2001, Empirical Validation of Iowa Energy Resource Station Building Energy Analysis Simulation Models, Task 22 Subtask A Report, June 2001
- Trisco Version 10.0w, 2002, A computer program to calculate 3D steady-state heat transfer, Physibel, Heirweg 21, B-9990, Maldegem, Belgium
- Tseng, C., and Goswami, D.Y., 2001, Effect of Tilt Angle and Temperature Difference on Solar Heat Gain Coefficient Measurement of Fenestration System, ASHRAE Transactions, Vol. 107(1):684-690
- Winklelmann, F.C., Selkowitz, S., 1985, Daylighting Simulation in the DOE-2 Building Energy Analysis Program, Energy and Building, 8:271-286
- Windows 5.2 version 5.2.17, 2003, Regents University of California

- Wise, D.J., and Shah, B.V., 2000, An Assessment of Interlaboratory Reproducibility in Fenestration Energy Ratings, ASHRAE Transactions Vol. 106(1)
- Wouters, P., Vandaele, L., Voit, P., and Fisch, N., 1993, The Use of Outdoor Test Cells for Thermal and Solar Building Research within the PASSYS Project, Building and Environment, Vol. 28, No.2:107-113
- WIS. 2004. Window Information System, <http://windat.ucd.ie/wis/html/index.html>
- Wright, J.L., and McGowan, A., 1999, Calculating the Solar Heat Gain of Window Frames, ASHRAE Transactions, 105(2):1011-1021
- Yahoda, D.S., and Wright, J.L., 2004A, Heat Transfer Analysis of a Between-Panes Venetian Blind Using Effective Longwave Radiative Properties, ASHRAE Transactions, Vol. 110(1):455-462
- Yahoda, D.S., and Wright, J.L., 2004B, Method for Calculating the Effective Longwave Radiative Properties of a Venetian Blind Layer, ASHRAE Transactions, Vol. 110(1): 463-473
- Ye, P., Harrision, S.J., and Oosthuizen, P.H., 1999, Convective Heat Transfer from a Window with a Venetian Blind: Detailed Modeling, ASHRAE Transactions, Vol. 105(2):1031-1037

**Chapter 2: Series of experiments for empirical validation of solar gain modeling in building energy simulation codes – Experimental setup, test cell characterization, specifications and uncertainty analysis**

A paper accepted in Building and Environment

H. Manz<sup>\*1,a</sup>, P. Loutzenhiser<sup>1,2,b</sup>, T. Frank<sup>1,c</sup>, P.A. Strachan<sup>3,d</sup>, R. Bindi<sup>1,e</sup>, and G. Maxwell<sup>2,f</sup>

<sup>1</sup> Empa, Materials Science & Technology, Laboratory for Applied Physics in Building, CH-8600 Duebendorf, Switzerland

<sup>2</sup> Iowa State University, Dept. of Mechanical Engineering, Ames, Iowa 50011, USA

<sup>3</sup> University of Strathclyde, Dept. of Mechanical Engineering, ESRU, Glasgow G1 1XJ, Scotland

\* Corresponding author (heinrich.manz@empa.ch)

<sup>a</sup> Wrote the original text and performed the original HELIOS simulations

<sup>b</sup> Added to the text, performed the EnergyPlus and DOE-2 simulations, developed the statistical analyses, added to the “Results” section, and wrote the “Discussion” section.

<sup>c</sup> Provided technical advice

<sup>d</sup> Performed the ESP-r simulations with the Monte Carlo Analysis

<sup>e</sup> Performed the TRISCO simulation

<sup>f</sup> Provided technical support

**Abstract**

Empirical validation of building energy simulation codes is an important component in understanding the capacity and limitations of the software. Within the framework of Task 34/Annex 43 of the International Energy Agency (IEA), a series of experiments was performed in an outdoor test cell. The objective of these experiments was to provide a high-quality data set for code developers and modelers to validate their solar gain models for windows with and without shading devices. A description of the necessary specifications for modeling these experiments is provided in this paper, which includes information about the test site location, experimental setup, geometrical and thermophysical cell properties including estimated uncertainties. Computed overall thermal cell properties were confirmed by conducting a steady-state experiment without solar gains. A transient experiment, also without solar gains, and corresponding simulations from four different building energy simulation codes showed that the provided specifications result in accurate thermal cell

modeling. A good foundation for the following experiments with solar gains was therefore accomplished.

*Keywords:* Building energy simulation; Empirical validation; Test cell specification

## **2.1. Introduction**

The use of building energy simulation codes has been continuously evolving since the 1970s and 1980s. The integral approach, by which all relevant energy transport paths are simultaneously processed, makes building energy simulation codes powerful tools for the design of energy-efficient buildings, which may explain their growing popularity. Numerous commercial and freeware codes are now available with varying levels of modeling versatility, complexity and user interfaces. An overview of the theory and application of this type of tool is given by Clarke [1].

Validation of models implemented in the codes is a prerequisite for a successful application. Studies performed by Judkoff [2] and Judkoff and Neymark [3] have shown large disagreements between different codes. Code validation is therefore seen as an essential part of the development of building energy simulation software. Clarke [1] stressed this point by noting that in new code development a code that has successfully passed a validation test may fail the same test at a later time. Hence, validation checks must be made on a regular basis to guarantee the accuracy of the code. An excellent way in which to do this was proposed and performed within IEA Annex 21 [3]: a set of diagnostic tests was implemented into a software package. A similar approach was pursued by Ben-Nakhi and Aasem [4], who developed a module for integrating into simulation codes to validate transient heat flow computation through opaque multi-layered constructions.

A number of authors have been working on validation methodology [2, 5, 6, 7, 8]. Code checking - i.e. testing if the code behaves as expected and is basically free of programming errors - and documentation of the functions of each routine can be thought of as the first steps towards quality assurance and validation. Judkoff [2] provides an overview of additional

validation techniques and discusses advantages and disadvantages of three different approaches, which are (i) analytical (comparison of simulation results with analytical solutions), (ii) comparative (code-to-code comparisons), and (iii) empirical (comparisons of simulation results with experimental data). The advantages of analytical and comparative tests are that there is no uncertainty associated with the input parameters and tests are relatively inexpensive to perform. The disadvantage of the analytical test is that a limited number of analytical solutions are available and that in comparative tests there is no truth standard. On the other hand, empirical validation has a truth standard within the limits of the experimental uncertainty and, in addition, complex cases can be performed. But empirical validation is the most time-consuming and expensive of the three techniques and has therefore only been performed on a very limited basis.

Highly glazed buildings are becoming increasingly popular around the world. It is particularly important to model the thermal performance of the transparent façade when predicting the thermal behavior of the building in summer. Energy flows through the glazing and shading devices are determined by optical, thermodynamic and fluid-dynamic processes [9]. Because of the complexities of the systems, no analytical solutions are available for such validations. Code-to-code comparisons are not sufficient because it is not obvious which model, if any, is correct. The only suitable approach is therefore to perform high-quality experiments for validation purposes.

The series of experiments discussed here was performed in a test cell on the EMPA campus in Dübendorf, Switzerland. According to Strachan [10], test cells represent an economic and practical alternative between laboratory experiments and full-scale monitoring of buildings and provide the best available environment providing high-quality data sets needed for the empirical whole-model validation. The facility used in this study, the cell concept was first described by Simmler et al. [11], has guarded zones for thermal shielding of the cell. Compared with previous empirical validation projects using test cells without guarded zones [10, 12, 13], the guarded zones offered much better control of boundary conditions in this study. The data acquired at the EMPA facility meet all nine criteria described by Lomas et al. [13] for high-quality data sets.

The goal of this project is to provide a set of empirical data from a series of experiments. The experiments will increase in complexity and can be used for validation of window models with and without external or internal shading devices. Previous test cell empirical validation work by Moinard and Guyon [14] has shown that determining the overall thermal cell characteristics is of the greatest importance. Thermal bridge losses are usually of greater importance in test cells compared to real buildings, because conduction through walls is the only heat loss mechanism (infiltration is excluded) and the test cells have smaller dimensions than real rooms. Therefore, particular attention was paid to identifying the magnitude of the thermal bridge losses. Two experiments without solar gains were therefore performed during the first phase of the project. These experiments included (i) a steady-state experiment to characterize the overall thermal performance of the cell, and (ii) a transient experiment with pseudo-random heat inputs.

Empirical validation exercises are always tests of (i) the experiment itself, (ii) the simulation tool, and (iii) the modeler. Four building energy simulation codes were used to model the transient experiment in this study. The specific codes were DOE-2.1E [15], EnergyPlus [16], ESP-r [17] and HELIOS [18]; inputs were made by different modelers. Results from those experiments, which included solar gains through a window with or without a shading device and corresponding building energy simulation code predictions, will be presented in future papers.

In empirical validation work measured and predicted uncertainty bands need to be evaluated and parameters identified to which the results are particularly sensitive. Lomas and Eppel [19] described three different sensitivity analysis techniques and their applicability to building simulation codes. Macdonald and Strachan [20] implemented algorithms for uncertainty analysis based on differential sensitivity and the Monte Carlo method into a building energy simulation code called ESP-r. In this paper, uncertainties are given for all measured and code input parameters as well as uncertainty bands of simulated results obtained using ESP-r.

## 2.2. Concept of Test Cells with Guarded Zones

Details of the test cell location and orientation are shown in Table 2.1. The facility comprising two identical test cells was designed for calorimetric measurements on façade elements and is shown in Figure 2.1. Table 2.2 depicts the main geometrical parameters of the cell, including estimated uncertainties. The wooden structure building surrounding the cells is insulated with a layer of 0.12 m glass wool. Both cuboid shape cells adjoin a guarded zone at five faces (Figure 2.2). Each test cell and each guarded zone employs its own air conditioning unit. The temperature in the test cells is controlled by means of an air-water heat exchanger. The cooling power (max. 5000 W) can be determined by measuring the mass flow rate and the temperature difference in the water circuit. The heating power (max. 3500 W) is directly determined by measuring the electrical power. If the temperature differences between the guarded zone and cell are small, energy flows through the external wall become far greater than the flows through the remaining faces and energy flows through the external wall can therefore be measured more precisely. A PC with data acquisition equipment was located in the guarded zone and was shielded from the test cell by an airtight curtain.

Table 2.1. Location of EMPA test cells.

Degree of longitude	-8.6°
Degree of latitude	47.4°
Altitude above sea-level	430 m
Time zone	Greenwich Mean Time (GMT) + 1h
Orientation of external wall	29° (south = 0°, west = 90°)

Table 2.2. Geometrical parameters of test cell. Areas shown in this table are in contact with internal air.

Internal height	2.360 m ± 0.02 m <sup>b</sup>
Internal width	2.850 m ± 0.02 m <sup>b</sup>
Internal length	4.626 m ± 0.02 m <sup>b</sup>
North / south wall	6.726 m <sup>2</sup> ± 0.074 m <sup>2</sup> <sup>a</sup>
East / west wall	10.917 m <sup>2</sup> ± 0.104 m <sup>2</sup> <sup>a</sup>
Floor / ceiling	13.184 m <sup>2</sup> ± 0.107 m <sup>2</sup> <sup>a</sup>
Internal volume	31.114 m <sup>3</sup> ± 0.368 m <sup>3</sup> <sup>a</sup>

*a is an estimate of error using propagation of error (uncertainty analysis) with individual Bayesian error estimates.*

*b is a Bayesian estimate of error.*

*c is a frequentist error which represents a sample standard deviation using literature values from different sources.*

*d is an estimate of error using propagation of error (uncertainty analysis) with estimates of error from linear regression analysis.*

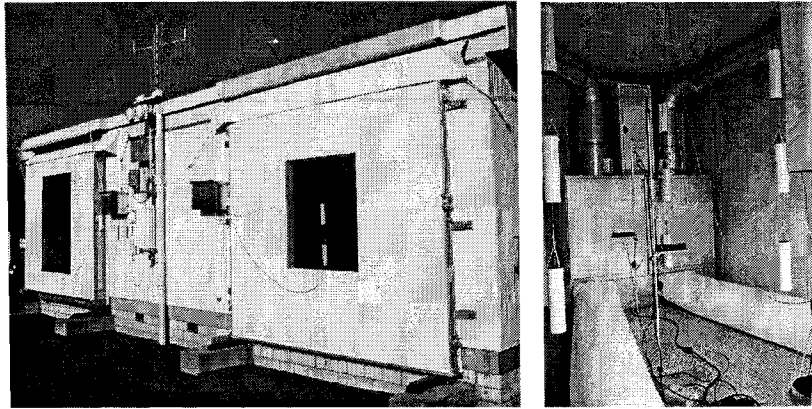


Figure 2.1. Outdoor view (left) of test cells with two removable façade elements (3.4 m × 3.4 m) and indoor view (right) showing HVAC cabinet and extract and supply ducts.

The goal of the test cell ventilation (Figure 2.2) was to minimize the temperature stratification and to obtain a well-defined cell air temperature. Temperature stratification of cell air was smaller than 0.5 K in the experiments presented in this paper. Air was extracted near the ceiling, while conditioned air was supplied close to the floor at low speed by means of two large cylindrical fabric outlets. Except for locations near the extract grills, air speeds in the whole cell were below 0.1 m/s. Using one fan only, the flow rate of recirculated air was ~ 40 air changes per hour; this value could be increased by switching on a second fan.

Equipment for air recirculation in the guarded zone maintained a more uniform air temperature distribution. Recirculated air was supplied near the south wall of the cell by means of four large cylindrical fabric outlets that were mounted horizontally and vertically around the test cell. The air was extracted near the north cell wall to obtain a flow pattern close to a piston flow. Outer surface temperatures of the cell adjacent to the guarded zone were within a range of 2 K during experiments described in this paper.

To control the outside environment of all six faces of the test cell, an external chamber shown in Figures 2.2 and 2.3 was mounted at the cell's south wall. The air temperature in this chamber was controlled by a water/air heat exchanger that was connected to a thermostat apparatus. As can be seen in Figure 2.3, the external chamber was covered with aluminum foil that reflects solar radiation, in order to minimize the impact of solar energy in the

chamber. Air temperature stratification in the exterior chamber was reduced by a fan. All outer surface temperatures of the south cell wall adjacent to the external chamber were within a band of 0.3 K during the experiments.

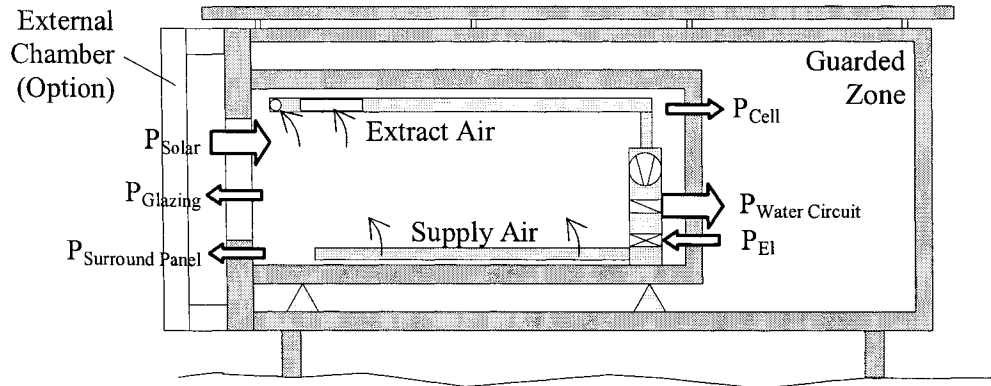


Figure 2.2. Concept of test facility with air conditioning of the cell, guarded zone, energy flows into and out of the test cell and optional external chamber.

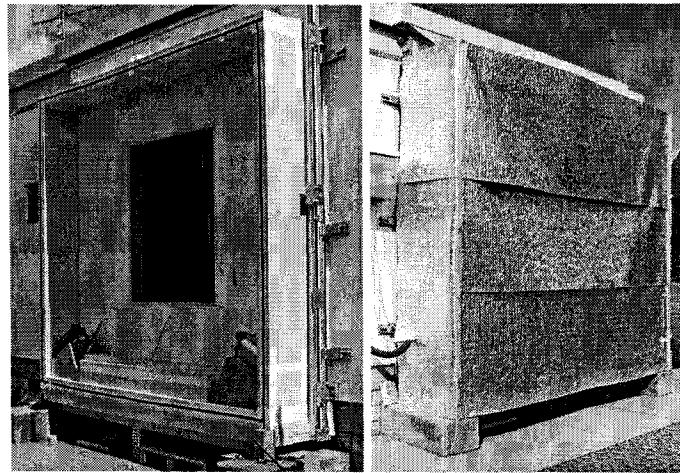


Figure 2.3. Thermally controlled external chamber mounted in front of one of the cells and viewed from outside during (left) and after construction (right).

## 2.3. Thermal Properties of Test Cell Envelope

### 2.3.1. Layer and Surface Properties

Tables 2.3 to 2.5 show layer sequences, thicknesses and thermophysical properties of all layers of the cell envelope. Modelers may wish to investigate the impact of uncertainties of input parameters on their results. Estimated uncertainties of all values are therefore given. Layer number 1 denotes the first layer from the outside. Numerical values of thermophysical properties were either based on product specifications, literature data or in-house measurements. If thermophysical properties had to be based on literature data, several literature sources were employed and the mean of these was taken.

Table 2.3. Layer properties: Ceiling, north (incl. door), east and west wall.

Layer number	Material	Thickness mm	Thermal conductivity W/(m K)	Density kg/m <sup>3</sup>	Specific heat J/(kg K)
1	Sheet steel	0.7 ± 0.1 <sup>b</sup>	53.62 ± 6.56 <sup>c</sup>	7837 ± 42 <sup>c</sup>	460.8 ± 25.4 <sup>c</sup>
2	PU foam	138.6 ± 1 <sup>b</sup>	0.01921 + 0.000137·θ ± 6.5 % <sup>*d</sup>	30 ± 0.3 <sup>b</sup>	1800 ± 72 <sup>b</sup>
3	Sheet steel	0.7 ± 0.1 <sup>b</sup>	53.62 ± 6.5 <sup>c</sup>	7837 ± 42 <sup>c</sup>	460.8 ± 25.4 <sup>c</sup>

<sup>\*</sup> Own measurement, θ Temperature in degree Celsius

Table 2.4. Layer properties: Floor.

Layer Number	Material	Thickness mm	Thermal conductivity W/(m K)	Density kg/m <sup>3</sup>	Specific heat J/(kg K)
1	Sheet steel	0.7 ± 0.1 <sup>b</sup>	53.62 ± 6.56 <sup>c</sup>	7837 ± 42 <sup>c</sup>	460.8 ± 25.4 <sup>c</sup>
2	PU foam	140 ± 1 <sup>b</sup>	0.01921 + 0.000137·θ ± 6.5 % <sup>*d</sup>	30 ± 0.3 <sup>b</sup>	1800 ± 72 <sup>b</sup>
3	PU foam (higher density)	20 ± 0.5 <sup>b</sup>	0.070 ± 0.0035 <sup>b</sup>	45 ± 0.45 <sup>b</sup>	1800 ± 72 <sup>b</sup>
4	Sheet steel with surface structure	2.5 ± 0.1 <sup>b</sup>	53.62 ± 6.56 <sup>c</sup>	7837 ± 42 <sup>c</sup>	460.8 ± 25.4 <sup>c</sup>

Table 2.5. Layer properties: External Wall.

Layer number	Material	Thickness mm	Thermal conductivity W/(m K)	Density kg/m <sup>3</sup>	Specific heat J/(kg K)
1	Plywood	10 ± 0.5 <sup>b</sup>	0.136359 + 0.000175·θ ± 2.5 % <sup>*d</sup>	850 ± 17 <sup>b</sup>	1605 ± 7.1 <sup>b</sup>
2	EPS foam	130 ± 1 <sup>b</sup>	0.03356 + 0.000127·θ ± 4.3 % <sup>*d</sup>	28 ± 0.28 <sup>b</sup>	1460 ± 58.4 <sup>b</sup>
3	Plywood	10 ± 0.5 <sup>b</sup>	0.136359 + 0.000175·θ ± 2.5 % <sup>*d</sup>	850 ± 17 <sup>b</sup>	1605 ± 7.1 <sup>b</sup>

The reflectances of samples of all relevant surfaces were measured in the wavelength interval of solar radiation (250 to 2500 nm) at approximately perpendicular incident solar radiation using a spectrophotometer. Integral values for solar and visual reflectances were

determined according to EN 410 [21] using GLAD software [22]. Emissivities were measured at room temperature using an integral method. Table 2.6 depicts optical properties of cell surfaces.

Table 2.6. Optical properties of cell surfaces.

	Solar reflectance	Visible reflectance	Emissivity
	-	-	-
Inner surfaces of walls and ceiling	$0.757 \pm 1 \%$	$0.874 \pm 1 \%$	$0.92 \pm 5 \%$
Inner surface of floor	$0.246 \pm 1 \%$	$0.300 \pm 1 \%$	$0.96 \pm 5 \%$
Outer / inner surfaces of south wall	$0.766 \pm 1 \%$	$0.884 \pm 1 \%$	$0.93 \pm 5 \%$

### 2.3.2. Thermal Bridges: Door, Edges, Etc.

Total thermal losses - including those at edges, door, sealing at external wall and intersections of pipes or flexes with the cell envelope - were computed using TRISCO software [23]. This code enables 3D steady-state analysis of heat conduction processes. Equivalent thermal conductivities of cavities were calculated according to prEN ISO 10077-2 [24]. The final model of the test cell employed  $5.6 \cdot 10^6$  nodes. Figures 2.4 and 2.5 show results of these simulations. High heat fluxes were computed at the sealing of the door and at the sealing between cell and removable external wall. Figure 2.6 shows a picture of the thermal bridges at the door taken with an infrared camera. Dark areas represent regions with higher radiation fluxes corresponding to increased surface temperatures.

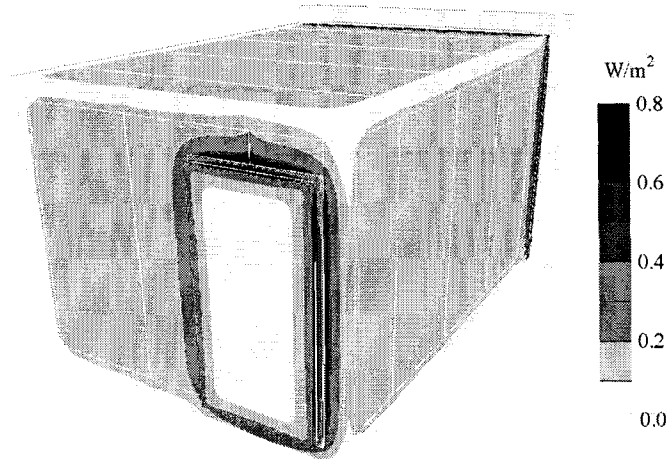


Figure 2.4. Computed heat fluxes at the outer surfaces of the test cell at a temperature difference of 1 K between cell air and guarded zone.

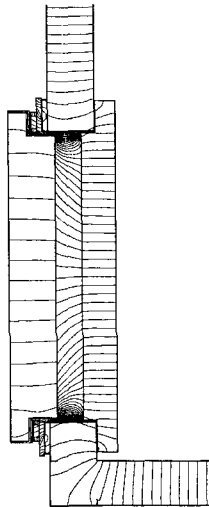


Figure 2.5. Computed heat flow lines in a horizontal cross-section of the door.

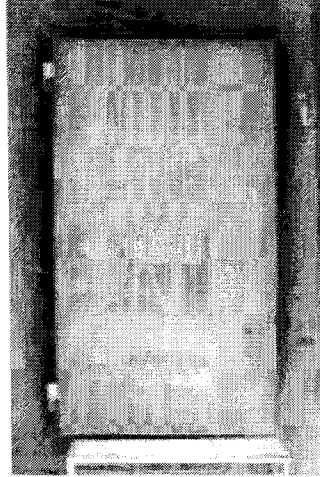


Figure 2.6. Infrared picture of the cell door, taken when temperature in the cell was 20 K higher than in the guarded zone, shows thermal bridges at the door frame.

Numerical values of additional thermophysical properties needed for these simulations were also based on product specifications and literature data. The total thermal conductance of the whole cell envelope from cell air to the outer surface of the cell envelope, including all flows at thermal bridges, were calculated at temperatures of 0°C and 20°C as being 13.539 W/K and 14.721 W/K, respectively.

### 2.3.3. Internal Thermal Mass

The heat capacity of the technical equipment in the cell, which consisted of metallic ducts, grills, fans, a heat exchanger apparatus inside a metallic casing, an electrical cabinet etc. was estimated to be  $200 \pm 30$  kJ/K (Fig. 2.1, right). Because the steel sheets were a major component of the thermal mass, the thermal response of the internal mass was assumed to be fast compared with the cell envelope. However, simulations showed that the impact of this thermal mass on the overall transient thermal behavior of the cell was rather small.

### 2.3.4 .Total Steady-State Thermal Properties

Tables 2.7 and 2.8 show the heat transfer coefficients  $A_i$  and the thermal conductances  $H_i$ . These parameters refer to the heat flow between the cell air and the outer surface of the cell

envelope. In all TRISCO simulations, the heat transfer resistance between cell inside air and the inner surface of the cell envelope was assumed to be  $0.13 \text{ m}^2\text{K/W}$  at all locations. It can be seen in Table 2.7 that 35 % of the heat flow between cell and guarded zone occurs at thermal bridges. Thermal conductances of the the guarded zones,  $H_{GZ}$ , and of the external wall,  $H_{EW}$ , are shown as a function of temperature,  $\theta$  in  $^{\circ}\text{C}$ , in Equations 2.1 and 2.2.

$$\text{Guarded zone: } H_{GZ}(\theta) = 11.877 + 0.0534 \cdot \theta \quad (\text{W/K}) \quad (2.1)$$

$$\text{Outside: } H_{EW}(\theta) = 1.662 + 0.0057 \cdot \theta \quad (\text{W/K}) \quad (2.2)$$

Table 2.7. Heat transfer coefficients and thermal conductances of cell to the guarded zone (cell air to outer surface of cell envelope).

	Area A $\text{m}^2$	Heat transfer coefficient $\Lambda_{20^{\circ}\text{C}}$ $\text{W}/(\text{m}^2\text{K})$	Thermal conductance $H_{20^{\circ}\text{C}}$ $\text{W/K}$
Ceiling, north (incl. door), east and west wall	41.745	0.155	6.478
Floor	13.184	0.147	1.941
Thermal bridges guarded zone	-	-	$4.526 \pm 10 \% ^b$
Total			12.945

Table 2.8. Heat transfer coefficients and thermal conductances of cell to the outside (cell air to outer surface of cell envelope).

	Area A $\text{m}^2$	Heat transfer coefficient $\Lambda_{20^{\circ}\text{C}}$ $\text{W}/(\text{m}^2\text{K})$	Thermal conductance $H_{20^{\circ}\text{C}}$ $\text{W/K}$
External wall	6.726	0.258	1.736
Thermal bridges outside	-	-	$0.040 \pm 10 \% ^b$
Total			1.776

This temperature dependence is caused by the temperature-dependent thermal conductivities shown in Tables 2.3 to 2.5. Losses at thermal bridges are almost independent of temperature as they are mainly due to heat conduction in metals which is only affected to a very minor extent by temperature changes within ranges considered here.

### 2.3.5. Sensitivity and Uncertainty of Steady-State Thermal Properties

The numerical accuracy of TRISCO simulations was investigated using a grid sensitivity study and was found to be below 2%. The total uncertainties of the thermal conductance in Equations 2.1 and 2.2 were therefore mainly determined by the uncertainty of the input

parameters. Assuming that each individual input parameter is independent of other inputs, the total or combined uncertainty,  $u_c$ , can be estimated from the square root of the quadrature sum of the uncertainties due to each of the inputs shown in Equation 2.3.

$$u_c = \sqrt{\sum_{i=1}^N u_i^2} \quad (2.3)$$

Table 2.9 shows the impact of the uncertainties of a few parameters on the uncertainties of thermal conductance. These values were found using TRISCO simulations. Additional uncertainties occurred due to deviations of the model geometry or due to uncertainties in calculating heat transfer in cavities. Total uncertainties of thermal conductance,  $H_{GZ}$  and  $H_{EW}$ , were assumed to be less than  $\pm 8\%$ .

Table 2.9. Sensitivity of thermal conductance to changes of important input parameters.

Input parameter	Change of input parameter	Impact on thermal conductances	
		$H_{GZ}$	$H_{EW}$
Thermal conductivity of PU foam	$\pm 5 \%$	$\pm 3.4 \%$	-
Thermal conductivity of EPS foam	$\pm 5 \%$	-	$\pm 4.7 \%$
Thermal conductivity of steel	$\pm 10 \%$	$\pm 0.3 \%$	-
Thermal conductivity of stainless steel	$\pm 10 \%$	$\pm 0.9 \%$	-

## 2.4. Sensors

All sensors were periodically calibrated according to an EMPA internal quality assurance system. About 150 parameters were acquired every 4 minutes during the experiments. After each full hour of data acquisition mean values were computed for the last hour and saved.

Table 2.10 shows all meteorological parameters measured at the facility, the type of sensor and uncertainties according to manufacturers' specifications. Table 2.11 depicts specifications of the most important parameters which were measured in the test cell, the external chamber and in the guarded zone.

Table 2.10. Weather data parameters and equipment.

Parameter	Unit	Type of sensor / measurement	Number of sensors	Accuracy
Solar global irradiance, façade plane	$W/m^2$	Pyranometer (Kipp & Zonen CM 21)	1	$\pm 2 \%$
Solar global horizontal irradiance	$W/m^2$	Pyranometer (Kipp & Zonen CM 21)	1	$\pm 2 \%$
Solar diffuse horizontal irradiance	$W/m^2$	Pyranometer, mounted under the shading ball of a tracker (Kipp & Zonen CM 21)	1	$\pm 3 \%$

Zonen CM 11)				
Direct-normal irradiance	W/m <sup>2</sup>	Pyrheliometer, mounted in an automatic sun-following tracker (Kipp & Zonen CH 1)	1	± 2 %
Infrared irradiance, façade plane	W/m <sup>2</sup>	Pyrgeometers (Kipp & Zonen CG 4)	1	± 2 %
Outside air temperature, in front of façade	°C	Radiation shielded, mechanically ventilated thermocouples	2	± 0.5 K
Wind speed, in front of façade	m/s	Ultrasonic anemometer (WindMaster )	1	± 1.5 %
Horizontal illuminance	Lx	Luxmeter (Kipp & Zonen LuxLite, Minolta T-10W)	2	± 3 %
Pressure	hPa	Barometric Pressure Measuring Device (Vaisala PTA 427)	1	± 0.5 hPa
Relative humidity	%	Humidity Transmitter (Vaisala HMP 130Y Series)	1	± 1% (0-90%) ± 2% (90-100%)

Table 2.11. Parameters measured in the test cell, the external chamber and the guarded zone and approximate accuracies according to manufacturer specifications.

Parameter	Unit	Type of sensor / measurement	Number of sensors	Accuracy
Air temperatures, inside test cell	°C	Thermocouple, radiation shielded by two cylinders	8	± 0.3 K
Air temperatures, in external chamber	°C	Thermocouple, radiation shielded by two cylinders	5	± 0.3 K
Air temperatures, in guarded zone, 0.1 m in front of cell surface	°C	Thermocouple, radiation shielded by two cylinders	25	± 0.3 K
Surface temperatures, inner surface of cell envelope	°C	Thermocouple	30	± 0.3 K
Surface temperatures, outer surface of cell envelope	°C	Thermocouple	30	± 0.3 K
Heating power, inside test cell	W	Electric power (Infratek 106A)	1	± 0.1 %
Cooling power, inside test cell	W	Electromagnetic flowmeter (Endress+Hauser Promag 53H) and temperature difference measurement (PT100)	3	± 2 %
Illuminance, horizontal inside cell	Lx	Luxmeter (Minolta T-1H)	3	± 2 %

The locations of sensors in the test cell and in the guarded zone can be seen in Figure 2.7. The vertical distances of air temperature sensors inside the cell from the floor to ceiling were 0.3 m, 1.1 m and 2.1 m.

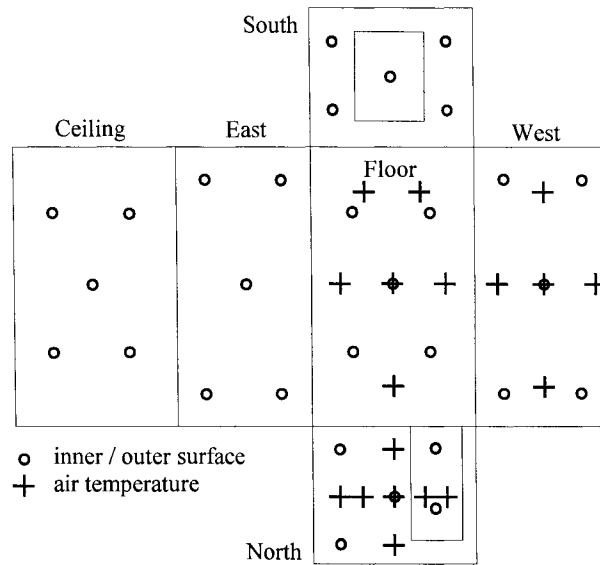


Figure 2.7. Location of temperature sensors on inner (30 sensors) and outer (30 sensors) surface of cell envelope. For air temperature (8 sensors) projections on floor, north and west wall are shown.

## 2.5. Air Tightness of the Cell

All inner and outer cell surfaces were made of steel sheets, and the gaps between the sheets were sealed with silicone. Two-stage rubber gaskets at the door and at the external wall made leak protection possible. The air tightness of the cell was measured using the blower door method. At an overpressure of 50 Pa in the test cell, air exchange was found to be  $0.2 \text{ h}^{-1}$ . The thermal effects of infiltration were therefore assumed to be negligible.

## 2.6. Experiment for Steady-State Cell Characterization

In addition to the computational approach described in Section 2.3, a steady-state experiment was performed in order to measure thermal conductances  $H_{GZ}$  and  $H_{EW}$  directly in the test facility. The external chamber was mounted over the external surface during these for conditioning of the sixth face of the cell. The air inside the test cell, the guarded zone and the external chamber were stirred in order to reduce temperature stratifications. Boundary

condition parameters were kept as close as possible to constant values. From a steady-state analysis of the cell results:

$$P_{el,A} + H_{GZ}(T_{TC,A} - T_{GZ,A}) + H_{EW}(T_{TC,A} - T_{EC,A}) = 0 \quad (2.4)$$

$$P_{el,B} + H_{GZ}(T_{TC,B} - T_{GZ,B}) + H_{EW}(T_{TC,B} - T_{EC,B}) = 0 \quad (2.5)$$

Parameters determined in the experiment were the heating power  $P_{el}$ , space-averaged air temperature in the test cell  $T_{TC}$  (8 sensors), space-averaged outer surface temperature of cell in guarded zone  $T_{GZ}$  (25 sensors) and space-averaged outer surface temperature of cell in external chamber  $T_{EC}$  (5 sensors). Because there were two unknowns,  $H_{GZ}$  and  $H_{EW}$ , two equations, representing two different temperature boundary conditions, were needed. Indices A and B denote these two phases of the experiment. The solutions for  $H_{GZ}$  and  $H_{EW}$  were found analytically by solving this set of equations (Equations 2.4 and 2.5).

No ideal steady-state situation could be reached in this experiment. Higher fluctuations in boundary conditions occurred particularly on days with high solar irradiances and large differences between daily minimum and maximum outside air temperature. Hence, time intervals with an overcast sky and, therefore, less fluctuating boundary conditions were chosen for analysis. Figure 2.8 shows temperatures and heating power in the cell as a function of time during Phase B. To eliminate small transient effects in the cell envelope, time-averaged values were used (Table 2.12). Taking into account that the uncertainties were dominated by systematic effects, the uncertainties given here were higher than uncertainties of individual sensors from information in Table 2.11. It was assumed that mean temperatures and heating power were independent of each other and the total uncertainty was therefore again estimated from the square root of the quadrature sum of the uncertainties due to each of the inputs (see Equation 2.3).

Table 2.12. Steady-state experiment: Time-averaged values and uncertainties for thermal conductance calculations.

	$P_{el}$	$T_{TC}$	$T_{GZ}$	$T_{EC}$
Phase A	$282.26 \text{ W} \pm 4 \text{ W}$	$43.13^\circ\text{C} \pm 0.5^\circ\text{C}$	$23.50^\circ\text{C} \pm 0.5^\circ\text{C}$	$23.24^\circ\text{C} \pm 0.5^\circ\text{C}$
Phase B	$145.04 \text{ W} \pm 3 \text{ W}$	$36.45^\circ\text{C} \pm 0.5^\circ\text{C}$	$23.33^\circ\text{C} \pm 0.5^\circ\text{C}$	$43.74^\circ\text{C} \pm 0.5^\circ\text{C}$

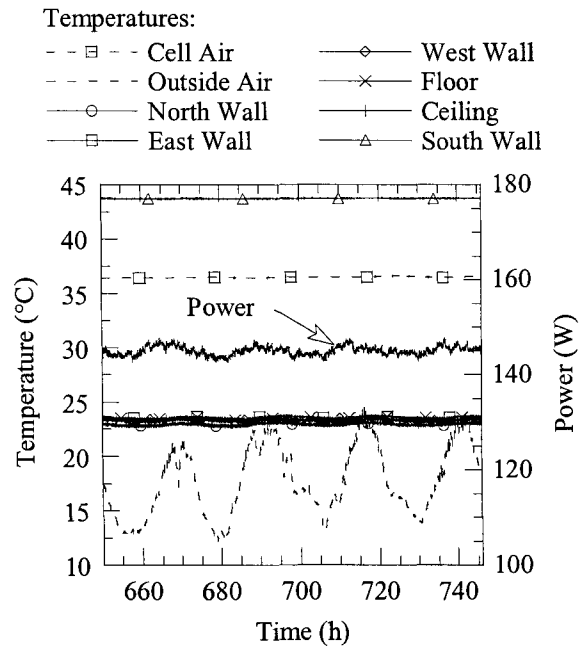


Figure 2.8. Mean air temperature inside cell and outside, mean surface temperatures of all six faces and heating power inside the cell as a function of time during phase B of the steady-state experiment (duration 96 h).

Based on this steady-state experiment and the procedure described above, numerical values and total uncertainties for the thermal conductances were calculated to be  $H_{GZ} = 12.23 \text{ W/K} \pm 0.53 \text{ W/K}$  and  $H_{EW} = 2.12 \text{ W/K} \pm 0.59 \text{ W/K}$ . These values refer to the mean temperatures in the cell envelope of  $36.6^\circ\text{C}$  in the external wall, and,  $31.6^\circ\text{C}$  in the cell envelope adjacent to the guarded zone, occurring during this experiment. Comparison of the values found in this steady-state experiment and those determined by the numerical method described in Section 2.3 are depicted in Figure 2.9. Uncertainty bands of the results of the two methods overlap in both cases. The uncertainty of  $H_{EW}$  determined in the steady-state

experiment was relatively large. The real value of  $H_{GZ}$  seems to be close to the lower end of the uncertainty band computed numerically by the method described in Section 2.3.

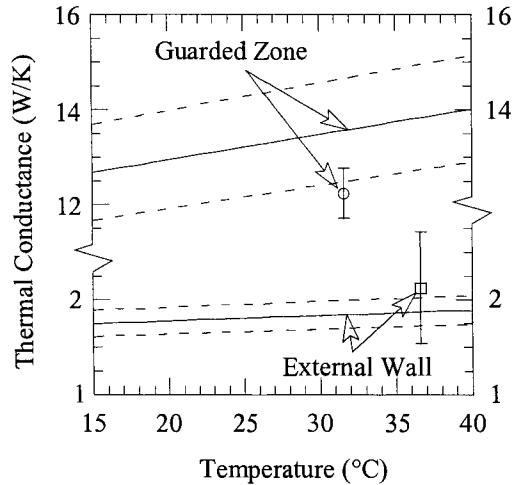


Figure 2.9. Comparison of thermal conductances  $H_{GZ}$  and  $H_{EW}$  as function of temperature found by simulation (curves) and the steady-state experiment (markers).

## 2.7. Transient Experiment for Cell Characterization

The goal of this transient experiment was to verify whether specifications given in Tables 2.2, 2.3, 2.4, 2.5, 2.7 and 2.8 provide an accurate characterization for modeling transient thermal behavior of the cell. This transient experiment was configured in the same way as the steady-state experiment. Constant temperatures of approximately 23°C were maintained in the guarded zone and the external chamber. Fluctuations of less than  $\pm 1$  K occurred during this experiment.

Due to one constantly running recirculation fan inside the cell, there was an internal heat source of  $\sim 77$  W during the entire experiment. After a preconditioning phase, the last 50 h of this phase shown in Figure 2.10, an additional pseudo-random heat source of  $\sim 196$  W was switched on and off in the cell. This source was located inside the recirculation / conditioning apparatus (Figures 2.1 right and 2.2) and can, therefore, be considered as a purely convective heat load. Figure 2.10 also depicts eight air temperatures measured in different locations and

heights in the cell and mean surface temperatures of all six faces as a function of time. During the experiment the measured air temperature stratification was less than 0.5 K.

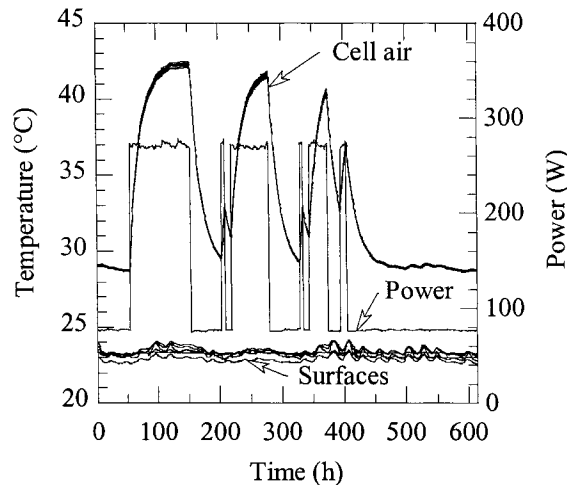


Figure 2.10. Measured pseudo-random internal heating power, cell air temperatures (total eight sensors) and mean surface temperatures of all six outer cell surfaces.

The time constant of the cell was determined by analyzing the temperature response of the cell to the first step increase of heating power and was found to be 17 h.

## 2.8. Simulation of Transient Experiment

Four building energy simulation codes were used to model the transient experiment. These codes included DOE-2.1E, EnergyPlus, ESP-r and HELIOS. When the experiment was modeled, hourly averaged values of six outside cell envelope surface temperatures as boundary conditions and thermal power, including the pseudo-random heat source, were scheduled into the models. For all simulations, the thermophysical cell properties were taken from Tables 2.2, 2.3, 2.4, 2.5, 2.7 and 2.8. As in most building energy simulation codes thermophysical properties cannot be defined as a function of temperature, constant values were therefore employed. The time-and-space averaged cell envelope temperature during the transient experiment of 28.38°C was used to calculate the thermal conductivities of the PU and EPS foam.

HELIOS [18, 25] was developed in the early 1980s and has been recently upgraded. In this code, the thermal bridges were simulated by adding an additional heat transfer surface with a fictitious area to the zone that had the same layer sequence as the walls and the ceiling. This element employed the same thermal conductance as computed for the thermal bridges (Tab. 2.7). Because the thermal bridges were not located at one face, a mean outer surface temperature of all five faces was used. The thermal mass in the room was modeled as a 2 mm metal sheet using thermophysical properties of steel. HELIOS requires a constant value as input for the combined radiative and convective inside heat transfer coefficient. With regard to radiative heat transfer, view factors were calculated using the test cell geometry and assuming grey and diffuse inside cell surfaces. Because the surface temperatures in the cell were nearly the same at any given hour in this experiment, it could be shown that radiation is of very minor importance, and radiative heat transfer coefficient was therefore assumed to be zero. The convective heat transfer coefficients for the walls, ceiling and floor were taken according to ISO/WD 6946 [26].

The development of EnergyPlus began in 1996 by the US Department of Energy (DOE), and is described in detail by Crawley et al. [27]. Thermal bridges were simulated in this code by adding non-radiating surfaces to the back of the space with a constant outer cell surface temperature of 23.22°C, which was the time-averaged outer cell surface temperature during the transient experiment. Because EnergyPlus calculates the radiation heat transfer using view factors and assuming gray and diffuse surfaces, six additional surfaces that faced each other were added to the model. For the other surfaces, a detailed approach was used to compute the convective heat transfer coefficient as a function of temperature difference between surface and cell air [28]. The thermal mass in the cell was modeled in a similar way as in HELIOS.

The original version of DOE-2.1E was released in November 1993 by Lawrence Berkley Laboratories (LBL). To use the outer surface temperatures as boundary conditions, adjacent zones were created with a single zone air conditioner for each test cell surface. The zone temperature was scheduled as the outer cell surface temperature. The inside film resistance for these zones was specified as zero, thus making the adjacent zone temperature and the

outer cell surface temperatures equal. For the inside of the test cell, numerical values of heat transfer coefficients were the same as in HELIOS. The thermal mass inside the cell was again modeled in a similar way as in HELIOS.

ESP-r [17] is an open source program, developed by the Energy Systems Research Unit at the University of Strathclyde with input from many other organizations. It has been developed over a 28 year period. Full details of the underlying theory can be found in [1]. Because ESP-r requires a fully bounded zone, it was not possible to simulate the thermal bridges by simply adding additional surfaces connecting the internal air temperature with the external environment to represent the thermal bridges. Different approaches for modeling edge effects were tried, but the one giving the best agreement with measured data was the use of a “fin” added to the back of the test cell with a total surface area equivalent to that used in the other simulation programs. This allowed the edge losses to be modeled without affecting the convective and radiative heat transfer from the 1-D heat transfer surfaces. Boundary temperatures were modeled by creating additional zones and imposing the measured temperatures. Several different convective regimes can be modeled by ESP-r, but the results presented here were based on the same convective coefficients as used in HELIOS. The thermal mass in the test cell was modeled as steel sheets in the room of appropriate dimensions.

A comparison plot between values of mean cell air temperature computed by all four codes is shown in Figure 2.11.

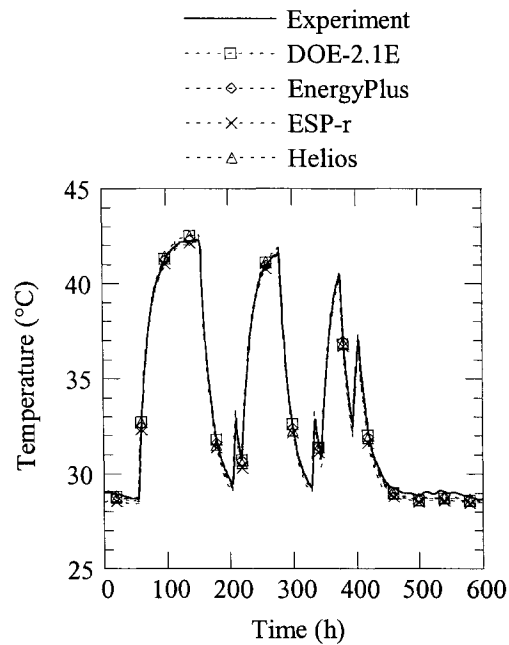


Figure 2.11. Comparison between measured mean cell air temperature and cell air temperature simulated by four different codes.

For HELIOS, discrepancies at the higher and lower temperatures were found that may mainly result from using a constant thermal conductivity (e.g. deviations tended to be smaller at the beginning and the end of the experiment, when a correct average envelope temperature of 26°C was used to calculate the thermophysical properties). Comparisons were made between the measured and predicted surface temperature for HELIOS. HELIOS under-predicted all cell surface temperatures. The wall surface temperatures were about 1 K lower at higher temperatures and 0.5 K lower at lower temperatures. Better agreement was seen at the ceiling where the temperature difference was about 0.3 K lower during the test. The largest discrepancies were seen when predicting the floor temperature; the error at high temperatures was nearly 3 K lower and at low temperatures was about 1 K lower.

For EnergyPlus, there were small discrepancies at the lower and higher temperatures. The deviations at lower temperatures may also be caused by using constant thermal conductivities for the PU and EPS foams. As in HELIOS, EnergyPlus under-predicted all the surface temperatures. The temperature differences for the walls were about 1 K at higher

temperatures and 0.5 K at lower temperatures. The temperature differences for the floor during the experiment remained relatively constant at about 0.6 K. At the ceiling, the temperature differences for the high temperatures and low temperatures were about 0.7 K and 0.3 K, respectively. Large differences between surface temperatures for EnergyPlus and HELIOS were thought to be due to the selection (constant values were used in HELIOS and a temperature dependent algorithm was used in EnergyPlus) of convective heat transfer coefficients and the modeling of radiative heat transfer.

Similar discrepancies seen in the other simulations were also apparent in DOE-2.1E and ESP-r and are thought to come from assuming constant thermophysical and convective heat transfer coefficient properties. For ESP-r, the surface temperatures were lower than measured values, with slightly higher temperature differences compared to those predicted with EnergyPlus. The surface temperature was not an available output in this version of DOE-2; comparisons between measured and predicted surface temperatures therefore could not be made.

## 2.9. Statistical Analysis of Transient Experiment Results

To quantitatively evaluate the measured and simulated air temperatures, a set of statistical and comparative quantities was chosen and will also be used in future work within this IEA project. The arithmetic mean,  $\bar{x}$ , maximum,  $x_{max}$ , and minimum,  $x_{min}$ , values and sample standard deviation,  $s$ , were computed for both the experimental and simulated results for all the 600 hours of the test.

To compare each simulation to the experiment, the differences between the experiment and the respective simulations,  $D_i$  (where  $i$  represents any given hour), were computed. The arithmetic mean,  $\bar{D}$ , maximum,  $D_{max}$ , and minimum,  $D_{min}$ , differences were determined for each simulation. The average absolute difference,  $|\bar{D}|$ , was computed using Equation 6. This quantity was used to show the overall magnitude of the difference between the simulations and the experiment.

$$|\bar{D}| = \frac{1}{n} \sum_{i=1}^n |D_i| \quad (2.6)$$

A root mean squared difference,  $D_{rms}$ , was used to compare the experiment and the simulations shown in Equation 2.7. In this analysis larger deviations in the simulations for the experiment are weighted more heavily; this quantity is essentially a standard deviation where the expected value would be zero.

$$D_{rms} = \sqrt{\frac{1}{n} \sum_{i=1}^n D_i^2} \quad (2.7)$$

For additional comparisons, 95% quantiles,  $D_{95\%}$  using the absolute values of the temperature differences were computed for all simulations. Uncertainties associated with the average temperature calculation,  $MU_i$ , were calculated using propagation of error analysis (sometimes referred to as an uncertainty analysis) shown in Equation 8 to estimate the impact of measurement error in the individual air temperature measurements on the average air temperature calculation. The uncertainty in the individual air temperature measurements,  $u_{ij}$ , (where j represents an individual thermocouple) was taken from Tab. 2.11. For this analysis, all the partial derivatives reduced to  $1/m$  (where m is the number of sensors).

$$MU_i = \left( \sum_{j=1}^m \left( \frac{1}{m} u_{ij} \right)^2 \right)^{1/2} = \frac{u_i}{\sqrt{m}} \quad (2.8)$$

The uncertainties associated with the position of the sensors,  $PU_i$ , were estimated by taking the sample variance for the eight air temperature sensors at each hour. Because the measurement errors were Bayesian in nature, overall 95 % error bounds,  $OU_{i,Experiment}$  for any given hour were estimated using Equation 2.9; the standard deviation for the measurement error was evaluated assuming a uniform distribution [29]. This analysis was done neglecting time-series interactions, which would also impact the overall uncertainty. The mean value,  $\overline{OU}$ , is reported in Table 2.13.

$$OU_{i,Experiment} = 1.96 \left( PU_i + \frac{MU_i^2}{3} \right)^{1/2} \quad (2.9)$$

An uncertainty analysis was performed in ESP-r using the Monte Carlo Analysis (MCA) to quantify overall output uncertainty for the building energy simulation codes due to uncertainties in input parameters. This analysis involves running a large number (100 in this

study) of simulations. In each simulation, all input parameters are perturbed by a random selection of their input values assuming a normal distribution with the standard deviation set as in the above table. The advantage of MCA over a Differential Sensitivity Analysis (DSA), which is often used to quantify uncertainty due to input parameters, is that it does not assume linearity and parameter independence and, therefore, gives a more accurate measure of overall output uncertainty bands.

Ninety-five percent error bounds,  $OU_{i,ESP-r}$ , for each hour were also calculated and the mean quantity,  $\overline{OU}$ , is reported in Table 2.13 under the ESP-r column.

To compare the performance of the individual building energy simulation codes, an uncertainty ratio,  $UR_i$ , was devised to compare hourly differences with experimental and input errors and is shown in Equation 2.10. Mean, maximum and minimum uncertainty ratios are reported in Table 2.13.

$$UR_i = \frac{|D_i|}{OU_{i,Experiment} + OU_{i,ESP-r}} \quad (2.10)$$

If  $UR \leq 1$  then the agreement between the code and the experiment is within the 95% uncertainty bands given by the experimental uncertainty and the uncertainties of the input parameters. A summary of these statistics is shown in Table 2.13. A plot of the input uncertainties, experimental uncertainties, and the summation of these two quantities is shown in Figure 2.12.

Table 2.13. A summary of the descriptive and comparative statistics.

Parameter	Experiment	Helios	EnergyPlus	DOE-2.1e	ESP-r
$\bar{x}$	33.55 °C	33.44 °C	33.41 °C	33.48 °C	33.18 °C
$s$	4.89 K	5.05 K	4.94 K	5.00 K	4.97 K
$x_{max}$	42.3 °C	42.54 °C	42.33 °C	42.6 °C	42.19 °C
$x_{min}$	28.65 °C	28.48 °C	28.57 °C	28.5 °C	28.37 °C
$\bar{D}$	-	0.11 K	0.14 K	0.06 K	0.36 K
$ \bar{D} $	-	0.31 K	0.18 K	0.25 K	0.37 K
$D_{max}$	-	0.8 K	0.72 K	1.22 K	0.94 K
$D_{min}$	-	0.01 K	0.00 K	0.00 K	0.01 K
$D_{rms}$	-	0.34 K	0.24 K	0.33 K	0.42 K
$D_{95\%}$	-	0.62 K	0.50 K	0.73 K	0.72 K
$\overline{OU}$	0.26 K	-	-	-	1.17 K
$\overline{UR}$	-	0.24	0.14	0.2	0.29
$UR_{max}$	-	0.8	0.6	1.16	0.65
$UR_{min}$	-	0.01	0	0	0.01

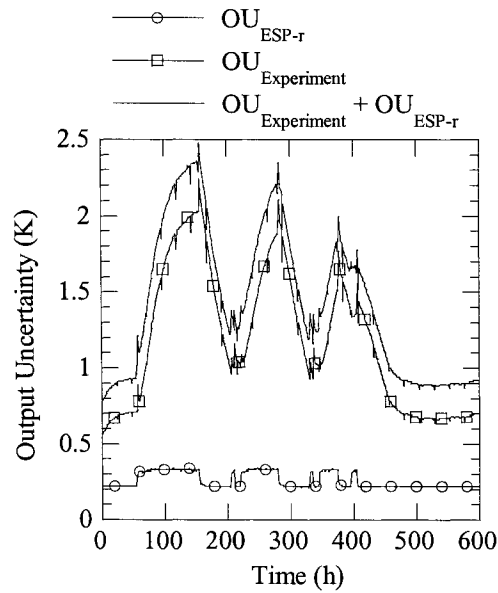


Figure 2.12. Experimental uncertainty, uncertainty of simulation results due to uncertainty in input parameters and total uncertainty.

A DSA using uncertainties provided in Table 2.2, 2.3, 2.4, 2.5, 2.7 and 2.8 revealed that computed cell air temperatures are most sensitive to (i) thermal bridge conductance, (ii) PU

foam thermal conductivity, (iii) cell surface temperatures, (iv) overall cell dimensions, (v) EPS foam thermal conductivity, and (vi) PU foam thickness (ranking with decreasing importance).

## **2.10. Conclusions and Outlook**

If test cells are used for empirical validation of building energy simulation codes, determining the overall thermal cell characteristics is very important. Hence, the thermal properties of the EMPA test cell were thoroughly analyzed both experimentally and numerically. Specifications were used as input parameters for modeling the cell in four building energy simulation codes. Taking into account the uncertainties of experimental data and those of computed cell air temperatures, it seems certain that specifications given in this paper adequately describe the transient thermal behavior of the EMPA test cell. These results are a good foundation to begin investigating solar gains with and without internal and/or external window shadings. The data of the transient experiment is of high quality and can therefore be used by code developers and modelers for validation purposes.

To our knowledge, this study is the most detailed and comprehensive work - in terms of reliability of input data and boundary conditions - in the field of empirical validation of solar gain models in building energy simulation codes using test cells. The additional work in the EMPA test cell in conjunction with the IEA Task 34/Annex 43 project includes a series of six experiments that are initially simple and increase in complexity. These six experiments include: (i) Glazing only, (ii) Glazing with external shading screens, (iii) Glazing with internal shading screens, (iv) Glazing with external Venetian blinds, (v) Glazing with internal Venetian blinds, and, (vi) Window (i.e. glazing with frames). The results from these experiments will be reported in future publications.

In view of the complexity and diversity of real building models and correspondingly huge parameter spaces, it is obvious that absolute validation of building energy simulation codes can never be achieved. However, high-quality empirical data remain absolutely essential for specific model and algorithm validations. Numerous modelers simulated the transient experiment presented in this paper using a number of different codes. These exercises have

confirmed that modeling has to be done very carefully and that the modeler can also be a major source of deviations even for very simple models such as that of a cuboid shape test cell, where detailed information about all the input parameters are available, because thermal bridges and/or convective heat transfer at surfaces can be modeled differently. In addition to validation, the provided data may also be valuable for educational purposes at universities and in engineering training courses.

Note: Data of the transient experiment (Exp. 2) and all subsequent experiments can be downloaded from our website at [www.empa.ch/ieatask34](http://www.empa.ch/ieatask34).

### **Acknowledgements**

We acknowledge with thanks the financial support of the Swiss Federal Office of Energy (BFE) for building and testing the experimental facility (Project 17'166) as well as the funding of EMPA participation in IEA Task 34/43 (Project 100'765). R. Judkoff (NREL, USA) and numerous Task 34 participants provided valuable input for this project. We thank also our colleagues at EMPA, B. Binder, R. Blessing, S. Carl, M. Christenson, C. Tanner and R. Vonbank for their contributions. We would also like to acknowledge the assistance provided by S. Vardeman at Iowa State University for his valuable direction in the statistical analysis.

## References

- [1] Clarke JA. Energy simulation in building design. Oxford: Butterworth Heinemann; 2001.
- [2] Judkoff RD. Validation of Building Energy Analysis Simulation Programs at the Solar Energy Research Institute. *Energy and Buildings* 1988; 10: 221-239.
- [3] Judkoff RD, Neymark J. International Energy Agency Building Simulation Test (BESTEST) and Diagnostic Report, Report TP-472-6231. NREL, Golden CO; 1995.
- [4] Ben-Nakhi AE, Aasem EO. Development and integration of a user friendly validation module within whole building dynamic simulation. *Energy Conversion and Management* 2003; 44 (1): 53-64.
- [5] Jensen SØ. Validation of building energy simulation programs: a methodology. *Energy and Buildings* 1995; 22: 133-144.
- [6] Palomo Del Barrio E, Guyon G. Theoretical basis for empirical model validation using parameters space analysis tools, *Energy and Buildings* 2003; 35 (10): 985-996.
- [7] Palomo Del Barrio E, Guyon G. Application of parameters space analysis tools for empirical model validation, *Energy and Buildings* 2004; 36 (1): 23-33.
- [8] Bloomfield DP. An overview of validation methods for energy and environmental software. *ASHRAE Transactions* 1999; 685-693.
- [9] Manz H, Frank T. Thermal simulation of buildings with double-skin façades. *Energy and Buildings*; accepted November 2004.
- [10] Strachan P. Model Validation using the PASSYS Test Cells. *Building and Environment* 1993; 28: 153-165.
- [11] Simmler H, Binder B, Vonbank R. Heat loads of transparent façade components and shading devices. *EMPA Materials Science & Technology*; 2000 (in German).
- [12] Wouters P, Vandaele L, Voit P, Fisch N. The use of outdoor test cells for thermal and solar building research within the PASSYS project. *Building and Environment* 1993; 28: 107-113.
- [13] Lomas KJ, Eppel H, Martin CJ, Bloomfield DP. Empirical validation of building energy simulation programs. *Energy and Building* 1997; 26: 253-275.
- [14] Moinard S, Guyon G. Empirical Validation of EDF ETNA and GENEC Test-Cell Models. A Report of Task 22, Project A.3 Empirical Validation. International Energy Agency; 1999.
- [15] DOE-2.1E Software (Version-119). Building Energy Simulation Code. Lawrence Berkley Laboratories (LBL), Berkley CA; 2002.
- [16] EnergyPlus Software (Version 1.2.0.029). Building Energy Simulation Code. <http://www.energyplus.gov>; 2004.
- [17] ESP-r Software (Version 9). Building Energy Simulation Code. University of Strathclyde, Glasgow. <http://www.esru.strath.ac.uk>; 1999.

- [18] HELIOS Software (Version 2000). Building Energy Simulation Code. EMPA Materials Science & Technology, Duebendorf, Switzerland; 2004.
- [19] Lomas KJ, Eppel H. Sensitivity analysis techniques for building thermal simulation programs. *Energy and Buildings* 1992; 19: 21-44.
- [20] Macdonald I, Strachan P. Practical application of uncertainty analysis. *Energy and Buildings* 2001; 33: 219-227.
- [21] European Standard EN 410. Glass in building – Determination of luminous and solar characteristics of glazing. European Committee for Standardization, Brussels, Belgium; 1998.
- [22] GLAD Software. EMPA Materials Science & Technology, Duebendorf, Switzerland; 2002.
- [23] TRISCO (Version 10.0w). A computer program to calculate 3D steady-state heat transfer. Physibel, Heirweg 21, Maldegem, Belgium.
- [24] prEN ISO 10077 - 2. Thermal performance of windows, doors and shutters - Calculation of thermal transmittance — Part 2: Numerical method for frames (Final Draft). European Committee for Standardization, Brussels; 2003.
- [25] Frank T. Manual HELIOS 1. NF-Project Report: Radiation Exchange at Building Surfaces. EMPA Materials Science & Technology, Duebendorf, Switzerland; 1982 (in German).
- [26] EN ISO 6945. Building components and building elements — Thermal resistance and thermal transmittance — Calculation methods. Draft Revision. ISO; 2004.
- [27] Crawey DB, Lawrie LK, Winkelmann FC, Buhl WF, Huang YJ, Pedersen CO, Strand RK, Liesen RJ, Fisher DE, Witte MJ, Glazer J. EnergyPlus: creating a new-generation building energy simulation program. *Energy and Buildings* 2001; 33: 319-331.
- [28] EnergyPlus Engineering Document. The Reference to EnergyPlus Calculations. University of Illinois and LBL, 2004.
- [29] Gleser LJ. Assessing Uncertainty in Measurement. *Statistical Science* 1998; 13: 277-290.

### Chapter 3: Empirical validation of models to compute solar irradiance on inclined surfaces for building energy simulation

A paper accepted by Solar Energy

P.G. Loutzenhiser<sup>\*,1,2,a</sup>, H. Manz<sup>1,b</sup>, C. Felmann<sup>3,c</sup>, P.A. Strachan<sup>4,d</sup>, T. Frank<sup>1,e</sup>, G.M. Maxwell<sup>2,f</sup>

\*Corresponding author. Tel.: +41 44 823 43 78; fax: +41 44 823 40 09 *E-mail Address:* peter.loutzenhiser@empa.ch

<sup>1</sup> Swiss Federal Laboratories for Materials Testing and Research (EMPA), Laboratory for Applied Physics in Buildings, CH-8600 Duebendorf, Switzerland

<sup>2</sup> Iowa State University, Department of Mechanical Engineering, Ames, IA 50011 USA

<sup>3</sup> Technical University of Dresden, Institute of Thermodynamics and Building Systems Engineering, D-01062 Dresden, Germany

<sup>4</sup> University of Strathclyde, Department of Mechanical Engineering, ESRU, Glasgow G1 1XJ, Scotland

<sup>a</sup> Wrote the text, performed the comparisons, and simulated the experiments with EnergyPlus and DOE-2.

<sup>b</sup> Supervised the text writing

<sup>c</sup> Provided TRNSYS-TUD results

<sup>d</sup> Provided ESP-r results and wrote the Muneer radiation model section

<sup>e</sup> Provided technical support

<sup>f</sup> Provided technical support

Keywords: Solar radiation models; empirical validation; building energy simulation; Uncertainty analysis

#### Abstract

Accurately computing solar irradiance on external facades is a prerequisite for reliably predicting thermal behavior and cooling loads of buildings. Validation of radiation models and algorithms implemented in building energy simulation codes is an essential endeavor for evaluating solar gain models. Seven solar radiation models implemented in four building energy simulation codes were investigated: 1) isotropic sky, 2) Klucher 3) Hay-Davies, 4) Reindl, 5) Muneer, 6) 1987 Perez, and 7) 1990 Perez models. The building energy simulation codes included: EnergyPlus, DOE-2.1E, TRNSYS-TUD, and ESP-r. Solar

radiation data from two 25 days periods in October and March/April, which included diverse atmospheric conditions and solar altitudes, measured on the EMPA campus in a suburban area in Duebendorf, Switzerland, were used for validation purposes. Two of the three measured components of solar irradiances—global horizontal, diffuse horizontal and direct-normal—were used as inputs for calculating global irradiance on a south-west façade. Numerous statistical parameters were employed to analyze hourly measured and predicted global vertical irradiances. Mean absolute differences for both periods were found to be: 1) 13.7% and 14.9% for the isotropic sky model, 2) 9.1% for the Hay-Davies model, 3) 9.4 % for the Reindl model, 4) 7.6% for the Muneer model, 5) 13.2% for the Klucher model, 6) 9.0%, 7.7%, 6.6%, and 7.1% for the 1990 Perez models, and 7) 7.9% for the 1987 Perez model. Detailed sensitivity analyses using Monte Carlo and Fitted Effects for N-way Factorial analyses were applied to assess how uncertainties in input parameters propagated through one of the building energy simulation codes and impacted the output parameter. The implications of deviations in computed solar irradiances on predicted thermal behavior and cooling load of buildings are discussed.

### **3.1. Introduction**

In the 21<sup>st</sup> century, engineers and architects are relying increasingly on building energy simulation codes to design more energy-efficient buildings. One of the common traits found in new commercial buildings across Europe and the United States is construction with large glazed façades. Accurate modeling of the impact of solar gains through glazing is imperative especially when simulating the thermal behavior of these buildings. Empirical validations of solar gain models are therefore an important and necessary endeavor to provide confidence to developers and modelers that their respective algorithms simulate reality.

A preliminary step in assessing the performance of the solar gain models is to examine and empirically validate models that compute irradiance on exterior surfaces. Various radiation models for inclined surfaces have been proposed—some of which have been implemented in building energy simulation codes—which include isotropic models (Hottel

and Woertz, 1942 as cited by Duffie and Beckman, 1991; Liu and Jordan 1960; Badescu, 2002), anisotropic models (Perez et al., 1990, 1986; Gueymard, 1987; Robledo and Soler, 2002; Li *et al.*, 2002; Olmo et al., 1999; Klucher, 1979; Muneer, 1997) and models for a clear sky (Robler and Soler, 2002). Comparisons and modifications to these models and their applications to specific regions in the world have also been undertaken (Behr, 1997; Remund et. al., 1998).

In all empirical validations, accounting for uncertainties in the experiment and input parameters is paramount. Sensitivity analysis is a well-established technique in computer simulations (Saltelli et al., 2004; 2000; Santer et al., 2003) and has been implemented in building energy simulation codes (Macdonald and Strachan, 2001) and empirical validations (Mara et al., 2001; Aude et al., 2000; Fürbringer and Roulet, 1999; 1995; Lomas and Eppel, 1992) for many years. A thorough methodology for sensitivity analysis for calculations, correlation analysis, principle component analysis, and implementation in the framework of empirical validations in International Energy Agency's (IEA) Task 22 are described by Palomo Del Barrio and Guyon (2003, 2004).

In the context of the IEA Task 34/Annex 43 Subtask C, a series of empirical validations is being performed in a test cell to assess the accuracy of solar gain models in building energy simulation codes with/without shading devices and frames. A thorough description of the proposed suite of experiments, description of the cell, rigorous evaluation of the cell thermophysical properties and thermal bridges, and a methodology for examining results are reported by Manz et al. (2005).

In virtually all building energy simulation applications, solar radiation must be calculated on tilted surfaces. These calculations are driven by solar irradiation inputs or appropriate correction factors and clear sky models. While the horizontal irradiation is virtually always measured, measuring of direct-normal and/or diffuse irradiance adds an additional level of accuracy (Note: In the absence of the latter two parameters, models have to be used to split global irradiation into direct and diffuse).

**Nomenclature**

$A$	anisotropic index, -	$OU$	Overall uncertainty at each hour for the experiment and EnergyPlus for 95% credible limits, $W/m^2$
$B$	radiation distribution index, -	$\overline{OU}$	average overall uncertainty calculated for 95% credible limits, $W/m^2$
$a, b$	terms that account for the incident angle on the sloped surface, -	$s$	sample standard deviation, $W/m^2$
$D$	Hourly difference between experimental and predicted values for a given array, $W/m^2$	$R_b$	variable geometric factor which is a ratio of tilted and horizontal solar beam irradiance
$D_{max}$	maximum difference between experimental and predicted values for a given array, $W/m^2$	$u$	is the individual or combined effects from the n-factorial study, $W/m^2$
$D_{min}$	minimum difference between experimental and predicted values for a given array, $W/m^2$	$TF$	tilt factor, -
$D_{rms}$	root mean squared difference between experimental and predicted values for a given array, $W/m^2$	$UR$	computed uncertainty ratio at each hour for comparing overall performance of a given model, -
$D_{95\%}$	Ninety-fifth percentile of the differences between experimental and predicted values for a given array, $W/m^2$	$\overline{UR}$	average uncertainty ratio, -
$d$	estimated error quantity provided by the manufacturer, units vary	$UR_{max}$	maximum uncertainty ratio, -
$F_1$	circumsolar coefficient, -	$UR_{min}$	minimum uncertainty ratio, -
$F_2$	brightness coefficient, -	$\bar{x}$	arithmetic mean for a given array of data, $W/m^2$
$F'$	clearness index, -	$x_{min}$	minimum quantity for a given array of data, $W/m^2$
$f_{11}, f_{12}, f_{13}, f_{21}, f_{22}, f_{23}$	statistically derived coefficients derived from empirical data for specific locations as a function of $\epsilon$ , -	$x_{max}$	maximum quantity for a given array of data, $W/m^2$
$I_{bn}$	direct-normal solar irradiance, $W/m^2$	<b>Greek Symbols</b>	
$I_h$	global horizontal solar irradiance, $W/m^2$	$\alpha$	absorptance, %
$I_{h,b}$	direct-normal component of solar irradiance on the horizontal surface, $W/m^2$	$\alpha_n$	normal absorptance, %
$I_{h,d}$	global diffuse horizontal solar irradiance, $W/m^2$	$\alpha_s$	solar altitude angle, °
$I_{on}$	direct extraterrestrial normal irradiance, $W/m^2$	$\beta$	surface tilt angle from horizon, °
$I_T$	solar irradiance on the tilted surface, $W/m^2$	$\Delta$	sky condition parameter for brightness, -
$I_{T,b}$	direct-normal (beam) component of solar irradiance on the tilted surface, $W/m^2$	$\epsilon$	sky condition parameter for clearness, -
$I_{T,d}$	diffuse component of solar irradiance on the tilted surface, $W/m^2$	$\phi_b$	building azimuth, °
$I_{T,d,iso}$	isotropic diffuse component of solar irradiance on the tilted surface, $W/m^2$	$\theta$	incident angle of the surface, °
$I_{T,d,cs}$	circumsolar diffuse component of solar irradiance on the tilted surface, $W/m^2$	$\theta_z$	zenith angle, °
$I_{T,d,hb}$	horizontal brightening diffuse component of solar irradiance on the tilted surface, $W/m^2$	$\xi$	input parameter n-way factorial, units vary
$I_{T,d,g}$	reflected ground diffuse component of solar irradiance on the tilted surface, $W/m^2$	$\rho$	hemispherical-hemispherical ground reflectance, -
$i, j$	indices the n-factorial study the represent different levels of input parameters, -	$\sigma$	standard deviation n-way factorial, units vary
$m$	relative optical air mass, -		

The purpose of this work is to validate seven solar radiation models on tilted surfaces that are implemented in widely used building energy simulation codes including: EnergyPlus (2005), DOE-2.1e (2002), ESP-r (2005), and TRNSYS-TUD (2005). The seven models examined include:

- Isotropic sky (Hottel and Woertz, 1942 as cited by Duffie and Beckman, 1991)
- Klucher (1979)
- Hay-Davies (1980)
- Reindl (1990)
- Muneer (1997)
- Perez (1987)
- Perez (1990)

Two of three measured irradiance components were used in each simulation and predictions of global vertical irradiance on a façade oriented 29° West of South were compared with measurements. Particular emphasis was placed on quantifying how uncertainty in the input parameters—direct-normal, diffuse and horizontal global solar irradiance as well as ground reflectance and surface azimuth angle—propagated through radiation calculation algorithms and impacted the global vertical irradiance calculation. Sensitivity analyses were performed using both the Monte Carlo Analysis (MCA) and Fitted Effects for N-way Factorials.

### 3.2. Solar Radiation Models

Total solar irradiance on a tilted surface can be divided into two components: 1) the beam component from direct irradiation of the tilted surface and 2) the diffuse component. The sum of these components equates to the total irradiance on the tilted surface and is described in Equation 3.1.

$$I_T = I_{T,b} + I_{T,d} \quad (3.1)$$

Studies of clear skies have led to a description of the diffuse component being composed of an isotropic diffuse component  $I_{T,d,iso}$  (uniform irradiance from the sky dome),

circumsolar diffuse component  $I_{T,d,cs}$  (resulting from the forward scattering of solar radiation and concentrated in an area close to the sun), horizon brightening component  $I_{T,d,hb}$  (concentrated in a band near the horizon and most pronounced in clear skies), and a reflected component that quantifies the radiation reflected from the ground to the tilted surface  $I_{T,d,g}$ . A more complete version of Equation 3.1 containing all diffuse components is given in Equation 3.2.

$$I_T = I_{T,b} + I_{T,d,iso} + I_{T,d,cs} + I_{T,d,hb} + I_{T,d,g} \quad (3.2)$$

For a given location (longitude, latitude) at any given time of the year (date, time) the solar azimuth and altitude can be determined applying geometrical relationships. Therefore, the incidence angle of beam radiation on a tilted surface can be computed. The models described in this paper all handle beam radiation in this way so the major modeling differences are calculations of the diffuse radiation. An overview of solar radiation modeling used for thermal engineering is provided in numerous textbooks including: Duffie and Beckman (1991) and Muneer (1997). Solar radiation models with different complexity which are widely implemented in building energy simulation codes will be briefly described in the following sections.

### 3.2.1. Isotropic Sky Model

The isotropic sky model (Hottel and Woerz, 1942 as cited by Duffie and Beckman, 1991; Liu and Jordan, 1960) is the simplest model that assumes all diffuse radiation is uniformly distributed over the sky dome and that reflection on the ground is diffuse. For surfaces tilted by an angle  $\beta$  from the horizontal plane, total solar irradiance can be written as shown in Equation 3.3.

$$I_T = I_{h,b}R_b + I_{h,d}\left(\frac{1+\cos\beta}{2}\right) + I_{h,\rho}\left(\frac{1-\cos\beta}{2}\right) \quad (3.3)$$

Circumsolar and horizon brightening parts (Eq. 3.2) are assumed to be zero.

### 3.2.2. Klucher Model

Klucher (1979) found that the isotropic model gave good results for overcast skies but underestimates irradiance under clear and partly overcast conditions, when there is increased intensity near the horizon and in the circumsolar region of the sky. The model developed by Klucher gives the total irradiation on a tilted plane shown in Equation 3.4.

$$I_T = I_{h,b}R_b + I_{h,d}\left(\frac{1 + \cos \beta}{2}\right)\left[I + F' \sin^3\left(\frac{\beta}{2}\right)\right]\left[I + F' \cos^2 \theta \sin^3 \theta_z\right] + I_h \rho \left(\frac{1 - \cos \beta}{2}\right) \quad (3.4)$$

$F'$  is a clearness index given by Equation 3.5.

$$F' = 1 - \left(\frac{I_{h,d}}{I_h}\right)^2 \quad (3.5)$$

The first of the modifying factors in the sky diffuse component takes into account horizon brightening; the second takes into account the effect of circumsolar radiation. Under overcast skies, the clearness index  $F'$  becomes zero and the model reduces to the isotropic model.

### 3.2.3. Hay-Davies Model

In the Hay-Davies model, diffuse radiation from the sky is composed of an isotropic and circumsolar component (Hay and Davies, 1980) and horizon brightening is not taken into account. The anisotropy index  $A$  defined in Equation 3.6 represents the transmittance through atmosphere for beam radiation.

$$A = \frac{I_{bn}}{I_{on}} \quad (3.6)$$

The anisotropy index is used to quantify a portion of the diffuse radiation treated as circumsolar with the remaining portion of diffuse radiation assumed isotropic. The circumsolar component is assumed to be from the sun's position. The total irradiance is then computed in Equation 3.7.

$$I_T = (I_{h,b} + I_{h,d}A)R_b + I_{h,d}(1 - A)\left(\frac{1 + \cos \beta}{2}\right) + I_h \rho \left(\frac{1 - \cos \beta}{2}\right) \quad (3.7)$$

Reflection from the ground is dealt with as for the isotropic model.

### 3.2.4. Reindl Model

In addition to isotropic diffuse and circumsolar radiation, the Reindl model also accounts for horizon brightening (Reindl *et al*, 1990a; Reindl *et al*, 1990b) and employs the same definition of the anisotropy index  $A$  as described in Equation 3.6. The total irradiance on a tilted surface can then be calculated using Equation 3.8.

$$I_T = (I_{h,b} + I_{h,d}A)R_b + I_{h,d}(1-A)\left(\frac{1+\cos\beta}{2}\right)\left[1 + \sqrt{\frac{I_{h,b}}{I_h}} \sin^3\left(\frac{\beta}{2}\right)\right] + I_h\rho\left(\frac{1-\cos\beta}{2}\right) \quad (3.8)$$

Reflection on the ground is again dealt with like the isotropic model. Due to the additional term in Equation 3.8 representing horizon brightening, the Reindl model provides slightly higher diffuse irradiances than the Hay-Davies model.

### 3.2.5. Muneer Model

Muneer's model is summarized by Muneer (1997). In this model the shaded and sunlit surfaces are treated separately, as are overcast and non-overcast conditions of the sunlit surface. A tilt factor  $T_F$  representing the ratio of the slope background diffuse irradiance to the horizontal diffuse irradiance is calculated from Equation 3.9.

$$T_F = \left(\frac{1+\cos\beta}{2}\right) + \frac{2B}{\pi(3+2B)}\left[\sin\beta - \beta\cos\beta - \pi\sin^2\frac{\beta}{2}\right] \quad (3.9)$$

For surfaces in shade and sunlit surfaces under overcast sky conditions, the total radiation on a tilted plane is given in Equation 3.10.

$$I_T = I_{h,b}R_b + I_{h,d}T_F + I_h\rho\left(\frac{1-\cos\beta}{2}\right) \quad (3.10)$$

Sunlit surfaces under non-overcast sky conditions can be calculated using Equation 3.11.

$$I_T = I_{h,b}R_b + I_{h,d}[T_F(1-A) + AR_b] + I_h\rho\left(\frac{1-\cos\beta}{2}\right) \quad (3.11)$$

The values of the radiation distribution index  $B$  depend on the particular sky and azimuthal conditions, and the location. For European locations, Muneer recommends fixed values for the cases of shaded surfaces and sun-facing surfaces under an overcast sky, and a function of the anisotropic index for non-overcast skies.

### 3.2.6. Perez Model

Compared with the other models described, the Perez model is more computationally intensive and represents a more detailed analysis of the isotropic diffuse, circumsolar and horizon brightening radiation by using empirically derived coefficients (Perez *et al*, 1990). The total irradiance on a tilted surface is given by Equation 3.12.

$$I_T = I_{h,b}R_b + I_{h,d} \left[ (1 - F_1) \left( \frac{1 + \cos \beta}{2} \right) + F_1 \frac{a}{b} + F_2 \sin \beta \right] + I_h \rho \left( \frac{1 - \cos \beta}{2} \right) \quad (3.12)$$

Here,  $F_1$  and  $F_2$  are circumsolar and horizon brightness coefficients, respectively, and  $a$  and  $b$  are terms that take the incidence angle of the sun on the considered slope into account. The terms  $a$  and  $b$  are computed using Equations 3.13 and 3.14, respectively.

$$a = \max(0^\circ, \cos \theta) \quad (3.13)$$

$$b = \max(\cos 85^\circ, \cos \theta_z) \quad (3.14)$$

The brightness coefficients  $F_1$  and  $F_2$  depend on the sky condition parameters clearness  $\varepsilon$  and brightness  $\Delta$ . These factors are defined in Equations 3.15 and 3.16, respectively.

$$\varepsilon = \frac{\frac{I_{h,d} + I_n}{I_{h,d}} + 5.535 \cdot 10^{-6} \theta_z^3}{1 + 5.535 \cdot 10^{-6} \theta_z^3} \quad (3.15)$$

$$\Delta = m \frac{I_{h,d}}{I_{on}} \quad (3.16)$$

$F_1$  and  $F_2$  are then computed in Equations 3.17 and 3.18, respectively.

$$F_1 = \max \left[ 0, \left( f_{11} + f_{12} \Delta + \frac{\pi \theta_z}{180} f_{13} \right) \right] \quad (3.17)$$

$$F_2 = f_{21} + f_{22} \Delta + \frac{\pi \theta_z}{180} f_{23} \quad (3.18)$$

The coefficients  $f_{11}$ ,  $f_{12}$ ,  $f_{13}$ ,  $f_{21}$ ,  $f_{22}$ , and  $f_{23}$  were derived based on a statistical analysis of empirical data for specific locations. Two different sets of coefficients were derived for this model (Perez *et al.*, 1990; 1987).

## 2.3. Facility and Measurements

### 2.3.1. Test Site and Setup

The solar radiation measurements were performed on the EMPA campus located in Duebendorf, Switzerland (Longitude 8°36'55" East, Latitude 47°24'12" North at an elevation of 430 m above sea level). Figure 3.1 shows the facility which was designed to measure solar gains of transparent façade components; a detailed description of the facility is provided by Manz *et al.* (2005). For this study, only the pyranometers and the pyr heliometer at the facility were used (Figures 3.1 and 3.2). For the diffuse measurements, a shading disk was mounted in front of the pyranometer with the same solid angle as the pyr heliometer that blocked out the beam irradiance component (Figure 3.2). In order to evaluate the robustness of various radiation models, two 25 day periods were studied to compare predicted irradiance on the tilted façade with measured data that were recorded by a pyranometer mounted on the vertical surface (29° West of South) of the test cell. The dates of the first and second periods were October 2 to October 26, 2004 and March 22 to April 16, 2005, respectively. Both periods include a range of different atmospheric conditions and solar positions. The solar radiation data were acquired for 600 h for each period.

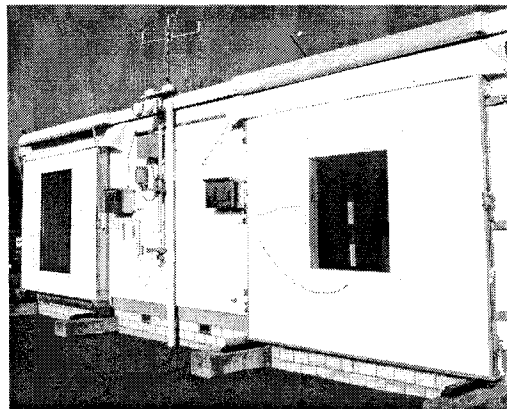


Figure 3.1. Test cells with pyranometers visible in the central part of the picture and green artificial turf installed in front of the test cell.



Figure 3.2. Pyrheliometer for measuring direct-normal and shaded pyranometer for measuring diffuse horizontal solar irradiance are positioned on the roof of the facility.

### 3.3.2. Solar Irradiance

Table 3.1 indicates measured parameters, type of instrument used and accuracies of sensors specified by the manufacturers. To verify the accuracy of the instrumentation, the global horizontal irradiance can be calculated using solar position and direct-normal and horizontal diffuse irradiance shown in Equation 3.19.

$$I_h = I_{b,n} \sin \alpha_s + I_{h,d} \quad (3.19)$$

The differences between global horizontal irradiance measured and computed based on direct-normal (beam) and horizontal diffuse irradiance were analyzed. Using the experimental uncertainties described in Table 3.1, 95% credible limits were calculated for the measured global horizontal irradiance using manufacturer's error and for the computed global irradiance using propagation of error techniques (uncertainty analysis) assuming uniform distributions (Glesner, 1998). From these comparisons, the 95% credible limits from the calculated and measured global horizontal irradiance for Periods 1 and 2 were found

to overlap 78.0% and 70.1% of the time, respectively; these calculations were only performed when the sun was up ( $\alpha_s > 0$ ). Careful examination of these results reveals that the discrepancies occurred when the solar altitude angles and irradiance were small or the solar irradiance were very large (especially for Period 2). Linear regression analysis was used to compare the computed using measured beam and diffuse irradiance and measured global irradiances. The results from this analysis are shown for Periods 1 and 2 in Figures 3.3a and 3.3b, respectively. The differences between calculated and measured quantities are apparent from the slopes of lines. These results reveal a slight systematic under-prediction by roughly 3% of global horizontal irradiance when calculating it from the beam and diffuse horizontal irradiance components.

Table 3.1. Instruments used for measuring solar irradiance.

Parameter	Unit	Type of sensor / measurement	Number of sensors	Accuracy
Solar global irradiance, façade plane (29° W of S)	W/m <sup>2</sup>	Pyranometer (Kipp & Zonen CM 21)	1	± 2% of reading
Solar global horizontal irradiance	W/m <sup>2</sup>	Pyranometer (Kipp & Zonen CM 21)	1	± 2% of reading
Solar diffuse horizontal irradiance	W/m <sup>2</sup>	Pyranometer, mounted under the shading disc of a tracker (Kipp & Zonen CM 11)	1	± 3% of reading
Direct-normal irradiance	W/m <sup>2</sup>	Pyrheliometer, mounted in an automatic sun-following tracker (Kipp & Zonen CH 1)	1	± 2% of reading

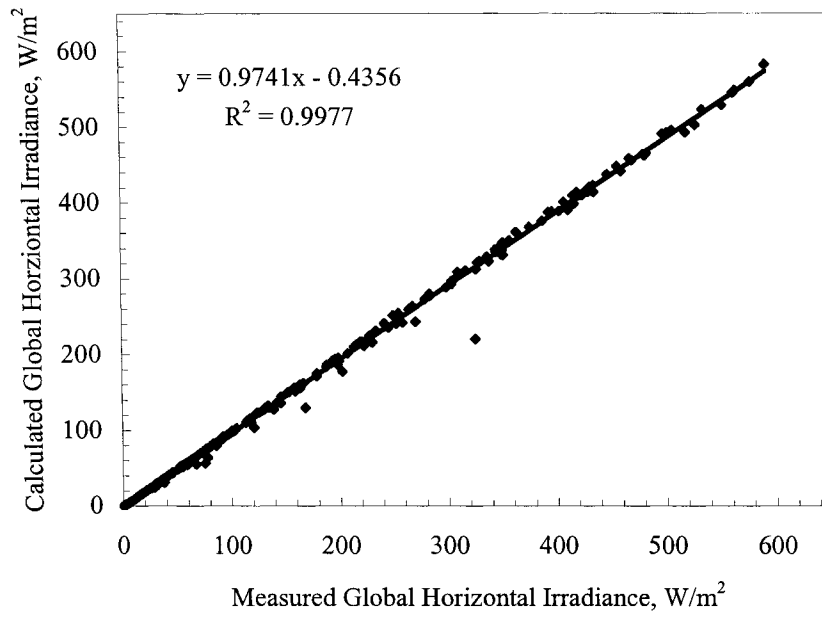


Figure 3.3a. Measured and calculated global horizontal irradiance for Period 1.

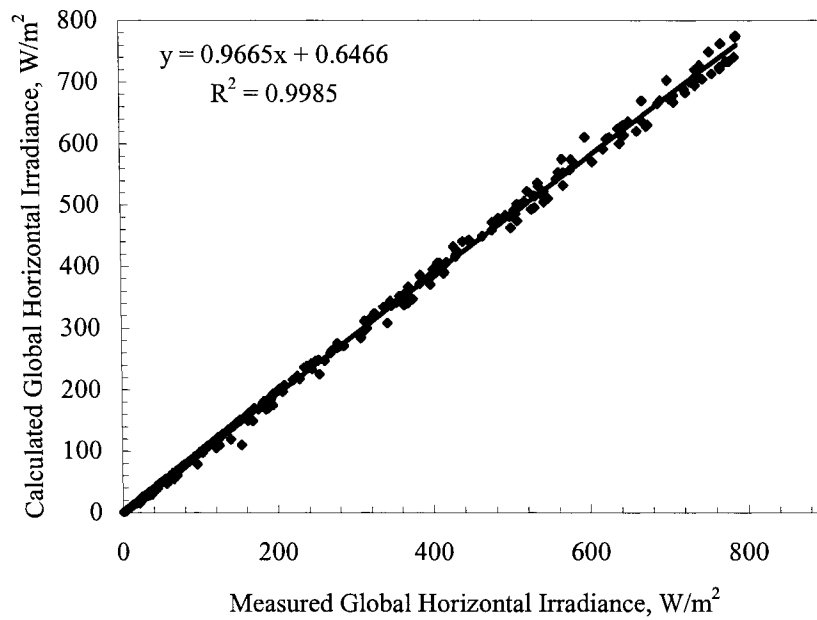


Figure 3.3b. Measured and calculated global horizontal irradiance for Period 2.

### 3.3.3. Ground Reflectance

The importance of accurately quantifying the albedo in lieu of relying on default values is discussed in detail by Ineichen *et al.* (1987). Therefore, in order to have a well-defined and uniform ground reflectance, artificial green turf was installed in front of the test cell to represent a typical outdoor surface (Figure 3.1).

Reflectance of a sample of the artificial turf was measured at almost perpendicular ( $3^\circ$ ) incident radiation in the wavelength interval between 250 nm and 2500 nm using an integrating sphere (Figure 3.4) which could not be employed for angular dependent measurements. Specular components of the reflectance were measured at incident angles of  $20^\circ$ ,  $40^\circ$ , and  $60^\circ$  and were found to be less than 1%; therefore the surface was considered to be a Lambertian surface (Modest, 2003). Integral values for reflectance were determined according to EN 410 (1998) by means of GLAD software (2002). Hemispherical-hemispherical reflectance was then determined at each wavelength assuming an angular dependent surface absorptance as shown in Equation 3.20 (from Duffie and Beckman, 1991).

$$\frac{\alpha(\theta)}{\alpha_n} = \begin{cases} 1 + 2.0345 \times 10^{-3} \theta - 1.99 \times 10^{-4} \theta^2 + 5.324 \times 10^{-6} \theta^3 - 4.799 \times 10^{-8} \theta^4 & 0^\circ \leq \theta \leq 80^\circ \\ -0.064\theta + 5.76 & 80^\circ \leq \theta \leq 90^\circ \end{cases} \quad (3.20)$$

Equation 3.21 was used to calculate the hemispherical-hemispherical reflectance.

$$\rho = 2 \int_{0^\circ}^{90^\circ} (1 - \alpha(\theta)) \sin(\theta) \cos(\theta) d\theta \quad (3.21)$$

This integral was evaluated numerically using the Engineering Equation Solver (Klein, 2004). The computed solar ground reflectance shown in Table 3.2a corresponds well with albedo measurements described by Ineichen *et al.* (1987) in Table 3.2b.

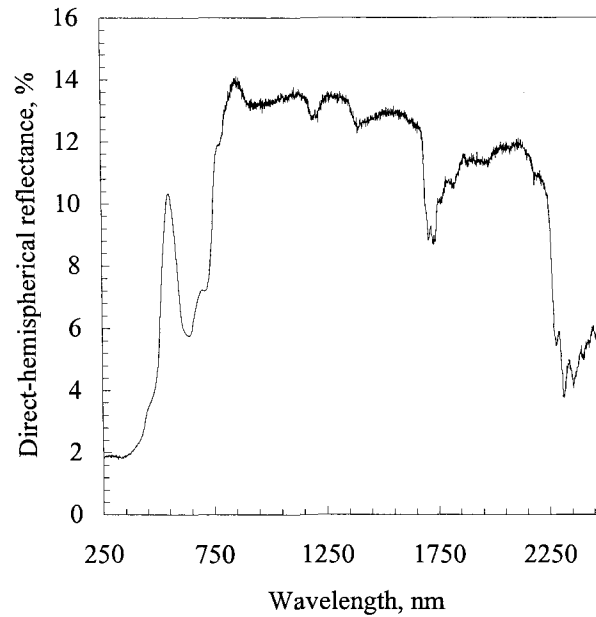


Figure 3.4. Near direct normal-hemispherical reflectance of the artificial turf.

Table 3.2a. Solar ground reflectance.

Parameter	Reflectance, %
Hemispherical-Hemispherical	14.8 ± 0.74
Near Direct Normal-Hemispherical	8.8

Table 3.2b. Ineichen et al. (1987) measurements for determining average albedo coefficients over a three-month period.

Parameter	Reflectance, %				
	Horizontal	North	East	South	West
Horizontal	13.4%	-	-	-	-
Differentiated		14.7%	15.5%	13.8%	14.8%
Morning		13.9%	14.3%	14.3%	15.7%
Afternoon		16.0%	17.2%	13.1%	13.5%

### 3.4. Simulations

The incident (global vertical) irradiance on the exterior façade for all the building energy simulation codes was a function of the solar irradiance and ground reflectance. Four building energy simulation codes, EnergyPlus, DOE-2.1e, ESP-r and TRNSYS-TUD, which encompassed seven different radiation models and were evaluated for both periods.

EnergyPlus version 1.2.2 uses the 1990 Perez model. For the simulation, measured direct-normal and diffuse horizontal solar irradiance were used as inputs in 10 minute and six timesteps each hour. DOE-2.1e also uses a Perez 1990 model to calculate irradiance on a tilted façade (Buhl, 2005) with hourly inputs of direct-normal and global horizontal solar irradiance. Both EnergyPlus and DOE-2.1e assumed a constant annual direct-normal extraterrestrial irradiation term (they do not factor in the elliptical orbit of the earth around the sun). TRNSYS-TUD allows the user to select from four models and various inputs for solar irradiance. For these experiments, the Isotropic, Hay-Davies, Reindl, and Perez 1990 model were used with inputs of measured direct normal and global horizontal irradiance; the inputs to the models were in 1 hour timesteps. The extraterrestrial irradiation was varied to account for the elliptical orbit of the sun for the Perez, Reindl, and Hay-Davies models. ESP-r has the Perez 1990 model as its default, but other models are available to the user, namely the Isotropic, Klucher, Muneer and Perez 1987 models. Measured six minute averaged data were input to the program. The program also takes into account variations in the extraterrestrial radiation in the Perez and Muneer models. It is also possible to use direct normal plus diffuse horizontal irradiances, or global horizontal plus diffuse horizontal irradiances as inputs to ESP-r; for this study, only the direct normal and diffuse horizontal inputs were used.

### **3.5. Sensitivity Analysis**

Sensitivity studies are an important component in thorough empirical validations; such studies were therefore also performed. The uncertainties in the input parameters were taken from information provided by the manufacturers (Table 3.1). The error in the ground reflectance calculation (models and measurements combined) was estimated as 5% (see Table 3.2a) and  $\pm 1^\circ$  for the building azimuth. Uniform distributions were assumed for estimated uncertainties and quantities provided by manufacturers (Glesner, 1998). Although all the codes perform solar angle calculations, uncertainties were not assigned to the test cell locations (latitude, longitude, and elevation). Two types of sensitivity analysis were

performed for this project in EnergyPlus which included Fitted Effects for N-way Factorials and MCA. For these analyses the source code was not modified, but rather a “wrap” was designed to modify input parameters in the weather file and the input file for EnergyPlus in MatLab 7.0 (2004). A Visual Basic program was written to create a command line executable program to run the “WeatherConverter” program and the “RunEplus.bat” program was run from the MatLab program. Output from each run was recorded in output files. A flowchart for this process is depicted in Figure 3.5.

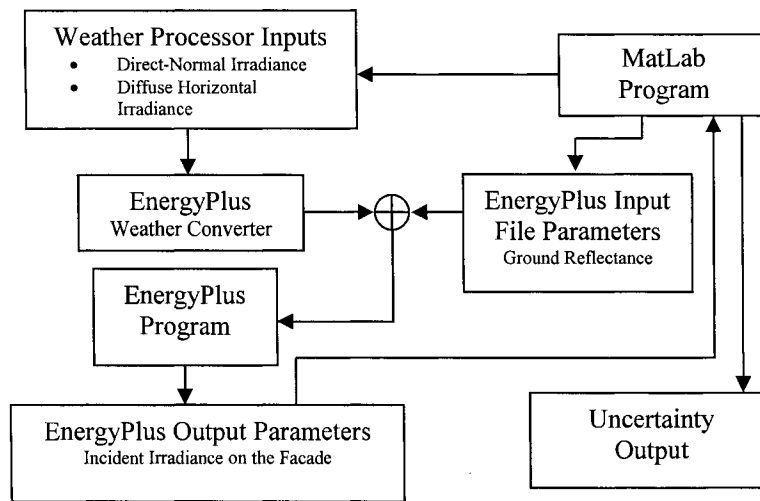


Figure 3.5. Flowchart for the sensitivity studies.

### 3.5.1. Fitted Effects for N-way Factorials

A Fitted Effects N-way Factorial method was used to identify the impact of uncertainties in various parameters on the results (Vardeman and Jobe, 2001). The parameters that were varied for this study included: ground reflectance, building azimuth, direct-normal irradiance, global horizontal irradiance (which was an unused parameter in EnergyPlus), and diffuse irradiance. Therefore, for this study a Fitted Effects for a Three-way Factorial analysis was performed. The first step in this process is to run a one-way factorial shown in Equation 3.22 varying each parameter. This equation is equivalent to the commonly used differential sensitivity analysis.

$$u_i = \phi(\xi_i + \sigma_i) - \phi(\xi_i) \quad (3.22)$$

For uniform distributions, the standard deviation is estimated in Equation 3.23.

$$\sigma_i = \frac{d}{\sqrt{3}} \quad (3.23)$$

The two-way factorials were estimated using Equation 3.24. Additional levels of interactions were considered but were found to be negligible.

$$u_{ij} = \phi(\xi_i + \sigma_i, \xi_j + \sigma_j) - (\phi(\xi_i, \xi_j) + u_i + u_j) \quad i \neq j \quad (3.24)$$

The overall uncertainty was estimated using the quadrature summation shown in Equation 3.25.

$$u = \sqrt{\sum u_i^2 + \sum u_{ij}^2} \quad (3.25)$$

This analysis assumes a localized linear relationship where the function is evaluated. To confirm this assumption, estimates were made by forward differencing ( $\xi_i + \sigma_i$ ) and backward differencing ( $\xi_i - \sigma_i$ ). The individual factorials can also be analyzed to assess their impact. In Table 3.3, the results from this analysis averaged over the entire test ( $\alpha_S > 0$ ) are shown for both forward and backward differencing. Looking at the results from forward and backward difference, the assumed localized linear relationship seems reasonable but may lead to minor discrepancies that are discussed later.

Table 3.3. Average factorial impacts ( $\alpha_S > 0$ ).

Factorial	Period 1		Period 2	
	Forward Differencing, W/m <sup>2</sup>	Backward Differencing, W/m <sup>2</sup>	Forward Differencing, W/m <sup>2</sup>	Backward Differencing, W/m <sup>2</sup>
$I_{bn}$	1.13	-1.10	1.23	-1.31
$I_{h,d}$	1.37	-1.28	1.50	-1.59
$\rho$	0.357	-0.357	0.566	-0.566
$\phi_b$	-0.499	0.500	-0.291	0.303
$I_{bn} \times I_{h,d}$	-0.05596	-0.0831	0.0663	0.0531
$I_{bn} \times \rho$	0.00155	0.00158	0.00308	0.00310
$I_{bn} \times \phi_b$	-0.00464	-0.00464	-0.0027	-0.00274
$I_{h,d} \times \rho$	0.00352	0.00380	0.00514	0.00516
$I_{h,d} \times \phi_b$	-0.00267	-0.00264	-0.00094	-0.000907
$\rho \times \phi_b$	No Interactions	No Interactions	No Interactions	No Interaction
$u$	2.40	2.40	2.85	2.95

### 3.5.2. Monte Carlo Analysis

The Monte Carlo method can be used to analyze the impact of all uncertainties simultaneously by randomly varying the main input parameters and performing multiple evaluations of the output parameter(s). When setting up the analysis, the inputs are modified according to a probability density function (pdf) and, after numerous iterations, the outputs are assumed to be Gaussian (normal) by the Central Limit Theorem. The error is estimated by taking the standard deviation of the multiple evaluations at each time step. MatLab 7.0 can be used to generate random numbers according to Gaussian, uniform, and many other distributions. A comprehensive description and the underlying theory behind the Monte Carlo Method are provided by Fishman (1996) and Rubinstein (1981).

#### 3.5.2.1. Sampling

For this study, Latin hypercube sampling was used. In this method, the range of each input factor is divided into equal probability intervals based on the number of runs of the simulation; one value is then taken from each interval. When applying this method for this study given parameters with non-uniform distributions, the intervals were defined using the cumulative distribution function and then one value was selected from each interval assuming a uniform distribution (again this was simplified in using MatLab because the functions were part of the code). This method of sampling is better when a few components of input dominate the output (Saltelli *et al.*, 2000). For this study, the input parameters were all sampled from a uniform distribution. Previous studies have shown that after 60-80 runs there are only slight gains in accuracy (Fürbringer and Roulet, 1995), but 120 runs were used to determine uncertainty. The average overall uncertainties ( $\alpha_S > 0$ ) for Periods 1 and 2 were  $2.35 \text{ W/m}^2$  and  $2.87 \text{ W/m}^2$ , respectively; the results corresponded well with the fitted effects model. The results at any given time step are discussed in the next section (3.5.3).

### 3.5.2.2. Analysis of Output

It can be shown that despite the pdf's for input parameters, the output parameters will always have a Gaussian distribution (given a large enough sample and sufficient number of inputs) by the Central Limit Theorem; therefore a Lilliefors Test for goodness of fit to normal distribution was used to test significance at 5% (when  $\alpha_S > 0$ ). Using this criterion, 27.5% and 11.5% of the outputs from Periods 1 and 2, respectively, were found not to be normally distributed. A careful study of these results reveals that the majority of these discrepancies occurred when the direct-normal irradiance is small or zero. This may be due to the proportional nature of the uncertainties used for these calculations. At low direct-normal irradiances, the calculation becomes a function of only three inputs rather than four, which could make the pdf for the output parameter more susceptible to the individual pdf's of the input parameters, which for these cases were uniform distributions.

### 3.5.3. Estimated Uncertainties

Estimates for uncertainties were obtained from both Fitted Effects for N-way Factorial and MCA. From these analyses, both methods yield similar results. The only discrepancies for both forward and backward differencing were that fitted effects estimates are sometimes overestimated at several individual timesteps. Careful inspection of the individual responses revealed that there was a significant jump in the two-way direct-normal/diffuse response (sometimes in the order of  $5 \text{ W/m}^2$ ) that corresponds to odd behavior in the one-way responses. The response for the rest of the timesteps was negligible. Additional review showed that these events do not occur during the same timesteps for forward and backward differencing. It was therefore assumed that these discrepancies result from localized nonlinearities at these timesteps.

### 3.6. Results

The computed results from the four simulation codes were compared with the measured global vertical irradiance. Comparisons were made using the nomenclature and methodology proposed by Manz *et al.* (2005). An important term used for comparing the performance of the respective models in the codes is the uncertainty ratio. This term was computed at each hour ( $\alpha_s > 0$ ) and is shown in Equation 3.26. The average, maximum, and minimum quantities are summarized in the statistical analyses for each test. Ninety-five percent credible limits were calculated from the MCA for EnergyPlus and the 95% credible limits for the experiment were estimated assuming a uniform distribution. The credible limits from EnergyPlus were used to calculate the uncertainty ratios for all the models and codes. For the uncertainty ratio, terms less than unity indicate that the codes are validated with 95% credible limits.

$$UR = \frac{|D|}{OU_{Experiment} + OU_{EnergyPlus}} \quad (3.26)$$

Tables 3.4, 3.5, and 3.6 show the results from Periods 1 and 2 and combined periods, respectively. Plots were constructed that depict the global vertical irradiation (hourly averaged irradiance values multiplied by a 1 hr interval) and credible limits. For these plots, the output and 95% credible limits for a given hour of the day were averaged to provide an overview of the performance of each model. Figures 3.6 to 3.8 contain results from Periods 1 and 2 and the combined results.

Table 3.4. Analysis of global vertical façade irradiance in  $W/m^2$  ( $\alpha_S > 0$ ) for Period 1.

	Experiment	EnergyPlus Perez 1990	DOE-2.1e Perez 1990	TRNSYS-TUD Hay-Davies	TRNSYS-TUD Isotropic	TRNSYS-TUD Reindl	TRNSYS-TUD Perez 1990	ESP-r Perez 1990	ESP-r Perez 1987	ESP-r Klucher	ESP-r Isotropic	ESP-r Muneer
$\bar{x}$	176.1	169.7	177.2	165.1	157.8	170.9	169.8	188.2	192.8	174.8	171.9	191.4
$s$	223.8	211.8	218.6	205.1	190.1	209.4	211.1	218.2	220.5	196.9	192.5	226.3
$x_{max}$	856.8	817.8	820.4	801.2	743.2	810.4	796.4	804.7	806.7	743.5	728.8	915.7
$x_{min}$	0.2	0.3	0.0	0.4	0.9	0.4	0.3	0.2	0.1	0.3	0.3	0.2
$\bar{D}$	-	-6.4	1.1	-11.0	-18.3	-5.2	-6.3	1.9	6.6	-11.5	-14.3	5.1
$ \bar{D} $	-	13.7	10.5	18.0	26.2	15.7	11.7	13.3	14.7	24.6	27.8	14.1
$D_{max}$	-	103.5	67.1	108.0	138.9	90.4	73.3	87.7	86.7	139.1	157.7	205.5
$D_{min}$	-	0.0	0.0	0.0	0.0	0.0	0.0	0.0	0.0	0.0	0.0	0.0
$D_{rms}$	-	24.2	17.0	28.9	44.4	24.0	21.0	21.4	22.1	39.1	44.7	24.6
$D_{95\%}$	-	56.4	40.3	71.7	111.2	56.3	57.1	50.9	51.5	96.5	110.7	53.3
$\overline{OU}$	6.90	4.62	-	-	-	-	-	-	-	-	-	-
$UR$	-	1.34	1.34	2.28	4.03	2.29	1.12	1.43	1.69	2.50	2.63	1.54
$UR_{max}$	-	12.42	20.41	20.41	129.05	20.41	10.20	11.22	12.09	17.04	17.04	13.48
$UR_{min}$	-	0.00	0.01	0.00	0.00	0.00	0.00	0.00	0.00	0.01	0.00	0.00
$ \bar{D} /\bar{x}$	-	7.8	5.9	10.2	14.9	8.9	6.7	6.7	6.7	14.8	16.7	7.2
$\bar{D}/\bar{x}$	-	-3.7	0.6	-6.2	-10.4	-3.0	-3.6	-2.7	-0.1	-11.3	-13.4	1.0

Table 3.5. Analysis of global vertical façade irradiance in  $W/m^2$  ( $\alpha_S > 0$ ) for Period 2.

	Experiment	EnergyPlus Perez 1990	DOE-2.1e Perez 1990	TRNSYS-TUD Hay-Davies	TRNSYS-TUD Isotropic	TRNSYS-TUD Reindl	TRNSYS-TUD Perez 1990	ESP-r Perez 1990	ESP-r Perez 1987	ESP-r Klucher	ESP-r Isotropic	ESP-r Muneer
$\bar{x}$	194.5	208.5	210.5	199.7	191.6	207.7	201.4	202.0	206.7	190.1	187.9	202.5
$s$	222.1	226.3	231.3	219.0	201.5	224.1	225.2	222.4	223.8	201.3	197.3	224.2
$x_{max}$	797.1	796.3	828.5	807.8	741.4	820.2	801.7	794.6	799.5	730.4	720.2	801.1
$x_{min}$	0.3	0.3	0.0	0.4	0.4	0.4	0.3	0.2	0.2	0.3	0.3	0.2
$\bar{D}$	-	14.0	16.0	5.2	-2.9	13.2	6.9	7.5	12.2	-4.4	-6.6	8.0
$ \bar{D} $	-	19.4	17.6	16.2	25.0	19.0	12.7	14.6	17.2	23.4	26.4	15.4
$D_{max}$	-	104.0	77.3	59.5	122.6	67.2	63.5	81.3	86.7	113.0	134.9	86.9
$D_{min}$	-	0.0	0.1	0.1	0.1	0.1	0.0	0.0	0.0	0.0	0.0	0.0
$D_{rms}$	-	29.2	26.3	20.9	35.2	24.5	19.2	22.2	24.5	33.6	38.8	24.0
$D_{95\%}$	-	70.1	62.4	42.6	81.7	51.1	46.3	50.9	58.0	79.9	93.2	55.6
$\overline{OU}$	7.62	5.62	-	-	-	-	-	-	-	-	-	-
$UR$	-	2.11	2.12	2.66	3.06	2.99	1.41	1.61	2.00	2.60	2.73	1.64
$UR_{max}$	-	12.83	21.70	20.62	20.63	21.41	11.21	9.70	11.24	14.94	14.94	13.48
$UR_{min}$	-	0.00	0.02	0.01	0.03	0.01	0.01	0.00	0.00	0.01	0.01	0.00
$ \bar{D} /\bar{x}$	-	10.0	9.1	8.3	12.9	9.8	6.5	7.5	8.8	12.0	13.6	7.9
$\bar{D}/\bar{x}$	-	7.2	8.2	2.7	-1.5	6.8	3.5	3.9	6.3	-2.3	-3.4	4.1

Table 3.6. Analysis of global vertical façade irradiance in  $W/m^2$  ( $\alpha_s > 0$ ) for both periods.

	Experiment	EnergyPlus Perez 1990	DOE-2.1e Perez 1990	TRNSYS-TUD Hay-Davies	TRNSYS-TUD Isotropic	TRNSYS-TUD Reindl	TRNSYS-TUD Perez 1990	ESP-r Perez 1990	ESP-r Perez 1987	ESP-r Klucher	ESP-r Isotropic	ESP-r Muneer
$\bar{x}$	186.2	191.0	195.5	184.1	176.3	191.1	187.1	188.2	192.8	174.8	171.9	191.4
$s$	222.9	220.6	226.1	213.4	197.0	218.2	219.4	218.2	220.5	196.9	192.5	226.3
$x_{max}$	856.8	817.8	828.5	807.8	743.2	820.2	801.7	804.7	806.7	743.5	728.8	915.7
$x_{min}$	0.2	0.3	0.0	0.4	0.4	0.4	0.3	0.2	0.1	0.3	0.3	0.2
$\bar{D}$	-	4.8	9.3	-2.1	-9.9	4.9	0.9	1.9	6.6	-11.5	-14.3	5.1
$ \bar{D} $	-	16.8	14.4	17.0	25.6	17.5	12.2	13.3	14.7	24.6	27.8	14.1
$D_{max}$	-	104.0	77.3	108.0	138.9	90.4	73.3	87.7	86.7	139.1	157.7	205.5
$D_{min}$	-	0.0	0.0	0.0	0.0	0.0	0.0	0.0	0.0	0.0	0.0	0.0
$D_{rms}$	-	27.1	22.6	24.8	39.6	24.3	20.0	21.4	22.1	39.1	44.7	24.6
$D_{95\%}$	-	65.7	55.1	54.9	99.4	54.2	48.7	50.9	51.5	96.5	110.7	53.3
$\overline{OU}$	7.30	4.46	-	-	-	-	-	-	-	-	-	-
$UR$	-	1.91	1.90	2.57	3.61	2.77	1.38	1.43	1.69	2.50	2.63	1.54
$UR_{max}$	-	17.62	29.31	28.31	129.05	29.39	15.38	11.22	12.09	17.04	17.04	13.48
$UR_{min}$	-	0.00	0.01	0.00	0.00	0.00	0.00	0.00	0.00	0.01	0.00	0.00
$ \bar{D} /\bar{x}$	-	9.0	7.7	9.1	13.7	9.4	6.6	7.2	7.9	13.2	14.9	7.6
$D/\bar{x}$	-	2.6	5.0	-1.1	-5.3	2.6	0.5	1.0	3.5	-6.2	-7.7	2.8

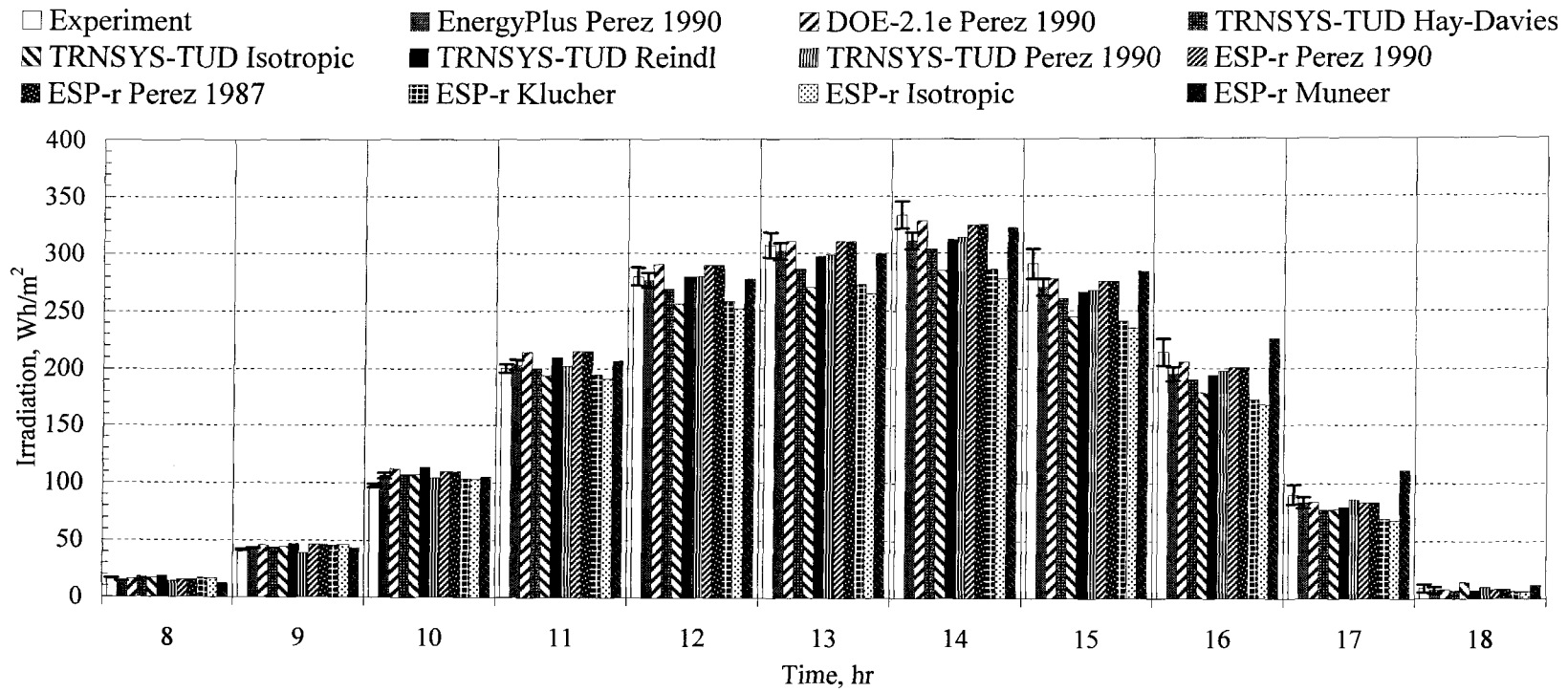


Figure 3.6. Average hourly irradiation comparisons for the vertical façade for Period 1.

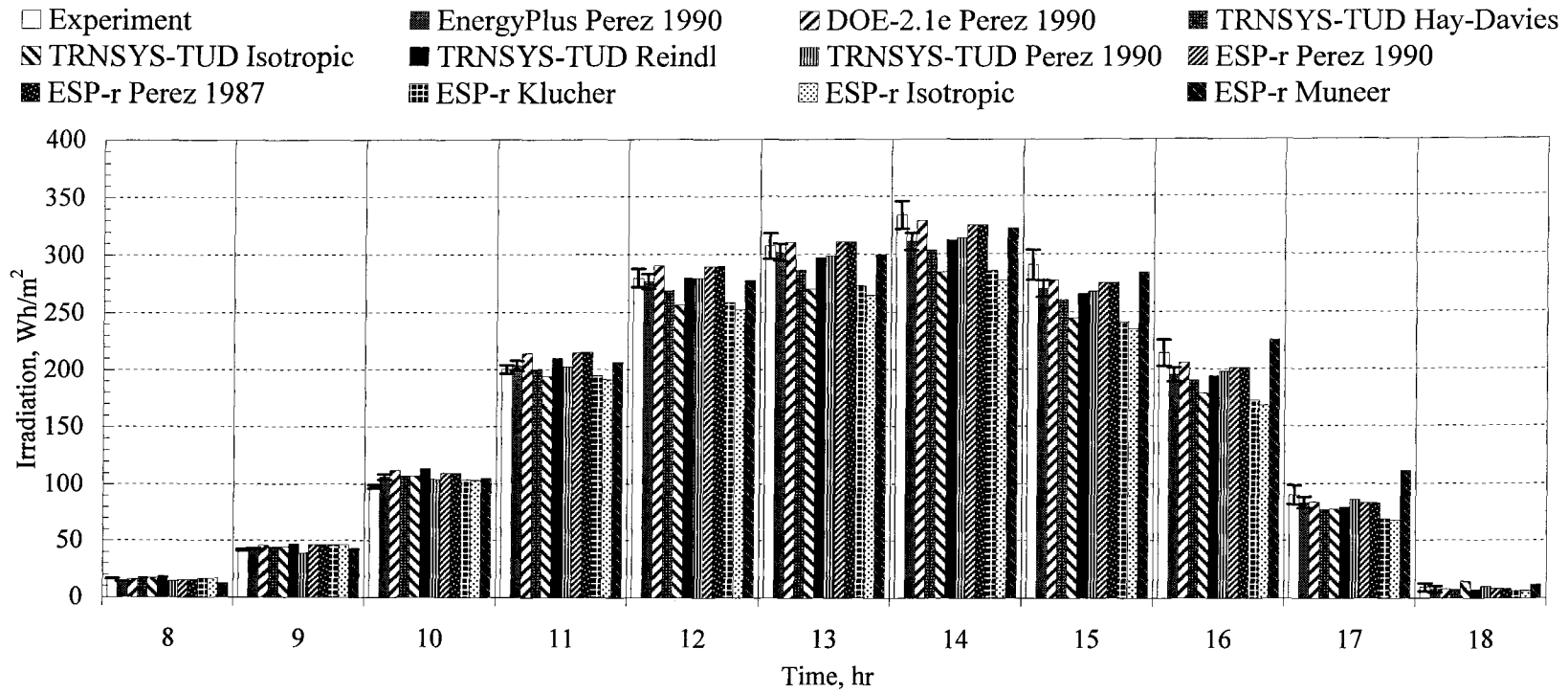


Figure 3.7. Average hourly irradiation comparisons for the vertical façade for Period 2.

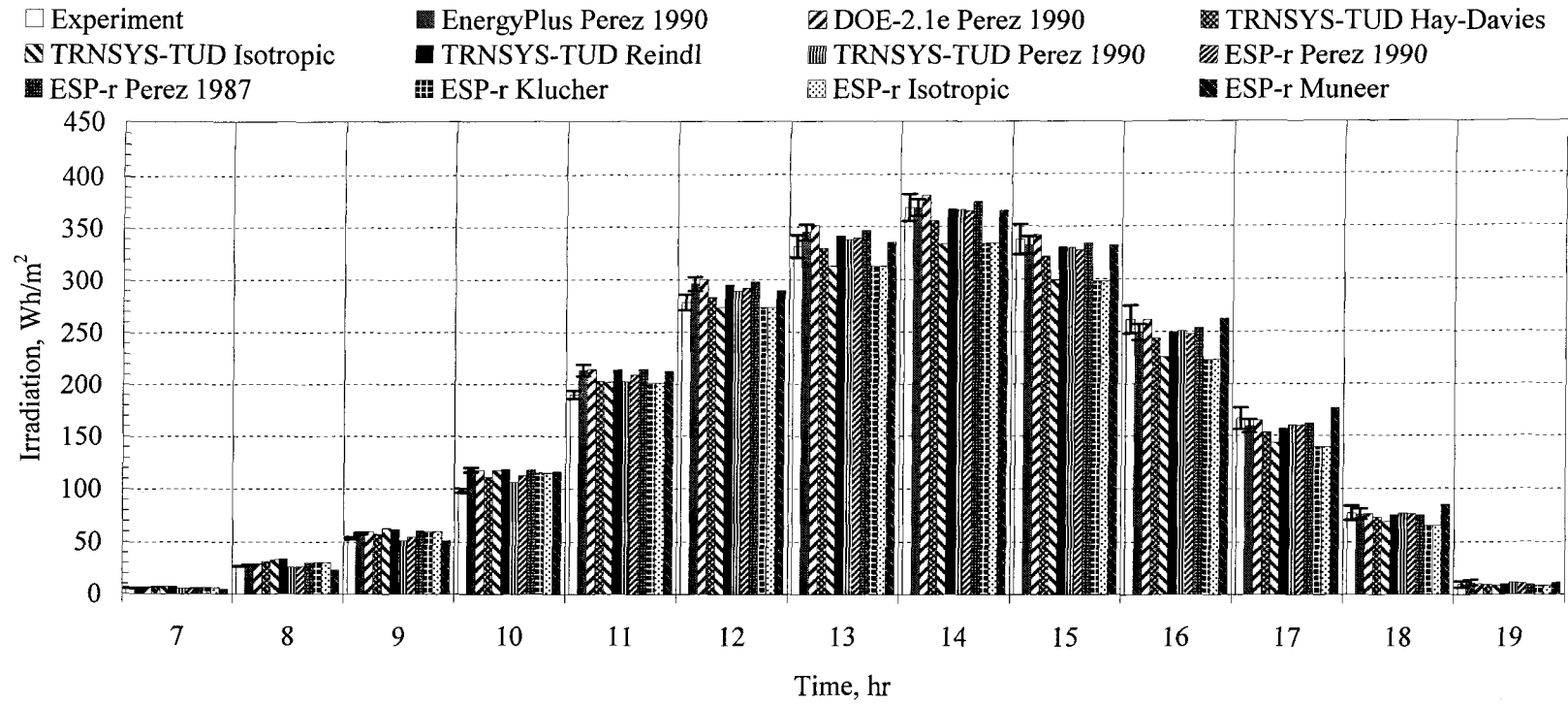


Figure 3.8. Average hourly irradiation comparisons for the vertical façade combining both periods.

### 3.7. Discussion and Conclusions

The accuracy of the individual radiation models and their implementation in each building energy simulation code for both periods can be accurately assessed from the statistical analyses and the plots from the results section. Figure 2.6 shows that in the morning, there are both over and under-prediction of the global vertical irradiance by the models for Period 1; in the afternoon the global vertical irradiance is significantly under-predicted by most models. During Period 2, the majority of the models over-predict the global vertical irradiance for most hours during the day. Combining these results helps to redistribute the hourly over and under-predictions from each model, but it is still clear when comparing the uncertainty ratios that all the models performed better during Period 1.

Using the average uncertainty ratio as a guide, it can be seen that for both periods none of the models were within overlapping 95% credible limits. Strictly speaking, none of the models can therefore be considered to be validated within the defined credible limits ( $\overline{UR} > 1$ ). This is partly due to the proportional nature of the error which at vertical irradiance predictions with small uncertainties leads to large hourly uncertainty ratio calculations and the difficulty in deriving a generic radiation model for every location in the world. This is also shown in Figures 2.6 to 2.8 where there is very little overlap in the experimental and MCA 95% credible limits. However, the average uncertainty ratio can also be used as a guide to rank the overall performance of the tilted radiation models. The Isotropic model performed the worst during these experiments, which can be expected because it was the most simplistic and did not account for the various individual components of diffuse irradiance. While the Reindl and Hay-Davies model accounted for the additional components of diffuse irradiance (both circumsolar and horizontal brightening for the Reindl and circumsolar for the Hay-Davies), the Perez formulation—which relied on empirical data to quantify the diffuse components—provided the best results for this location and wall orientation. Differences between the Perez models in the four building energy simulation codes can be attributed to solar irradiance input parameters (beam, global horizontal, and diffuse), timesteps of the weather measurements, solar angle algorithms, and assumptions made by the programmers (constant direct-normal extraterrestrial radiations for DOE-2.1 e

and EnergyPlus). For both periods, the assumptions made in the TRNSYS-TUD formulation Perez radiation model performed best. Also from these results, the Muneer model performed quite well without the detail used in the Perez models. In fact, the Muneer model performed better than Perez models formulated in EnergyPlus and DOE-2.1e.

The presented results reveal distinct differences between radiation models that will ultimately manifest themselves in the solar gain calculations. Mean absolute deviations in predicting solar irradiance for both time periods were: 1) 13.7% and 14.9% for the isotropic sky model, 2) 9.1% for the Hay-Davies, 3) 9.4 % for the Reindl, 4) 7.6% for the Muneer model, 5) 13.2% for the Klucher, 6) 9.0%, 7.7%, 6.6%, and 7.1% for the 1990 Perez, and 7) 7.9% for the 1987 Perez models. This parameter is a good estimate of the instantaneous error that would impact peak load calculations. The mean deviations calculations for these time periods were: 1) -5.3% and -7.7% for the isotropic sky model, 2) -1.1% for the Hay-Davies, 3) 2.6% for the Reindl, 4) 2.8% for the Muneer model, 5) -6.2% for the Klucher, 6) 2.6%, 5.0%, 0.5%, and 1.0% for the 1990 Perez, and 7) 3.5% for the 1987 Perez models. From this parameter it can be concluded that building energy simulation codes with advanced radiation models are capable of computing total irradiated solar energy on building façades with a high precision for longer time periods (such as months). Hence, the calculations of building energy consumption with high prediction accuracy is achievable even in today's highly glazed buildings, which are largely affected by solar gains. On the other hand, even the most advanced models deviate significantly at specific hourly timesteps (up to roughly  $100 \text{ W/m}^2$ ), which poses serious limitations to accuracy of predictions of cooling power at a specific point in time, the short-time temperature fluctuations in the case of non-air conditioned buildings or the control and/or sizing of HVAC equipment or shading devices. When performing building simulations, engineers must consider much higher uncertainties at specific timesteps.

Additional factors that were not investigated include the number of components of solar irradiance measured at a given weather station (often only global horizontal irradiance is measured and other models are used to compute beam irradiance), locations and densities of the weather stations used as inputs for building simulation codes, and reliability of weather

files used by building energy simulation codes. While this study is somewhat limited to a specific location and time period, it reveals the importance of making proper assessments concerning tilted radiation models and their implementations in building energy simulation codes.

Note: Radiation data and data of all other experiments within the IEA Task 34 project can be downloaded from our website at [www.empa.ch/ieatask34](http://www.empa.ch/ieatask34).

### **Acknowledgements**

We gratefully acknowledge with thanks the financial support from the Swiss Federal Office of Energy (BFE) for building and testing the experimental facility (Project 17'166) as well as the funding for EMPA participation in IEA Task 34/43 (Project 100'765). We would also like to acknowledge Dr. M. Morris from the Iowa State University Statistics Department for his clear direction with regard to formulating the sensitivity analysis and the many contributions from our colleagues R. Blessing, S. Carl, M. Camenzind, and R. Vonbank.

### **References**

- Aude, P., Tabary, L., and Depecker, P., 2000. Sensitivity analysis and validation of buildings' thermal models using adjoint-code method. *Energy and Buildings* 30:267-283
- Badescu, V., 2002. 3D Isotropic approximation for solar diffuse irradiance on tilted surfaces. *Renewable Energy* 26:221-233
- Behr, H.D., 1997. Solar radiation on tilted south oriented surfaces: validation of transfer-models. *Solar Energy* Vol. 61 No.6:399-413
- Buhl, F., 2005. Private email correspondence exchanged on March 9, 2005 with Peter Loutzenhiser at EMPA that contained the radiation model portion of the DOE-2.1E source code, Lawrence Berkley National Laboratories (LBNL)
- DOE-2.1E (Version-119). 2002. Building Energy Simulation Code, (LBL), Berkley, CA, April 9, 2002
- Duffie, J.A., and Beckman, W.A., 1991. *Solar Engineering of Thermal Processes 2<sup>nd</sup> Edition*, John Wiley & Sons, New York, Chichester, Brisbane, Toronto, Singapore
- EnergyPlus Version 1.2.2.030. 2005. Building Energy simulation code, [www.energyplus.gov](http://www.energyplus.gov)
- ESP-r, Version 10.12, 2005, University of Strathclyde, [www.esru.strath.ac.uk](http://www.esru.strath.ac.uk)

- European Standard EN 410, 1998. Glass in building – Determination of luminous and solar characteristics of glazing. European Committee for Standardization, Brussels, Belgium
- Fishman, G.S., 2000. *Monte Carlo: Concepts, Algorithms, and Applications*, Springer, New York, Berlin, Heidelberg
- Fürbringer, J.M. and Roulet, C.A., 1999. Confidence of simulation results: put a sensitivity analysis module in you MODEL: The IEA-ECBCS Annex 23 experience of model evaluation. *Energy and Buildings* 30:61-71
- Fürbringer, J.M., and Roulet, C.A., 1995, Comparison and Combination of Factorial and Monte-Carlo Design in Sensitivity Analysis. *Building and Environment* Vol. 30 No.4:505-519
- GLAD Software, 2002. Swiss Federal Laboratories for Material Testing and Research (EMPA), Duebendorf, Switzerland
- Glesner, J.L., 1998. Assessing Uncertainty in Measurement. *Statistical Science* Vol. 13 No.3:277-290
- Gueymard, C., 1987. An anisotropic solar irradiance model for tilted surfaces and its comparison with selected engineering algorithms. *Solar Energy* Vol.38 No.5:367-386
- Hay, J.E. and Davies, J.A., 1980. Calculations of the solar radiation incident on an inclined surface, Proc. of First Canadian Solar Radiation Data Workshop (Eds: J.E. Hay and T.K. Won), Ministry of Supply and Services Canada, 59
- Hottel, H.C. and Woertz, B.B., 1942. Evaluation of flat-plate solar heat collector. *Trans. ASME* 64, 91
- Ineichen, P., Perez, R., and Seals, R., 1987. The importance of correct albedo determination for adequately modeling energy received by a tilted surface. *Solar Energy* Vol.39 No.4:301-305
- Klein, S.A., 2004. Engineering Equation Solver (EES) Software, Department of Mechanical Engineering, University of Wisconsin—Madison
- Klucher, T.M., 1979. Evaluation of models to predict insolation on tilted surfaces. *Solar Energy* Vol.23 No.2:111-114
- Li, D.H.W., Lam, J.C., Lau, and Chris C.S., 2002. A new approach for predicting vertical global solar irradiance. *Renewable Energy* 25:591-606
- Liu, B.Y.H. and Jordan, R.C. 1960. The interrelationship and characteristic distribution of direct, diffuse, and total solar radiation, *Solar Energy* Vol. 4 No.3:1-19
- Lomas, K.J. and Eppel, H., 1992. Sensivity analysis techniques for building thermal simulation programs. *Energy and Buildings* 19:21-44
- Macdonald, I. and Strachan, P., 2001. Practical applications of uncertainty analysis. *Energy and Buildings*, 33:219-227
- Mara, T.A., Garde, F., Boyer, H., and Mamode, M., 2001. Empirical validation of the thermal model of a passive solar test cell. *Energy and Buildings* 33:589-599
- MatLab Version 7.0.0.19920, 2004. The MathWorks Inc.

- Manz, H., Loutzenhiser, P., Frank, T., Strachan, P.A., Bindi, R., and Maxwell, G. (Accepted for publication in *Building and Environment* on July 12, 2005) Series of experiments for empirical validation of solar gain modeling in building energy simulation codes – Experimental setup, test cell characterization, specifications and uncertainty analysis.
- Modest, M., 2003. *Radiative Heat Transfer 2<sup>nd</sup> Edition*, Academic Press, Amsterdam.
- Muneer, T., 1997. *Solar radiation and daylight models for the energy efficient design of buildings*, Architectural Press, Oxford.
- Olmo, F.J., Vida, J., Castro-Diez, Y., and Alados-Arboledas, L., 1999. Prediction of global irradiance on inclined surfaces from horizontal global irradiance. *Energy* 24:689-704
- Palomo del Barrio, E., and Guyon, G., 2004. Application of parameters space analysis tools for empirical model validation. *Energy and Buildings* 36:23-33
- Palomo del Barrio, E., and Guyon, G., 2003. Theoretical basis for empirical model validation using parameter space analysis tools. *Energy and Buildings* 35:985-996
- Perez, R., Seals, R., Ineichen, P., Stewart, R., and Menicucci D., 1987. A new simplified version of the Perez diffuse irradiance model for tilted surfaces. *Solar Energy* Vol.39 No.3:221-232
- Perez, R., Ineichen, P., Seals, R., Michalsky, J., and Stewart, R., 1990. Modeling daylight availability and irradiance components from direct and global irradiance. *Solar Energy* Vol.44 No.5:271-289
- Reindl, D.T., Beckmann, and W.A., Duffie, J.A. 1990a. Diffuse fraction correlations. *Solar Energy* Vol.45 No. 1:1-7
- Reindl, D.T., Beckmann, and W.A., Duffie, J.A. 1990b. Evaluation of hourly tilted surface radiation models. *Solar Energy* Vol.45 No.1:9-17
- Remund, J., Salvisberg, E., and Kunz, S., 1998. On the generation of hourly shortwave radiation data on tilted surfaces. *Solar Energy* Vol.62 No.5:331-334
- Robledo, L. and Soler, A., 2002. A simple clear skies model for the luminous efficacy of diffuse solar radiation on inclined surfaces. *Renewable Energy* 26:169-176
- Rubinstein, R.Y., 1981. *Simulation and the Monte Carlo Method*, John Wiley & Sons, New York, Chichester, Brisbane, Toronto
- Saltelli, A., Tarantola, S., Campolongo, F., and Ratto, M., 2004. *Sensitivity Analysis in Practice: A Guide to Assessing Scientific Models*, John Wiley & Sons, LTD
- Saltelli, A., Chan, K., and Scott, E.M., 2000. *Sensitivity Analysis*, John Wiley & Sons, LTD, Chichester, New York, Weinheim, Brisbane, Singapore, Toronto
- Santner, T.J., Williams, B.J., and Notz, W.I., 2003. *The Design and Analysis of Computer Experiments*, Springer, New York, Berlin, Heidelberg
- TRNSYS-TUD, 2005, Technical University of Dresden research code based on the frame of TRNSYS 14.2, Solar Energy Laboratory, University of Wisconsin-Madison, Madison, WI, 1996
- Vardeman, S.B., and Jobe, J.M., 2001. *Data Collection and Analysis*, Duxbury Thomson Learning, Australia, Canada, Mexico, Singapore, Spain, United Kingdom, United States

## **Chapter 4: An Empirical Validation of Solar Gain Models Found in Building Energy Simulation Programs**

A paper accepted by HVAC&R Research

Peter G. Loutzenhiser<sup>a</sup>  
Student Member ASHRAE  
Swiss Federal Laboratories for Material Testing and Research (EMPA)  
Laboratory for Applied Physics in Buildings  
Ueberlandstrasse 129  
CH-8600 Duebendorf  
Switzerland

Telephone: +41 44 823 43 78  
Fax: +41 44 823 40 09  
Email: [peter.loutzenhiser@empa.ch](mailto:peter.loutzenhiser@empa.ch)

Peter Loutzenhiser currently works at the Swiss Federal Laboratories for Material Testing and Research (EMPA) in the Laboratory for Applied Physics in Buildings in Duebendorf, Switzerland and is a PhD Candidate in the Mechanical Engineering Department at Iowa State University in Ames, Iowa USA.

Heinrich Manz<sup>b</sup>, PhD  
Swiss Federal Laboratories for Material Testing and Research (EMPA)  
Laboratory for Applied Physics in Buildings  
Ueberlandstrasse 129  
CH-8600 Duebendorf  
Switzerland

Heinrich Manz is a senior scientist at the Swiss Federal Laboratories for Material Testing and Research (EMPA) working in the Laboratory for Applied Physics in Buildings in Duebendorf, Switzerland.

Paul A. Strachan<sup>c</sup>, PhD  
University of Strathclyde  
Department of Mechanical Engineering  
Glasgow G1 9 1XJ  
Scotland

Paul Strachan is a senior lecturer of Mechanical Engineering at the University of Stathclyde in Glasgow, Scotland.

Clemens Felsmann<sup>d</sup>, PhD  
Requested ASHRAE Membership  
Technical University of Dresden  
Department of Mechanical Engineering  
Institute of Thermodynamics and Building Systems 11 Engineering  
D-01062 Dresden  
Germany

Clemens Felsmann is a member of the scientific staff in the Mechanical Engineering Department at the Technical University of Dresden in Dresden, Germany.

Thomas Frank<sup>e</sup>  
Associate Member ASHRAE  
Swiss Federal Laboratories for Material Testing and Research (EMPA)  
Laboratory for Applied Physics in Buildings  
Ueberlandstrasse 129  
CH-8600 Duebendorf  
Switzerland

Thomas Frank is the department head of the Laboratory for Applied Physics in Buildings at the Swiss Federal Laboratories for Material Testing and Research (EMPA) in Duebendorf, Switzerland.

Gregory M. Maxwell<sup>f</sup>, PhD  
Member ASHRAE  
Iowa State University  
H.M. Black Engineering  
Ames, IA 50011  
USA

Gregory Maxwell is an associate professor of Mechanical Engineering at Iowa State University in Ames, Iowa USA.

Peter Oelhafen<sup>g</sup>, PhD  
University of Basel  
Institute of Physics  
Klingelbergstrasse 82  
CH-4056 Basel  
Switzerland

Peter Oelhafen is a Professor of Physics at the University of Basel in Basel, Switzerland.

- <sup>a</sup> Wrote the majority of the text, simulated the experiment with EnergyPlus and DOE-2, and performed the linear transmittance calculations
- <sup>b</sup> Supervised the writing of the text
- <sup>c</sup> Provided ESP-r results and wrote the ESP-r modeling section
- <sup>d</sup> Provided TRNSYS-TUD results and wrote the TRNSYS-TUD modeling section
- <sup>e</sup> Provided technical support
- <sup>f</sup> Provided technical support
- <sup>g</sup> Performed the angular dependent measurements for the glazing unit

## **Abstract**

Empirical validation of building energy simulation tools is an important component in assessing the reliability of the software. An experiment performed in conjunction with the International Energy Agency's (IEA) Task 34/Annex 43 was used to assess the performance of four building energy simulation codes used to model an outdoor test cell with a glazing unit. The experiment was run for a 20 day period during October 2004, and experimental cooling powers were compared with predictions from: 1) EnergyPlus, 2) DOE-2.1E, 3) TRNSYS-TUD, and 4) ESP-r. Detailed code inputs for optical and thermophysical properties as well as the impact of thermal bridges were quantified through experiments and simulations; numerous statistical parameters and sensitivity analyses were implemented to facilitate a thorough comparison of predicted and experimental cooling powers. The mean absolute differences for all four codes were: 1) 1.9% for EnergyPlus, 2) -3.6% for DOE-2.1E, 3) -6.2% for TRNSYS-TUD, and 4) 3.1% for ESP-r. The implications of various modeling procedures as well as a detailed discussion of the results are provided, specifically concerning the sensitivity of the code cooling power predictions to the selection of convective heat transfer coefficients and algorithms.

## **4.1. Introduction**

Commercial buildings with highly glazed facades are becoming increasingly popular in the United States and Europe. Many of these buildings are now being designed and evaluated for energy performance by engineers and architects using building energy

simulation programs. Most building energy simulation programs utilize the integral approach by which all relevant energy transport paths, including energy flow through windows, are simultaneously processed; this makes building energy simulation codes powerful tools that are becoming an important component in the design of energy efficient buildings. An overview of theory and application of building energy simulation programs is provided by Clarke (2001).

Code validation is a vital part of code development and a prerequisite for successful application of building energy simulation tools. Judkoff (1988) provides an overview of validation techniques and identifies three categories of validations: 1) analytical (comparisons of simulation results with an analytical solution), 2) comparative (code-to-code comparisons), and 3) empirical (comparisons of simulation results with experimental measurements). Analytical and comparative validations are both relatively inexpensive to perform and are useful for code diagnostics; empirical validation is a necessary component for comparing the overall accuracy of codes with reality. Unfortunately, empirical validation is also the most time-consuming and expensive approach and has, therefore, been performed only to a very limited extent.

For highly glazed buildings, it is particularly important to accurately model the energy performance of transparent facade and roof areas when predicting the thermal behavior of buildings, especially in the summer when sizing air-conditioning equipment or calculating the peak free floating temperature. Energy flows through glazing and shading devices are determined by optical, thermodynamic, and fluid-dynamic processes (Manz and Frank, 2005). Because of the complexities associated with these systems, no analytical solutions are available for such validations. Code-to-code comparisons are insufficient because it is not obvious which model(s), if any, is (are) correct. Therefore the only suitable approach is to perform high-quality experiments to evaluate the solar gain algorithms contained in building energy simulation codes and subsidiary software; such exercises are very important when assessing the reliability of the outputs and provide confidence to both code developers and users that their respective codes simulate reality.

Empirical validation of building energy simulation codes can be done using test rooms in a real building (Maxwell et al., 2003) and test cells. Test cells represent an intermediate between a real building and an experiment in the laboratory. Test cells also have a significant advantage in that the initial and particularly important boundary conditions can be controlled to a much higher degree than in real buildings while still maintaining dimensions and thermophysical properties that are very close to those found in rooms of real buildings. Empirical validations using test cells were performed in conjunction with the International Energy Agency's (IEA) Annex 21/Task 8 (Lomas et al., 1997), the PASSYS project (Jensen, 1995; Strachan, 1993; Wouters et al., 1993), and IEA Task 22 (Moinard and Guyon, 1999). Precise determination of initial and boundary conditions during the experiment is of primary importance for work in empirical validations. Moinard and Guyon (1999) have also shown that determining the overall thermal cell characteristics is also crucial.

An empirical validation using a test cell was pursued using a test facility located on the Swiss Federal Laboratories for Material Testing and Research (EMPA) campus in Duebendorf, Switzerland and was done in conjunction with the IEA Task 34/Annex 43 Subtask C; a series of experiments was performed to assess the accuracy of building energy simulation codes when evaluating solar gains with glazing with and without shading. Compared with previous empirical validation projects using test cells without guarded zones, such as the PASSYS cells, the guarded zones of the EMPA test cells offered much better control of boundary conditions. The data acquired meet all nine criteria described by Lomas et al. (1997) for high-quality data sets.

The focus of this paper is to evaluate the solar gains through an insulating glazing unit with wavelength selective properties (solar protection glazing) mounted in the exterior wall of a test cell by analyzing the cooling/heating load of the cell. The EMPA facility comprises two test cells, one of which was used for the experiment described in this paper. Preliminary work to characterize the cell was performed by Manz et al. (2005). Additional work in the context of evaluating irradiance models on tilted surfaces commonly used in building energy simulation codes on the exterior surface of the building using a solar irradiance data set for the same time period and location was carried out by Loutzenhiser et al. (2005). Detailed

information about the optical properties of the glazing as well as rigorous analysis coupling calorimetric measurements and two-dimensional heat transfer simulation results were used as inputs into four building energy simulation codes. Sensitivity analyses were used to quantify the impact of input uncertainties on output parameters. These analyses were coupled with thorough evaluations of experimental and measurement uncertainties in the experiment.

#### 4.2. Experiment

After a preconditioning phase of five days (test cell time constant 17 h), the experiment was run for a 20 day period from October 7 to October 26, 2004 and was configured to maintain a near-constant cell air temperature by adjusting heating and cooling power (because of the internal loads only cooling power was required). During this period, the cell was subjected to diverse atmospheric conditions. Air temperatures in the test cell were measured using 18 double-shielded thermocouples. Conditioned air was supplied to the cell at low speed near the floor through two large textile ducts. Air was extracted close to the external wall through two metallic ducts located near the ceiling to minimize temperature stratification as shown on the right in Figure 4.1.

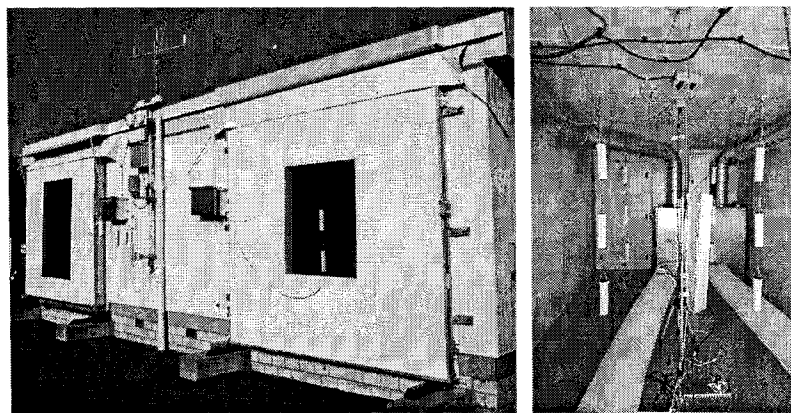


Figure 4.1. The external view (left) of the test facility shows sensors for weather data acquisition between the two test frames with glazing; the internal view (right) of the test cell shows supply (bottom) and extract (top) ducts.

#### **4.2.1. Facility**

The EMPA outdoor test facility depicted on the left in Figure 4.1 is located in a suburban area on the Swiss Plateau in Duebendorf, Switzerland (8.6°E, 47.4°N; 430 m ASL). The orientation of the test facade is 29° west of south. Thorough documentation of the cell, including descriptions of geometry, ventilation, air conditioning and guarded zone concepts, tables listing all relevant thermophysical cell properties, and a detailed thermal bridge analysis is provided by Manz et al. (2005). Information about type, location, and measurement uncertainty of sensors for acquiring weather data and measuring test cell parameters is provided in the same reference.

#### **4.2.2. Glazing Unit**

An insulating glazing unit with wavelength selective properties was employed. The outer pane had a solar protection / low-e coating and the inner pane was clear float glass; the cavity was filled with argon. The pane and glazing properties were determined through optical and thermal measurements.

##### **4.2.2.1. Spectral Optical Properties and Emittances**

Optical properties of the glazing and the individual glass panes were measured in the wavelength interval between 250 nm to 2500 nm at near normal (3°) incident angles using a spectrometer. Figure 4.2 shows transmittances and reflectances (front and back) as a function of wavelength for the whole glazing. Spectral transmittances and reflectances for the individual panes were measured in the same wavelength interval and integral solar properties were computed according to European Standard EN 410 (1998) using Glad Software (2002). The hemispherical emittances of all the surfaces for both panes of glass were measured using an emissometer based on a calorimetric method. These optical quantities are shown in Table 4.1.

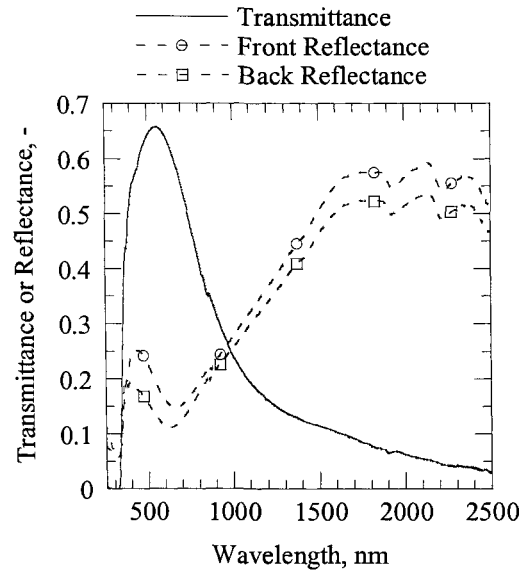


Figure 4.2. Measured transmittance and reflectances of solar protection glazing unit as a function of wavelength.

Table 4.1. Properties of individual panes of glass.

Parameter	Outer Pane	Inner Pane
Normal Solar Transmittance	0.509	0.808
Normal Solar Exterior Reflectance	0.285	0.076
Normal Solar Interior Reflectance	0.296	0.076
Outer Hemispherical Emittance	0.894	0.878
Inner Hemispherical Emittance	0.097	0.887

#### 4.2.2.2. Angular Dependent Optical Properties

To calculate angular dependent properties, measured near normal spectral transmittances and reflectances were imported into Optics5 (documented by Rubin et al., 1998) for each pane of glass, because Window 5.2 (2005) required an Optics5 output of integral properties to compute angular dependent transmittances, reflectances, absorptances, and solar heat gain coefficients SHGC (or total solar energy transmittance). The algorithms employed for calculations of angular dependence of optical properties were developed by Furler (1991). A

summary of how to calculate the SHGC is provided by ASHRAE (2001). General discussions and evaluations of various models used to compute angular dependent optical properties are given by Karlsson et al. (2001), Roos et al. (2000), and Rubin et al. (1999).

At the University of Basel in Switzerland, an experimental setup to measure wavelength and angular dependent direct-direct transmittances and reflectances of glazing was constructed (Reber et al., 2005). In this setup, the radiation source consisted of numerous lamps positioned in a cuboid-shape casing with highly reflective interior surfaces that generate a homogeneously radiating area. The glazing sample was mounted on a rotatable disk and may have dimensions larger than 1.0 m. Behind the glazing sample, a wavelength and direction selective sensor measured radiation. The accuracy of the experimental setup was successfully tested for several applications. Measurements for incident angles up to  $75^\circ$  in the wavelength interval from 300 nm to 1650 nm were run.

Angular dependent optical properties were calculated based on measured normal properties using Window 5.2 software. Comparisons between the calculated and measured optical properties at different angles of incident are shown in Figure 4.3 where each marker represents a measurement. Because the entire solar spectrum was not measured, integral visible optical properties were computed for comparisons. Calculations for the transmittances and back reflectances corresponded within 0.02 with measured quantities, and within 0.03 for the front reflectances.

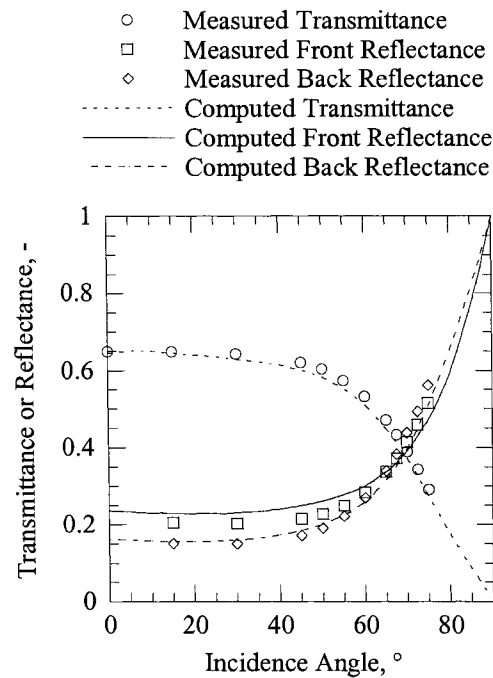


Figure 4.3. Measured and computed (Window 5.2) angular dependent visible transmittances and reflectances of the glazing unit (Measurements: University of Basel).

#### 4.2.2.3. Thermal Properties

In order to investigate the thermal bridge effect in the glazing edge region, a program called BISCO (2004) was employed to compute two-dimensional heat transfer for a steady-state case. To model the aluminum spacer between the panes of glass, a dimensioned cross-section of the aluminum spacer provided by the manufacturer was used. Figure 4.4 shows a cross-section of the portion of the glazing and exterior wall that was simulated and a detailed picture of the spacer. Thermal conductivities of the construction materials were taken from literature and in-house measurements. For temperature dependent properties, the thermal conductivity was evaluated at a mean envelope temperature of 10°C. The simulation results were then coupled with calorimetric hotbox measurements, performed according to ISO 12567-1 (2000) and described in detail by Nussbaumer and Frank (2004); a drawing of the hotbox is shown in Figure 4.5.

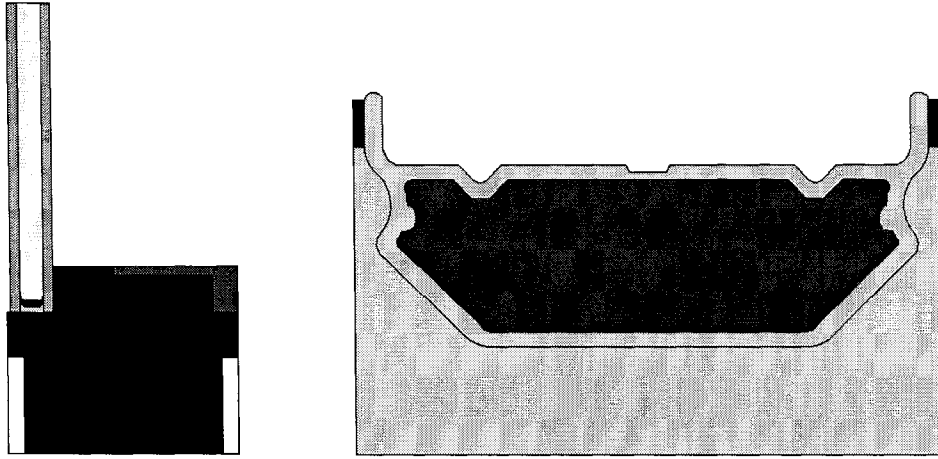


Figure 4.4. The section shows the mounting of the glazing in the frame (left) and a detailed view of the spacer between the glass sheets (right).

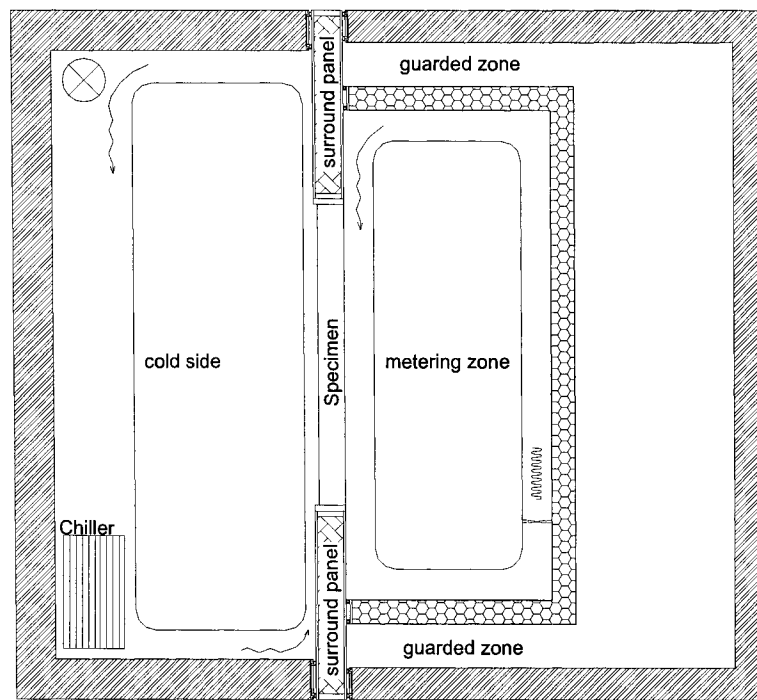


Figure 4.5. Hotbox apparatus featuring a cold zone (left) and a guarded hot zone (right). The test specimen is mounted between the two zones.

The specified properties for the boundary conditions in the simulation included the temperature and the heat transfer coefficients for the outside and inside; these quantities were taken from EN ISO 10077-2 (2003) and are presented in Table 4.2. Computed heat flow lines in Figure 4.6 visualize the increased heat flux in the glazing edge region.

Table 4.2. BISCO simulation boundary conditions.

Boundary Condition	Temperature °C	Heat Transfer Coefficient W/m <sup>2</sup> -K
Inside Air	20	7.7
Outside Air	0	25.0

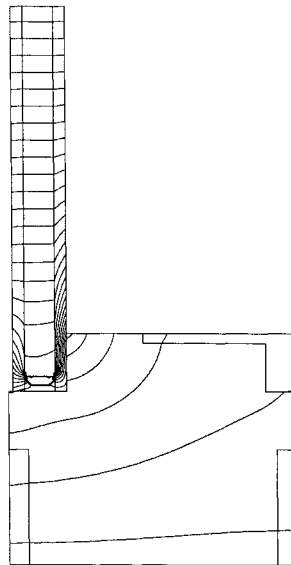


Figure 4.6. Computed heat flow lines at glazing edge.

Because the total heat transfer through the entire frame with mounted glazing – the same setup was later used in the outdoor test cell – was measured in the hotbox, the modified linear thermal transmittance not only includes the impact from the spacer, but also two-dimensional heat transfer effects due to the mounting of the glazing in the frame. The steady-state one-dimensional heat transfer across the element was calculated using Equation 4.1.

$$\dot{Q}_{l-D} = \left\{ L_g U_g + \frac{L_w}{\left( \frac{1}{h_i} + \frac{2d_{ply}}{\lambda_{ply}} + \frac{d_{eps}}{\lambda_{eps}} + \frac{1}{h_o} \right)} \right\} (\theta_i - \theta_o) \quad (4.1)$$

A linear thermal transmittance was calculated using Equation 4.2. After each calculation, heat transfer measurements from the hotbox were used to recalculate the center-of-glazing thermal transmittance and an updated equivalent conductance was calculated for the argon cavity and the simulation was rerun. This was done until the linear and center-of-glazing thermal transmittances converged.

$$\psi = \frac{\dot{Q}_{2-D} - \dot{Q}_{l-D}}{\theta_i - \theta_o} \quad (4.2)$$

Table 4.3 contains a list of input parameters as well as results used for the calculations in Equations 4.1 and 4.2 not previously quantified in Table 4.2.

Table 4.3. Inputs and results for Equations 4.1 and 4.2.

Parameter	Quantity
$U_g$	1.144 W/m <sup>2</sup> -K
$\psi$	0.08899 W/m-K
$L_g$	0.190 m
$L_w$	0.120 m
$d_{ply}$	0.010 m
$d_{eps}$	0.130 m
$\dot{Q}_{2-D}$	6.72 W/m
$\dot{Q}_{l-D}$	4.94 W/m

### 4.3. Simulations

Simulations were run using four building energy simulation codes: EnergyPlus (2005), DOE-2.1E (2002), ESP-r (2005), and TRNSYS-TUD (2005). A summary of the inputs and methodologies employed when modeling this experiment are provided in this section.

### 4.3.1. Inputs

The code inputs included: measured weather parameters, outer surface temperatures for all five faces of the cell envelope adjacent to the guarded zone, internal loads (constant fan power of ~160 W), and volume weighted average hourly air temperature ( $22.66 \pm 0.16$  °C). For each hour, the maximum air temperature difference between any two air temperature sensors was calculated. Mean, minimum, and maximum temperature differences during the experiment were 0.41°C, 0.13°C and 1.77°C, respectively.

Hourly measurements for all these quantities were scheduled into all the building energy simulation codes. The internal loads in the room were modeled as purely convective. Thermal conductivities for the exterior wall, floor, and the remaining elements were fixed at average envelope temperatures of 17.49°C, 22.72°C, and 22.78°C, respectively.

### 4.3.2. Modeling

Brief narratives of the modeling procedure for EnergyPlus, DOE-2.1E, ESP-r, and TRNSYS-TUD are contained in this section. The modeling procedures described by Manz et al. (2005) were used with modifications that accounted for the addition of a glazing in the exterior wall.

Previous work by Loutzenhiser et al. (2005) showed that the solar irradiance model of Perez et al. (1990) best described the vertical solar irradiance measured on the cell external wall during the time period analyzed here. Therefore, in order to reduce discrepancies associated with computing solar irradiance on the external surface of the glazing, the Perez Model was used in all simulations.

#### 4.3.2.1. EnergyPlus

For both panes of glass, reflectances and transmittances at near normal incident angle in the wavelength interval between 250 nm to 2500 nm were used as inputs for EnergyPlus so that angular dependent calculations similar to those found in Window 5.2 could be made. The edge effects were modeled by modifying the “Ratio of Frame-Edge Glass Conductance”

field. In EnergyPlus, the edge is defined as a 63.5 mm distance from the frame; therefore, an additional simulation was run in Bisco software applying the same procedure described in Section 4.2.2.3 to calculate a new center-of-glazing thermal transmittance using this definition. The impact of thermal bridges at the external wall edges (Manz et al., 2005) was accounted for by adding additional thermal transmittance to the glazing edge calculation. Because EnergyPlus employs an algorithm for equivalent thermal conductivity of the glazing cavity that provides slightly higher values than those calculated in Section 4.2.2.3, the thermal conductivities of the glass were reduced accordingly. A general overview for modeling windows in EnergyPlus is provided by Winkelmann (2001). Six hourly timesteps were used with weather data at 10 minute intervals. Measured diffuse and direct-normal solar irradiance were employed as inputs for the calculations of global vertical solar irradiance of the exterior façade. A detailed convective heat transfer coefficient algorithm was chosen that factored in the temperature differences between the air temperature and surfaces, surface orientation, and height/length at each timestep.

#### **4.3.2.2. DOE-2.1E**

For DOE-2.1E, the glazing unit was modeled using Window 5.2 coupled with wavelength dependent near normal optical measurements from a custom database file from Optics. Background information for this type of modeling is provided by Reilly et al. (1995). Because there was no quantitative input for edge effects in DOE-2.1E (there were spacer types), a 3.0 cm window frame was modeled with an equivalent thermal conductivity to account for the edge effects, exterior thermal bridges, one-dimensional heat transfer of the construction displaced by the frame, and two-dimensional heat transfer. The thermal transmittance from the Window 5.2 DOE-2 output file was modified to reflect the center-of-glazing thermal transmittance calculated in Section 4.2.2.3 with adjustments made to account for different heat transfer coefficients. Hourly weather data were put into TMY2 weather format and read into the code; the outputs were verified with the measured data. In TMY2 weather format, the horizontal infrared irradiance is not explicitly described; therefore, the

opaque sky cover quantity from the weather inputs (including the infrared irradiance) was calculated by reversing the algorithm used to calculate infrared irradiance in the code (Walton, 1983; Clark and Allen, 1978). Measured direct-normal and global horizontal solar irradiance were used as inputs for the calculations of the global vertical solar irradiance on the external facades. Combined constant heat transfer coefficients that factored in the impact of radiation and convection as a function of surface orientation using design standards were taken from *ASHRAE Fundamentals* (2001).

#### **4.3.2.3. ESP-r**

For ESP-r, the glazing unit was modeled using WIS software (2004). The inputs were the optical and emittance values at normal incidence for the two panes of glass. The calculated angular dependent transmission and absorption properties over the solar spectrum were then used in the ESP-r model. The glazing thermal bridge was modeled by adding a window frame with an equivalent thermal conductivity to account for the thermal bridges and the one-dimensional heat transfer of the construction displaced by the frame. The thermal transmittance from the WIS output for the center-of-glazing thermal transmittance was used to calculate an equivalent air gap resistance of the argon filled glazing cavity. Simulations were undertaken with six minute climate data, using the measured direct normal and diffuse horizontal irradiances. The internal convection was modeled using the buoyancy correlations reported by Alamdari and Hammond (1983) for vertical and horizontal surfaces which take into account direction of heat flow, surface dimensions and temperature differences.

#### **4.3.2.4. TRNSYS-TUD**

For TRNSYS-TUD, the glazing unit was modeled using a Window 5.2 output file as in DOE-2.1E. The calculated angular dependent SHGC were then used by TRNSYS-TUD for the load calculations. Although edge effects are almost negligible, they were taken into account by a modified steady-state heat loss coefficient of the 6.0 cm window frame. The heat loss was calculated based on the given two-dimensional heat transfer data. The thermal

bridges for both exterior surfaces and surfaces adjacent to the guarded zone were modeled in the envelope of the test cell using an infiltration model; the steady-state heat loss coefficient for the thermal bridges was converted into two fictitious air change rates. A detailed algorithm was used to calculate the convective heat transfer coefficients as a function of temperature differences (average surface and air temperatures) and surface orientation. The radiative heat transfer was calculated assuming gray diffuse surfaces using view factors. Simulations were performed using measured hourly weather data in 1 hour timesteps. Measured diffuse and global horizontal irradiance were employed as inputs to calculate the global vertical irradiance on the exterior facade.

#### **4.4. Error and Sensitivity Analyses**

This section describes the methodology used for estimating different types of uncertainties. A detailed description of the Monte Carlo Analysis (MCA) and Fitted Effects for N-way Factorial Analysis is provided by Loutzenhiser et al. (2005).

##### **4.4.1. Assessing Uncertainties**

For any empirical validation, particular attention should be paid to ascertaining uncertainties and their impacts on the results. Accurately accounting for the experimental uncertainty is vital in empirical validations. Several methods were employed to correctly deal with the various types of uncertainties associated with the simulation inputs and experimental measurements.

###### **4.4.1.1. Temperature Dependent Properties**

Measurements taken for the thermal conductivities revealed temperature dependence for the plywood, EPS foam, and PU foam. Thermal conductivities were found to be linear functions of temperature as shown in Equation 4.3.

$$\lambda_j = b_o + b_1\theta_j + \varepsilon_j \quad (4.3)$$

Because most codes do not have the capacity to use temperature dependent thermophysical properties, the uncertainties as a function of the mean envelope temperature were estimated using propagation error techniques (Weisstein, 1999) incorporating results from analysis of variance (ANOVA) for linear regression (Neter et al., 1996). The variance in the thermal conductivity was calculated using Equation 4.4.

$$Var\lambda_i = \left(\frac{\partial\lambda}{\partial b_0}\right)^2 Var(b_0) + \left(\frac{\partial\lambda}{\partial b_1}\right)^2 Var(b_1) + \left(\frac{\partial\lambda}{\partial \varepsilon}\right)^2 Var(\varepsilon_i) + 2\left(\frac{\partial\lambda}{\partial b_0}\right)\left(\frac{\partial\lambda}{\partial b_1}\right)Cov(b_0, b_1) \quad (4.4)$$

Taking the partial derivative and substituting the ANOVA nomenclature for the error, Equation 4 can be simplified to Equation 4.5.

$$Var\lambda_j = Var(b_0) + \theta_j^2 Var(b_1) + MSE + 2\theta_j Cov(b_0, b_1) \quad (4.5)$$

The standard deviation is calculated as shown in Equation 4.6.

$$\sigma_\lambda = \sqrt{Var\lambda} \quad (4.6)$$

Table 4.4 contains the temperature dependent functions for the standard deviations.

Table 4.4. Standard deviations of the temperature dependent thermal conductivities.

Thermal Conductivity	Standard Deviation, W/m-K
Plywood	$\sqrt{2.2 \times 10^{-11} \theta^2 - 7.68 \times 10^{-10} \theta + 3.60 \times 10^{-8}}$
PU Foam	$\sqrt{1.2 \times 10^{-11} \theta^2 - 5.80 \times 10^{-10} \theta + 1.07 \times 10^{-8}}$
EPS Foam	$\sqrt{5.0 \times 10^{-12} \theta^2 - 5.80 \times 10^{-9} \theta + 6.80 \times 10^{-8}}$

#### 4.4.1.2. Temperature Inputs

Average hourly mean air temperatures in the cell and outer cell envelope surface temperatures (guarded zone) were used as boundary conditions for the simulations. Because there were multiple temperature measurements for each quantity, the overall variance was estimated using the sample variance and propagation of error analysis for the average temperature calculation described in greater depth by Manz et al. (2005) (Equation 9 in this reference of their overall uncertainty calculation employing the same assumptions). Table 4.5

contains average error estimates from the experiment for the temperature boundary conditions.

Table 4.5. Input temperature uncertainties.

Temperature	$\sigma_{\theta, sensor}$ , °C
Zone Air	0.117
North Wall	0.165
Ceiling	0.288
Floor	0.369
West Wall	0.181
East Wall	0.220

#### 4.4.1.3. Additional Errors

Standard deviations for other cell properties and weather inputs were quantified by Manz et al. (2005) and Loutzenhiser et al. (2005). Input errors associated with addition of the glazing are described in Table 4.6; the additional uncertainties were all of a Bayesian nature.

Table 4.6. Additional uncertainties.

Parameter	Uncertainty
Spectrometer Measurements (Transmittances and Reflectances)	± 0.01
Center-of-Glazing Thermal Transmittance	± 5%
Modified Linear Thermal Transmittance	± 5%

#### 4.4.2. Sensitivity Studies

One and 2-way factorial analyses were performed to quantify the impact of uncertainties of inputs on the outputs. Table 4.7 contains a list of the average overall uncertainty and the average impact of the 10 most important input parameters.

Table 4.7. Overall uncertainty and 10 most influential input parameters from the factorial analyses in Watts.

Parameter	Forward	Backward
Overall Uncertainty	3.08	3.06
Average Inside Air Temperature	-1.82	1.82
Floor Temperature	0.919	-0.919
Fan Power	0.916	-0.916
Outside Air Temperature	0.819	-0.818
Ceiling Temperature	0.727	-0.728
North Wall Temperature	0.519	-0.519
East Wall Temperature	0.460	-0.460
Outer Pane Transmittance	0.388	-0.385
Diffuse Irradiance	0.385	-0.360
West Wall Temperature	0.378	-0.379

A MCA was used to quantify the hourly uncertainties and calculate 95% credible limits in EnergyPlus. For this study, 120 runs were made and the average standard deviation for the experiment was 3.01 W, which corresponded well with results from the factorial analysis in Table 4.7. A Lilliefors Test for goodness of fit for normal distributions was used to confirm that the distribution was Gaussian at a 1% significance level; there was no evidence that any hourly outputs were not normally distributed.

#### 4.5. Results

Several comparisons were made to try to ascertain the accuracies of each code and evaluate the impact of modelers' assumptions. Statistical analyses between the predicted and measured cooling power were performed, a comparative study of solar gain calculations (which could not be empirically validated), and an evaluation of the impact of the convective heat transfer coefficients.

#### **4.5.1. Cooling Power Comparisons**

The computed cooling powers from the four building energy simulation codes were compared with measured hourly quantities taken during the experiment. Figure 4.7 contains plots that compare at any given hour in the day averages taken during the experiment. Ninety-five percent credible limits from the experiment and MCA are also displayed on the plot. To provide an additional evaluation of the code behavior for each hour, the mean, maximum, and minimum absolute differences between measured and predicted cooling powers were calculated and are displayed in Figure 4.8.

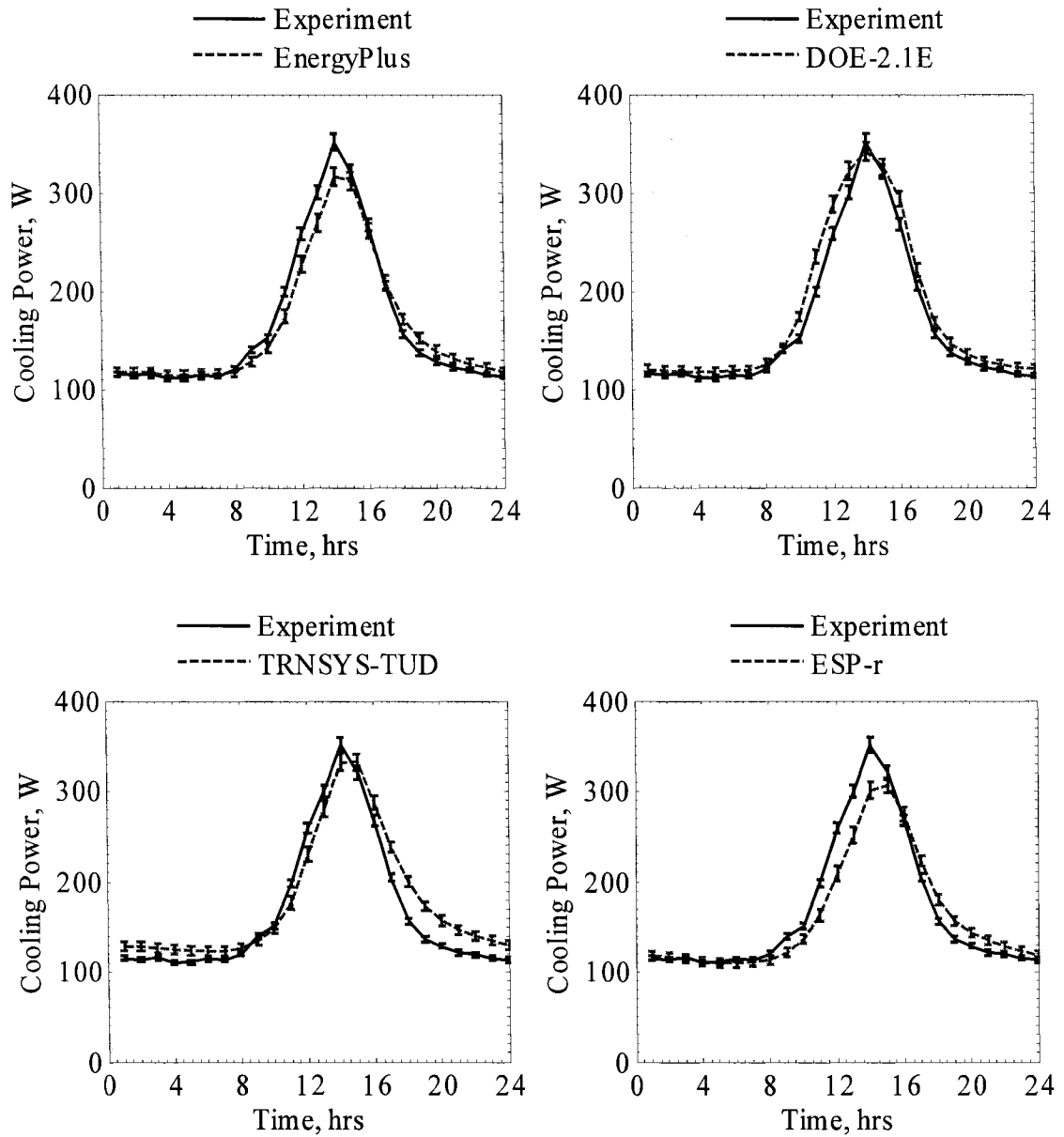


Figure 4.7. Comparisons between measured and computed cooling powers as a function of the hour of the day (averaged over 480 h).

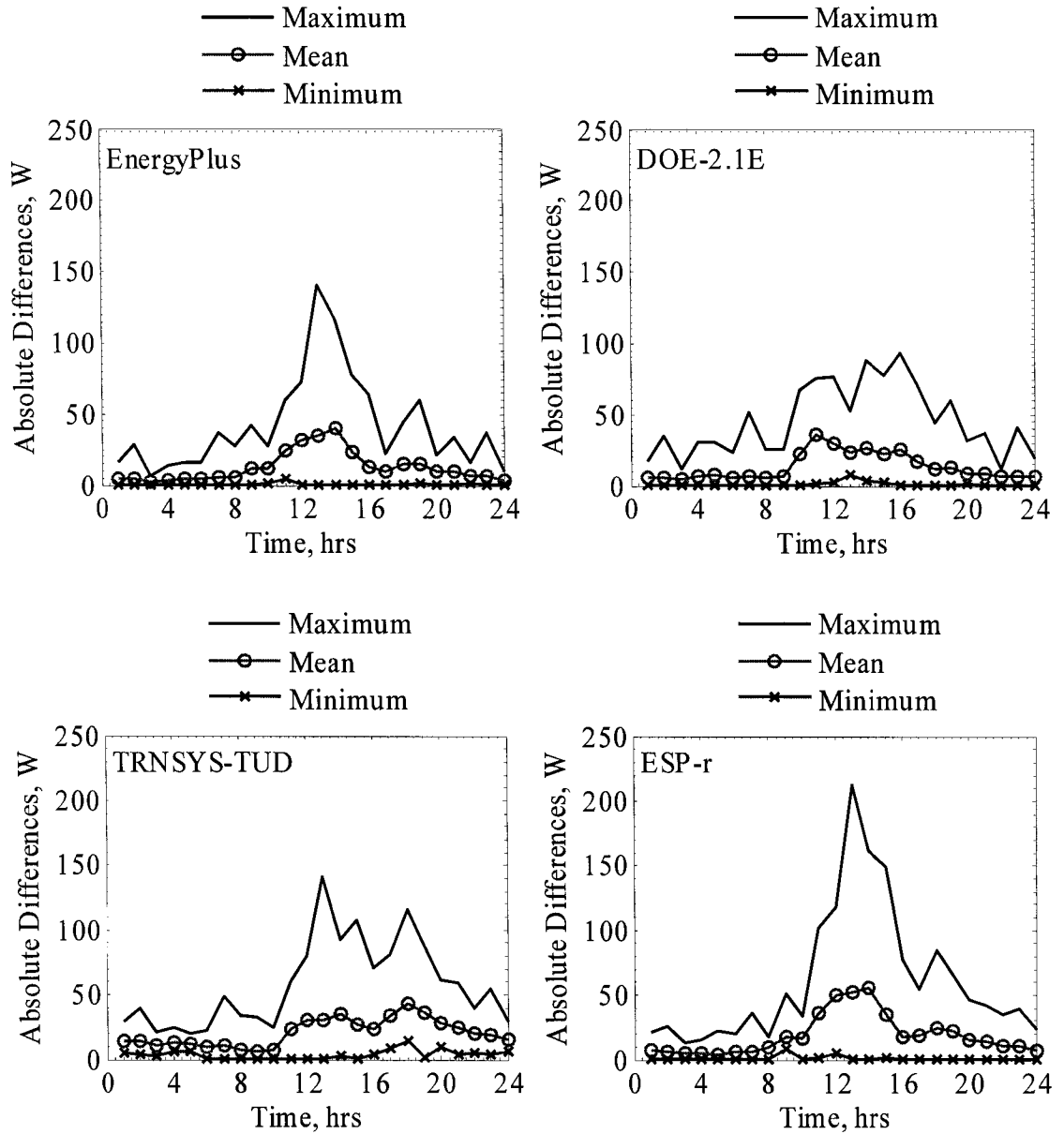


Figure 4.8. Maximum, mean, and minimum hourly absolute differences between experiment and predicted quantities as a function of hour of the day (calculated over 480 h).

Statistical analyses were performed to compare the output from the simulations with the experiment and are contained in Table 4.8. The methodologies and nomenclature are described by Manz et al. (2005). One important parameter worth noting is the uncertainty ratio calculated using Equation 4.7. This provides a measure of the performance of the

respective simulations. The codes can be considered validated within 95% credible limits if the ratio is less than or equal to unity.

$$UR = \frac{|D|}{OU_{Exp} + OU_{E+}} \quad (4.7)$$

Table 4.8. Summary of statistics and comparisons of cooling power.

	Experiment	EnergyPlus	DOE-2.1E	TRNSYS-TUD	ESP-r
$\bar{x}$	166.6 W	163.4 W	172.6 W	176.9 W	161.4 W
$s$	116.1 W	101.5 W	129.2 W	106.2 W	99.0 W
$x_{max}$	847.9 W	767.5 W	831.0 W	816.1 W	750.2 W
$x_{min}$	54.1 W	83.5 W	93.0 W	93.2 W	82.3 W
$\bar{D}$	-	3.2 W	-6.0 W	-10.3 W	5.2 W
$ \bar{D} $	-	12.8 W	13.9 W	20.8 W	19.0 W
$D_{max}$	-	140.5 W	136.6 W	140.7 W	213.1 W
$D_{min}$	-	0.07 W	0.00 W	0.24 W	0.01 W
$D_{rms}$	-	22.18 W	24.88 W	28.23 W	33.42 W
$D_{95\%}$	-	52.29 W	54.54 W	60.30 W	79.15 W
$\overline{OU}$	3.77 W	5.91 W	-	-	-
$\overline{UR}$	-	1.14	1.24	2.14	1.63
$UR_{max}$	-	9.30	7.72	13.78	10.35
$UR_{min}$	-	0.01	0.00	0.03	0.00
$ \bar{D} /\bar{x} \times 100\%$	-	7.7%	8.3%	12.5%	11.4%
$\bar{D}/\bar{x} \times 100\%$	-	1.9%	-3.6%	-6.2%	3.1%

#### 4.5.2. Solar Gains

For comparative purposes, the solar gains were computed by each program for this period and are shown in Figure 4.9. However, because this parameter could not be measured in the experimental setup, the empirical validation focused on cooling power

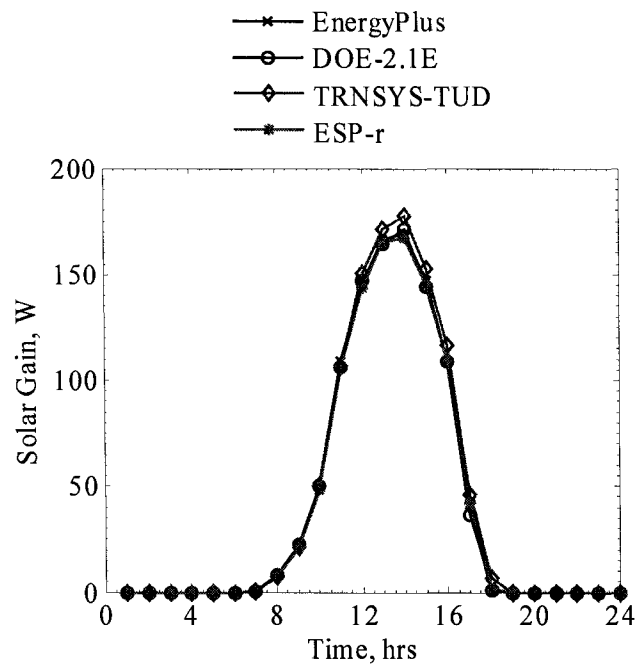


Figure 4.9. Computed solar gains from the building energy simulation codes as a function of hour of the day for the entire period (averaged over 480 h).

#### 4.5.3 Convective Heat Transfer Coefficients

Because the solar gains were nearly the identical (Figure 4.9), differences between modeling procedures were investigated; the delayed response depended significantly on the selection of convective heat transfer coefficient algorithms. For DOE-2.1E, constant combined radiative and convective heat transfer coefficients were used, while in EnergyPlus, TRNSYS-TUD, and ESP-r dynamic heat transfer coefficients that were functions of surface orientation, surface and air temperature, and surface height/length were chosen. Because of concerns pertaining to the appropriate selection of convective heat transfer coefficient algorithms expressed by Beausoleil-Morrison and Strachan (1999), an additional simulation was performed in EnergyPlus assuming constant convective heat transfer coefficients; descriptions of both algorithms are provided by *EnergyPlus Engineering Reference* (2005). Comparisons between the results for both algorithms are shown in Figure 4.10.

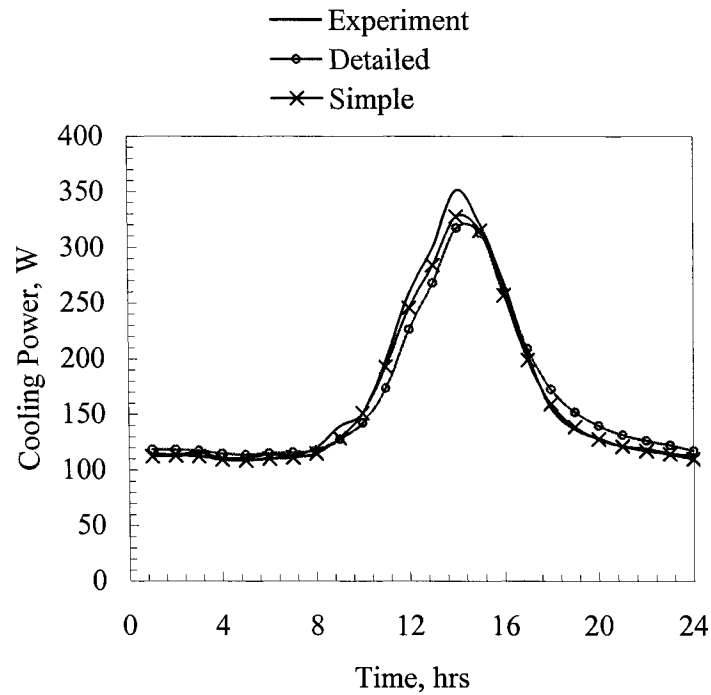


Figure 4.10. Impact comparisons of convective heat transfer coefficient algorithms on cooling power using EnergyPlus.

To further examine the sensitivity of the codes to the convective heat transfer coefficient algorithms, a parametric study was conducted where a detailed convective heat transfer coefficient algorithm was assigned to all surfaces except one, which was assigned constant heat transfer coefficients. Plots were constructed comparing mean absolute and mean differences in cooling power for each surface using the different constant convective heat transfer coefficients and are shown in Figure 4.11.

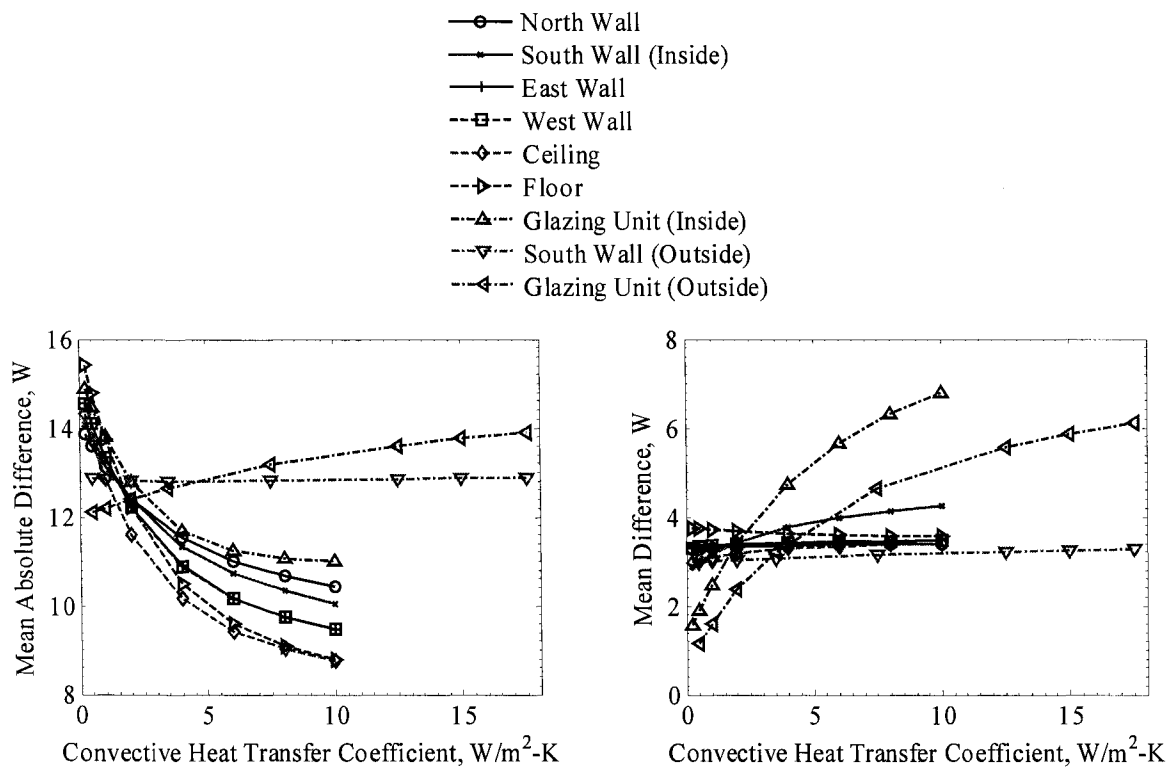


Figure 4.11. Parametric study of the impact of heat transfer coefficients on the mean absolute and mean differences.

#### 4.6. Discussion

According to Table 4.8, the average uncertainty ratio was greater than unity for all the codes, which strictly means that the codes were not validated within 95% credible limits. During the experiment, EnergyPlus and ESP-r generally under-predicted and DOE-2.1E and TRNSYS-TUD over-predicted the cooling power. For all codes, there were certain hours where the differences were relatively high. The mean absolute differences for EnergyPlus, DOE-2.1E, TRNSYS-TUD, and ESP-r were 12.8 W, 13.9 W, 20.8 W, and 11.4 W, respectively. This quantity provides a good overall assessment of the performance at any given hour. Often it is more important to evaluate overall energy performance for an extended period of time. Here the mean difference is an important parameter to describe the overall performance; for EnergyPlus, DOE-2.1E, TRNSYS-TUD, and ESP-r the mean

differences were 3.2 W, -6.0 W, -10.3 W, and 3.1 W, respectively. EnergyPlus, TRNSYS-TUD, and ESP-r all had delayed responses for the cooling power predictions compared with experimental measurements and DOE-2.1E predictions; this is further magnified by the maximum absolute differences that occur during the 13 h of the day for all three codes (Figure 4.8).

Much better instantaneous results were obtained using the constant heat transfer coefficients in EnergyPlus (Figure 4.10). The overall cooling energy remained nearly the same, the mean difference for the detailed and simple algorithms were 3.2 W and 4.7 W, respectively. The results using the simple (fixed) convective heat transfer algorithm yield better instantaneous predictions which resulted in quantities within the 95% credible limits and would be considered validated ( $\overline{UR} = 0.75$ ).

The sensitivity of the building energy simulation code predictions to the selection of convective heat transfer algorithms found in this survey concurs with the findings of Beausoleil-Morrison and Strachan. The results from the parametric study (Figure 4.11) show that the overall impact of convective heat transfer coefficient was significant for all interior surfaces and the exterior glazing when making cooling power predictions. While the largest impact can be seen when adjusting interior convective heat transfer coefficients across the glazing and the south (exterior) wall where there were large fluctuating temperature gradients, the cooling power predictions (and thus the heat flux calculations) were also very sensitive to convective heat transfer coefficients across the interior surfaces, where the temperature gradients in the walls and differences across the walls were very small (less than 3.6 K/m and 0.5 K, respectively). Changes in the exterior convective heat transfer coefficients across the exterior wall seem to have very little impact on the results; in contrast, the impact of the exterior convective heat transfer for the glazing is much greater than that for the exterior wall (although much smaller compared with internal convective heat transfer coefficients) on the predicted cooling power.

The impact of convective heat transfer coefficients at internal surfaces on the required cooling energy (mean differences from Figure 4.11) was much smaller than on the required

cooling power. This is because changes in the interior convective heat transfer coefficients alter the time constant and thus the thermal storage process (and the required cooling power). However, changes for the convective heat transfer coefficients for the glazing unit – both internal and external – significantly impacted the cooling energy predictions. Here, changes in the convective heat transfer coefficients impeded the flow of energy via convection into or out of the cell depending on the outside temperature and affected the required overall cooling power/energy. The glazing unit area was particularly important because the thermal conductance of the glazing unit was relatively high compared with the well-insulated exterior wall; therefore, the overall thermal transmittance of the glazing unit was much more sensitive to changes in convective heat transfer coefficients than that of the exterior wall.

While, for this experiment, steps were taken in the experimental design to minimize the impact of the convective heat transfer for all guarded surfaces (maintaining the guarded zone at nearly the same temperature as the inside of the test cell), the impact of the convective heat transfer coefficients is clearly seen in Figures 4.10 and 4.11; this reiterates concerns expressed by Beausoleil-Morrison and Strachan about convective heat transfer coefficient algorithm selections in building energy simulation codes and is clearly a topic for future investigation outside the scope of these validations. However, the impact of convective heat transfer coefficient on predicted heating/cooling power may be smaller in real buildings compared with very airtight test cells, because infiltration can be a significant heat transfer mechanism.

Other modeling deficiencies and their impact on results could not be fully examined in this study. The modeling of the angular dependence of the solar transmittances and time dependent heating/cooling power predictions may contribute to some of the discrepancies noted in the experiment. These topics will have to be investigated in future studies.

This work has also shown that using the four building energy simulation codes employed here, the solar energy gains through a glazing can be accurately modeled and cooling/heating energy for longer periods of time can be computed with relatively high accuracies. But much

lower accuracies are obtained for cooling power predictions at a specific timestep. This uncertainty must be accounted for when sizing HVAC equipment.

These results do indicate that the measured data, calorimetric measurements, simulation for center-of-glazing, modified linear thermal transmittances, and the modeling methodology accurately describe the behavior of the test cell. Overall, this experiment is well-suited for rigorous empirical validations of solar gain models in building energy simulation codes but also identifies the impact of various assumptions that modelers and code designers might make, particularly when selecting convective heat transfer coefficients.

The data and descriptions of this experiment are available for download at [www.empa.ch/ieatask34](http://www.empa.ch/ieatask34). Future studies planned in conjunction with IEA Task 34/Annex 43 will deal with internal and external shading devices and a window (i.e. glazing with frame). Therefore, this work is also to be seen as a starting point for investigating more complex cases.

### **Acknowledgements**

We gratefully acknowledge the financial support of the Swiss Federal Office of Energy (BFE) for building and testing the experimental facility (Project 17'166) as well as the funding for EMPA participation in IEA Task 34/43 (Project 100'765). We would also like to acknowledge the many contributions from: R. Blessing, M. Camenzind, K. Meyer, T. Nussbaumer, G. Reber, R. Steiner, and R. Vonbank.

## Nomenclature

$b_o$	= intercept coefficient from linear regression, W/m-K
$b_l$	= slope coefficient from linear regression, W/m-K-°C
$d_{ply}$	= width of plywood, m
$d_{eps}$	= width of the EPS foam, m
$D$	= difference between experiment and predicted values for a given value, W
$\bar{D}$	= mean difference for a given array, W
$ \bar{D} $	= mean absolute difference for a given array, W
$D_{max}$	= maximum difference between experimental and predicted values for a given array, W
$D_{min}$	= minimum difference between experimental and predicted values for a given array, W
$D_{rms}$	= root mean squared difference between experimental and predicted values for a given array, W
$D_{95\%}$	= ninety-fifth percentile of the differences between experimental and predicted values for a given array, W
$h_i$	= combined interior radiative and convective heat transfer coefficient, W/m <sup>2</sup> -K
$h_o$	= combined exterior radiative and convective heat transfer coefficient, W/m <sup>2</sup> -K
$L_g$	= length of glazing in 2-D model, m
$L_w$	= length of wall in 2-D model, m
$MSE$	= mean squared error from ANOVA regression, (W/m-K) <sup>2</sup>
$OU_{Exp}$	= 95% credible limits or overall uncertainty from experiment, W
$OU_{E+}$	= 95% credible limits or overall uncertainty from MCA, W
$\overline{OU}$	= average overall uncertainty calculated for 95% credible limits, W
$\dot{Q}'_{1-D}$	= one-dimensional heat transfer, W/m
$\dot{Q}'_{2-D}$	= heat transfer computed from BISCO, W/m
$U_g$	= center-of-glazing thermal transmittance, W/m <sup>2</sup> -K
$UR$	= uncertainty ratio for a given value, no units
$\overline{UR}$	= average uncertainty ratio for a given array, no unit
$UR_{max}$	= maximum uncertainty ratio for a given array, no units
$UR_{minx}$	= minimum uncertainty ratio for a given array, no units
$\bar{x}$	= arithmetic mean for a given array, W
$x_{min}$	= minimum quantity for a given array, W/m <sup>2</sup>
$x_{max}$	= maximum quantity for a given array, W/m <sup>2</sup>

$\theta_i$	= inside temperature, °C
$\theta_o$	= outside temperature, °C
$\theta_j$	= input temperature for linear regression, °C
$\psi$	= modified linear thermal transmittance, W/m-K
$\lambda_{eps}$	= thermal conductivity of the EPS foam, W/m-K
$\lambda_{ply}$	= thermal conductivity of the plywood, W/m-K
$\lambda_i$	= thermal conductivity of a temperature dependent property, W/m-K
$\varepsilon_j$	= residuals from the linear regression, W/m-K
$\sigma_\lambda$	= standard deviation for thermal conductivity, W/m-K

## References

- Alamdari F. and G.P. Hammond. 1983. *Improved Data Correlation for Buoyancy-Driven Convection in Rooms, Building Services Engineering Research and Technology*, Vol. 4:106-112.
- ASHRAE. 2001. *ASHRAE Fundamentals 2001 SI Edition*, American Society of Heating, Refrigeration and Air-Condition Engineers, Inc, Atlanta, GA.
- Beausoleil-Morrison, I. and P. Stachan. 1999. On the Significance of Modeling Internal Surface Convection in Dynamic Whole-Building Simulation Programs. *ASHRAE Transactions* Vol. 105(2):929-940
- BISCO Version 7.0w, 2004. A computer program to calculate 2D steady-state heat transfer, Physibel, Heirweg 21, B-9990 Maldegem, Belgium
- Clark G. and C. Allen. 1978. The Estimation of Atmospheric Radiation for Clear and Cloudy Skies. *Proc. 2nd National Passive Solar Conference (AS/ISES)*, 675-678
- Clarke, J.A. 2001. *Energy simulation in building design*. Oxford: Butterworth Heinemann; 2001.
- DOE-2.1E (Version-119). 2002. Building Energy Simulation Code, Lawrence Berkley Laboratories (LBL), Berkley, CA, April 9, 2002
- EnergyPlus. 2005. *EnergyPlus Engineering Reference: The Reference to EnergyPlus Calculations*. The Board of Trustees of the University of Illinois and the Regents of the University of California through the Ernst Orlando Lawrence Berkley National Laboratory
- EnergyPlus Version 1.2.2.030. 2005. Building Energy simulation code, [www.energyplus.gov](http://www.energyplus.gov)
- ESP-r Software (Version 10.12). 2005. Building Energy Simulation Code. University of Strathclyde, Glasgow. <http://www.esru.strath.ac.uk>
- European Standard EN 410. 1998. Glass in building – Determination of luminous and solar characteristics of glazing. European Committee for Standardization, Brussels, Belgium
- European Standard EN ISO 10077–2. 2003. Thermal performance of windows, doors and shutters – Calculation of thermal transmittance – Part 2: Numerical method for frames, European Committee for Standardization, Brussels
- Furler, R.A. 1991. Angular dependence of optical properties of homogenous glasses. *ASHRAE Transactions* Vol. 97(2):1129-1137
- GLAD Software. 2002. Swiss Federal Laboratories for Materials Testing and Research (EMPA), Duebendorf, Switzerland
- International Standard ISO 12567-1. 2000. Thermal performance of windows and doors – Determination of thermal transmittance by hotbox method – Part 1: Complete windows and doors, ISO, Geneva, Switzerland
- Jensen, S.Ø. 1995. Validation of building energy simulation programs: a methodology. *Energy and Buildings* 22: 133-144.

- Judkoff R.D. 1988. Validation of Building Energy Analysis Simulation Programs at the Solar Energy Research Institute. *Energy and Buildings* 10:221-239.
- Karlsson, J., M. Rubin, and A. Roos. 2001. Evaluation of predictive models for the angle-dependent total solar energy transmittance of glazing materials. *Solar Energy* Vol. 71 No.1:22-31
- Lomas, K.J., H. Eppel, C.J. Martin, and D.P. Bloomfield. 1997. Empirical validations of building energy simulation programs. *Energy and Buildings* 26:253-275
- Loutzenhiser, P.G., H. Manz, C. Felsmann, P.A. Strachan, T. Frank, and G.M. Maxwell. (Submitted July 14, 2005 to *Solar Energy*). Empirical validation of models to compute solar irradiance on inclined surfaces for building energy simulation.
- Manz, H., P. Loutzenhiser, T. Frank, P.A. Strachan, R. Bindi, and G. Maxwell. (Accepted for publication in *Building and Environment* on July 12, 2005) Series of experiments for empirical validation of solar gain modeling in building energy simulation codes – Experimental setup, test cell characterization, specifications and uncertainty analysis.
- Manz, H. and T. Frank. 2005. Thermal simulation of buildings with double-skin façades. *Energy and Buildings*, 37:1114–1121
- Maxwell, G.M., P.G. Loutzenhiser, and C.J. Klaassen. 2003. *Daylighting – HVAC Interaction Tests for the Empirical Validation of Building Energy Analysis Tools*, A Report of Task 22 Subtask D. Building Energy Analysis Tools Project D Empirical Validation. [http://www.iea-shc.org/task22/reports/IEA\\_Daylighting\\_Report\\_Final.pdf](http://www.iea-shc.org/task22/reports/IEA_Daylighting_Report_Final.pdf)
- Moinard, S. and G. Guyon. 1999. *Empirical Validation of EDF ETNA and GENEC Test-Cell Models*, A Report of Task 22, Project A.3 Empirical Validation, International Energy Agency, [http://www.iea-shc.org/task22/reports/Final\\_report.pdf](http://www.iea-shc.org/task22/reports/Final_report.pdf)
- Neter, J., M.H. Kutner, C.J. Nachtsheim, and W. Wasserman. 1996. *Applied Linear Statistics Model*, WCB McGraw-Hill. Boston, MA
- Nussbaumer, T. and T. Frank. 2004. Bestimmung des Wärmedurchgangskoeffizienten  $U_g$  einer 2-fach Isolierverglasung, Nr. 880'097, STS-Nr. 086. EMPA, Dübendorf, Switzerland, Nov. 30, 2004, (In German)
- Perez, R., P. Ineichen, R. Seals, J. Michalsky, and R. Stewart. 1990. Modeling daylight availability and irradiance components from direct and global irradiance. *Solar Energy* Vol. 44 No.5:271-289
- Reber, G., R. Steiner, P. Oelhafen, and A. Romanyuk. 2005. Angular dependent solar gain for insulating glasses from experimental optical and thermal data. *CISBAT 2005 Proceedings*, 173-178, Lausanne, Switzerland
- Reilly, M.S., F.C. Winkelmann, D.K. Arasteh, and W.L. Carrol. 1995. Modeling windows in DOE-2.1E. *Energy and Buildings* 22:59-66
- Roos, A., P. Polato, P.A. Van Nijnatten, M.G. Hutchins, F. Olive, and C. Anderson. 2000. Angular-dependent optical properties of low-e and solar control windows—simulations versus measurements. *Solar Energy*, Vol. 69 (Suppl) No:1-6:15-26

- Rubin, M., R. Powles, and K. Von Rottkay. 1999. Models for the angle-dependent optical properties of coated glazing materials. *Solar Energy* Vol.66 No.4:267-276
- Rubin, M., K. Von Rottkay, and R. Powles. 1998. Window Optics. *Solar Energy* Vol.65 No. 3:149-161
- Strachan, P. 1993. Model Validation using the PASSYS Test Cells. *Building and Environment*, 28:153-165
- TRNSYS-TUD. 2005. Technical University of Dresden research code based on the frame of TRNSYS 14.2, Solar Energy Laboratory, University of Wisconsin-Madison, Madison, WI, 1996
- Walton, G.N. 1983. *Thermal Analysis Research Program Reference Manual*. NBSIR 83-2655, March 1983, 21
- Weisstein, E.W. 1999. Error Propagation. From *MathWorld*--A Wolfram Web Resource. <http://mathworld.wolfram.com/ErrorPropagation.html>
- Window 5.2 Version 5.2.17a. 2005. Code to calculate window properties, LBL, <http://windows.lbl.gov/software/window/window.html>
- Winkelmann, F.C. 2001. Modeling windows in EnergyPlus. *Proceedings IBPSA Building Simulation 2001*, Rio de Janeiro (listed as LBNL Report 47972)
- WIS. 2004. Window Information System, <http://windat.ucd.ie/wis/html/index.html>
- Wouters, P., L. Vandaele, P. Voit, and N. Fisch. 1993. The use of outdoor test cells for thermal and solar building research within the PASSYS project. *Building and Environment*, 28:107-113

## Chapter 5: An empirical validation of modeling solar gain through a glazing unit with external and internal shading screens

A paper submitted to Applied Thermal Engineering

P.G. Loutzenhiser<sup>1,2,a</sup>, H. Manz<sup>1,b</sup>, C. Felmann<sup>3,c</sup>, P.A. Strachan<sup>4,d</sup>, G.M. Maxwell<sup>2,e</sup>

<sup>1</sup> Swiss Federal Laboratories for Material Testing and Research (EMPA), Laboratory for Building Technologies, CH-8600 Duebendorf, Switzerland

<sup>2</sup> Iowa State University, Department of Mechanical Engineering, Ames, Iowa 50011 USA

<sup>3</sup> Technical University of Dresden, Institute of Thermodynamics and Building Systems Engineering, D-01062 Dresden, Germany

<sup>4</sup> University of Strathclyde, Department of Mechanical Engineering, ESRU, Glasgow G1 1XJ, Scotland

<sup>a</sup> Wrote the majority of the text and performed the EnergyPlus and DOE-2 simulations

<sup>b</sup> Supervised the text writing

<sup>c</sup> Performed the TRNSYS-TUD simulations and wrote the TRNSYS-TUD modeling descriptions

<sup>d</sup> Performed the ESP-r simulations and wrote the ESP-r modeling descriptions

<sup>e</sup> Provided technical support

### Abstract

Empirical validations are integral components in assessing the overall accuracies of building energy simulation programs. Two test cell experiments were performed at the Swiss Federal Laboratories for Material Testing and Research's (EMPA) campus in Duebendorf, Switzerland to evaluate the solar gain models with external and internal shading screens in four building energy simulation programs including: 1) EnergyPlus, 2) DOE-2.1E, 3) TRNSYS-TUD, and 4) ESP-r. Detailed information about the shading screen properties, modeling procedures, and thorough statistical and sensitivity analyses of simulation results are provided. For the external shading screen experiment, the mean percentage of the absolute difference between measured and simulated cooling power to maintain a near-constant cell air temperature for EnergyPlus, DOE-2.1E, TRNSYS-TUD and ESP-r were 3.7%, 5.5%, 10.6%, and 7.5%, respectively. EnergyPlus and DOE-2.1E were considered validated within 95% credible limits. For the internal shading screen experiment, the mean percentage of the absolute mean differences for EnergyPlus, DOE-2.1E, TRNSYS-TUD and

ESP-r were 6.7%, 13.8%, 5.7%, and 4.3%, respectively; only ESP-r was considered validated within 95% credible limits.

## 5.1. Introduction

Window shading devices are important components in the design of modern highly glazed buildings. They allow occupants to avoid glare and provide flexibility to reduce solar gains through windows in the summer and yet the shading devices can be retracted in the winter to subsidize heating requirements. Assessing the potential energy and/or demand savings associated with the implementation of various types and configurations of window shading devices in summer can be done prior to constructing an actual building using building energy simulations programs. Building energy simulation programs are widely used today and allow engineers and architects to optimize the energy performance in a building before construction and size building heating and/or cooling equipment. Clarke [1] gives the basic underlying theory behind the development of building energy simulation programs.

Several studies have been performed using building energy simulation programs to calculate annual cooling energy savings from the installation of interior and/or exterior shading devices. One study using DOE-2.1 [2] found a cooling energy saving of up to 30% in northern US climate with the installation of external shading devices. A similar study [3] using TRNSYS with TMY weather from Cyprus revealed cooling load reductions of up to 20% depending on the room construction and using internal shading devices. However, efficient (external) shading in combination with solar control windows can even make cooling unnecessary in most well-designed buildings in moderate climates. Therefore, accurate modeling and simulation of solar gains is a prerequisite for reliable predictions of summertime behavior of buildings, especially for highly glazed buildings.

To ensure the overall accuracies of building energy simulation programs, thorough validations of programs are important endeavors that provide confidence to program developers and users that their respective programs simulate reality. Judkoff [4] describes the three types of validation procedures: 1) analytical, 2) program-to-program, and 3)

empirical validations. Each of these approaches has its own strengths and weaknesses making them all powerful tools for assessing very different types of problems. In analytical validation (comparing program results with an analytical solution) all the input parameters are perfectly known and outputs can be compared to an absolute mathematical truth standard within the limitation of the physical theory. Unfortunately these types of validations can only be performed if the analytical solution is known and are therefore limited to only very simple problems. There are no such limitations in program-to-program comparisons (results from different programs are compared), but there are also no absolute truth standards, and, so, it is impossible to ascertain which program(s), if any, perform best. Empirical validations (comparisons of experimental quantities and simulated results) provide comparisons to an absolute truth standard within limits of experimental uncertainties and are not limited to simple cases. While analytical and program-to-program comparisons are relatively inexpensive to perform, empirical validations are time-consuming and expensive; therefore very few empirical validations have been performed.

While it is impossible to say with absolute certainty that a given building energy simulation program is completely validated, it is possible to evaluate and validate specific components and algorithms of the programs. Test cells offer a unique median between an actual building and an experimental setup in a laboratory for empirical validations of energy flow algorithms through windows and shading devices. In a test cell, it is possible to accurately control and measure all relevant boundary conditions (surface temperatures of interior walls and weather parameters) while still maintaining dimensions and thermophysical properties similar to those of office or residential spaces. Test cells were used extensively in the PASSYS project [5-7] where empirical validations were conducted all across Europe using numerous sites. Additional studies using test cells were performed in conjunction with the International Energy Agency's (IEA) Annex 21/Task 8 [8] and IEA Task 22 [9]. Another study using an actual building designed for research purposes was performed in conjunction with IEA Task 22 [10, 11].

The experiments for this research were performed in conjunction with IEA Task 34/Annex 43 Subtask C in a test facility on the campus of the Swiss Federal Laboratories for

Material Testing and Research (EMPA) in Dübendorf, Switzerland. The test facility consists of two test cells where all interior walls are adjacent to a temperature controlled guarded zone for better control of boundary conditions. Data taken at this facility meet all nine criteria for a high quality data set [8].

The purpose of this paper is to describe and discuss results from experiments performed with exterior and interior shading screens. Prior works to characterize the test cell [12], evaluate radiation models for the exterior façade [13], and characterize the glazing unit and validate solar gain models without shading devices [14] were considered in earlier publications. The emphasis of this paper is on assessing the performance of four building energy simulation programs when external and internal diffuse window shading screens were mounted over the glazing unit. Detailed information concerning the optical properties and modeling of the shading screens are presented along with comparisons between measured and predicted cooling powers for each building energy simulation program. Because experimental uncertainty is such an integral component in evaluating the performance of experiments and programs, detailed sensitivity analyses were also conducted.

## **5.2. Experiments**

Two experiments were run with external and internal window shading screens. The experiments were set up to maintain a near-constant temperature inside the test cell by adjusting the cooling power. During the experiment, two fans operating with a combined load of  $\sim 160$  W were used to distribute the air to the test cell through two textile ducts along the floor and extracted through metal ducts hanging from the ceiling. The air temperature inside the cell was measured by 18 double-shielded thermocouples. Figure 5.1 shows a drawing of the test cell that depicts the air distribution system. A brief description of both experiments is provided in this section. Optical and thermophysical properties for the test cell and the glazing unit are described in [12] and [14], respectively. An additional calculation related to quantifying the ground reflectance is described by [13].

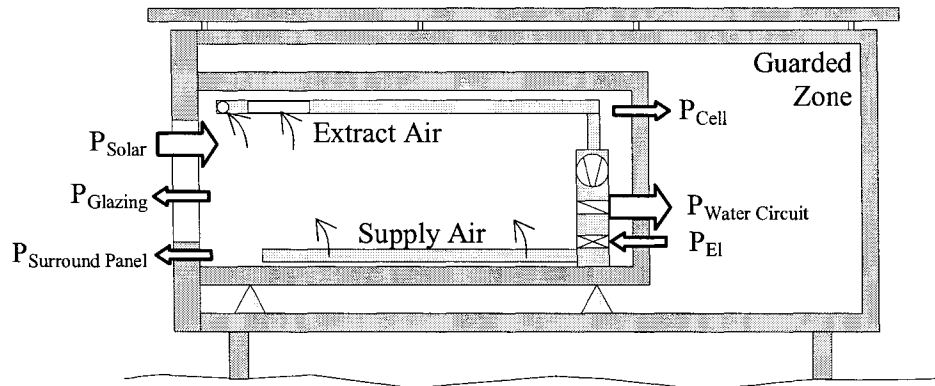


Figure 5.1. Side view of the test facility showing energy flows and cell ventilation system.

### 5.2.1. External Shading Screen

An experiment with an external shading screen mounted over the glazing unit was run for a 20 day period from March 28 to April 16, 2005. Prior to the experiment, five days of preconditioning were run with an opaque insulating foil mounted over the glazing unit to prevent solar gain. During the experiment, the external shading screen was installed 0.10 m from the glazing unit. The top and the bottom of the shade were not sealed off and air was allowed to circulate along the sides through notches cut in the mounting. The external shading screen was a closed weave fabric shown in Figure 5.2. Near-normal transmittance and reflectances of the shading screen were measured in the wavelength interval of 250 nm to 2500 nm and are shown in Figure 5.3 indicating that the screen is not solar selective. No difference between the outside and inside reflectance was found. The integral optical properties for the shade were computed according to EN 410 [15] using GLAD software [16]. The normal integral solar transmittance and reflectance were calculated as 21.5% and 59.6%, respectively. A photograph of the experimental setup is provided in Figure 5.4.

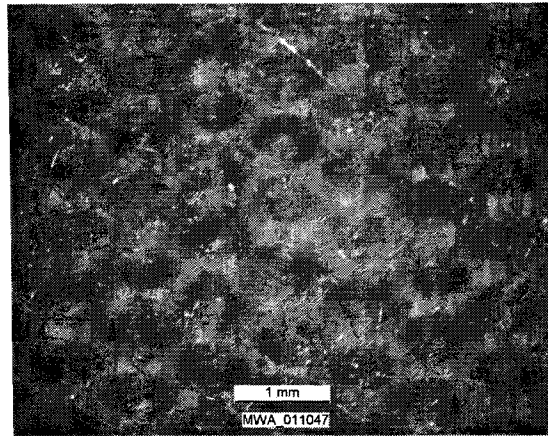


Figure 5.2. Photograph of the external shading screen taken using a microscope.

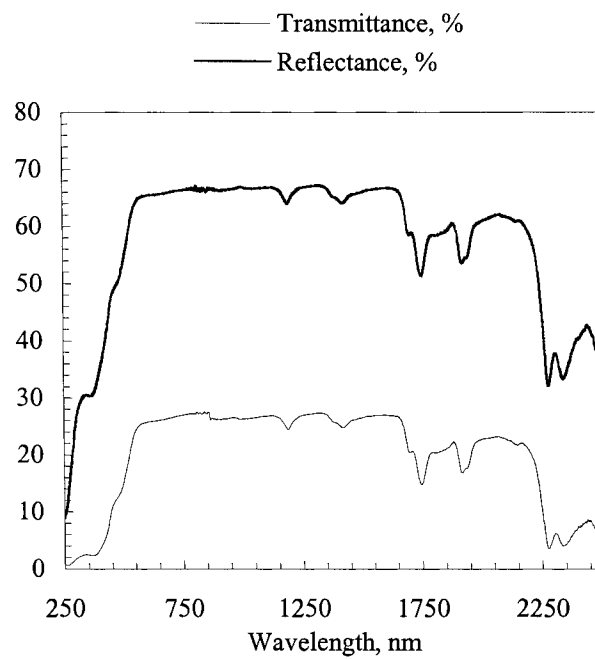


Figure 5.3. Transmittance and reflectance of the external shade as a function of wavelength.

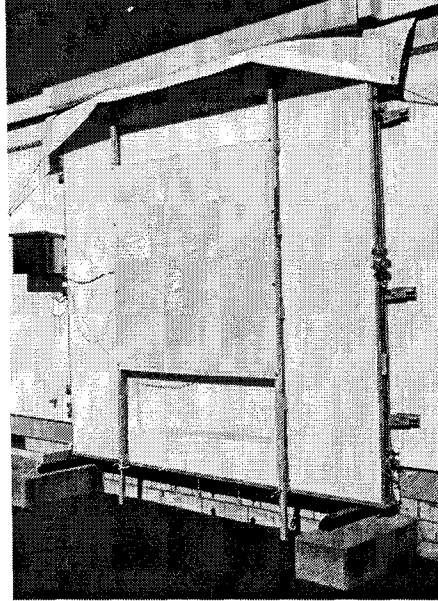


Figure 5.4. External shading screen mounted on the test cell.

### 5.2.2. Internal Shading Screen

An internal shading screen was mounted over the glazing unit and an experiment was run for a 20 day period from June 13 to July 2, 2005. Prior to running the experiment, there was a five day preconditioning phase with an opaque insulating foil covering the glazing unit. The internal screen was positioned 0.16 m from the surface of the glazing unit and 0.04 m from the internal surface of the external wall. The openness factor of the fabric [22] was found to be 10%, which is considered a semi-open weave fabric as shown in Figure 5.5. The screen was mounted so that air could move freely around the shading screen. The transmittance and reflectance of the shading screen were measured at near-normal incident angles from 250 nm to 2500 nm and are shown in Figure 5.6 revealing that the screen is not solar selective. The normal integral solar transmittance and reflectance were computed as 30.4% and 59.4%, respectively. The photograph shown in Figure 5.7 was taken from inside the test cell and shows the glazing unit covered by the internal shade.

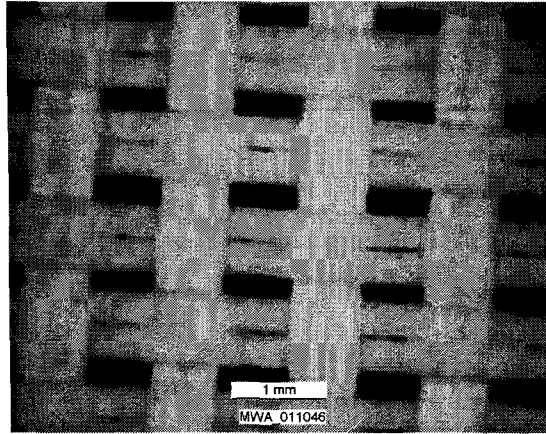


Figure 5.5. Photograph of the internal shading screen taken using a microscope.

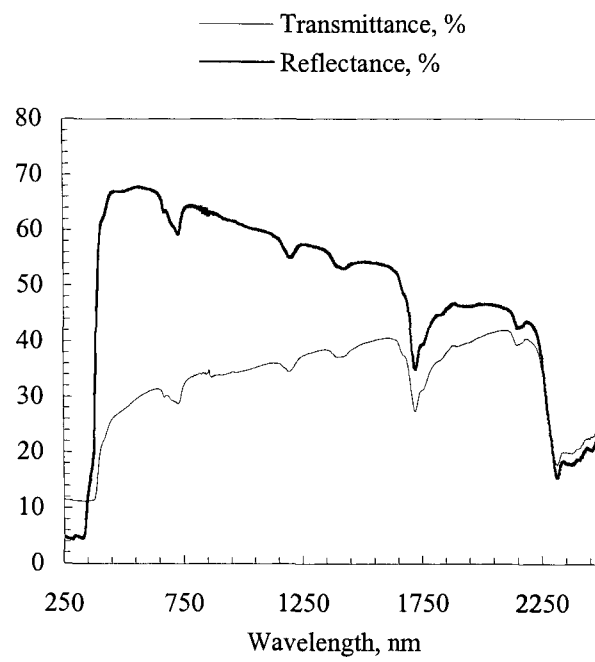


Figure 5.6. Transmittance and reflectance of the interior shade as a function of wavelength.

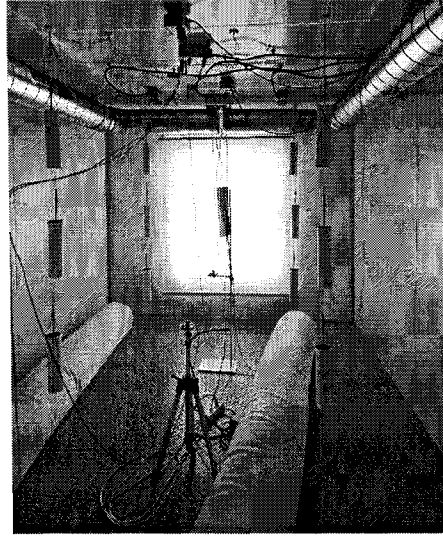


Figure 5.7. Internal shading screen mounted in the test cell.

### 5.3. Simulation Modeling

Both experiments were simulated using four building energy simulation programs: 1) EnergyPlus [17], 2) DOE-2.1e [18], 3) TRNSYS-TUD [19], and 4) ESP-r [20]. The same models described by [14] were used with the addition of internal and external shading devices. To maintain consistency between the models, the Perez 1990 [21] model for predicting solar radiation on tilted surfaces was used in all models. Because some of the thermal conductivities in the test cell were temperature dependent, the properties were fixed at the mean envelope temperatures for the construction elements shown in Table 5.1. The input parameters for the programs were exactly the same as in [14] and included outer envelope surface temperatures for all elements except the external wall, internal loads ( $\sim 160$  W), volume-weighted average cell air temperature, and weather data. The volume-weighted average test cell air temperatures were also averaged in time. For the duration of the experiments, the average temperatures for external and internal shading configurations were found to be  $22.50 \pm 0.072^\circ\text{C}$  and  $22.61 \pm 0.088^\circ\text{C}$ , respectively.

Table 5.1. Mean envelope temperatures for test cell construction elements during the experiments.

Element	Mean temperature, °C	
	External Screen	Internal Screen
Ceiling, East, West, and North Walls	22.58	22.83
Floor	22.34	22.75
South Wall	16.34	20.91

Air temperature stratification inside the cell was also considered. For the external screen experiment, the maximum, minimum, and average temperature differences for the maximum difference between any double shielded thermocouples for any given hour were 0.63 K, 0.13 K, and 0.36 K, respectively. The maximum, minimum, and average temperature differences for any given hour for the internal shading screen were 0.80 K, 0.13 K, and 0.31 K, respectively.

### 5.3.1. EnergyPlus

In the EnergyPlus optical model, all window layers such as glass panes and shading device(s), are assumed to be flat, parallel, and infinite. System reflectances and transmittances are computed based on a ray tracing technique. Spectral optical properties can be used for determining glazing reflectance and transmittance. The shading screen is, however, modeled using only a non-spectral method.

For these experiments, the integral solar transmittances and reflectances of the screen based on measurements were used as program inputs. The ratios of the open sides as well as the openness factors of the shading devices were calculated and entered into the program. The screen thickness was assumed to be 0.5 mm and estimates for screen thermal conductivities ( $0.9 \text{ Wm}^{-1}\text{K}^{-1}$ ) were taken from *ASHRAE Fundamentals* [22]; these parameters were of very minor importance. The methodology employed to calculate the total heat transfer between the shade and the window in the program was taken from EN ISO 15099 [23], which factored in surface temperatures of the glazing and the screens to calculate the heat transfer through the air gap at each time step. According to a methodology proposed in [24], the emittances of the shading screens were assumed to be the product  $0.9 \cdot (1 - \text{openness factor})$ . The calculation performed in EnergyPlus assumed buoyancy driven flow. Weather

data measured in 10 minute intervals were input into the program as boundary conditions. Measured direct-normal and diffuse horizontal solar irradiance were used to calculate the global vertical irradiance on the façade.

### **5.3.2. DOE-2.1E**

The optical model of DOE-2.1E is much simpler than the EnergyPlus model. The transmitted solar energy through the glazing unit is reduced by the integral solar transmittance of the shading screen (i.e., no solar radiation reflected from the glazing and then back-reflected into the room is taken into account). Because the outer surface temperature of the glazing unit and the screen were not known, a less robust method was used to account for the heat transfer in the gap between the shade and the window. The amount of additional heat transfer through the gap between the glazing and the shading screen was calculated assuming the same screen properties used for EnergyPlus and the thermal resistance for a well-ventilated air layer using EN ISO 6946 [25]. Hourly weather data in TMY2 weather format were inputs to the program and direct-normal and global horizontal solar irradiances were used to calculate the global vertical irradiance on the façade. The methodology described by [14] was used to input horizontal infrared irradiance into TMY2 weather format.

### **5.3.3. TRNSYS-TUD**

The TRNSYS-TUD window model consisted of a thermal and optical calculation algorithm. For the external shading device case, the only coupling between both algorithms was the solar absorptance of the glass panes that leads to heat sources in the panes. An equivalent thermal conductivity of the glazing cavity was calculated according to EN ISO 15099 and temperature dependent internal and external heat transfer coefficients were used. Interior and exterior shading devices were treated as additional heat transfer resistances.

Optical properties of the window construction were pre-calculated using WINDOW and OPTICS software [26, 27] based on spectral optical data for the different glass panes. The

model accounted for re-reflections between window, shading device, and inside wall surfaces.

If there was an internal shading device, then a convective component that represented solar radiation absorbed at the internal shading was directly linked to the air temperature node. The outside shading device consisted only of a transmittance shield that reduced irradiation at the outside surface of the window.

There was no algorithm implemented that calculates the impact of the air flow between window and shading devices or the heat transfer coefficients.

#### **5.3.4. ESP-r**

The two situations of external and internal free-hanging shading screens required the modeling of ventilation between the screen and the glazing. This was accomplished in ESP-r by modeling the gap between the shading screen and the glazing as a thermal zone. The advantage of modeling the air gap as a thermal zone is that the heat transfer processes of long-wave radiant exchange, surface convection and solar transmission, reflection, and absorption can be fully modeled. A network airflow model was defined to predict the airflow due to buoyancy in the case of the internal blind, and due to both buoyancy and wind pressure in the case of the external blind. There were uncertainties regarding suitable boundary pressure coefficients for the edge of the external blind, but the results were found to be not particularly sensitive to the chosen values.

For the external shading screen, the thermal zone representing the air gap between the screen and the window was modeled with the shading screen material on the external surface. The glazing unit separated the two thermal zones representing the test cell and the air gap. This was reversed for the internal shading screen, with the shading screen material separating the two thermal zones. The optical properties of the window (without shading screens) were obtained using the software WIS [28], given the optical properties at normal incidence for the two panes of glass. The calculated angular dependent transmission and absorption properties over the solar spectrum were then used in the ESP-r model. The thermophysical properties of the shading screens were assumed in a similar way to those described above for EnergyPlus.

Simulations were undertaken with six minute climatic data, using the measured direct-normal and diffuse horizontal irradiances. Measured temperatures from the test cell guard spaces were input as boundary conditions, together with the measured average test cell air temperature and internal fan power. The internal convection for all internal test cell surfaces, including those for the internal shading screen, was modeled using the buoyancy correlations reported by [29] for vertical and horizontal surfaces which take into account direction of heat flow, surface dimensions and temperature differences. Cooling power and internal surface temperatures were also predicted.

#### **5.4. Sensitivity Study**

Monte Carlo Analysis (MCA) and N-way factorial analysis were used to quantify the influence of experimental uncertainties on the input parameters and how they propagated through the programs and impacted output parameters; these analyses were only performed in EnergyPlus. Thorough descriptions of the methodologies used to perform the sensitivity studies are provided by [13]; robust quantifications of the uncertainties are provided by [12] and [14].

One and two-way factorial analyses were run to identify the sensitivity of the cooling power output to specific uncertainties in program input parameters and associated interactions. Tables 5.2 and 5.3 contain lists of the 10 input parameters that affected the cooling power the most and the overall uncertainty for each experiment averaged over the entire periods. Similar values for the forward and backward differencing for both experiments confirm the assumption of localized linear responses. From this analysis, it appears that uncertainties in the glazing properties play a much more prominent role in the overall error of the cooling power for the internal shading screen compared with the external shading screen.

Table 5.2. Overall uncertainty and 10 most influential parameters that impacted the cooling power uncertainty in Watts for the external screen experiment.

Parameter	Forward	Backward
Overall Uncertainty	3.04	3.04
Average Room Temperature	-1.83	1.83
Floor Temperature	1.29	-1.30
Ceiling Temperature	1.02	-1.02
Fan Power	0.908	-0.909
Outside Air Temperature	0.889	-0.889
East Wall Temperature	0.678	-0.679
North Wall Temperature	0.497	-0.498
West Wall Temperature	0.367	-0.368
Transmittance of the Outer Glass Pane	0.181	-0.189
Diffuse Solar Irradiance	0.173	-0.178

Table 5.3. Overall uncertainty and 10 most influential parameters that impacted the cooling power uncertainty in Watts for the internal screen experiment.

Parameter	Forward	Backward
Overall Uncertainty	2.74	2.70
Average Room Temperature	-1.39	1.40
Fan Power	0.893	-0.893
Outside Air Temperature	0.879	-0.878
North Wall Temperature	0.712	-0.712
Ceiling Temperature	0.604	-0.604
West Wall Temperature	0.477	-0.478
Front Reflectance Inner Pane	-0.406	0.302
Front Transmittance Outer Pane	0.395	-0.392
Floor Temperature	0.394	-0.395
Diffuse Solar Irradiance	0.369	-0.375

The MCA was run 120 times and the hourly results were tested for normal distributions using a Lilliefors Test for goodness of fit at a 1% significance level; there was no evidence that any of the hourly uncertainties were not normally distributed. The average uncertainties for the experiments with exterior and interior shades were 2.94 W and 2.66 W, respectively. Hourly uncertainties were used to calculate 95% credible limits for assessing the overall performance of the programs. These results corresponded quite well with the results from the factorial analyses (Tables 5.2 and 5.3).

## **5.5. Results**

Several parameters were compared to evaluate the overall performance of each building energy simulation program and are described in this section.

### **5.5.1. Cooling Power**

The measured cooling powers were compared with the predicted cooling powers for all four building energy simulation programs. Plots to compare the cooling powers for both the internal and external shading screens were constructed and are described in this section.

#### **5.5.1.1. External Shading Screen**

Plots to compare the measured cooling power with predicted quantities for the external shading screen are shown in Figure 5.8. The plots include error bars that contain 95% credible limits from the experiment and 95% credible limits from the MCA fixed to the simulation results. Additional information about the cooling power predictions is provided in Figure 5.9, where the maximum, mean, and minimum absolute differences between measured and predicted cooling powers are displayed.

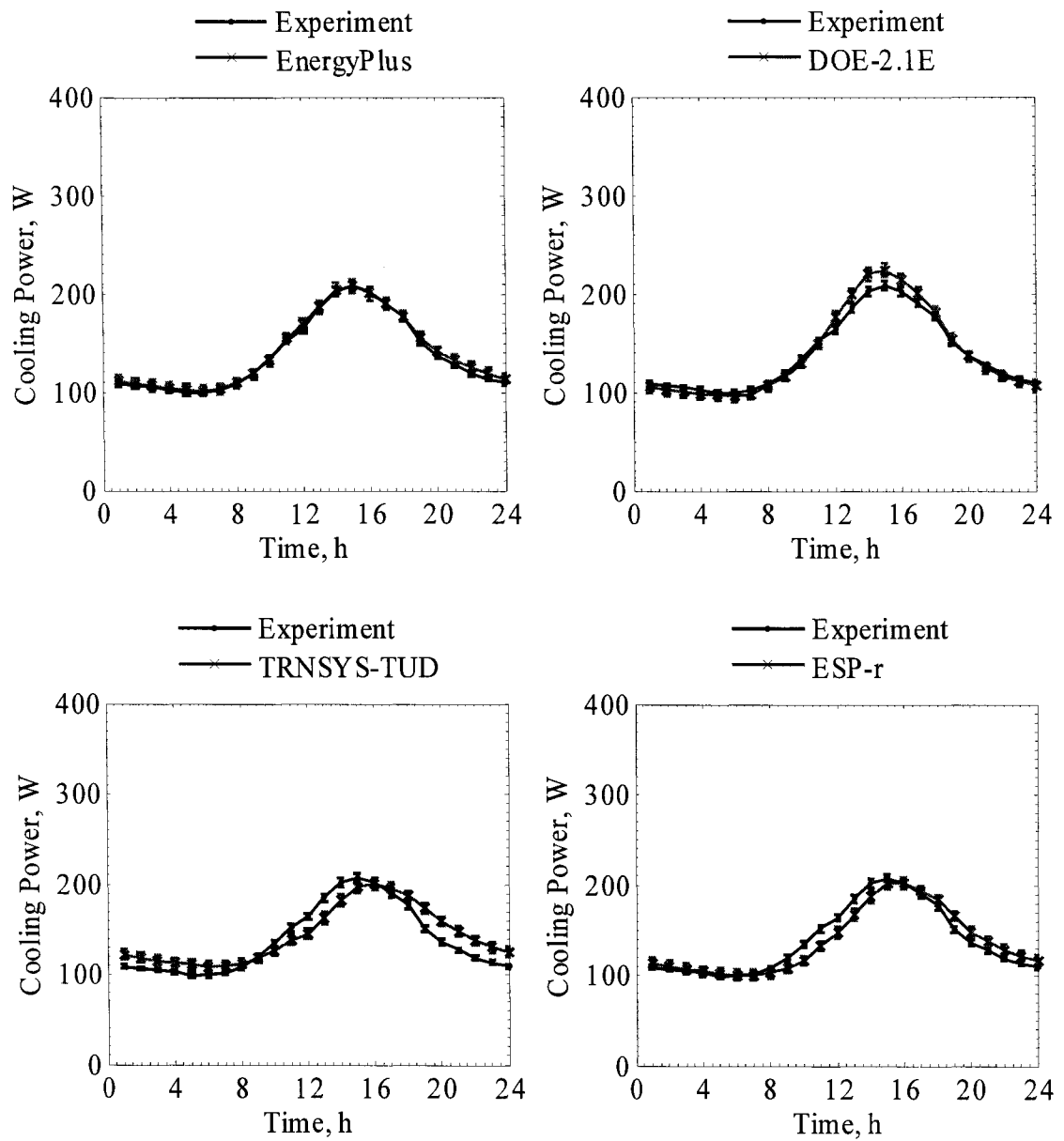


Figure 5.8. Cooling power comparisons averaged over a given hour of the day for the external shading screen experiment (480 h).

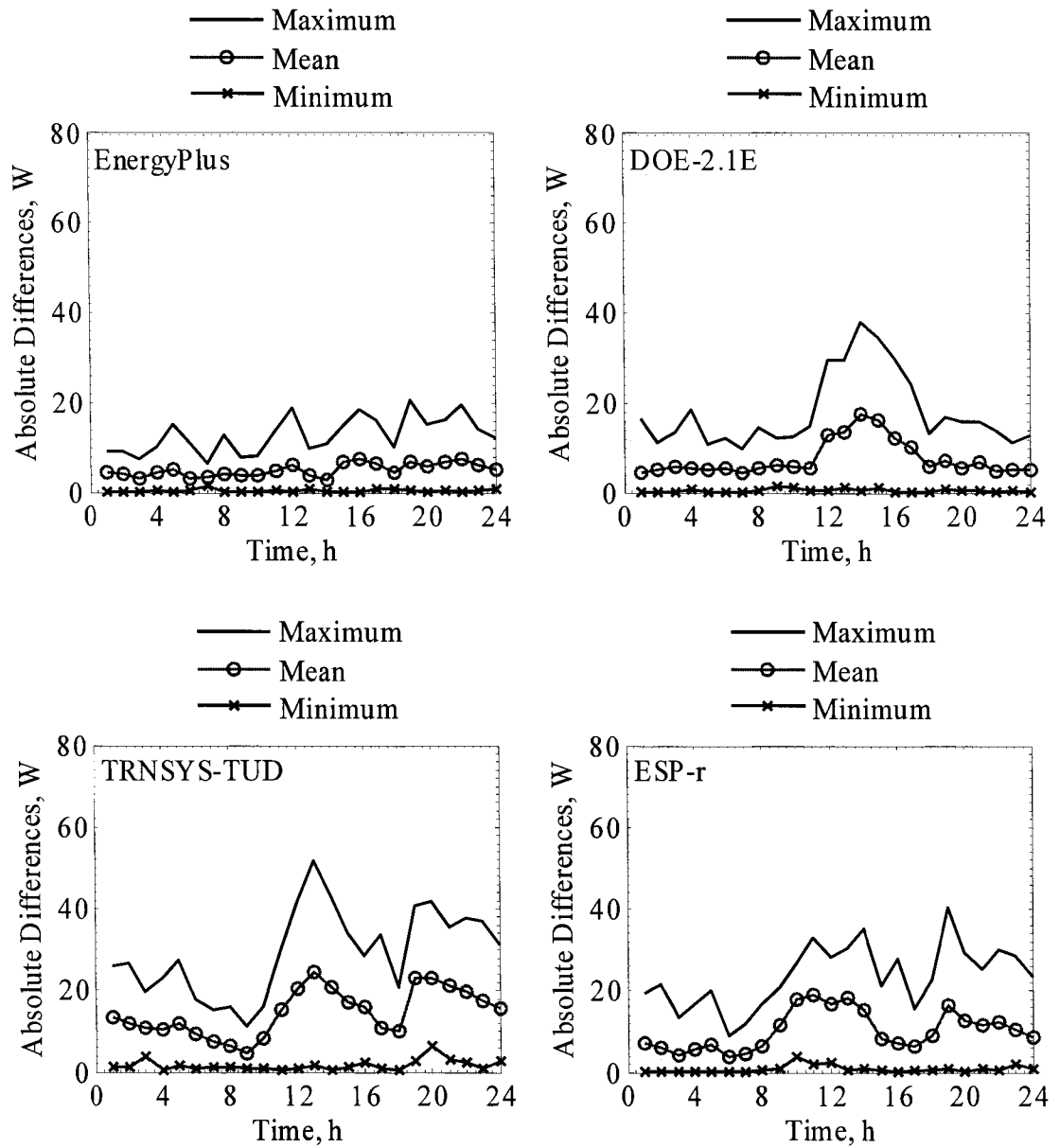


Figure 5.9. Absolute maximum, mean, and minimum differences between measured and predicted cooling power for the external shading screen at any given hour of the day (480 h).

### 5.5.1.2. Internal Shading Screen

Similar plots were constructed for experiment with the internal shading screen. The cooling power plots and the maximum, mean, and minimum absolute difference plots for each program are shown in Figures 5.10 and 5.11, respectively.

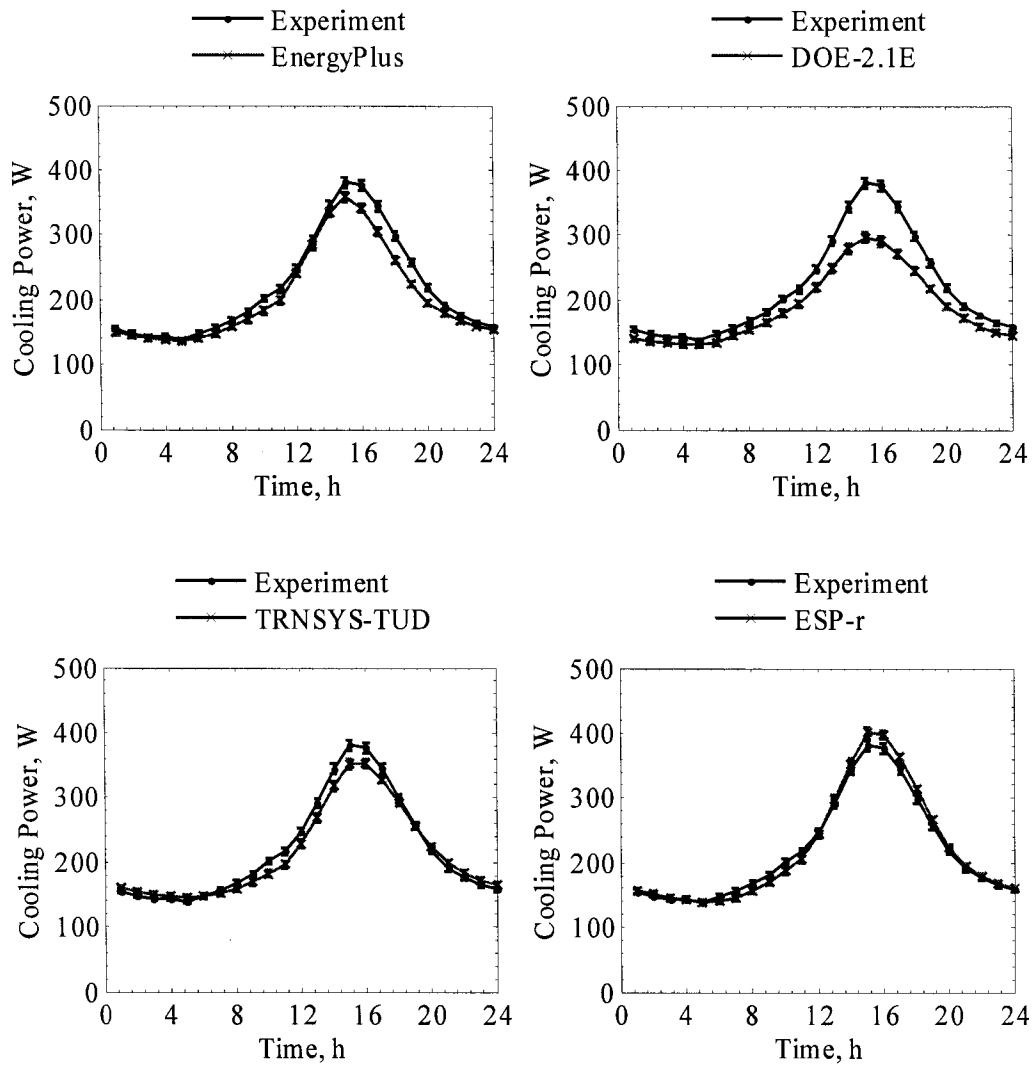


Figure 5.10. Cooling power comparisons averaged over a given hour of the day for the internal shading screen experiment (480 h).

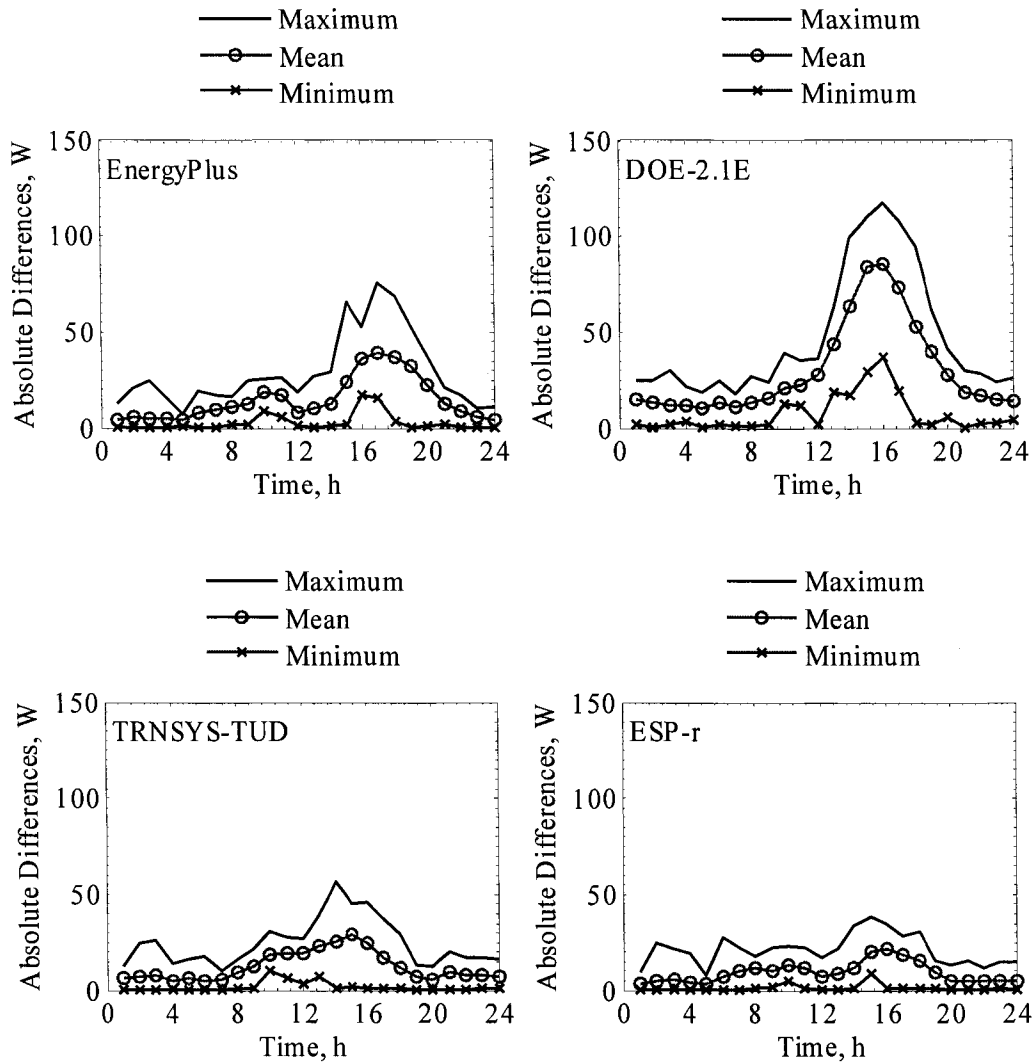


Figure 5.11. Absolute maximum, mean, and average differences between measured and predicted cooling power for the internal shading screen at any given hour of the day (480 h).

### 5.5.1.3 Statistical Comparisons

Statistical analyses employing formulations proposed by [12] were used to quantify the difference between the experimental results and predictions for the cooling powers. A useful

quantify developed to indicate whether a building energy simulation program was validated within 95% credible limits is the uncertainty ratio shown in Equation 5.1. The programs were considered validated within 95% credible limits if the uncertainty was less than or equal to unity.

$$UR = \frac{|D|}{OU_{Exp} + OU_{E+}} \quad (5.1)$$

The statistical comparisons for the external and internal shading screen experiments are shown in Tables 5.4 and 5.5, respectively.

Table 5.4. Statistical and comparative parameters of cooling power for the external shading screen experiment.

	Experiment	EnergyPlus	DOE-2.1E	TRNSYS-TUD	ESP-r
$\bar{x}$	138.6 W	140.7 W	140.1 W	143.5 W	137.6 W
$s$	50.4 W	48.1 W	57.1 W	42.5 W	48.7 W
$x_{max}$	317.4 W	303.4 W	337.0 W	290.9 W	310.2 W
$x_{min}$	73.2 W	84.5 W	83.0 W	91.0 W	82.0 W
$\bar{D}$	-	-2.11 W	-1.58 W	-4.92 W	0.92 W
$ \bar{D} $	-	5.09 W	7.59 W	14.61 W	10.33 W
$D_{max}$	-	20.69 W	38.12 W	51.74 W	40.36 W
$D_{min}$	-	0.01 W	0.07 W	0.40 W	0.02 W
$D_{rms}$	-	6.54 W	10.32 W	18.08 W	13.30 W
$D_{95\%}$	-	13.28 W	23.93 W	35.84 W	26.79 W
$\overline{OU}$	3.14 W	5.78 W	-	-	-
$\overline{UR}$	-	0.58	0.80	1.61	1.14 W
$UR_{max}$	-	2.65	2.77	5.14	4.10 W
$UR_{min}$	-	0.00	0.01	0.05	0.00 W
$ \bar{D} /\bar{x} \times 100\%$	-	3.7%	5.5%	10.6%	7.5%
$\bar{D}/\bar{x} \times 100\%$	-	-1.5%	-1.1%	-3.6%	0.7%

Table 5.5. Statistical and comparative parameters of cooling power for the internal shading screen experiment.

	Experiment	EnergyPlus	DOE-2.1E	TRNSYS-TUD	ESP-r
$\bar{x}$	218.7 W	204.8 W	188.9 W	212.8 W	221.2 W
$s$	85.2 W	76.5 W	58.8 W	74.4 W	92.1 W
$x_{max}$	459.4 W	419.5 W	342.0 W	426.3 W	477.4 W
$x_{min}$	100.6 W	119.9 W	119.0 W	124.5 W	116.7 W
$\bar{D}$	-	13.9 W	29.7 W	5.9 W	-2.5 W
$ \bar{D} $	-	14.7 W	30.1 W	12.5 W	9.4 W
$D_{max}$	-	75.7 W	117.4 W	56.6 W	38.7 W
$D_{min}$	-	0.1 W	0.0 W	0.1 W	0.0 W
$D_{rms}$	-	20.2 W	40.6 W	16.2 W	12.3 W
$D_{95\%}$	-	44.0 W	94.8 W	34.6 W	25.7 W
$\overline{OU}$	4.9 W	5.2 W	-	-	-
$\overline{UR}$	-	1.35	2.58	1.14	0.90
$UR_{max}$	-	5.85	7.68	3.74	3.52
$UR_{min}$	-	0.01	0.00	0.01	0.00
$ \bar{D} /\bar{x} \times 100\%$	-	6.7%	13.8%	5.7%	4.3%
$\bar{D}/\bar{x} \times 100\%$	-	6.4%	13.6%	2.7%	-1.1%

### 5.5.2. Transmitted Solar Power

For comparative purposes to identify differences in the program algorithms, the predictions for transmitted solar power through the window were compared. This parameter refers to the heat gain of the room due only to short-wave solar radiation and does not include secondary heat gain. Figures 5.12 and 5.13 contain predictions for any given hour for the external and internal shading screen experiments, respectively, for all four building energy simulation programs.

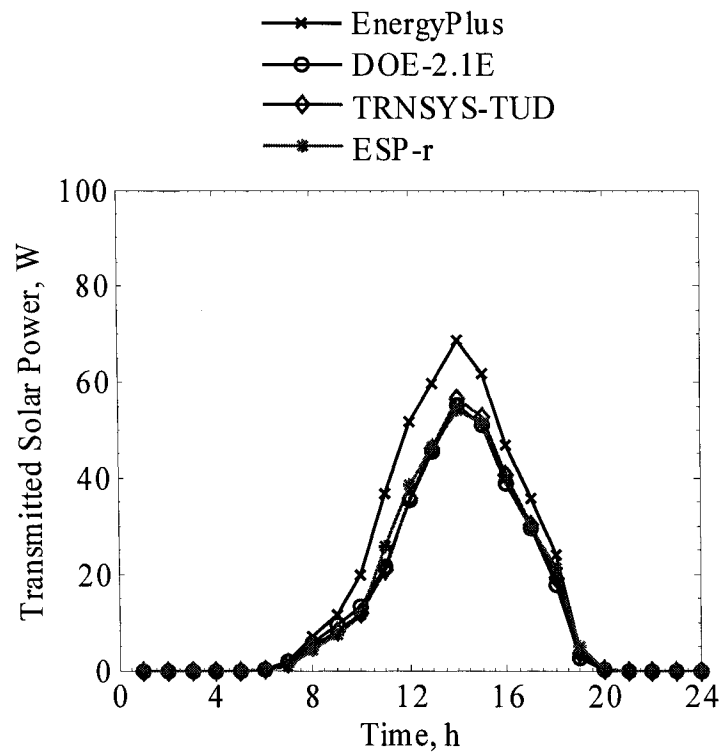


Figure 5.12. Predicted transmitted solar power for a given hour of the day during the external shading screen experiment (480 h).

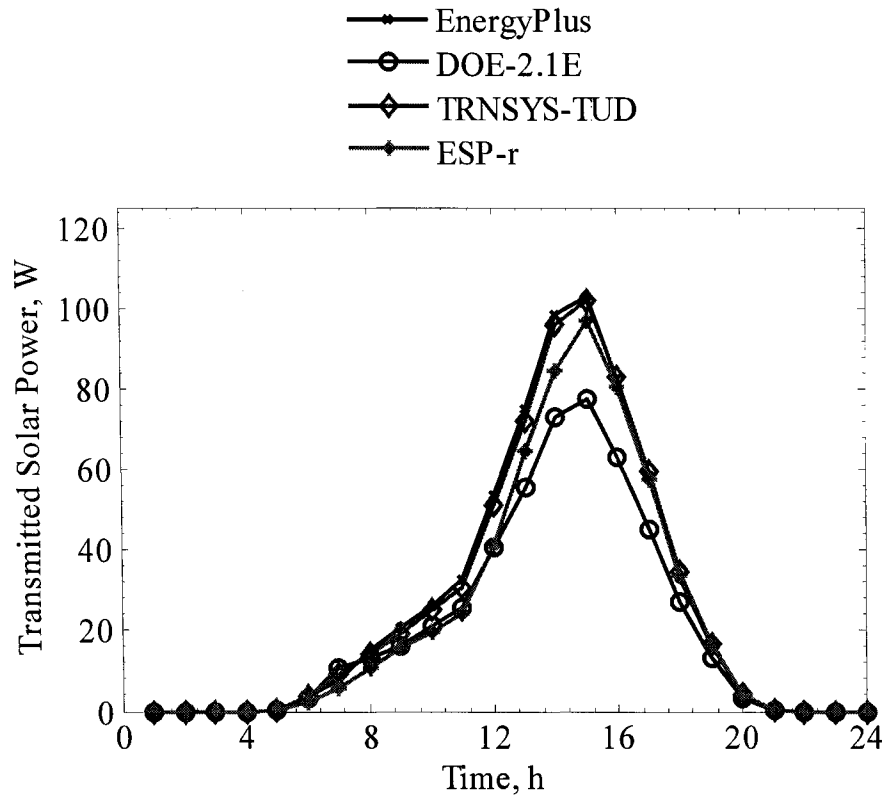


Figure 5.13. Predicted transmitted solar power for a given hour of the day during the internal shading screen experiment (480 h).

## 5.6. Discussion

Overall comparisons of the performances of the building energy simulation programs indicate that, strictly speaking, the cooling power predictions for the external shading screen experiment using EnergyPlus and DOE-2.1E were validated within 95% credible limits (shown by the average uncertainty ratio); the cooling power predictions for the internal shading screen experiment were only validated within these 95% credible limits for ESP-r.

More in-depth comparisons of the overall cooling energy can be made using mean differences described in the statistical analyses for both experiments. For the external shading screen experiment, the mean differences for EnergyPlus, DOE-2.1E, TRNSYS-TUD, and ESP-r were 2.11 W, 1.58 W, 4.92 W, and -0.92 W, respectively. When comparing these

values with the sum of the average overall 95% credible limits ( $3.14 \text{ W} + 5.78 \text{ W} = 8.92 \text{ W}$ ), all programs accurately computed the amount of cooling energy required to account for energy paths into and out of the cell for the entire experiment. For the instantaneous cooling power predictions from the external shading experiment, the mean absolute difference is an important parameter for comparisons. For EnergyPlus, DOE-2.1E, TRNSYS-TUD, and ESP-r the mean absolute differences were 5.09 W, 7.59 W, 14.61 W, and 10.33 W, respectively. For TRNSYS-TUD, there appears to be an offset which may indicate a slightly different test cell time constant and the results from ESP-r seem to be shifted by one hour but very accurate otherwise. A comparative validation (Figure 12) using the transmitted solar power shows that there was very little difference between the predicted transmitted power into the test cell between DOE-2.1E, TRNSYS-TUD, and ESP-r and slight differences with EnergyPlus. In DOE-2.1E, the solar properties of the shading screen were described using only solar transmittance, whereas in EnergyPlus, the solar transmittance and reflectances were used for calculating the transmitted solar power (accounting for higher order reflections and transmissions resulting in more solar irradiance entering the test cell). A similar experiment performed with just a glazing unit [14] without shading showed that the transmitted solar powers were nearly identical for all four building energy simulation programs, which indicates that the differences were primarily due to the modeling of the shading screen. But because these differences were small and DOE-2.1E predicts more required cooling power than EnergyPlus and TRNSYS-TUD and ESP-r results were shifted, differences in the predictions must be due to modeling mechanisms for internal heat transfer within test cell which could include: convective heat transfer coefficients, radiative heat transfer (geometrical view factors or constant coefficients), algorithms used to approximate transient conduction, and modeling thermal bridges, rather than differences between the solar processing algorithms.

Predictions from the internal shading screen experiment were much less accurate for EnergyPlus and DOE-2.1e than those seen in the external shading screen experiment and more accurate for TRNSYS-TUD and ESP-r, where the modeling of the shading device and air gap appear to more accurately account for all mechanisms of heat transfer. Only ESP-r

was validated within 95% credible limits for this experiment. All the simulations under-predicted the amount of cooling power required to offset the thermal load in the cell except ESP-r, which over-predicting it. Evaluating the cooling power predictions, the mean differences for EnergyPlus, DOE-2.1E, and TRNSYS-TUD were 13.9 W, 29.7 W, 5.9 W, and -2.5, respectively. Comparing these quantities to the sum of the uncertainties ( $4.95 \text{ W} + 5.22 \text{ W} = 10.17 \text{ W}$ ), TRNSYS-TUD and ESP-r's predictions were within average overlapping uncertainties. Similar comparisons can be made for cooling power to assess the instantaneous predictions, the mean absolute differences for EnergyPlus, DOE-2.1E, TRNSYS-TUD, and ESP-r were 14.7 W, 30.1 W, 12.5 W, and 9.4 W, respectively. The EnergyPlus and DOE-2.1E mean absolute differences are very close to the mean differences, which indicates that there were systematic under-predictions during the entire experiment; this was not true for TRNSYS-TUD where over-predictions occurred during the night and under-predictions during the day and in ESP-r, where there were under-predictions in the morning and over-predictions in the afternoon. The under-predictions during the day in EnergyPlus, DOE-2.1E, and TRNSYS-TUD may be a result of the semi-open weave fabric that was used that may have been impacted by the assumptions made for simulating the longwave and convective heat exchange in the gap and through the screen (Figure 5.5). Comparisons of the predicted transmitted solar powers (Figure 5.13) into the test cell reveal similar patterns seen in the external shading screen experiment, but, due to shade properties, retransmitted solar power is much more important. In this experiment, both TRNSYS-TUD and ESP-r account for retransmitted solar power. Many differences between program cooling power predictions must again be attributed to effects other than the solar processors.

## 5.7. Conclusions

The results reveal the limitations that can be expected when modeling scattering shading screens in building energy simulation programs. Even for relatively simple cases where almost all input parameters are well-defined, results from even the most robust building energy simulation programs are not always within experimental uncertainties as seen in the internal shading screen experiment.

An additional limitation of the shading algorithms in these building energy simulation programs is the failure to account for solar selective shading screens. For all of the programs, integral transmittances and, in some programs, reflectances were required inputs. Because the optical properties of the shading screens used in this study did not significantly depend on wavelength in the solar spectrum, overall transmittance was affected only to a minor extent due to these modeling deficiencies. However, for solar-selective shading screens, these inputs would have failed to adequately address the overall transmission through a solar selective glazing unit and shading screen. However, these studies were beyond the scope of this validation and will need to be addressed in future studies.

### Acknowledgements

We gratefully acknowledge the financial support of the Swiss Federal Office of Energy (BFE) for building and testing the experimental facility (Project 17'166) as well as the funding for EMPA participation in IEA Task 34/43 (Project 100'765). We would also like to acknowledge the many contributions from: R. Blessing, M. Camenzind, K. Meyer, T. Nussbaumer, and R. Vonbank.

### Nomenclature

$D$	= difference between experiment and predicted values for a given hour, W
$\bar{D}$	= mean difference, W
$ \bar{D} $	= mean absolute difference, W
$D_{max}$	= maximum difference between experimental and predicted values for a given array, W
$D_{min}$	= minimum difference between experimental and predicted values for a given array, W
$D_{rms}$	= root mean squared difference between experimental and predicted values for a given array, W
$D_{95\%}$	= ninety-fifth percentile of the differences between experimental and predicted values for a given array, W
$OU_{Exp}$	= 95% credible limits or overall uncertainty from experiment for a given hour, W
$OU_{E+}$	= 95% credible limits or overall uncertainty from MCA for a given hour, W
$\overline{OU}$	= average overall uncertainty calculated for 95% credible limits, W

$UR$	= uncertainty ratio for a given hour, no units
$\overline{UR}$	= arithmetic mean of the uncertainty ratio, no unit
$UR_{max}$	= maximum uncertainty ratio, no units
$UR_{min}$	= minimum uncertainty ratio, no units
$\bar{x}$	= arithmetic mean for a given array of data, W
$x_{min}$	= minimum quantity for a given array of data, W
$x_{max}$	= maximum quantity for a given array of data, W

## References

- [1] J.A. Clarke, *Energy simulation in building design*, Butterworth Heinemann, Oxford, 2001
- [2] B.D. Hunn, J.W. Jones, M.M. Grasso, and J.D. Hitzfelder, Effectiveness of shading devices on buildings in heat-dominated climates, *ASHRAE Transactions* Vol. 99(1), 1993, 207-222
- [3] G.A. Florides, S.A. Kalogirou, S.A. Tassou, and L.C. Wrobel, Modeling of the modern houses of Cyprus and energy consumption analysis, *Energy* 25, 2000, 915-937
- [4] R.D. Judkoff, Validation of Building Energy Analysis Simulation Programs at the Solar Energy Research Institute, *Energy and Buildings*, 10, 1998, 221-239,
- [5] P. Strachan, Model Validation using the PASSYS Test Cells, *Building and Environment* 28, 1993, 153-165
- [6] P. Wouters, L. Vandaele, P. Voit, N. Fisch, The use of outdoor test cells for thermal and solar building research within the PASSYS project, *Building and Environment* 28, 1993, 107-113
- [7] S.Ø. Jensen, Validation of building energy simulation programs: a methodology, *Energy and Buildings* 22, 1995, 133-144
- [8] K.J. Lomas, H. Eppel, C.J. Martin, D.P. Bloomfield, Empirical validation of building energy simulation programs, *Energy and Buildings* 26, 1997, 253-275
- [9] S. Moinard, G. Guyon, *Empirical Validation of EDF ETNA and GENEC Test-Cell Models*, A Report of Task 22, Project A.3 Empirical Validation, International Energy Agency, 1999
- [10] P.G. Loutzenhiser and G.M. Maxwell, A Comparison of DOE-2.1E Daylighting and HVAC System Interactions to Actual Building Performance, (Revised and submitted to *ASHRAE Transactions* January 12, 2006)
- [11] G.M. Maxwell, P.G. Loutzenhiser, and C.J. Klaassen, *Daylighting – HVAC Interaction Tests for the Empirical Validation of Building Energy Analysis Tools*, A Report of Task 22 Subtask D. Building Energy Analysis Tools Project D Empirical Validation. [http://www.iea-shc.org/task22/reports/IEA\\_Daylighting\\_Report\\_Final.pdf](http://www.iea-shc.org/task22/reports/IEA_Daylighting_Report_Final.pdf), 2003
- [12] H. Manz, P. Loutzenhiser, T. Frank, P.A. Strachan, R. Bindi, and G. Maxwell. (Accepted for publication in *Building and Environment* and available online September 8, 2005 at [www.sciencedirect.com](http://www.sciencedirect.com)) Series of experiments for empirical validation of solar gain modeling in building energy simulation codes – Experimental setup, test cell characterization, specifications and uncertainty analysis.

- [13] P.G. Loutzenhiser, H. Manz, C. Felsmann, P.A. Strachan, T. Frank, and G.M. Maxwell, (Submitted July 14, 2005 to *Solar Energy*), Empirical validation of models to compute solar irradiance on inclined surfaces for building energy simulation.
- [14] P.G. Loutzenhiser, H. Manz, P.A. Strachan, C. Felsmann, T. Frank, G.M. Maxwell, and P. Oelhafen, An Empirical Validation of Solar Gain Models Found in Building Energy Simulation Programs, (Submitted to *HVAC&R Research* on November 24, 2005)
- [15] European Standard EN 410. Glass in building – Determination of luminous and solar characteristics of glazing. European Committee for Standardization, Brussels, Belgium, 1998
- [16] GLAD Software. Swiss Federal Laboratories for Materials Testing and Research (EMPA), Duebendorf, Switzerland, 2002
- [17] EnergyPlus 1.2.3.023 Building energy simulation code, [www.energyplus.gov](http://www.energyplus.gov), 2005
- [18] DOE-2.1E(Version-119) Building Energy Simulation Code, Lawrence Berkley National Laboratories (LBNL), Berkley, CA, April 9, 2002
- [19] TRNSYS-TUD Technical University of Dresden research code based on the frame of TRNSYS 14.2, Solar Energy Laboratory, University of Wisconsin-Madison, Madison, WI, 2005
- [20] ESP-r Software (Version 10.12). Building Energy Simulation Code. University of Strathclyde, Glasgow, <http://www.esru.strath.ac.uk>, 2005
- [21] R. Perez, P. Ineichen, R. Seals, J. Michalsky, and R. Stewart, Modeling daylight availability and irradiance components from direct and global irradiance. *Solar Energy* Vol. 44 No.5, 1990, 271-289
- [22] ASHRAE, *2001 ASHRAE Handbook of Fundamentals SI Edition*, Atlanta: America Society of Heating, Refrigeration and Air-Conditioning Engineers, Inc, 2001
- [23] ISO/FDIS 15099: 2003(E), Thermal performances of windows, doors, and shading devices—Detailed calculations, 2003
- [24] EnergyPlus, Input Output Reference, Board of Trustees of University of Illinois and the University of California through Orlando Lawrence Berkley Laboratories, October 11, 2005
- [25] EN ISO 6946, Building components and building elements – Thermal resistance and thermal transmittance –Calculation Method, August 1996
- [26] WINDOW 5.2a Version 5.2.17a, LBNL
- [27] OPTICS 5, LBNL
- [28] WIS, Window Information System, <http://windat.ucd.ie/wis/html/index.html>, 2004

- [29] F. Alamdari and G.P. Hammond, Improved Data Correlation for Buoyancy-Driven Convection in Rooms, Building Services Engineering Research and Technology, Vol.4, 1983, 106-112

## **Chapter 6: Empirical validations of solar gain models for a glazing unit with exterior Venetian blinds**

A paper to be submitted to Energy and Buildings

P.G. Loutzenhiser<sup>1,2,a</sup>, H. Manz<sup>1,b</sup>, G.M. Maxwell<sup>2,c</sup>

<sup>1</sup> Swiss Federal Laboratories for Materials Testing and Research (EMPA), Laboratory for Building Technologies, CH-8600 Duebendorf, Switzerland

<sup>2</sup> Iowa State University, Department of Mechanical Engineering, Ames, Iowa 50011 USA

<sup>a</sup> Wrote the text and ran the EnergyPlus Simulation

<sup>b</sup> Supervised the text writing

<sup>c</sup> Provided technical support

### **Abstract**

Experiments performed at the Swiss Federal Laboratories for Materials Testing and Research (EMPA) test cell located in Duebendorf, Switzerland were used for empirical validations of building energy simulation programs. Two experiments were run with exterior Venetian blinds mounted over a glazing unit with the blinds in the horizontal position and the blind slat tilted 45° with the outer slat edge toward the ground. A model of the facility was constructed in EnergyPlus and the measured cooling power in the test cell was compared with the predicted cooling power from EnergyPlus for both experiments. When the blind slats were horizontal and tilted 45° downward, the results were within 95% credible limits. The absolute average differences for the horizontal and tilted 45° downward experiments were 4.4% and 3.8%, respectively. The paper also contains detailed information concerning the blind slat optical properties and robust sensitivity analyses.

### **6.1. Introduction**

The modern office buildings are being designed to link today's occupants to their environments and provide daylight on the work planes by using highly glazed façades. Shading devices enable control to office dwellers to manage the extent of their interactions with the outside world. Venetian blinds are very popular shading devices that are used in office spaces around the world and play an integral role in reducing solar gains in the

summer and transmitting solar energy to the space in the winter through windows to offset of heating requirements. They also provide flexibility to the occupants for eliminating beam radiation into the space and prevent glare while still allowing diffuse natural light to enter. When exterior Venetian blinds are installed over the windows, the energy absorbed by the blind assembly, for the most part, remains outside of the office space, which is highly advantageous in order to reduce overheating of the building.

Quantifying the impact of both interior and exterior blinds has been the focus of prior research. A great deal of experimental work has been undertaken to examine various permutations of Venetian blinds and windows in order to better understand and model the solar optical behavior and different heat transfer mechanisms (longwave radiation, air flow patterns and convective heat transfer) [1-8]. Using some of these experiments, validated models have been constructed for simulating the impact of blinds outside of the laboratory for practical analysis of actual window/blind assemblies for construction buildings [9-17].

Implementing models like these into building energy simulation programs increases the potency of the software—making them powerful tools for designing modern buildings optimized for energy efficiency and user comfort. Building energy simulation programs can be employed to evaluate different window/shading combinations prior to constructing a building and provide valuable information for assessing annual energy performance and sizing heating, ventilation, and air-conditioning equipment. There are different levels of complexities for blind simulations that are currently used in building energy simulation programs and subsidiary software. Various standards and handbooks provide guidance for estimating the impact of blind assemblies as a function of slat angle and properties that range from very simple to very complicated in their method and application.

The simplest methods rely on estimating an unshaded fraction where direct irradiance can penetrate the space and, for simplicity sake, assume the rest of the irradiation is diffuse. General guidelines for approximating the impact of blinds, especially solar heat gain coefficients, are provided by [18].

More robust methods outlined in several standards use viewfactor approaches for estimating radiative transfer through blind assemblies. The calculation procedures given in

prEN 13363-2 [19] assume the blinds are adjusted to eliminate direct irradiance as well as flat diffuse reflecting and transmitting slats. For each blind slat, a view factor is computed for the entire slat for estimating diffuse transmittance and a second blind slat view factor is determined to account for direct-diffuse transmissions and reflections. The standard does not consider the wavelength-dependence of optical properties of glazing and blind properties. Additional calculations for longwave radiation transmittance are also provided.

A similar strategy is employed in ISO/FDIS 15099:2003 [20]. Here the blind slats are divided up in five equal segments and diffuse view factors are calculated for all surfaces, including the glazing unit. The curvature of the blind slat is also ignored and direct-direct, direct-diffuse, and diffuse-diffuse transmissions and reflections are computed as a function of wavelength. Integral solar and visible properties can then be calculated.

Programs are also available for evaluating glazing units with blind assemblies. WIS [21] can compute angular dependent overall transmittance and reflectance using spectral glazing and blind slat properties. The software also accounts for curvature in the blind slats and uses both view factor and ray tracing methods.

Before using building energy simulation programs in actual practice, an intense regiment of validations should be pursued to ensure that the programs are performing as intended. Judkoff [22] identifies three different types of validations, namely: 1) analytical, 2) comparative, and 3) empirical validations and describes the advantages and disadvantages, applications, and the importance of each type of validation approach. Because empirical validations are relatively expensive to perform, only a few studies using building energy simulation programs have been undertaken.

Test cells provide a unique environment for empirical validations and lie between a carefully controlled laboratory environment and an actual building. They have the advantage that the inside cell boundary conditions can be well-controlled while also maintaining an environment that is similar to an actual office space envelope (i.e. dimensions, optical and thermophysical properties, air flow patterns). The PASSYS project [23-25] used test cells situated throughout Europe to evaluate ESP-r. The International Energy Agency's (IEA) Annex 21/ Task 8 [26] also used test cells to assess the performances of programs. Further

investigations were performed in IEA Task 22 in two test cells at different locations in Europe [27, 28, 29].

This research focuses on empirical validation of solar gain algorithms for a solar selective glazing unit with exterior mounted Venetian blind slats positioned horizontally and tilted  $45^\circ$  with the outer edge the slat towards the ground. The experiments were performed in a test cell located on the Swiss Federal Laboratories for Material Testing and Research (EMPA) on the campus in Duebendorf, Switzerland. The series of experiments was conducted in conjunction with IEA Task 34/Annex 43 Subtask C. Prior work has been completed that characterized the test cell [30], examined radiation models on tilted surfaces [31], and evaluated solar gain models in building energy simulation programs through a glazing unit without [32] and with [33] shading screens. In addition to the information described in these previous studies, thorough documentation of optical properties, construction, and mounting of the external Venetian blinds are described in this paper.

The building energy simulation program EnergyPlus [34] was evaluated using experimental data to predict the cooling power required to maintain a fixed temperature in the test cell. These results were accompanied by sensitivity analyses designed to evaluate the impact of experimental uncertainties and how they propagated through building energy simulation program and the robustness of EnergyPlus.

## 6.2. Experiment

The EMPA test cells are located on the institution's Duebendorf campus in Switzerland. The longitude, latitude, and altitude above sea level are  $8.6^\circ\text{E}$ ,  $47.4^\circ\text{N}$  and 430 m, respectively. The interior building elements (floor, ceiling, and interior walls) are all adjacent to a temperature controlled guarded zone for better definition of boundary conditions, and the exterior wall faces  $29^\circ$  West of South. The facility meets all nine criteria for a high-quality data set for empirical validation [26]. Additional information about the test cell (i.e. dimensions, thermophysical properties, thermal bridges etc.) is described by [30].

Two experiments were run for 20 day periods in the test cell with exterior Venetian blinds. The slats in the horizontal position and tilted  $45^\circ$  downward (outer slat edge pointed towards the ground) experiments were performed from July 24 to August 12, 2005 and August 17 to September 5, 2005, respectively. The test cell was configured to maintain a near-constant temperature by adjusting the cooling power. A photograph taken from outside shows the test cell during the experiment when the blinds were in the horizontal position (refer to Figure 6.1). Boundary conditions and Venetian blind slat optical properties are provided in this section. Other information pertaining to the test cell construction and glazing unit are provided by [30] and [32], respectively. Prior to the experiment, a computational fluid dynamics (CFD) model was constructed to examine airflow and temperature patterns around the blinds assuming natural convection. Heat source assigned to the blind slats were used to model solar irradiance. The velocity and temperature patterns around the blinds when in the horizontal slat position are shown in Figure 6.2.

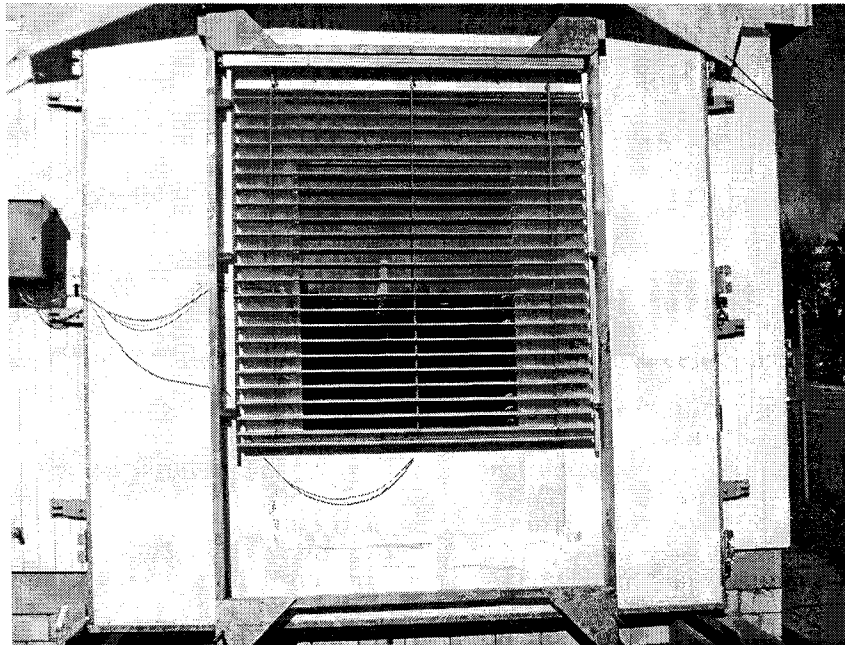


Figure 6.1. Venetian blind assembly mounted over the test cell glazing unit.

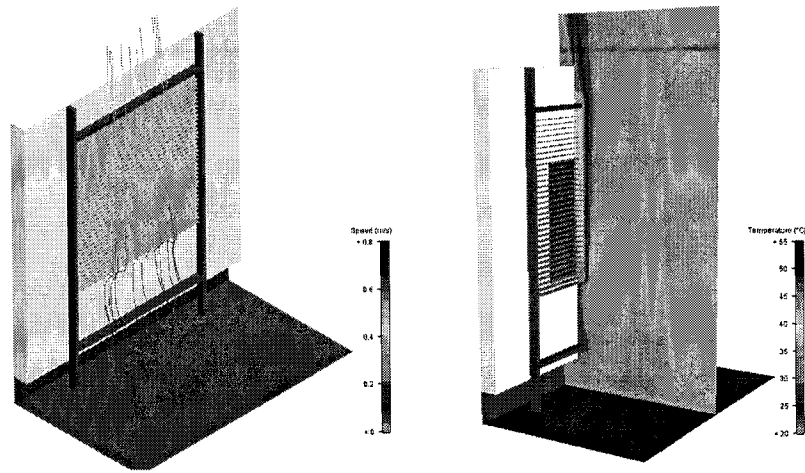


Figure 6.2. Airflow and temperature patterns around the blind slats from a CFD analysis.

### 6.2.1. Boundary Conditions

The outer surface temperatures for the construction elements adjacent to the guarded zone were used as inputs to the building energy simulation programs in hourly averaged increments. During the experiment, the air temperature inside the test cell was measured by 18 double-shielded thermocouples and the volume averaged temperatures averaged over each hour were used as inputs for the programs. The mean air temperatures also averaged in time for experiments in the horizontal and 45° downward slat positions were  $22.64 \pm 0.09^\circ\text{C}$  and  $22.62 \pm 0.08^\circ\text{C}$ , respectively. The conditioned air entered the test cell through two textile ducts on the floors and exited through metal ducts hanging slightly below the ceiling. This configuration was used to reduce temperature stratification in the test cell. The mean, maximum, and minimum temperature differences between the thermocouples that recorded the highest and lowest temperatures for a given hour during experiment when the slats were horizontally positioned were 0.25 K, 0.59 K, and 0.13 K, respectively, and were 0.22 K, 0.41 K, and 0.12 K, respectively, when the slats were tilted 45° downward. The temperature dependent thermal conductivities of the construction elements were fixed using the mean temperature in the elements for each experiment.

### 6.2.2. Blind Slat Properties

The properties of the blind slats were measured for effective simulation of the blind assembly. Wavelength dependent reflectance was measured at near-normal incident angles from 250 nm to 2500 nm shown in Figure 6.3. The integral reflectance was computed using Glad Software [35] according to EN 410 [36]. The hemispherical emittance of the blind slats was measured using an emissometer based on a calorimetric method. The computed properties are shown in Table 6.1. A detailed drawing of the two blind slats that describes the slat geometry, orientation, and distance from the outer window pane is provided in Figure 6.4. The slats were rotated around the center when 45° tilted and, thus, the distance between slat edge and the glazing increased.

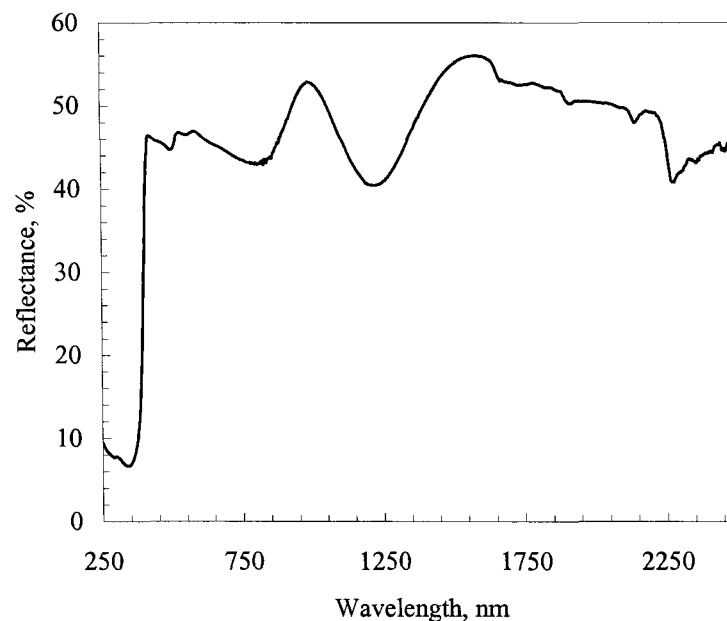


Figure 6.3. Blind slat reflectance as a function of wavelength.

Table 6.1. Optical properties of the slat surfaces.

Property	Quantity
Normal Solar Reflectance, %	44.1
Hemispherical Emittance, %	86.2

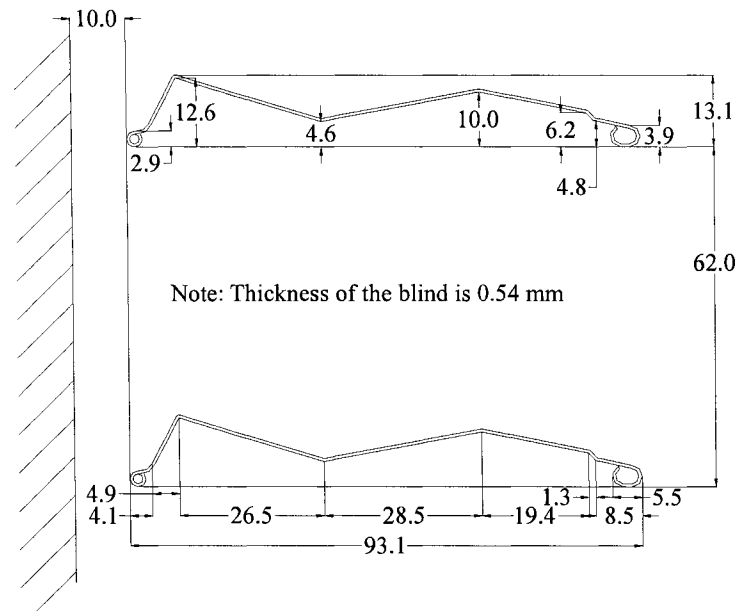


Figure 6.4. Dimensioned blind slats relative to the outer glazing in millimeters.

### 6.3. Modeling

The experiments were modeled in EnergyPlus. The same modeling procedures employed by [30, 32] were also used here with the addition of an exterior Venetian blind assembly. For this experiment, outer surface temperatures for the construction elements adjacent to the guarded zones in one hour increments were used as program inputs. The Perez 1990 model [37] was used to compute the diffuse irradiance on the tilted surface.

Direct-normal and diffuse horizontal irradiances were weather file inputs for computing the transmitted solar power along with other parameters used in 10 minute increments. EnergyPlus contains a blind model that assumes flat diffuse slats [38] similar to the model proposed in prEN 13363-2. The slat's normal solar reflectance, hemispherical emittance, width, thickness, distance from the outer pane of glass (measured from the center of the blind slats), and distance between individual slats were entered into the program. The heat transfer between the window and the shading devices was calculated using ISO 15099 assuming natural buoyancy; this was performed as an iterative procedure in the program. A detailed

algorithm that factored in surface orientation and temperatures was used to compute dynamic convective heat transfer coefficients for the interior surfaces.

#### 6.4. Sensitivity Analyses

Monte Carlo Analysis (MCA) and fitted effects for an n-way factorial analysis were used to assess how input uncertainties propagated through the building energy simulation program and impacted output parameters. The theory and implementation of these analyses are discussed by [31].

##### 6.4.1. Fitted Effects for N-way Factorial Analysis

One and two-way factorial analyses were performed for both experiments. The results for the overall uncertainty and the 10 most influential parameters for the horizontal slat and 45° downward tilted slat experiments are contained in Tables 6.2 and 6.3, respectively. To verify the assumption of localized linearity, both forward and backward differencing were performed.

Table 6.2. Overall uncertainty and 10 most influential input parameters from the factorial analyses for the horizontally positioned slat experiment in Watts.

Parameter	Forward	Backward
Overall Uncertainty	2.24	2.24
Average Air Temperature	-1.36	1.36
Fan Power	0.889	-0.888
Outside Air Temperature	0.822	-0.823
North Wall Temperature	0.708	-0.709
Ceiling Temperature	0.597	-0.599
West Wall Temperature	0.471	-0.472
Floor Temperature	0.388	-0.389
East Wall Temperature	0.315	-0.316
Ground Reflectance	0.162	-0.163
Global Horizontal Infrared Irradiance	0.155	-0.158

Table 6.3. Overall uncertainty and 10 most influential input parameters from the factorial analyses for the 45° downward tilted slat experiment in Watts.

Parameter	Forward	Backward
Overall Uncertainty	2.24	2.24
Average Temperature	-1.36	1.36
Fan Power	0.893	-0.893
Outside Air Temperature	0.824	-0.822
North Wall Temperature	0.708	-0.708
Ceiling Temperature	0.598	-0.598
West Wall Temperature	0.471	-0.471
Floor Temperature	0.388	-0.388
East Wall Temperature	0.315	-0.315
Global Horizontal Infrared Irradiance	0.158	-0.157
Ground Reflectance	0.140	-0.141

#### 6.4.2. Monte Carlo Analysis

A MCA was used to quantify the overall hourly uncertainties for the experiments and generate 95% credible limits used for comparisons in the statistical analyses. The average overall cooling power uncertainties for experiments with the blinds in horizontal position and tilted 45° downward were 2.47 W and 2.25 W, respectively. These results corresponded well with the results from the factorial analyses (Tables 6.2 and 6.3).

#### 6.5. Results

The empirical validation focused on the required cooling power needed to maintain the space at a constant temperature. Figure 6.5 contains a plot of the measured and predicted cooling power for the experiment when the blind slats were in the horizontal position. In the plot, each hour represents the average cooling power for that hour of the day averaged over all 20 days of the experiment. Averaged 95% credible limits for the experiment were fixed to the measured results and the averaged 95% credible limits from the MCA were fixed to the simulation results. For any given hour, the maximum, minimum, and mean absolute differences for each hour of the day of the experiment are plotted in Figure 6.6.

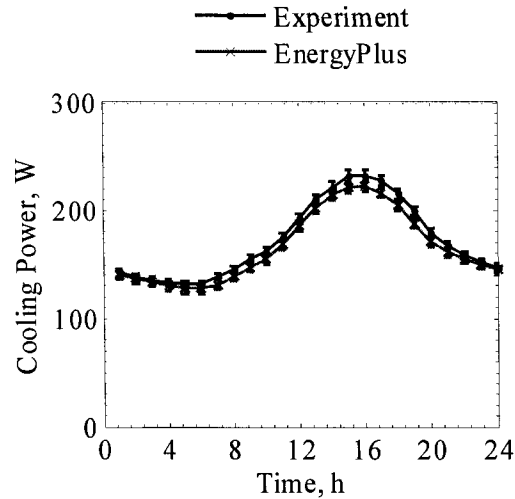


Figure 6.5. Measured and prediction cooling power for the horizontally positioned blind experiment averaged for a given hour of the day.

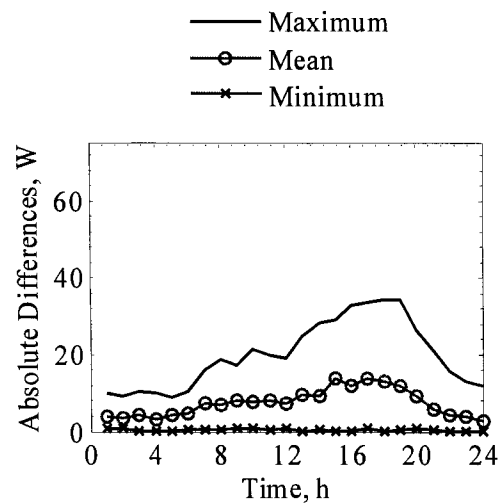


Figure 6.6. Maximum, minimum, and mean absolute cooling power differences for the horizontally positioned blind experiment for a given hour of the day.

Figure 6.7 contains a measured and predicted cooling power plot for the experiment where the slats were tilted  $45^\circ$  downward averaged for every given hour of the day over all

20 days of the experiment. The maximum, minimum, and mean absolute differences for the experiment are contained in Figure 6.8.

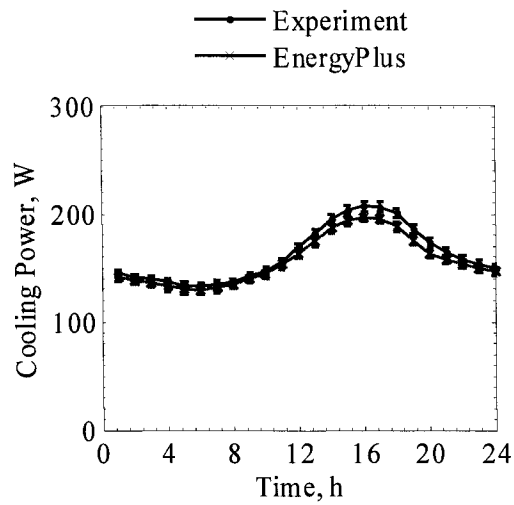


Figure 6.7. Measured and prediction cooling power for the 45° tilted downward blind experiment averaged for a given hour of the day.

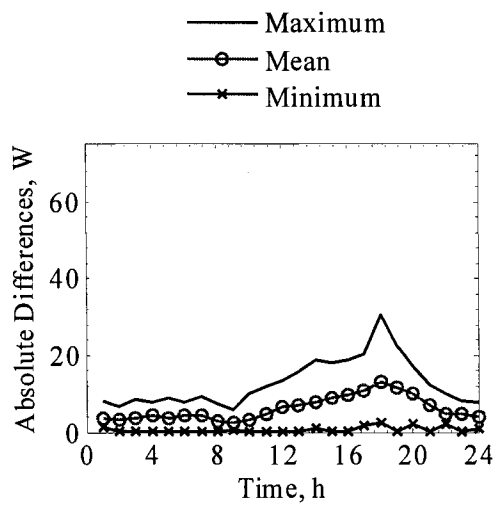


Figure 6.8. Maximum, minimum, and mean absolute cooling power differences for the 45° tilted downward blind experiment for a given hour of the day.

Statistical analyses were performed using the methodology proposed by [30]. An important parameter for assessing the overall performance of the program is the uncertainty ratio given in Equation 6.1. This relationship relates the hourly uncertainties to measurements and predictions. If the uncertainty ratio is less than or equal to unity, then the program is considered validated within the 95% credible limits.

$$UR = \frac{|D|}{OU_{Exp} + OU_{E+}} \quad (6.1)$$

The statistical comparisons for both experiments are shown in Table 6.4.

Table 6.4. Summary of statistics and comparisons of cooling power.

	Horizontal Position		45° Tilted Downward	
	Experiment	EnergyPlus	Experiment	EnergyPlus
$\bar{x}$	171.6 W	165.4 W	162.2 W	156.4 W
$s$	43.2 W	38.5 W	32.2 W	28.1 W
$x_{max}$	330.4 W	297.4 W	260.6 W	242.7 W
$x_{min}$	102.4 W	102.8 W	112.7 W	107.8 W
$\bar{D}$	-	6.20 W	-	5.80 W
$ \bar{D} $	-	7.52 W	-	6.16 W
$D_{max}$	-	34.4 W	-	30.5 W
$D_{min}$	-	0.0 W	-	0.0 W
$D_{rms}$	-	10.4 W	-	7.9 W
$D_{95\%}$	-	22.8 W	-	16.5 W
$\overline{OU}$	3.9 W	4.8 W	3.7 W	4.4 W
$\overline{UR}$	-	0.80	-	0.72
$UR_{max}$	-	3.0	-	3.1
$UR_{min}$	-	0.0	-	0.0
$ \bar{D} /\bar{x} \times 100\%$	-	4.4%	-	3.8%
$\bar{D}/\bar{x} \times 100\%$	-	3.6%	-	3.6%

## 6.6. Discussion and Conclusions

Due to different geometries of the blind slats, no solar beam radiation was transmitted into the room during the blind slat tilted 45° downward experiment. However, when blind slats were horizontal, it was possible for beam radiation to enter the room when angles lower than the cut-off angle of 32° occurred. However, this situation occurred only for the last two

hours before sunset and, therefore, the additional modeling challenge of having to split global radiation into diffuse and beam components was not relevant for this case.

Using the uncertainty ratios, EnergyPlus was validated within 95% credible limits for both blind slat positions over the entire experiment. These results do provide confidence in the assumptions employed in the EnergyPlus blind model and other assumptions made concerning the heat transfer within the air gap between the blinds and the outer pane of the glazing unit.

The absolute percent differences can be used to make a general assessment of hourly predictions. These predictions specifically impact calculations used for equipment sizing and peak operating demand of cooling equipment. For the horizontal and 45° downward blind orientations, the absolute percent differences were 4.4% and 3.8%, respectively. The percent differences can provide an evaluation of the overall energy predictions into the cell. When in the horizontal position, the percent difference was 3.6% and the percent difference when the blind slats were tilted downward 45° was 3.6%, which indicates that for both experiments, EnergyPlus under-predicted the cooling power.

The experiments performed here were designed for empirical validations of building energy simulation programs. All relevant inputs into the programs were well-described and methods used to evaluate the programs accounted for uncertainties in the experiment and program inputs. The results from EnergyPlus provide confidence that a given level of empirical validation can be attained.

### **Acknowledgements**

We gratefully acknowledge the financial support of the Swiss Federal Office of Energy (BFE) for building and testing the experimental facility (Project 17'166) as well as the funding for EMPA participation in IEA Task 34/43 (Project 100'765). We would also like to acknowledge the many contributions from: R. Blessing, M. Camenzind, K. Meyer, and R. Vonbank.

**Nomenclature**

$D$	= difference between experiment and predicted values for a given hour, W
$\overline{D}$	= mean difference, W
$ \overline{D} $	= mean absolute difference, W
$D_{max}$	= maximum difference between experimental and predicted values for a given array, W
$D_{min}$	= minimum difference between experimental and predicted values for a given array, W
$D_{rms}$	= root mean squared difference between experimental and predicted values for a given array, W
$D_{95\%}$	= ninety-fifth percentile of the differences between experimental and predicted values for a given array, W
$OU_{Exp}$	= 95% credible limits or overall uncertainty from experiment for a given hour, W
$OU_{E+}$	= 95% credible limits or overall uncertainty from MCA for a given hour, W
$\overline{OU}$	= average overall uncertainty calculated for 95% credible limits, W
$UR$	= uncertainty ratio for a given hour, no units
$\overline{UR}$	= arithmetic mean of the uncertainty ratio, no unit
$UR_{max}$	= maximum uncertainty ratio, no units
$UR_{min}$	= minimum uncertainty ratio, no units
$\bar{x}$	= arithmetic mean for a given array of data, W
$x_{min}$	= minimum quantity for a given array of data, W
$x_{max}$	= maximum quantity for a given array of data, W

**References**

- [1] M.R. Collins and S.J. Harrison, Calorimetric Analysis of the Solar and Thermal Performance of Windows with Interior Louvered Blinds. ASHRAE Transaction 110(1): 474-485, 2004
- [2] X.D.Fang, A study of the U-factor of the window with a high-reflectivity Venetian blind, Solar Energy Vol. 68, No.2:207-217, 2000
- [3] M.R. Collins and S.J. Harrison, Test of Measured Solar Heat Gain Variation in a Fenestration and Shade Combination with Respect to Test Specimen Tilt, ASHRAE Transactions 107(1): 691-699, 2001
- [4] J.H. Klems and J.L. Warner, Solar Heat Gain Coefficient of Complex Fenestrations with a Venetian Blind for differing Slat Angles, ASHRAE Transactions 103(1): 1026-1034, 1997
- [5] J.H. Klems and J.L. Warner, Measurements of Bidirectional Optical Properties of Complex Shading Devices, ASHRAE Transactions 101(1): 791-801, 1995
- [6] J.H. Klems and G.O. Kelly, Calorimetric Measurements of Inward-Flowing Fraction for Complex Glazing and Shading Systems, ASHRAE Transactions 102(1): 947-954, 1996
- [7] M.R. Collins and S.J. Harrison, Calorimetric Measurements of the Inward-Flowing Fraction of Absorbed Solar Radiation in Venetian Blinds, ASHRAE Transactions 105(2): 1022-1030, 1999
- [8] M.R. Collins and S.J. Harrison, Calorimetric Analysis of the Solar and Thermal Performance of Windows with Interior Louvered Blinds, ASHRAE Transactions 110(1): 474-485, 2004
- [9] S.J. Harrison and S.J. van Wonderen, Evaluation of Solar Heat Gain Coefficient for Solar-Control Glazings and Shading Devices, ASHRAE Transactions 104(1): 1051-1062,
- [10] D.S. Yahoda and J.L. Wright, Method for Calculating the Effective Longwave Radiation Properties of a Venetian Blind Layer, ASHRAE Transactions 110(1): 463-473, 2004
- [11] D.S. Yahoda and J.L. Wright, Heat Transfer Analysis of a Between-Panes Venetian Blind Using Effective Longwave Radiative Properties, ASHRAE Transactions 110(1): 455-462, 2004
- [12] M.R. Collins, S.J. Harrison, P.H. Oosthuizen, and D. Naylor, Sensitivity Analysis of Heat Transfer from an Irradiated Window and Horizontal Louvered Blind Assembly, ASHRAE Transactions 108(1): 503-511, 2002
- [13] M.R. Collins and S.J. Harrison, Estimating the Solar Heat and Thermal Gain from a Window with and Interior Venetian Blind, 110(1): 486-500, 2004
- [14] H. Shahid and D. Naylor, Energy performance assessment of a window with a horizontal Venetian blind, Energy and Buildings 37: 836-843. 2005
- [15] P. Pfrommer, K.J. Lomas, and C. Kupke, Solar radiation transport through slat-type blinds: A new model and its application for the thermal simulation of buildings, Solar Energy Vol.57, No.2:77-91, 1996

- [16] M. Andersen, M. Rubin, R. Powles, and J.L. Scartezzini, Bi-directional transmission properties of Venetian blinds: experiments assessment compared to ray-tracing calculation, *Solar Energy* 78:187-198, 2005
- [17] J. Breitenbach, S. Lart, I. Längle, J.L.J. Rosenfeld, Optical and thermal performance of glazing with integral Venetian blinds, *Energy and Buildings* 33:433-442, 2001
- [18] ASHRAE, ASHRAE Fundamentals 2001 SI Edition, American Society of Heating, Refrigeration and Air-Condition Engineers, Inc, Atlanta, GA, 2001
- [19] prEN 13363-2 (Final Draft), Solar protection devices combined with glazing - Calculation of total solar energy transmittance and light transmittance - Part 2: Detailed calculation method (English Version), October 2004
- [20] ISO/FDIS 15099: 2003(E), Thermal performances of windows, doors, and shading devices—Detailed calculations, 2003
- [21] WIS, Window Information System, <http://windat.ucd.ie/wis/html/index.html>, 2004
- [22] R.D. Judkoff, Validation of Building Energy Analysis Simulation Programs at the Solar Energy Research Institute, *Energy and Buildings*, 10, 1998, 221-239
- [23] P. Strachan, Model Validation using the PASSYS Test Cells, *Building and Environment* 28, 1993, 153-165
- [24] P. Wouters, L. Vandaele, P. Voit, N. Fisch, The use of outdoor test cells for thermal and solar building research within the PASSYS project, *Building and Environment* 28, 1993, 107-113
- [25] S.Ø. Jensen, Validation of building energy simulation programs: a methodology, *Energy and Buildings* 22, 1995, 133-144
- [26] K.J. Lomas, H. Eppel, C.J. Martin, D.P. Bloomfield, Empirical validation of building energy simulation programs, *Energy and Buildings* 26, 1997, 253-275
- [27] S. Moinard, G. Guyon, Empirical Validation of EDF ETNA and GENEC Test-Cell Models, A Report of Task 22, Project A.3 Empirical Validation, International Energy Agency, 1999
- [28] P.G. Loutzenhiser and G.M. Maxwell, A Comparison of DOE-2.1E Daylighting and HVAC System Interactions to Actual Building Performance, (Revised and submitted to *ASHRAE Transactions* January 12, 2006)
- [29] G.M. Maxwell, P.G. Loutzenhiser, and C.J. Klaassen, *Daylighting – HVAC Interaction Tests for the Empirical Validation of Building Energy Analysis Tools*, A Report of Task 22 Subtask D. Building Energy Analysis Tools Project D Empirical Validation. [http://www.iea-shc.org/task22/reports/IEA\\_Daylighting\\_Report\\_Final.pdf](http://www.iea-shc.org/task22/reports/IEA_Daylighting_Report_Final.pdf), 2003
- [30] H. Manz, P. Loutzenhiser, T. Frank, P.A. Strachan, R. Bindi, and G. Maxwell. (Accepted for publication in *Building and Environment* and available online September 8, 2005 at [www.sciencedirect.com](http://www.sciencedirect.com)) Series of experiments for empirical validation of solar gain modeling in building energy simulation codes – Experimental setup, test cell characterization, specifications and uncertainty analysis.

- [31] P.G. Loutzenhiser, H. Manz, C. Felsmann, P.A. Strachan, T. Frank, and G.M. Maxwell, (Submitted July 14, 2005 to *Solar Energy*), Empirical validation of models to compute solar irradiance on inclined surfaces for building energy simulation.
- [32] P.G. Loutzenhiser, H. Manz, P.A. Strachan, C. Felsmann, T. Frank, G.M. Maxwell, and P. Oelhafen, An Empirical Validation of Solar Gain Models Found in Building Energy Simulation Programs, (Submitted to *HVAC&R Research* on November 24, 2005)
- [33] P.G. Loutzenhiser, H. Manz, C. Felsmann, P.A. Strachan, and G.M. Maxwell, An empirical validation of modeling solar gain through a glazing unit with external and internal shading screens (In preparation for submission to *Applied Thermal Engineering*)
- [34] EnergyPlus 1.2.3.023 Building Energy simulation program, [www.energyplus.gov](http://www.energyplus.gov), 2005
- [35] GLAD Software. Swiss Federal Laboratories for Materials Testing and Research (EMPA), Duebendorf, Switzerland, 2002
- [36] [15] European Standard EN 410. Glass in building – Determination of luminous and solar characteristics of glazing. European Committee for Standardization, Brussels, Belgium, 1998
- [37] R. Perez, P. Ineichen, R. Seals, J. Michalsky, and R. Stewart, Modeling daylight availability and irradiance components from direct and global irradiance. *Solar Energy* Vol. 44 No.5, 1990, 271-289
- [38] EnergyPlus, Input Output Reference, Board of Trustees of University of Illinois and the University of California through Orlando Lawrence Berkley Laboratories, October 11, 2005

## **Chapter 7: Empirical Validation of the Daylighting Algorithms and Associated Interactions Using Various Shading Devices and Windows in Building Energy Simulation Programs**

A paper to be submitted to Energy and Buildings

Peter G. Loutzenhiser<sup>1,2,a</sup>, Gregory M. Maxwell<sup>1,b</sup>, Heinrich Manz<sup>2,c</sup>

<sup>1</sup> Iowa State University, Department of Mechanical Engineering

<sup>2</sup> Swiss Federal Laboratories for Materials Testing and Research (EMPA)

<sup>a</sup> Wrote the text and ran the EnergyPlus and DOE-2 simulations

<sup>b</sup> Supervised the text writing

<sup>c</sup> Provided technical support

### **Abstract**

Empirical validation of building energy simulation programs is an important tool in examining the effectiveness of building energy simulation algorithms. In recent years, daylighting algorithms have become increasingly sophisticated in their abilities to predict the illuminance, light power reductions, and the associated thermal load interactions. The focus of this research was to examine measured and simulated light levels in an actual building constructed for research purposes. Daylighting models were constructed in EnergyPlus and DOE-2.1e and the predicted illuminance and light power were compared with measurements; an assessment of heating and cooling interactions using a variable-air-volume reheat (VAVRH) system was also performed by analyzing reheat coil powers for the VAV boxes. The average differences from EnergyPlus for reference point daylight illuminance, light power, and reheat coil power predictions were within 124.1%, 14.9%, and 39.0%. DOE-2.1E predicted reference point daylight illuminances were within 54.2%, light powers were within 10.9%, and reheat coil power were within 40.2%.

**KEYWORDS:** Daylighting, empirical validation, building energy simulation tools

## 7.1. Introduction

During the last 30 years, engineers and architects have increasingly relied on building energy simulation programs to design and retrofit commercial buildings. Increased computer capacity has allowed for the implementation of complex control algorithms used in modern structures to be simulated by various programs. One such control strategy is daylighting control. Daylighting controls take advantage of ambient light (daylight) entering the space through exterior windows and/or light wells and adjusts the amount of artificial light to the space to control the light level at a given point. Typically, a controller mounted in the ceiling measures the illuminance on a reference plane. When the illuminance on this reference plane deviates from a specified set point, the controller sends feedback to dimmable ballasts which cause the lights to dim or illuminate to maintain prescribed light levels. Building energy simulation programs combine room geometry and surface optical properties, window information, and window shading (if installed) into the algorithms to compute illuminance(s) at a reference point(s) in the zones. This information along with detailed lighting and ballast specifications is used calculate the amount of light dimming required to maintain a fixed illuminance.

Important and necessary components for evaluating these types of programs are rigorous validations. Judkoff [1] identifies three types of validations for building energy simulation programs: analytical validations, program-to-program comparisons, and empirical validations. In analytical validations, the building energy simulation programs are configured according to a known analytical solution. Program outputs are then compared with the results of the analytical solution. The advantages for this type of validation include: no input uncertainties, an absolute truth standard within the limitation of the theory, and low costs; the primary disadvantage is that analytical solutions are limited to very simple cases. In program-to-program comparisons, specifications are written and the outputs from each program are then compared. The advantages include: relative inexpensive and straightforward and the validations can be as complex as necessary. The disadvantage is that there is not absolute truth standard; so it is impossible to ascertain which program(s), if any,

is (are) correct. For empirical validations, an actual experiment is run and then modeled in building energy simulation programs. The advantages are that there is an absolute truth standard within experimental uncertainty limits, and it can be as complex as required. The primary disadvantage is that empirical validations are expensive to perform.

Numerous daylighting algorithms have been developed and validated that explore different types of shading devices and illuminance predictions [2-6]. The International Energy Agency's Task 21 [7] was assembled to investigate daylighting for design tools and software in buildings. One of the most popular daylighting algorithms used in the design of buildings [8] was installed in DOE-2.1E and is analyzed in this paper.

Different facets of the DOE-2.1E daylighting algorithm has been already explored in earlier studies, including numerous empirical validations [9-13] and several studies that used the program as a tool for optimizing the daylighting performance of buildings [14-17]. Other empirical validations that did not emphasize daylighting have been performed in the PASSYS project [18-20], IEA Annex 21/Task 8 [21], and IEA Task 34/Annex 43 [22-24] that explored different facets of the building envelope and the associated solar gains with and without solar shading devices.

The focus of this research is to evaluate the daylighting algorithms and connected load interactions in EnergyPlus [25] and DOE-2.1E [26]. The experiment was performed in test rooms in a research facility and was done in conjunction with the International Energy Agency's Task 34/ Annex 43 Subtask C. For this study, various shading devices (internal and external) and windows were installed in different combinations to assess the performances of each building energy simulation program. Various statistical parameters were used to compare the results. Experimental uncertainties were computed and a Monte Carlo Analysis (MCA) was used to quantify how uncertainties in program input parameters (thermophysical properties and instrumentation uncertainties) propagated through a building energy simulation program (in this case EnergyPlus) and impacted output predictions.

## 7.2. Facility Layout

The building where the research was performed is uniquely equipped for empirical validations and meets all nine criteria for a high quality validation data set [19]. The facility is located on the campus of a community college in Ankeny, Iowa USA. The structure is comprised of eight test rooms, a computer room, offices, two classrooms and other rooms necessary for the support and operation of the facility. A drawing of the building is shown in Figure 7.1. The test rooms were constructed in symmetrical pairs to provide side-by-side testing with exposures to nearly identical outside thermal loads; three of pairs of test rooms are located at the perimeter of the building (east, south, and west) and the other two test rooms are situated inside the facility. There are three air-handling units (AHU's) in the facility. Test rooms denoted as A and B are served by different two nearly identical AHU's; the other AHU serves the rest of the facility. The building also contains a weather station, pyranometer, pyrliometer, precision infrared radiometer, and numerous exterior light sensors. Additional information concerning the construction and layout of the building is provided by [27].

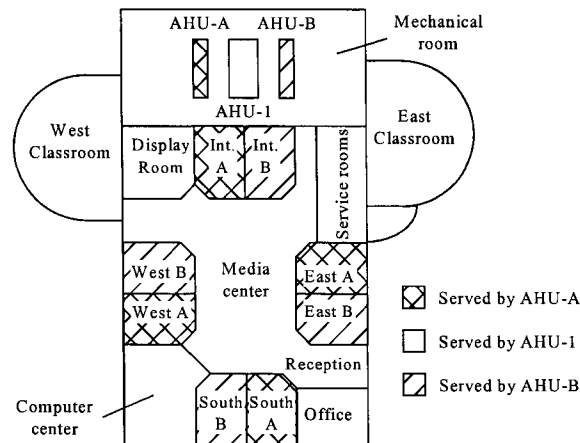


Figure 7.1. Facility layout (courtesy of [27]).

### 7.3. Experiment

A daylighting experiment was run from July 1 to July 7, 2005 using variable-air-volume systems with electric reheat coils (VAVRH) to evaluate the performances of building energy simulation programs. For the experiment, the supply air temperatures from the AHU's were fixed at 13°C and the temperature rise from the AHU to the inlets of the VAV terminal units associated with heat duct gain was 0.6 K. The maximum and minimum room airflow rates for the exterior test rooms were 1000 m<sup>3</sup>/h and 800 m<sup>3</sup>/h, respectively. The maximum airflow rate in the interior test rooms was 700 m<sup>3</sup>/h and the minimum airflow rate was 425 m<sup>3</sup>/h. The path of the return air was through the plenum spaces. The room heating and cooling temperature set points for all the test rooms were 22°C and 23°C, respectively. One stage of installed baseboard heat with rated power of ~890 W was operated during the entire experiment to add a sensible load to the spaces. In the exterior test rooms, box fans, used to reduce temperature stratification, were mounted near the ceiling during the experiment with a measured power of ~125 W. Specific information concerning other aspects of the experiment pertaining to the daylighting setup is contained in this section.

#### 7.3.1. Windows and Shading Devices

Various windows and shading devices were installed in the exterior test rooms. Brief descriptions of specifications of the shading devices and windows installed for this experiment are presented in this section. Shading screens, mini-blinds (motorized and fixed), and exterior fins were configured in different combinations with windows shown in Table 7.1. A description of the properties and installation of the windows, interior shading devices, and exterior fins is provided below.

Table 7.1. Test rooms shading and window configurations for the experiment.

Test Room	Window Type	Interior Window Treatment	Exterior Window Treatment
East A	25.2 mm Low-E#3 Glazing System	Motorized Mini-blinds	none
East B	25.2 mm Low-E#3 Glazing System	Fixed Slat Angle Horizontal Mini-blinds	none
South A	25.2 mm Clear Glass Glazing System	Nysan Roller Shades	none
South B	25.2 mm Clear Glass Glazing System	Fixed Slat Angle Horizontal Mini-blinds	none
West A	25.2 mm Low-E#2 Glazing System	Nysan Roller Shades	Exterior Fins
West B	25.2 mm Low-E#2 Glazing System	none	Exterior Fins

### 7.3.1.1. Windows

Three different types of windows were installed for each for each pair of test rooms.

Optical properties and the thermal transmittances of the windows are provided in Table 7.2.

Table 7.2. Test room window properties.

Type	25.2 mm OA LOW-E #3	25.2 mm OA LOW-E #2	25.2 mm OA Clear Glass
Layers	6 mm Clear (103) <sup>1</sup> 13.2 mm airspace 6 mm Lof Pyro Low-E #3 (9924) <sup>1</sup>	6 mm VE3-55 #2 (6059) <sup>1</sup> 13.2 mm airspace 6 mm Clear (103) <sup>1</sup>	6 mm Clear (103) <sup>1</sup> 13.2 mm airspace 6 mm Clear (103) <sup>1</sup>
Visible Transmittance	73%	23%	79%
Solar Transmittance	52%	14%	61%
Visible Light-Exterior Reflectance	17%	6%	14%
Visible Light-Interior Reflectance	16%	15%	14%
Solar Exterior Reflectance	15%	10%	11%
ASHRAE U-Value Winter Nighttime	1.87 W/m <sup>2</sup> -K	1.76 W/m <sup>2</sup> -K	2.68 W/m <sup>2</sup> -K
ASHRAE U-Value Summer Daytime	2.0 W/m <sup>2</sup> -K	1.87 W/m <sup>2</sup> -K	2.81 W/m <sup>2</sup> -K
Shading Coefficient	0.79	0.26	0.81
Solar Heat Gain Coefficient	0.66	0.22	0.70
Relative Heat Gain	497.7 W/m <sup>2</sup>	176.4 W/m <sup>2</sup>	533 W/m <sup>2</sup>

<sup>1</sup>ID number from the Window 5.2 Glazing System Library.

Note: All properties are center pane values.

### 7.3.1.2. Interior Shading Devices

Interior mini-blinds with white slats and white shading screens were installed in four of six exterior test rooms (Table 7.1). Optical properties of the blind slats and the shading screens were measured. The integral transmittance and reflectance of the shading screen and

the reflectance of the blind slats were computed according to EN 410 [28] using Glad software [29] using wavelength dependent near direct-hemispherical measurements taken from 250 nm to 2500 nm. The hemispherical emittance of the blind slats was also measured; a summary of these properties is shown in Table 7.3.

Table 7.3. Optical properties of the interior shading devices.

Type	Nysan Superweave 1000 (10% open) White Fabric	White Mini-Blind Slats
Normal Visible Transmittance, %	30.5	0.0
Normal Solar Transmittance, %	30.4	0.0
Normal Visible Reflectance, %	67.3	73.1
Normal Solar Reflectance, %	59.4	63.9
Hemispherical Emittance, %	-	72.1

In the East A test room, motorized mini-blinds were installed. The blinds were designed to block beam radiation from entering the room. Solar angles were calculated according to [30] using the building location and orientation to derive a control algorithm used to vary the blade angles so that the slats were always normal to the sun during the morning when beam irradiance entered the space. In the afternoon, the blinds slats were controlled to the horizontal position and then closed at 16:00 Central Local Standard Time (GMT-6). When in the horizontal position, the inner edges of the blind slats were 38.1 mm from the inner glass pane of the window. In the East B and South B test rooms, mini-blinds were installed with the slats fixed in the horizontal position 76.2 mm from the inner edges of the blind slats to the inner pane of glass. Nysan Superweave 1000 (10% openness factor) shading screens were installed in the West A and South A test rooms. The shading screens were mounted 108.0 mm from the inner glass pane.

### 7.3.1.3 Exterior Fins

Opaque exterior fins were constructed around the windows of the west test rooms. A dimensioned drawing of the fins is shown in Figure 7.2. The exterior fins were constructed out of a dark brown material to minimize reflection from the fins through the windows to the space.

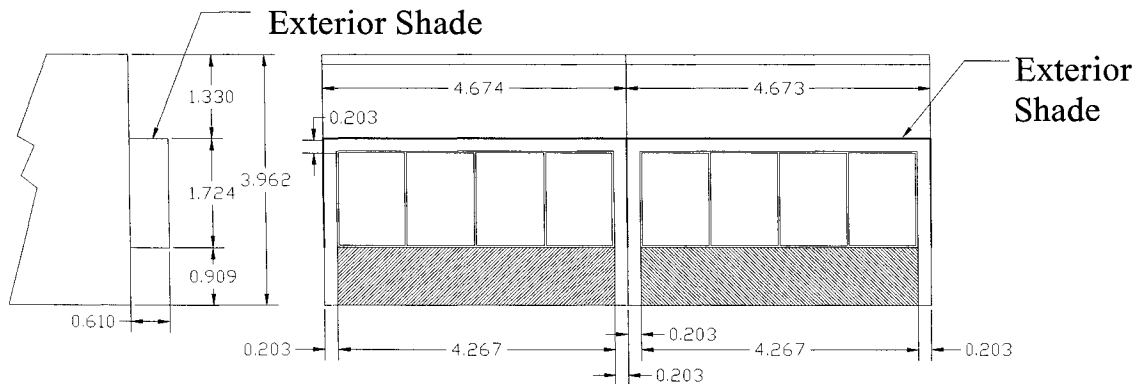


Figure 7.2. Drawing and dimensions in meters of the exterior shades for west test rooms.

### 7.3.2. Lighting and Daylighting Controls

Four fluorescent light fixtures with dimmable ballasts were mounted in each exterior test room. A light sensor with a 180° field of view, located on a table near the center of each room shown in Figure 7.3, provided feedback to the lighting control algorithm which maintained the illuminance at the reference point by controlling the ballasts. The lights were turned off when they were at maximum dimming and illuminance exceeded the set point, the lights were then turned back on when the illuminance dropped 108 Lux below the set point. Table 7.4 contains a list of maximum and minimum light power measured prior to the experiment and illuminance set points and at minimum lighting and corresponding reference point illuminance for the exterior test rooms. Measurements prior to the experiment indicated a linear relationship between reference point illuminance and light power in the absence of daylight to the space (the measurements were taken at night).

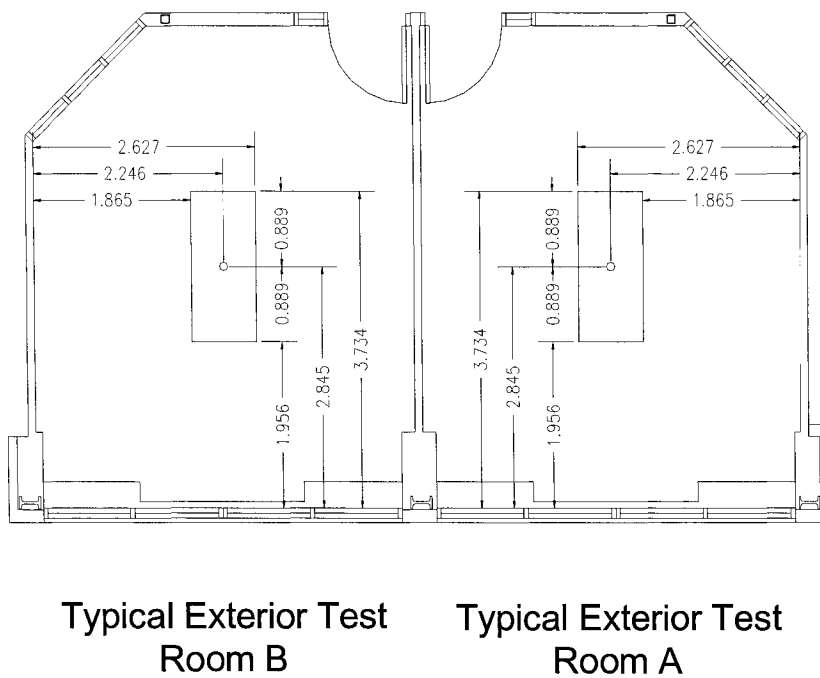


Figure 7.3 Light sensor reference point (the sensor height is 0.7239 m from the floor).

Table 7.4. Maximum and minimum light power and corresponding illuminance.

Test Room	Maximum Light Power W	Minimum Light Power W	Set Point Illuminance Lux	Illuminance without daylighting at reference point for minimum light power, Lux
East A	356	86.1	645	17.5
East B	362	89.3	645	29.2
South A	364	88.1	700	34.1
South B	362	89.3	700	26.9
West A	362	88.4	645	28.7
West B	348	86.9	645	23.6

#### 7.4. Simulations

This section contains brief narratives concerning the modeling of the facility in EnergyPlus and DOE-2.1E. Detailed architectural drawing of the facility, construction material properties, and optical properties of the interior surfaces of the test rooms (visible and solar) were used to model the facility along with the information described in Section 7.3. Weather parameters which included: dry-bulb temperature, relative humidity, barometric pressure, direct-normal solar irradiance, global horizontal solar irradiance, global horizontal infrared irradiance, global horizontal illuminance, and global vertical illuminance

on the east, west and south exterior façade were measured in one minute increments. During the experiment, spaces adjacent to the test rooms were maintained at nearly the same air temperature as the test rooms to provide near-adiabatic conditions. For confirmation, the adjacent space air temperatures were also verified and could be used as input into the building energy simulation programs.

#### **7.4.1. EnergyPlus**

A simulation model of the facility was constructed in EnergyPlus. The construction elements adjacent to occupied zones in the building were modeled as adiabatic boundaries. The internal heat loads in the test rooms were considered purely sensible convective loads and the light fixtures were modeled as recessed fluorescent lamps. Weather data measured at the facility were averaged in 10 minute intervals and used as boundary conditions. Because diffuse global solar irradiance was not measured at the facility but was a required input, it was computed using the solar altitudes calculated from EnergyPlus (to ensure the same solar angle algorithm was used) and direct-normal and global horizontal solar irradiances measured with the solar instruments.

The “DAYLIGHTING:DETAILED” model in EnergyPlus was used (there are two additional models available); this model seemed best suited for this validation. The inputs required for this model included: maximum and minimum light powers and corresponding illuminances (input as ratios), a daylight reference point(s) (a maximum of two), and illuminance set points. This model is similar to the daylighting model used in DOE-2.1e with two addition sky luminance distributions [31]. The vertical solar irradiances and illuminances on the exterior facades were computed in the program using a Perez 1990 [32] model for the solar irradiance inputs. The ground reflectance was estimated using measurements from [23, 33] was approximated as 15%.

The windows were modeled in Window 5.2.1 [34] and an output file was used that accounted for angular dependent properties. The window spacer and frame were described as a generic aluminum spacers and aluminum frames, respectively. The roller shades were

modeled as diffuse transmitters. EnergyPlus contains a blind algorithm used to estimate the visible and solar transmittance of the blind assemblies. This model assumes that the blinds are perfectly flat diffuse reflectors which are infinitely long. Cross-strings for two-dimensional configuration factor calculations were used for blind slats and the window described by [31]. The shading screens were described in the program using integral visible and solar transmittances and reflectance described in Table 7.3. The heat transfer between the window and the shading devices was calculated using ISO 15099 [35] assuming natural buoyancy; this was performed as an iterative procedure in the program. The exterior fins were modeled as opaque projected around the west windows. The HVAC equipment was auto-sized in the program and zone heating and cooling set points for temperatures and maximum and minimum airflow rates were fixed.

A detailed algorithm as a function of surface orientation and surface temperatures was used to quantify convective heat transfer and approximate geometric view factors in the program were used to calculate the radiative heat exchange between surfaces.

#### **7.4.2. DOE-2.1E**

The facility was also modeled in DOE-2.1E. All the zones and AHUs were described in the input files; therefore the simulation also included results from the occupied spaces. The test rooms were described as cuboids with room widths and heights that corresponded with the actual dimensions of the space and an equivalent room length corresponding to the room volume was implemented. Custom weighting factors were used in program to account for transient heat transfer of the building elements (Floor-Weight=0). The test rooms' internal loads were considered sensible and purely convective and recessed light fixture models were employed. The daylighting model in DOE-2.1e is described in detail by [8]. Hourly averaged weather data measured at the facility were put into TMY2 weather format and used as inputs into the program. Measured global horizontal and direct-normal solar irradiances were used to calculate the global vertical irradiances and illuminances on the east, south, and west facades using the Perez 1990 model using the same ground reflectance as in

EnergyPlus. In TMY2 weather, it is impossible to input global horizontal infrared irradiance; therefore the opaque sky cover was calculated by reversing the code algorithm for calculating infrared global horizontal irradiance used in the TMY2 weather file [36, 37].

The windows were modeled in Window 5.2.1, which accounted for angular dependent properties. Generic aluminum spacers and frames were used. Integral solar and visible shading transmittances were used for simulating the shading screens. Because surface temperatures of the inner glass panes, shading screen, and the air temperatures in the gap were not known, the heat transfer between in the air gap between the inner glazing and shading screen was estimated using EN ISO 6946 [38] for an unventilated air layer. The exterior fins over the east windows were described in the input file as opaque non-reflecting surfaces. Currently, DOE-2.1E does not have an algorithm to model mini-blinds and there is no subsidiary software designed to be used in conjunction with this building energy simulation program; therefore, comparisons between for the test rooms with mini-blinds did not include results from DOE-2.1E.

A combined design heat transfer coefficient was taken from [30] as  $8.5 \text{ W/m}^2\text{-K}$  for all elements (floor, ceiling, and walls) to estimated total impact of convective and radiative heat transfer. This was done because element surface temperatures in the program were not known.

## **7.5. Uncertainties**

Accounting for experimental uncertainties is of utmost importance when performing empirical validations. For this study, the experimental uncertainties of measured parameters were calculated and compared with program outputs. The uncertainties of program outputs as a function of program inputs were accounted for by using a MCA. Ninety-five credible limits from these calculations were used in the statistical analysis to assess the overall performance of the building energy simulation programs.

### **7.5.1. Experimental Uncertainties**

The uncertainties of experimental measurements were estimated based on manufacturers' specifications assembled by [28]. Using criteria proposed by [39], the uncertainties were considered Bayesian and estimated according to a uniform probability distribution function (pdf); ninety-five percent credible limits were then calculated.

### **7.5.2. Monte Carlo Analysis**

A MCA was used to evaluate how uncertainties of input parameters propagated through the building energy simulation programs and impacted simulation outputs and was performed using EnergyPlus. A thorough description of how this analysis was performed is provided by [23]. Input uncertainties for measuring equipment were again taken from information provided by product manufacturers that were compiled by [28]. Thermophysical and optical property uncertainties were estimated to be  $\pm 5\%$  of the quantity and  $\pm 0.01$ , respectively. The physical dimensions of the rooms were not perturbed because of associated interactions with other zones. Because the uncertainties were of Bayesian nature, they were perturbed in the MCA according to a uniform pdf. For this study, 120 runs were used to estimate 95% credible limits assumed normal by the Central Limit Theorem and verified using a Lilliefors Test for a Normal Distribution at a 1% significance level. Because it was impossible to modify the Window 5.2.1 output file, visible and solar integral transmittances and reflectance for each pane were entered into the program and perturbed for the MCA.

## **7.6. Results**

Several zone output parameters from the building energy simulation programs were compared with quantities measured at the facility during the experiment for the exterior test rooms. These outputs included: illuminance at the reference point due daylight, light power, reheat coil power, and one example of zone temperature. Because the minimum airflow rate set points in the test rooms was relatively high, reheat was required during most of the test to overcome the ventilation load of the entering air; therefore the airflows remained at the

minimum position and were not compared. The global exterior illuminances in the test room facades (east, south, and west) and on the horizontal plane were measured during the experiment. From this information, hypotheses can be made to assess general trends expected with respect to daylight in the test rooms. The exterior global illuminances are plotted in Figure 7.4.

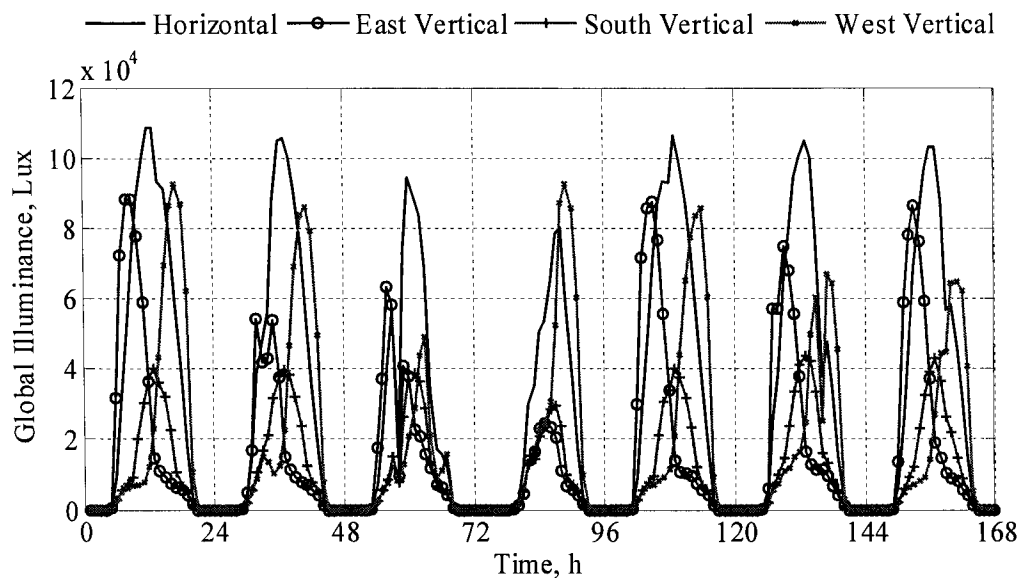


Figure 7.4. Horizontal and vertical global exterior illuminance.

From this plot, there were initially two fairly sunny days, following by two relatively cloudy days, and, finally, three sunny days. The global vertical illuminances provide information concerning the amount of potential visible light incident upon the windows (this was reduced for the west test rooms where exterior fins were installed. Because of the high path that the sun takes across the sky during the year, beam illuminances were never incident upon the south windows but were incident in the morning and evenings on the east and west windows, respectively.

The statistical analysis proposed by [22] was used to assess the performances of the building energy simulation programs. An important parameter is the uncertainty ratio shown in Equation 7.1. If this parameter is less than or equal to unity, then the programs were considered validated within 95% credible limits.

$$UR_i = \frac{|D_i|}{OU_{i,Experiment} + OU_{i,EnergyPlus}} \quad (7.1)$$

In order not to divide by zero when computing the uncertainty ratios, data were only analyzed if the sum of the uncertainties (experimental and MCA) for the daylight reference point illuminance, light power, and reheat power exceeded 1.0 Lux, 1.0 W, and 1.0 W, respectively, which were arbitrarily chosen for mathematical reasons to ensure that the uncertainty ratio never exceeded the absolute differences.

### 7.6.1. Daylight Illuminance

The daylight illuminances were predicted at the reference points in the exterior test rooms. The experimental daylight illuminances were calculated by subtracting from the measured illuminance the illuminance from the lights using light power versus total illuminance relationships from Table 7.4. The results from the east, south and west test rooms are presented in this section.

#### 7.6.1.1. East Test Rooms

During the morning, the east test rooms were subjected to beam solar irradiation entering the space. The blinds slats were automatically adjusted in the A Test Room to ensure only diffuse solar irradiation entered the rooms, while in the B Test Room, blind slats in the horizontal position did little to impede beam radiation during sunrise. From Table 7.2, 73% of the visible light penetrated the space through the windows when the mini-blinds failed to stop beam radiation. The measured and predicted daylight illuminances for the east test rooms are shown in Figure 7.5.

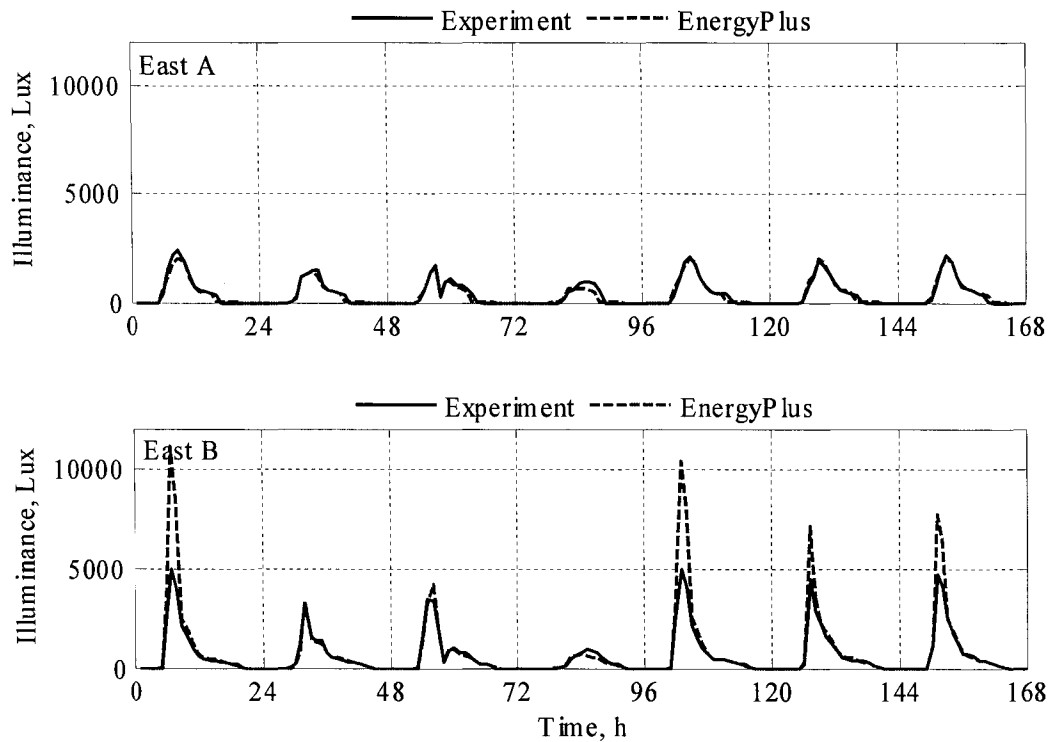


Figure 7.5. Reference point illuminance for the east test rooms.

#### 7.6.1.2. South Test Rooms

The south test room had double clear glazing windows. Roller shades and mini-blinds in the horizontal positions were installed in the A and B Test Rooms, respectively. During this time of the year, beam radiation was never incident upon the outer window pane of south-facing windows. Therefore, only diffuse light entered the space. Daylight illuminance measurements and predictions at the references points are shown in Figure 7.6.

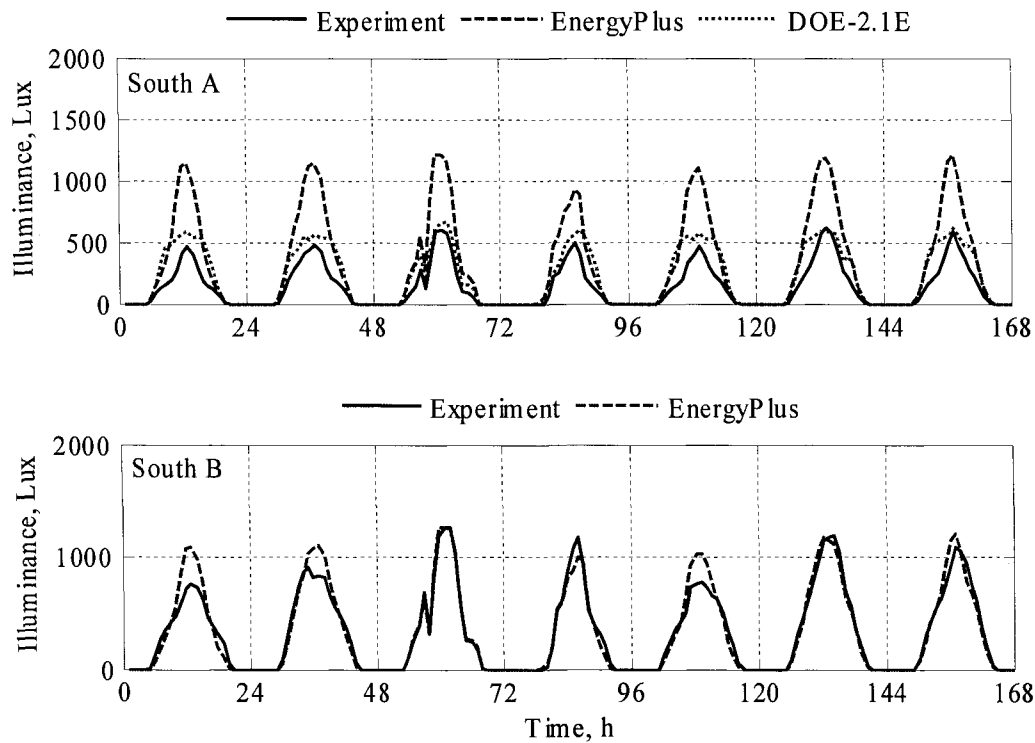


Figure 7.6. Reference point illuminance for the south test rooms.

### 7.6.1.3 West Test Rooms

In the west test rooms, exterior fins were installed over the test room windows to reduce the beam radiation entering the space. Beam radiation was only incident on the outer window panes in the evening when the sun was setting. Predictions are compared with measurements in Figure 7.7 for reference point daylight illuminance.

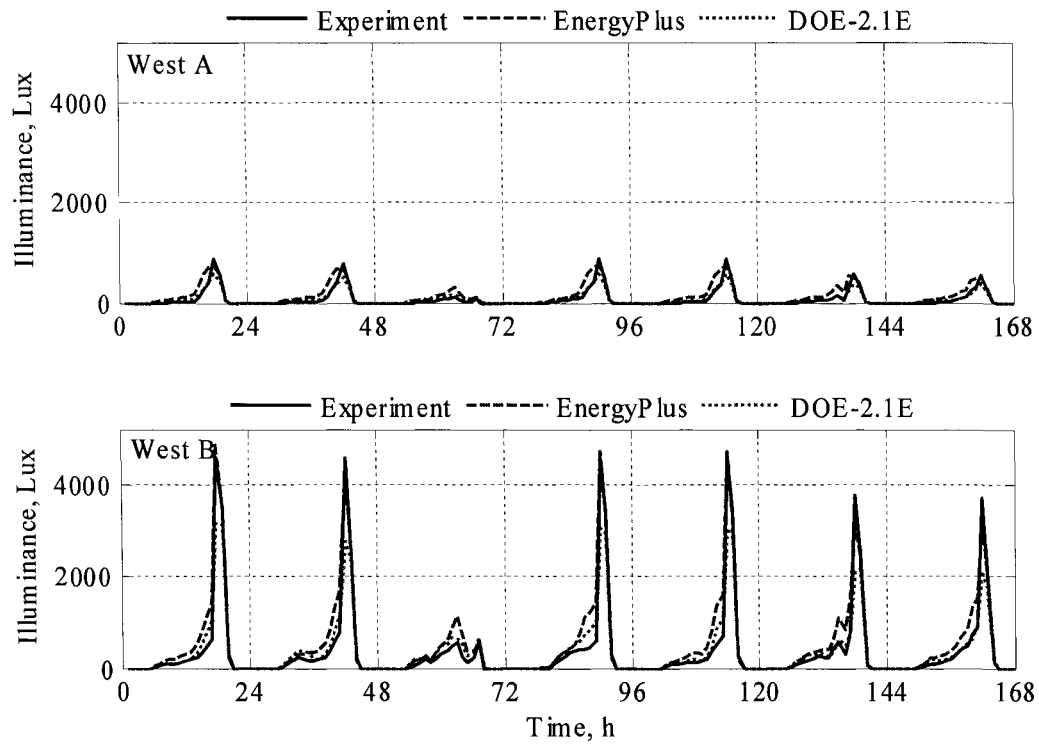


Figure 7.7. Reference point illuminance for the west test rooms.

#### 7.6.1.4. Statistical Comparisons

An assessment of the overall performance of the programs for each test room was performed by employing statistical parameters for each test room. Table 7.5 contains the comparisons for the daylight reference point illuminance for the exterior test rooms and corresponding predictions from the building energy simulation programs.

Table 7.5. Statistical analysis for the room daylight illuminance at the reference point in Lux.

	East A		East B		South A			South B		West A			West B		
	Experiment	EnergyPlus	Experiment	EnergyPlus	Experiment	EnergyPlus	DOE-2.1E	Experiment	EnergyPlus	Experiment	EnergyPlus	DOE-2.1E	Experiment	EnergyPlus	DOE-2.1E
$\bar{x}$	692.8	656.7	1050.3	1367.4	248.1	555.9	382.4	545.5	561.8	129.4	218.3	129.8	647.3	840.2	611.8
$s$	640.4	615.3	1214.5	2171.6	167.9	372.9	186.5	334.1	380.8	209.5	215.7	145.9	1136.3	1098.7	790.5
$x_{max}$	2375.0	2034.7	4937.0	11145.2	609.0	1215.3	666.9	1272.0	1269.4	873.0	749.7	588.1	4593.0	4870.4	3160.4
$x_{min}$	0.0	2.1	12.0	10.8	0.0	40.74	24.30	28.0	9.89	0.0	9.06	5.40	0.0	13.33	26.70
$\bar{D}$	-	36.1	-	-317.2	-	307.8	134.3	-	16.3	-	88.9	0.4	-	192.9	-35.6
$ \bar{D} $	-	108.5	-	392.2	-	307.8	134.7	-	81.2	-	100.3	46.5	-	236.2	205.1
$D_{max}$	-	550.5	-	6212.2	-	698.3	341.1	-	349.1	-	311.4	301.8	-	915.5	1837.8
$D_{min}$	-	0.3	-	0.6	-	21.1	4.5	-	0.5	-	0.5	1.5	-	3.4	0.9
$D_{rms}$	-	166.0	-	1127.7	-	373.0	163.1	-	112.1	-	128.0	74.0	-	332.8	420.1
$D_{95\%}$	-	366.9	-	2613.7	-	638.2	296.5	-	252.5	-	283.8	159.7	-	748.1	1432.6
$\overline{OU}$	39.2	12.3	59.4	26.0	14.0	17.8	-	30.9	21.3	7.3	23.7	-	36.6	88.8	-
$\overline{UR}$	-	4.2	-	3.2	-	9.9	6.2	-	2.3	-	5.5	2.7	-	3.6	2.6
$UR_{max}$	-	58.0	-	21.3	-	31.1	18.5	-	12.8	-	9.3	9.0	-	11.5	25.7
$UR_{min}$	-	0.1	-	0.0	-	4.7	0.2	-	0.0	-	0.1	0.0	-	0.0	0.0
$ \bar{D} /\bar{x} \times 100\%$	-	15.7%	-	37.3%	-	124.1%	54.3%	-	14.9%	-	77.5%	35.9%	-	36.5%	31.7%
$\bar{D}/\bar{x} \times 100\%$	-	5.2%	-	-30.2%	-	124.1%	54.2%	-	3.0%	-	68.7%	0.3%	-	29.8%	-5.5%

## 7.6.2. Light Power

Dimmable ballasts were used to maintain reference point illuminance on the table light sensor (used as a reference point in the programs). The measured and predicted light powers for the east, south, and west test rooms and statistical comparisons are provided in this section.

### 7.6.2.1. East Test Rooms

Figure 7.8 contains plots of the experimental and predicted light power for the east test rooms.

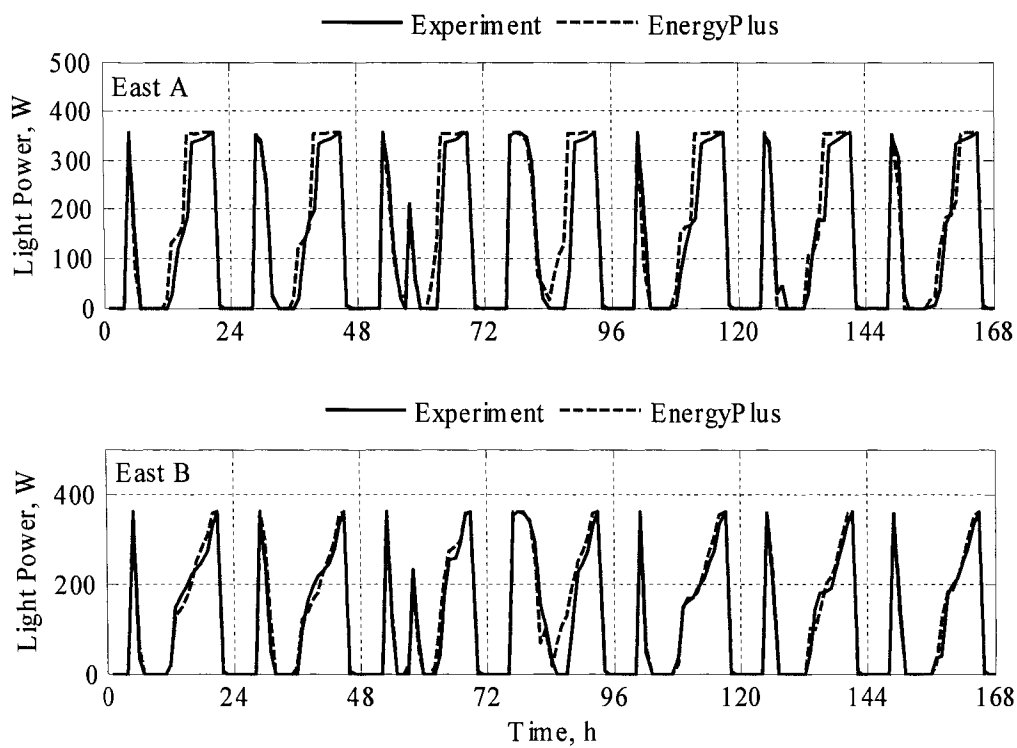


Figure 7.8. Light power for the east test rooms.

### 7.6.2.2. South Test Rooms

Results for the light power in the south test rooms from the measured and predicted light power are contained in Figure 7.9.

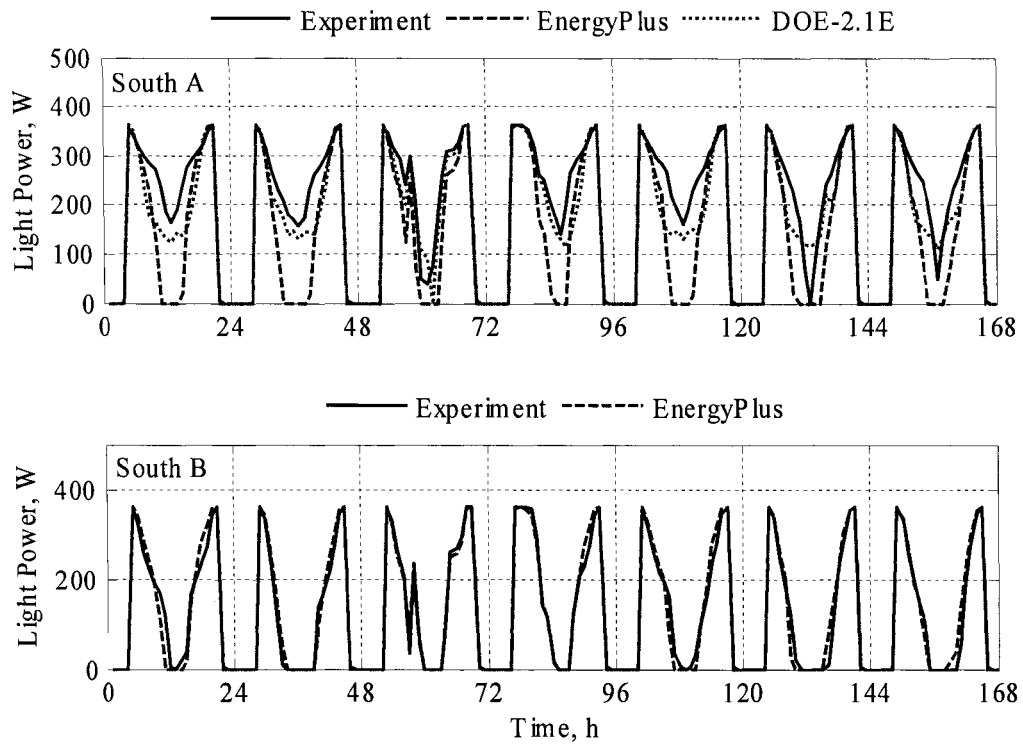


Figure 7.9. Light power for the south test rooms.

### 7.6.2.3 West Test Rooms

Light power measurements and predictions for the west test rooms are shown in Figure 7.10.

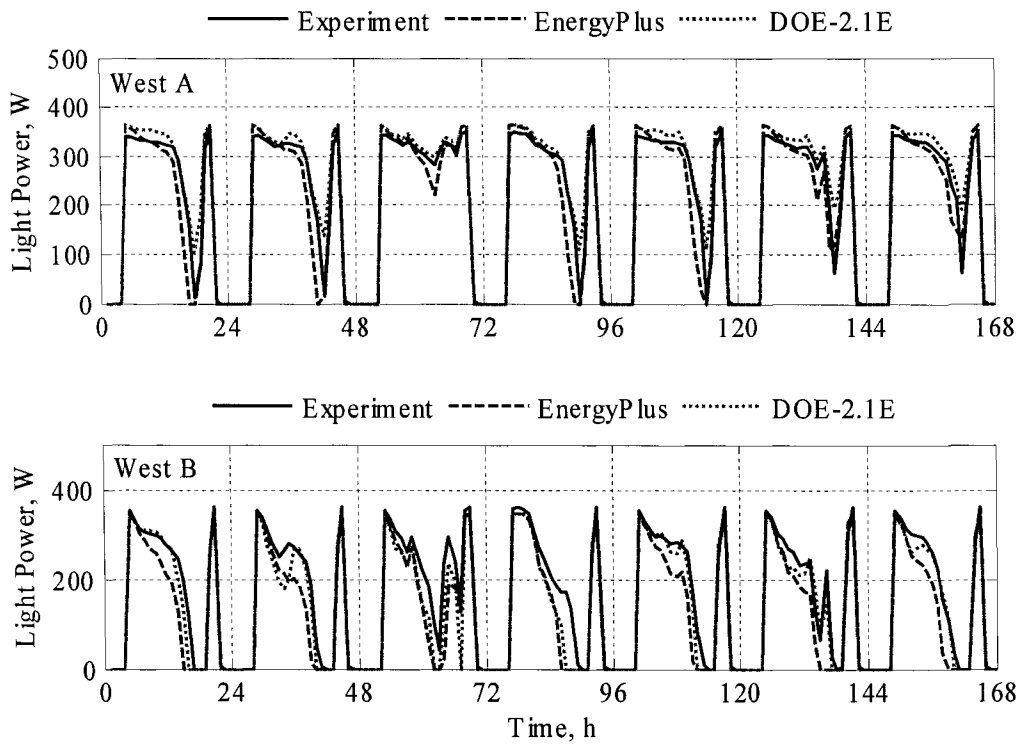


Figure 7.10. Light power for the west test rooms.

#### 7.6.2.4. Statistical Comparisons

Statistical analyses of the predictions compared with the measurements are presented in Table 7.6.

Table 7.6. Statistical analysis for the room light power in Watts.

	East A		East B		South A			South B		West A			West B		
	Experiment	EnergyPlus	Experiment	EnergyPlus	Experiment	EnergyPlus	DOE-2.1E	Experiment	EnergyPlus	Experiment	EnergyPlus	DOE-2.1E	Experiment	EnergyPlus	DOE-2.1E
$\bar{x}$	182.0	199.0	175.6	185.5	307.4	261.6	274.0	239.8	247.2	328.3	329.4	344.8	318.6	306.5	305.0
$s$	152.2	151.9	132.3	133.0	44.1	96.9	79.2	106.3	106.8	19.0	34.2	17.0	43.6	45.5	57.9
$x_{max}$	356.0	356.0	362.0	362.0	364.0	364.0	364.0	362.0	362.0	348.0	362.0	362.0	362.0	348.0	348.0
$x_{min}$	0.0	0.0	0.0	0.0	199.0	18.30	135.19	0.0	15.75	193.0	110.46	250.69	144.0	126.16	0.00
$\bar{D}$	-	-17.0	-	-9.8	-	-45.9	-33.4	-	7.4	-	1.1	16.5	-	-12.1	-13.6
$ D $	-	30.0	-	20.3	-	48.2	36.6	-	19.1	-	13.9	16.5	-	15.0	18.4
$D_{max}$	-	284.8	-	127.1	-	216.7	127.5	-	98.3	-	82.5	57.7	-	48.4	144.0
$D_{min}$	-	0.0	-	0.0	-	0.0	0.0	-	0.0	-	0.2	3.1	-	1.4	0.5
$D_{rms}$	-	57.5	-	31.5	-	71.4	54.1	-	28.2	-	17.6	18.0	-	17.6	28.3
$D_{95\%}$	-	130.8	-	75.5	-	150.3	111.6	-	57.7	-	31.0	26.9	-	34.0	41.1
$OU$	0.4	12.2	0.4	9.7	0.7	11.7	0.0	0.5	12.2	0.7	11.7	0.0	0.7	9.0	0.0
$\overline{UR}$	-	3.3	-	2.2	-	4.6	3.1	-	1.9	-	1.3	1.6	-	2.0	2.7
$UR_{max}$	-	33.8	-	13.5	-	51.0	23.5	-	33.7	-	7.1	4.9	-	10.4	19.0
$UR_{min}$	-	0.0	-	0.0	-	0.0	0.0	-	0.0	-	0.0	0.1	-	0.2	0.1
$\frac{ D }{\bar{x}} \times 100\%$	-	16.5%	-	11.6%	-	15.7%	11.9%	-	8.0%	-	4.2%	5.0%	-	4.7%	5.8%
$\frac{\bar{D}}{\bar{x}} \times 100\%$	-	-9.3%	-	-5.6%	-	-14.9%	-10.9%	-	3.1%	-	0.3%	5.0%	-	-3.8%	-4.3%

### 7.6.3. Reheat Coil Power

The VAVRH system used electric reheat coils. VAV boxes that use electric heat require relatively high minimum airflow rates to satisfy the safety systems which prevent the coils from being energized if the airflow is too low. Heating and cooling temperature set points for the test rooms were used as inputs to the programs with a 1 K temperature deadband. During the experiment, there were only cooling loads in the test rooms because of the internal loads introduced into the space and summertime conditions. However, due to high ventilation loads attributed to the incoming supply air, the reheat coils in the VAV boxes were nearly always energized. In EnergyPlus, the program assumed that when the test rooms required cooling (i.e. the temperature of the entering air from the diffuser was less than the room air temperature), the room temperature was at the cooling set point, despite the fact that reheat coils were still required to overcome the ventilation load; this can be seen in Figure 7.11, which shows plots for the room temperatures for the South Test Rooms.

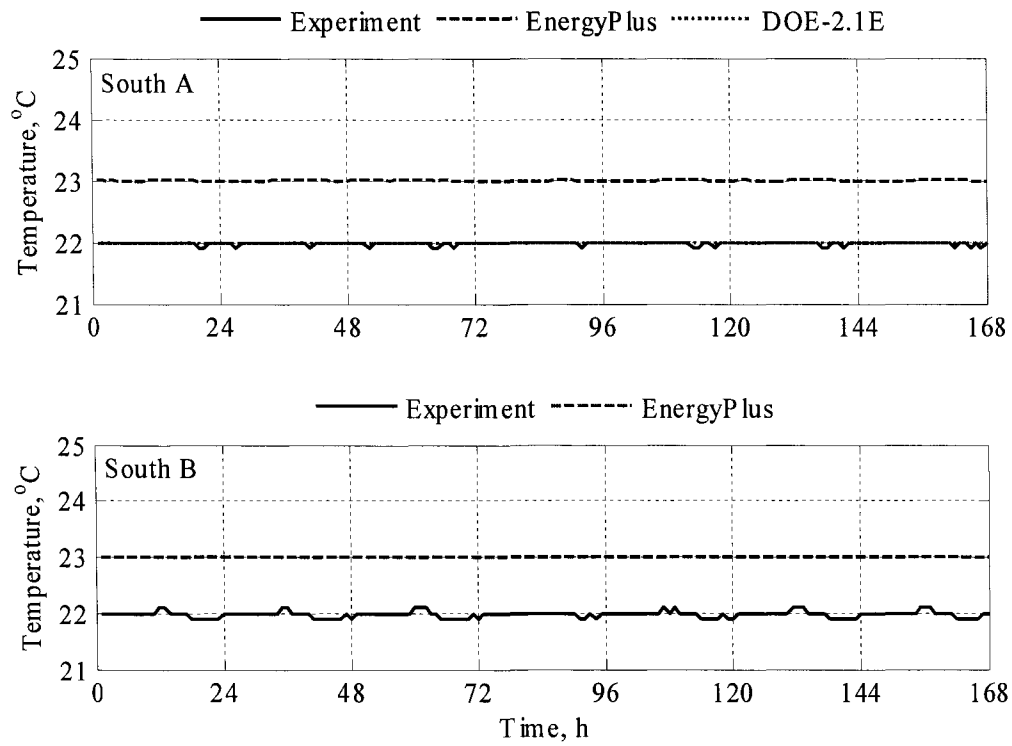


Figure 7.11. Room temperature for the south test rooms.

The predicted and measured reheat powers for the east, south, and west test rooms are reported in this section.

### 7.6.3.1. East Test Rooms

The measured and predicted reheat powers from the electric coils for the east test rooms are shown in Figure 7.12. Reheat power was not required in the east test rooms for only three mornings when beam radiation entered the rooms.

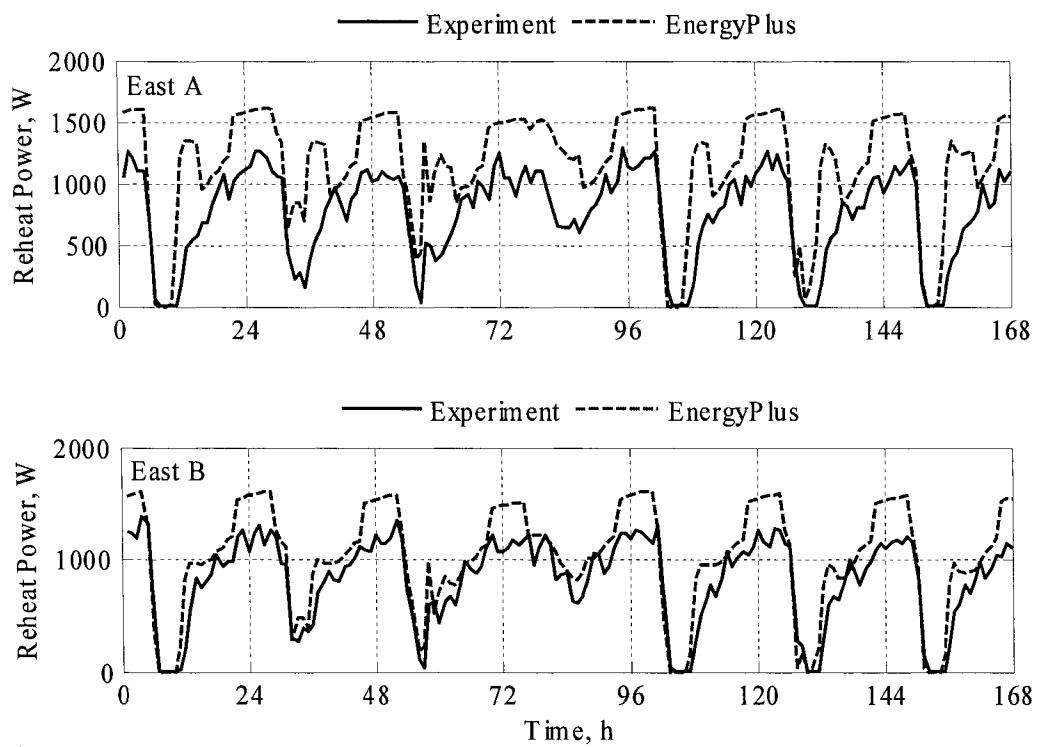


Figure 7.12. Reheat power for the east test rooms.

### 7.6.3.2. South Test Rooms

Comparison plots between the measured and predicted reheat powers for the south test rooms are shown in Figure 7.13.

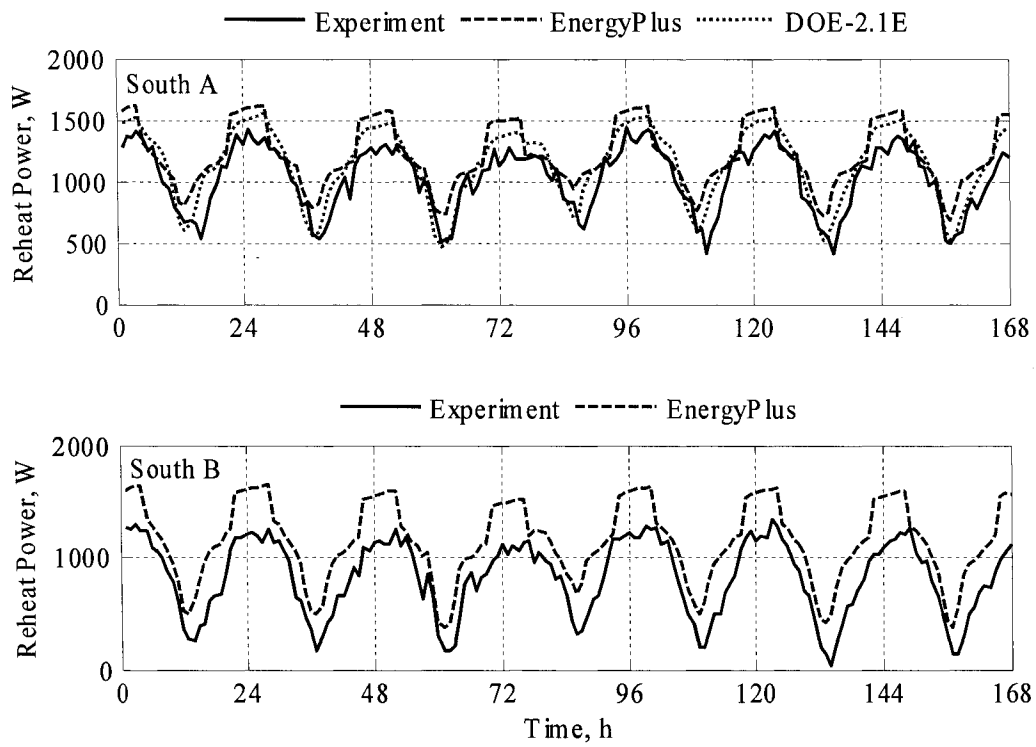


Figure 7.13. Reheat power for the south test rooms.

### 7.6.3.3. West Test Rooms

Measured and predicted reheat powers for the west test rooms are shown in Figure 7.14.

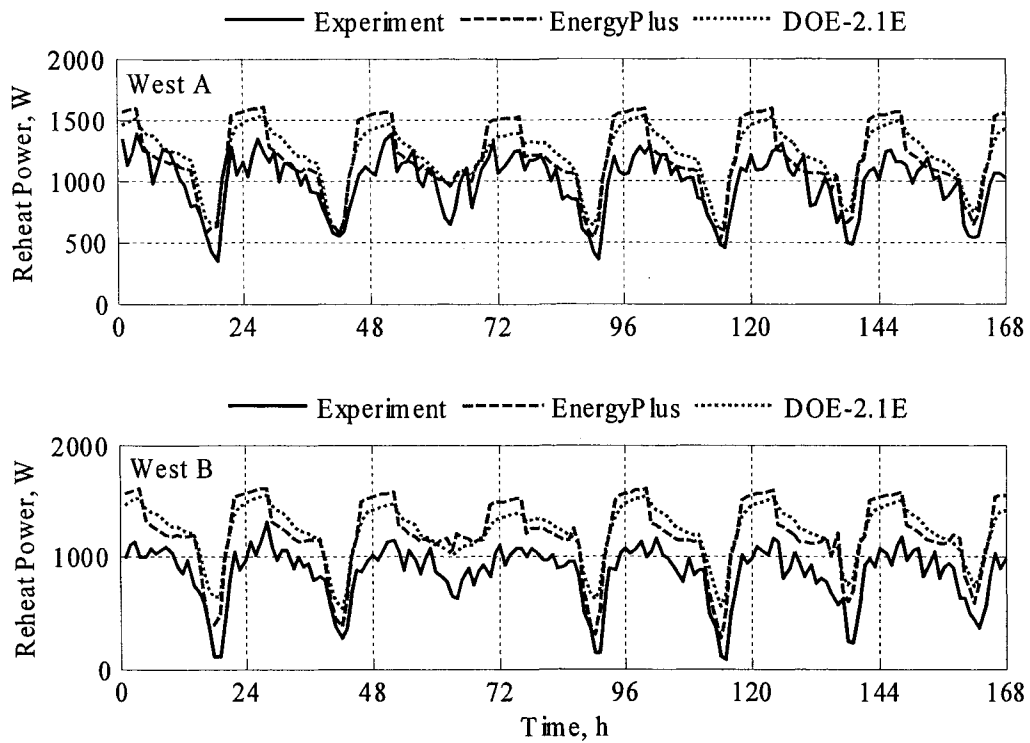


Figure 7.14. Reheat power for the west test rooms.

#### 7.6.3.4. Statistical Comparisons

Statistical analyses of the predictions compared with the measurements are presented in Table 7.7.

Table 7.7. Statistical analysis for the room reheat coil power in Watts.

	East A		East B		South A			South B		West A			West B		
	Experiment	EnergyPlus	Experiment	EnergyPlus	Experiment	EnergyPlus	DOE-2.1E	Experiment	EnergyPlus	Experiment	EnergyPlus	DOE-2.1E	Experiment	EnergyPlus	DOE-2.1E
$\bar{x}$	819.0	1075.9	886.7	1103.5	1028.8	1212.0	1142.6	828.0	1143.4	991.5	1182.4	1212.5	899.2	1249.6	1260.3
$s$	327.7	429.3	337.8	401.2	268.8	256.7	302.0	340.0	353.7	230.6	286.3	232.4	194.2	247.7	191.7
$x_{max}$	1284.0	1619.2	1378.0	1611.9	1433.0	1621.5	1557.0	1338.0	1646.9	1390.0	1595.1	1538.0	1308.0	1607.8	1555.0
$x_{min}$	3.0	31.47	2.0	33.03	410.0	688.89	469.00	31.0	379.96	339.0	502.75	575.00	226.0	589.63	683.00
$\bar{D}$	-	256.9	-	216.8	-	183.2	113.8	-	315.4	-	190.9	221.0	-	350.4	361.1
$ \bar{D} $	-	287.9	-	233.6	-	191.2	132.2	-	315.4	-	202.1	221.3	-	350.4	361.1
$D_{max}$	-	609.8	-	628.0	-	555.0	424.0	-	554.8	-	543.8	463.0	-	660.9	576.0
$D_{min}$	-	1.8	-	5.0	-	1.1	0.0	-	7.7	-	0.5	6.0	-	51.5	86.0
$D_{rms}$	-	326.5	-	274.3	-	229.9	155.1	-	339.3	-	252.9	245.6	-	383.0	373.7
$D_{95\%}$	-	523.8	-	456.9	-	403.3	280.0	-	500.1	-	469.5	392.0	-	610.3	525.0
$OU$	1.9	74.9	2.0	74.3	2.3	77.6	0.0	1.9	76.6	2.2	74.8	0.0	2.0	74.8	0.0
$UR$	-	4.0	-	3.1	-	2.4	1.7	-	4.0	-	2.9	3.9	-	6.1	7.3
$UR_{max}$	-	33.7	-	11.3	-	6.8	5.4	-	7.1	-	24.8	107.7	-	115.1	147.8
$UR_{min}$	-	0.0	-	0.1	-	0.0	0.0	-	0.1	-	0.0	0.1	-	0.6	1.1
$ \bar{D} /\bar{x} \times 100\%$	-	35.2%	-	26.3%	-	18.6%	12.8%	-	38.1%	-	20.4%	22.3%	-	39.0%	40.2%
$D/\bar{x} \times 100\%$	-	31.4%	-	24.4%	-	17.8%	11.1%	-	38.1%	-	19.3%	22.3%	-	39.0%	40.2%

## 7.7. Discussion

The discussion is divided up into three sections: daylight illuminances, light power, and reheat power.

### 7.7.1. Daylight Illuminance

Strictly speaking with respect to the daylight illuminance predictions, none of the programs predicted daylight illuminance at the reference points within 95% credible limits. The EnergyPlus model performed best in the South B test room and worst in the East B room; in both cases mini-blinds were installed.

A general assessment of how the mini-blind algorithm performed can be seen in the South B and east test rooms. The daylight algorithm performed best when diffuse light entered the space and the mini-blind slats were in the horizontal position. Good agreement was also seen in the East A test room where the blinds were adjusted to prevent beam radiation from entering the space. When the blinds were closed for the experiments, blind curvature allowed some penetration of daylight into the space not predicted by EnergyPlus. In the East B test room, the model performed well when diffuse radiation was entered the space (afternoons and on cloudy days). During the mornings when the sun was incident on the window, the EnergyPlus daylighting/window/shading algorithms significantly over-predicted the magnitude of illuminance at the daylight reference point. These over-predictions could be due to the fact that in its blind model, EnergyPlus assumes the blinds are flat slats, even though the actual blades have curvature. When in the horizontal position and exposed to beam radiation, the flat slat assumption increases the surface area of the window compared with reality; therefore, the flat slat assumptions seems viable for diffuse light in entering the space but over-predicted the illuminance when exposed to beam radiation.

When shading screens were installed over the windows (South A and West A test rooms), both DOE-2.1E and EnergyPlus were used. While both programs contain similar algorithms for daylight and window (Window 5.2 output files were used) calculations,

the EnergyPlus shading model accounted for back reflectances and re-transmission of both visible and solar light between the window and the shading screen, whereas DOE-2.1E used only visible and solar transmittances in its shading calculation and neglected re-transmitted light. Accounting for re-transmitted light resulted in over-predictions of the daylight illuminance at the reference point in the both South A and West A test rooms, whereas the simpler shading model used in DOE-2.1E for reference point daylight illuminances produced results much closer to reality. Other factors that may have resulted in offsetting errors may also be present.

Both EnergyPlus and DOE-2.1E were used in the west test rooms with exterior fins installed over the windows. During the morning when diffuse light entered the space (Figure 7.7), the predictions appear quite accurate. In the afternoon, when beam radiation was incident upon the projections the transition from to the window, both DOE-2.1E and EnergyPlus over-predicted the daylight reference point illuminance for most days. When beam radiation entered the space in the West B test room (where no interior shading was installed), EnergyPlus more accurately predicted reference point illuminances. From these results, the opaque non-reflecting exterior fin model seems plausible.

### **7.7.2. Light Power**

Again, none of the programs were with within the overlapping 95% credible limits from the MCA and experiment (the uncertainty ratios). The MCA credible limits are much higher than the experimental credible limits, primarily due to uncertainties in shading and window optical properties and daylight reference point illuminance setpoints. One of the limitations of the statistical analysis was that the analyses were only performed when the sum of the credible limits was great than 1.0 W — done to ensure a conceivable calculations for the uncertainty ratios. This criterion limited the extent of the analysis and excluded results when the lights were turned off by the controllers and the programs because credible limits were equal to zero during this time.

However, the statistics do provide a good basis for comparisons and program assessment.

The light powers in the rooms were directly correlated to the illuminance predictions at low daylight levels. When the daylight illuminances at the reference points exceeded the setpoints in the rooms (700 Lux for the south test rooms and 645 Lux for the east and west test rooms), the lights were turned off; therefore discrepancies in predictions for daylight illuminance reference points at higher values than the set point did not result in inconsistencies in the light power predictions.

For the east test rooms, accurate daylight illuminance predictions at the reference points when diffuse radiation entered the space translated into accurate predictions from EnergyPlus in the East B room (motorized mini-blinds). In the East A test room, the results mimicked the general trend of the experiment, but were not entirely consistent with the experiment.

In the South A test room, the over-predictions from EnergyPlus for daylight illuminance resulted in too much dimming in the space; DOE-2.1E results appear much better which can be verified in the statistical analysis (Table 7.6). In the South B test room, the EnergyPlus blind model (in the absence of beam radiation entering the space) performed quite well correlating illuminance predictions to light power. Again this accuracy is under-stated in the statistical analysis because of the cutoff criterion employed for evaluating statistical parameters.

In the west test rooms, the exterior shading algorithms in the programs accounted for the absence of beam radiation incident on the window until the afternoon when the sun is setting. For both test rooms, EnergyPlus generally under-predicted the light power (over-predicted the daylight illuminance at the reference point), while DOE-2.1E generally over-predicted the light power. In the West A test room where shading screens were used, part of this can be attributed to differences in the shading models. In the West B test room, the same exterior shading model was used with the same window models and differences can be accounted for by comparing the daylight model differences

(EnergyPlus used four sky models compared with two used in DOE-2.1E) and room geometries (the DOE-2.1E model assumes the test rooms are cuboids).

### 7.7.3. Reheat Coil Power

The statistical comparisons for the reheat coil power reveal that none of the predictions were within 95% credible limits. The credible limits from the MCA were much larger than from the experiment. This is due to the high uncertainties associated with thermophysical properties, optical properties (particularly solar transmittance and reflectance), thermal transmittances of the window, room set points (airflow rates and temperatures), which all impacted the load calculations and the required reheat coil power predictions. The experimental uncertainties only reflect the uncertainties associated with measurement of the electrical power to the coils, but do not factor in the uncertainties of the entering and leaving coil air temperatures and airflow rates, which most certainly added additional levels of uncertainty to the measurement beyond the scope of this study.

Examining the predictions from EnergyPlus, it is apparent that the reheat coil powers are always over-predicted for all rooms when required; this is primarily due to the assumption concerning zones heating and cooling set points (Figure 7.10) as discussed in Section 7.6.3. While assumption that the room is at the cooling set point temperature when cooling is required for the space reduces thermal load of the space, it significantly increases the ventilation loads with high minimum airflow rates. The control algorithm programmed in EnergyPlus does not appear to be consistent with controllers used for VAV boxes with reheat coils used in office spaces.

Generally, DOE-2.1E predictions for reheat coil power were over-predicted compared with the experiment but less than the EnergyPlus predictions. Less robust inputs were used in DOE-2.1E to describe the heat transfer between the shading screen air gap and interior window pane. There seems to be little difference between the reheat coil predictions for the east test rooms where shading screens were installed in the East A test

room and interior shading was not used in the East B test room; therefore the shade air gap modeling assumption does not appear to significantly impact the results.

## 7.8. Conclusions

While the daylight algorithms and associated interactions for EnergyPlus and DOE-2.1E performed quite well, none of the parameters were validated within 95% credible limits. In general, the blind model implemented in EnergyPlus accurately predicted visible transmittance with the window/mini-blind assembly and the controllers accurately equated daylight illuminance predictions to light power adjustments (dimming or brightening the light). However, the limitations of the model were clearly seen when beam radiation entered the space. The program also seems quite flexible when making predictions for different types of windows and combinations of shades for different times of the year.

From these results, DOE-2.1E provided better estimates for the associated performance. However, DOE-2.1E does not contain a model for mini-blinds, which severely limits the application of the program because mini-blinds are commonly installed in office spaces.

DOE-2.1E also performed better with a less robust shading algorithm, which may simply be due to offsetting errors. However, this study does provide confidence that both daylighting algorithm implementation do predict with some accuracy daylight illuminance and the associated interactions. These programs can provide insight into potential energy savings associated with the implementation of daylight controls in an office space. Building energy simulation programs can also be very valuable tools in the design phase of a new building to assess potentially daylight control energy savings by performing parametric studies varying windows and shading devices to optimize the energy performance of a building.

An indicator of overall performance during the experiment is the average differences between measured and predicted parameters. For EnergyPlus, the reference point

daylight illuminance, light power, and reheat coil power predictions were within 124.1%, 14.9%, and 39.0%. DOE-2.1E predicted reference point daylight illuminances were within 54.2%, light powers were within 10.9%, and reheat coil power were within 40.2%.

An interesting discovery in EnergyPlus was the assumption concerning dual temperature set points (heating and cooling) coupled with VAV boxes with reheat coils. The current algorithm used to determine the room temperature is not consistent with how offices and VAV systems are currently designed and constructed and results in over-predictions of reheat coil power (or heat transfer rates associated with hydronic reheat coils).

This paper provides real assessments of the building energy simulation programs when simulating daylighting in a real building. The advantage of this type of validation is that nearly all the inputs about the constructing of the room, particularly the optical properties, fixture illuminances, and light powers that impacted the daylighting calculations, were known and well-described inputs to the programs. This allowed for accurate comparisons, within levels of experimental uncertainties, of the programs and a foundation for adjusting algorithms contained in building energy simulation programs to reflect actual building performance.

### **Acknowledgements**

We would like to gratefully acknowledge the financial support of the Iowa Energy Center under Grant 9608. We would also like to thank the people at the Wisconsin Energy Center for providing the windows and the people at Nysan Shading Systems Inc. for the shading screens. We would like to thank Som Shrestha for his hard work designing and implementing the motorized blind controls. We would also acknowledge the staff at the Energy Resource Station for their assistance in running these experiments. The people specifically involved in this endeavor included: Curt Klaassen, Dave Perry, Xiao Hui Zhou, and Emir Kadic. We also thank the staff at EMPA for performing optical measurement, these people included: Martin Camenzind and Kaethe Meyer.

## Nomenclature

$D_i$	= difference between experiment and predicted values for a given value
$\overline{D}$	= mean difference for a given array
$ \overline{D} $	= mean absolute difference for a given array
$D_{max}$	= maximum difference between experimental and predicted values for a given array
$D_{min}$	= minimum difference between experimental and predicted values for a given array
$D_{rms}$	= root mean squared difference between experimental and predicted values for a given array
$D_{95\%}$	= ninety-fifth percentile of the differences between experimental and predicted values for a given array
$OU_{Experiment}$	= 95% credible limits or overall uncertainty from experiment
$OU_{EnergyPlus}$	= 95% credible limits or overall uncertainty from MCA
$\overline{OU}$	= average overall uncertainty calculated for 95% credible limits
$UR_i$	= uncertainty ratio for a given hour, no units
$\overline{UR}$	= average uncertainty ratio for a given array, no unit
$UR_{max}$	= maximum uncertainty ratio for a given array, no units
$UR_{min}$	= minimum uncertainty ratio for a given array, no units
$\bar{x}$	= arithmetic mean for a given array
$x_{min}$	= minimum quantity for a given array
$x_{max}$	= maximum quantity for a given array

## References

- [1] R.D. Judkoff, Validation of Building Energy Analysis Simulation Programs at the Solar Energy Research Institute, *Energy and Buildings*, 10, 1988, 221-239
- [2] F. Gulgermetti and F. Bisegna, Daylighting with external shading devices: design and simulation algorithm, *Building and Environment*, (Article in press and available at [www.sciencedirect.com](http://www.sciencedirect.com))
- [3] K. Park and A.K. Athienitic, Workplance illuminance prediction method for daylighting control systems, *Solar Energy*, 75, 2003, 277-284
- [4] A. Tzempelikos and A.K. Athienitis, Integrated thermal and daylighting analysis for design of office buildings, *ASHRAE Transactions*, Winter Meeting, 2005, 227-238
- [5] K. Park and A.K. Athienitic, Development and testing of an integrated daylighting control system, *ASHRAE Transactions*, Winter Meeting, 2005, 218-226
- [6] L. Bellia, A. Cesarano, F. Minisheillo, and S. Sibilio, De-Light: a software tool for the evaluation of direct daylighting illuminances both indoors and outdoors-comparison with Superlite 2.0 and Lumin Micro 7.1, *Building and Environment*, 35, 2000, 281-295
- [7] K. Johnsen, Daylight in Buildings, Collaborative research in the International Energy Agency (IEA Task 21), *Renewable Energy*, 15, 1998, 142-150
- [8] F.C. Winkelmann, and S. Selkowitz, Daylighting simulation in DOE-2 building energy analysis program, *Energy and Building*, 8, No.5, 1985, 271-286
- [9] P.G. Loutzenhiser and G.M. Maxwell, A Comparison of DOE-2.1E Daylighting and HVAC System Interactions to Actual Building Performance, Submitted to *ASHRAE Transactions* (July 14, 2005)
- [10] P.G. Loutzenhiser, Empirical validations of the DOE-2.1E building simulation software for daylighting and economizer controls, Thesis (Masters), Iowa State University, Ames, Iowa, 2003
- [11] G.M. Maxwell, P.G. Loutzenhiser, and C. Klaassen, Daylighting – HVAC Interaction Tests for the Empirical Validation of Building Energy Analysis Tools, A Report of IEA Task 22, Subtask D Building Energy Analysis Tools Project D Empirical Validation, <http://www.iea-shc.org/task22>, 2003
- [12] S. Lee, Empirical Validation of Building Energy Simulation Software: DOE-2.1E, HAP, and TRACE, Thesis (PhD), Iowa State University, Ames, Iowa, 1999
- [13] T.A. Kuiken, Energy savings in a commercial building with daylighting controls : empirical study and DOE-2 validation. Thesis (Masters), Iowa State University, Ames, Iowa, 2002

- [14] M. Bodart and A. De Herde, Global energy savings in offices buildings by use of daylighting, *Energy and Buildings*, 34, 2002, 421-429
- [15] D.H.W. Li, J.C. Lam, and S.L. Wong, Daylighting and its effect on peak load determination, *Energy*, 30, 2005, 1817-1831
- [16] S. Gates and J. Wilcox, Daylighting analysis for classrooms using DOE-2.1b, *Energy and Buildings*, Vol. 6, Issue 4:331-341, 1984
- [17] G.H. Hart, R.S. Blancett, and K.F. Charter, The use of DOE-2 to determine the relative energy performance of daylighted retail stores covered with tension supported fabric roofs, *Energy and Buildings*, Vol.6, Issue 4:343-352, 1984
- [18] P. Strachan, Model Validation using the PASSYS Test Cells, *Building and Environment*, 28, 1993, 153-165
- [19] P. Wouters, L. Vandaele, P. Voit, and N. Fisch, The use of outdoor test cells for thermal and solar building research within the PASSYS project, *Building and Environment* 28, 1993, 107-113
- [20] S.Ø. Jensen, Validation of building energy simulation programs: a methodology, *Energy and Buildings* 22, 1995, 133-144
- [21] K.J. Lomas, H. Eppel, C.J. Martin, D.P. Bloomfield, Empirical validation of building energy simulation programs, *Energy and building*, 26, 1997, 253-275
- [22] H. Manz, P. Loutzenhiser, T. Frank, P.A. Strachan, R. Bundi, and G. Maxwell. (Accepted for publication in *Building and Environment* and available online September 8, 2005 at [www.sciencedirect.com](http://www.sciencedirect.com)) Series of experiments for empirical validation of solar gain modeling in building energy simulation codes – Experimental setup, test cell characterization, specifications and uncertainty analysis.
- [23] P.G. Loutzenhiser, H. Manz, C. Felsmann, P.A. Strachan, T. Frank, and G.M. Maxwell, (Submitted July 14, 2005 to *Solar Energy*), Empirical validation of models to compute solar irradiance on inclined surfaces for building energy simulation.
- [24] P.G. Loutzenhiser, H. Manz, P.A. Strachan, C. Felsmann, T. Frank, G.M. Maxwell, and Peter Oelhafen, An Empirical Validation of Solar Gain Models Found in Building Energy Simulation Programs, (Submitted to *HVAC&R Research* on November 24, 2005)
- [25] EnergyPlus Software (Version 1.2.3), Building Energy Simulation Code, <http://www.energyplus.gov>, 2005
- [26] DOE-2.1E (Version-119) Building Energy Simulation Code, Lawrence Berkley National Laboratories (LBNL), Berkley, CA, April 9, 2002

- [27] B.A. Price and T.F.Smith, Description of the Iowa Energy Center Energy Resource Station: Facility Update III, University of Iowa, Iowa City, IA, 2000
- [28] European Standard EN 410. Glass in building – Determination of luminous and solar characteristics of glazing. European Committee for Standardization, Brussels, Belgium, 1998
- [29] GLAD Software. Swiss Federal Laboratories for Materials Testing and Research (EMPA), Duebendorf, Switzerland, 2002
- [30] ASHRAE, 2001 ASHRAE Handbook of Fundamentals SI Edition, Atlanta: America Society of Heating, Refrigeration and Air-Conditioning Engineers, Inc, 2001
- [31] EnergyPlus, Engineering Reference, Board of Trustees of University of Illinois and the University of California through Orlando Lawrance Berkley Laboratories, October 11, 2005
- [32] R. Perez, P. Ineichen, R. Seals, J. Michalsky, and R. Stewart, Modeling daylight availability and irradiance components from direct and global irradiance. Solar Energy 44, No.5, 1990, 271-289
- [33] P.Ineichen, R.Perez, and R,Seals, The importance of correct albeto determination for adequately modeling energy received by a tilted surface. Solar Energy Vol.39 No.4, 1987, 301-305
- [34] Window 5.2 Version 5.2.17, LBNL, June 3, 2003
- [35] ISO/FDIS 15099: 2003(E), Thermal performances of windows, doors, and shading devices—Detailed calculations, 2003
- [36] G.N. Walton, Thermal Analysis Research Program Reference Manual. NBSIR 83-2655, March 1983, 21
- [37] Clark G. and C. Allen.. The Estimation of Atmospheric Radiation for Clear and Cloudy Skies. Proc. 2nd National Passive Solar Conference (AS/ISES), 1978, 675-678
- [38] EN ISO 6946, Building components and building elements – Thermal resistance and thermal transmittance –Calculation Method, August 1996
- [39] G.L. Gleser, Assessing Uncertainty in Measurement, Statistical Science, Vol. 13, No.3, 1998, 277-290

## **Chapter 8: Conclusions**

Empirical validations of building energy simulation programs are intensive undertakings that require well-instrumented facilities, experienced staff, and extensive collaboration between the people designing and running the experiments and modelers. While programs are being continually improved to better simulate reality, the experimental design and data sets from these studies are available for evaluating and improving building energy simulation programs and algorithms and can be a lasting contribution for continued improvements in the area of building energy simulation.

The focus of empirical validations was to evaluate the performance within the constraints of the programs. Therefore, it was impossible to use an occupied building with changing internal loads, infiltration between zone, changing shading conditions, and other parameters that are varied by occupants. In such cases, the uncertainties associated with these predictions would make it impossible to assess the performance of programs. For this research, nearly every facet of the experiments was controlled.

Particular emphasis was placed on ensuring the inputs to the building energy simulation programs were well-described. Specific examples and conclusions for the EMPA and ERS components of the research and an overall assessment of the study are documented below.

### **8.1. EMPA Experiments**

For the series of experiments performed at EMPA, the optical properties of the glass panes, shading devices and interior surfaces over the entire solar spectrum, thermal conductivities of the construction materials, two and three-dimensional heat transfer simulation programs, and well-described boundary conditions (outside surface temperatures for construction elements adjacent to the guarded zone, measured internal loads, and accurate weather inputs) were measured or simulated for use in evaluating building energy simulation programs. While this level of detail could not be attained in actual practice, the precise determination in the study allowed for careful assessments and

comparisons; in many cases, quantifying the input properties, particularly the thermal bridges, required calorimetric hotbox experiments and software calculations that were much more computationally intensive than what is currently found in building energy simulation programs. However, from these comparisons, conclusions were drawn concerning heat transfer coefficients, transmitted solar energy, radiative heat exchange, heat transfer in the air gap between shading devices and window panes, tilted radiation models, and many more topics. Preliminary results from these studies are already being realized in HELIOS, a building energy simulation program designed and maintained at EMPA. These studies have resulted in the implementation of a more accurate tilted radiation model, an angular dependent window algorithm, and a blind assembly model.

The order of experiments from simple to complex provided clear levels for identifying specific problems within the various models. This step-by-step method allowed for accurate diagnosis of potential deviations and a determination of how the discrepancies in the models propagated through the various experiments. The list below identifies some of these items.

- The transient characterization experiment provided evidence that the thermophysical properties and thermal bridges within the test cell were well-described and could accurately characterize the test cell in the programs for subsequent experiments.
- An evaluation of tilted radiation models prior to evaluating solar gains through the glazing unit revealed differences associated with incident radiation on the exterior wall and glazing unit, which impacted the solar gain models. This study also identified differences between the components of irradiance (direct-normal, diffuse horizontal, and global horizontal). The predictions were compared and the most reliable tilted radiation model for this region was used for remaining experiments.
- The glazing unit experiment provided reliable information concerning the quantifying and modeling the thermal bridges associated with the glazing unit spacer and mounting. The experiment also offered insight into the performance of algorithms for modeling angular dependent window properties.
- Diffuse interior and exterior shading screens were the simplest of all shading devices used in this study. The two experiments revealed discrepancies and shortcomings in various programs' abilities to account for transmissions through the screens and model the heat transfer in the air gap between the shading device and the glazing unit.

- The Venetian blind assembly was a much more complicated shading device that could not be simulated by all building energy simulation programs. However, the study revealed that there were models specifically designed to address these issues, one of which was implemented in EnergyPlus.

In some instances, some of the effects in the glazing unit experiment did not affect the shading experiments. For example, the magnitude of the transmitted solar power to the cell impacted the convective heat transfer coefficient algorithms which altered the time constant of the test cell in some programs; this was somewhat mitigated in EnergyPlus and ESP-r by the installation of shading devices where mostly diffuse radiation entered the test cell.

But for all the planning and preparation that went into the experiments, there were some issues that could not be addressed within this study and will be discussed in a subsequent chapter.

## **8.2. ERS Experiment**

The experiment performed at the ERS was well-documented and designed for assessing the performance of daylighting algorithms and their implementations within the building energy simulation programs. While analyses of thermophysical properties and thermal bridges were not as extensive as that done at EMPA, high airflow rates into the test rooms offset many of these uncertainties. Inputs that pertained to daylighting like optical properties of the shading screens, blinds slats, and interior surfaces were measured over the entire solar spectrum and integrated over both the solar and visible spectrums. The windows were simulated using software and an international database of glass spectral data. Light power versus illuminance measurements accurately describe of the daylighting input for the building energy simulation programs, and the reference point was fixed on the table with a light sensor that controlled the dimming of the lights.

Again, while many of the inputs and control strategies used for this exercise would not be known or used by design engineers, they do provide for a comprehensive evaluation of the daylighting algorithms. The comparisons between the different test

rooms oriented in different direction and combinations of windows and shading devices provided a unique assessment about the performance of building energy simulation programs.

### **8.3. Overall Assessments**

Many things can be taken from this study and used in future empirical validation efforts. The reasons for the relative success of the project was due to careful examination of the literature prior to initiating the endeavor, thoughtful design of the experimental setup using simulation tools, vigilant monitoring of the data, emphasis on thoroughly quantifying input parameters, careful consideration of uncertainties, collaboration with IEA Task 34/Annex 43 Subtask C, and a cohesive set of statistical parameters used for assessing the performance of the programs. While in retrospect, it is always possible to improve the experiments, this study was the one of most detailed empirical validations for building energy simulation programs ever performed.

## **Chapter 9: Recommendation for Future Work**

This research provides a solid foundation for future work in this field. Validation of building energy simulation programs is an ongoing task continually evolving to address changes in technology and building energy simulation programs. The research focused on very simple models of glazing units, shading devices, and daylighting that can be expanded upon to evaluate more complex cases described in the subsequent sections.

### **9.1. Glazing Units**

For this research, typical glazing units were used for empirical validation. Additional validation could assess the simulation of switchable glazing units that change optical characteristics to address different levels of light entering the zone. As glazing technology continues to improve, so-called smart glazings will become more important in building construction, and, thus, the need for reliable predictions will become necessary.

### **9.2. Window Shading Devices**

The shading devices investigated in this study were very simple and the optical properties were nearly independent of wavelength over the solar spectrum. This allowed the use of integral transmittance and reflectance in the building energy simulation programs that were reasonably precise. The accuracy of this method for shading devices with wavelength selective properties in the solar spectrum coupled with wavelength selective glazing units should be studied in future work to investigate the viability of this assumption made in some building energy simulation programs with respect to optical properties of shading devices.

### **9.3. Daylighting**

The most fundamental component of daylight controls were investigated in this study. However, there are many additional facets of daylighting including: light shelves, light

well, dome fenestration, and double skin facades that need to be validated on should be the topic of future studies.

**Appendix A: Test Cell Transient Characteristic Exercise**

**IEA Task 34/Annex 43  
Empirical Validation Project of Building Energy  
Simulation Tools  
Shading / Daylighting / Load Interaction**

**Test Cell Transient Characteristic Exercise**

Written by  
Heinrich Manz  
Peter Loutzenhiser  
Thomas Frank

August 25, 2004  
Revised March 15, 2005

## Introduction

This document contains information regarding the parameters and conditions used for an experiment performed at the Swiss Federal Laboratories for Material Testing and Research (EMPA) outdoor test cell facility. The experiment was designed to describe the transient characteristics of the test cell and was done in conjunction with the International Energy Agency Task 34/Annex 43 Subtask C. This experiment used pseudo-random heat inputs by which modelers can check the accuracy of their respective simulation tools. Information about the test cell location, experimental setup, geometrical and thermophysical properties, and results from a steady-state experiment for the overall thermal characteristics of the cell are contained within this document and an associated file.

## Test Cell

The test facility is comprised of two identical test cells designed for calorimetric measurements on façade elements shown in Figure 1a. Only one of the test cells was used for this experiment. The five faces of the test cell are adjacent to guarded zones. Each test cell and guarded zone has its own climate control system that can provide heating or cooling to maintain space temperatures. Figure 1b contains a diagram of the test cell configuration along with the guarded zones. For each test cell, a climate controlled exterior chamber can be mounted over an exterior surround panel. A picture of this external chamber is shown in Figure 1c. Specific information concerning the test cell construction and location are described in this section.

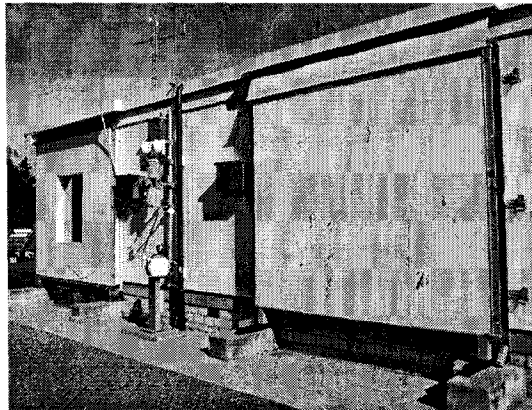


Figure 1a Outdoor test facility with removable façade element.

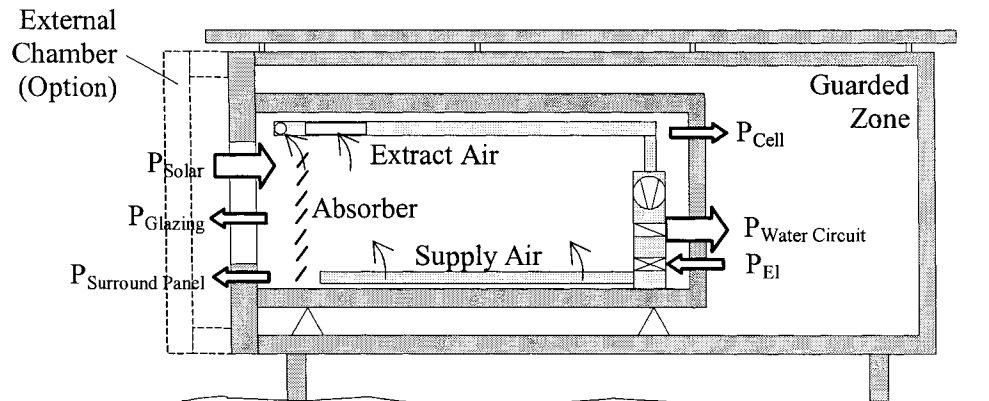


Figure 1b Diagram of test toom with an optional external chamer.

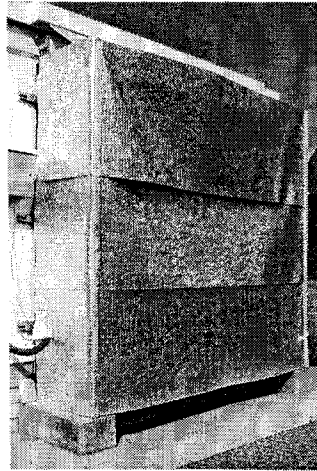


Figure 1c Photograph of test toom with external chamber.

### Test cell location

The test cell is located at EMPA in Duebendorf, Switzerland. Table 1 contains information concerning the global location, time zone, and orientation of the test cell.

Table 1 Location of the EMPA test cell.

Degrees of longitude	-8.6°
Degrees of latitude	47.7°
Altitude above sea-level	430 m
Time Zone	Greenwich Mean Time (GMT) + 1 hr
Orientation of external wall	29° (south = 0°, west =90°)

### Test cell construction

The internal dimensions of the test cell are shown in Table 2.

Table 2 Dimensions of the test cell.

Internal height	2.360 m
Internal width	2.850 m
Internal length	4.626 m
Area of the north/south wall	6.726 m <sup>2</sup>
Area of the east/west wall	10.917 m <sup>2</sup>
Area of the floor/ceiling	13.184 m <sup>2</sup>
Internal volume	31.114 m <sup>3</sup>

The thermophysical properties of the cell were obtained from measurements, literature, product specification, a three dimensional whole cell simulation, and a steady-state experiment used for overall thermal characterization of the cell. Tables 3 to 5 show layer sequences, thicknesses and thermophysical properties for all layers of the cell envelope. Layer Number 1 denotes the outside layer of the test cell. In the case of the thermal conductivity for the insulation layers, the quantity is based on a linear regression analysis calculated as a function of the average temperature in the material. A second set of tables is provided where the temperature dependent properties are evaluated at an average mean temperature of 28.38°C.

The outer surface of the removable external wall, the south wall of the cell, was painted white. Reflectance of a sample was measured in the wavelength interval of solar radiation at approximately perpendicular incident solar radiation and by means of a spectrophotometer. An integral value for reflectance of  $\rho = 0.76$  was determined according to EN 410 [1] by means of GLAD software [2]. The emissivity was measured to be  $\varepsilon = 0.93$  using an integral method (3-100  $\mu\text{m}$ ). The internal surfaces of the cell were also painted white and the emissivity was approximated to be  $\varepsilon = 0.9$ . The initial temperatures of the material can be estimated using initial surface temperature data that are provided in an Excel file entitled "Experiment 2.xls".

Table 4a Ceiling, North, East and West wall construction as a function of temperature.

Layer number	Material	Thickness mm	Thermal conductivity W/m-K	Density kg/m <sup>3</sup>	Specific heat J/kg-K
1	Sheet steel	0.7	53.62	7837	460.8
2	PU foam	139	0.01921 + 0.000137· $\theta$	30	1800
3	Sheet steel	0.7	53.62	7837	460.8

Table 4b Ceiling, North, East and West wall construction evaluated at  $\theta = 28.38^\circ\text{C}$ .

Layer number	Material	Thickness mm	Thermal conductivity W/m-K	Density kg/m <sup>3</sup>	Specific heat J/kg-K
1	Sheet steel	0.7	53.62	7837	460.8
2	PU foam	139	0.023098	30	1800
3	Sheet steel	0.7	53.62	7837	460.8

Table 5a Floor construction as a function of temperature.

Layer number	Material	Thickness mm	Thermal conductivity W/m-K	Density kg/m <sup>3</sup>	Specific heat J/kg-K
1	Sheet steel	0.7	53.62	7837	460.8
2	PU foam	140	0.01921 + 0.000137·θ	30	1800
3	PU foam (higher density)	20	0.070	45	1800
4	Sheet steel with surface structure	2.5	53.62	7837	460.8

Table 5b Floor construction evaluated at  $\theta = 28.38^\circ\text{C}$ .

Layer number	Material	Thickness mm	Thermal conductivity W/m-K	Density kg/m <sup>3</sup>	Specific heat J/kg-K
1	Sheet steel	0.7	53.62	7837	460.8
2	PU foam	140	0.023098	30	1800
3	PU foam (higher density)	20	0.070	45	1800
4	Sheet steel with surface structure	2.5	53.62	7837	460.8

Table 6a South wall construction as a function of temperature.

Layer number	Material	Thickness mm	Thermal conductivity W/m-K	Density kg/m <sup>3</sup>	Specific heat J/kg-K
1	Plywood	10	0.13636+0.000175·θ	850	1605
2	EPS foam	130	0.03356 + 0.000127·θ	28	1460
3	Plywood	10	0.13636+0.000175·θ	850	1605

Table 6b South wall construction evaluated at  $\theta = 28.38^\circ\text{C}$ .

Layer number	Material	Thickness mm	Thermal conductivity W/m-K	Density kg/m <sup>3</sup>	Specific heat J/kg-K
1	Plywood	10	0.14133	850	1605
2	EPS foam	130	0.03716	28	1460
3	Plywood	10	0.14133	850	1605

Total thermal losses--including those at edges, door, sealing at external wall and intersections of pipes or flexes with the cell envelope--were computed using TRISCO software [3]. This code allowed a three dimensional steady-state analysis of heat conduction processes. Equivalent thermal conductivities of cavities were calculated according to prEN ISO 10077-2 [4]. The final model of the test cell employed  $5.6 \cdot 10^6$  nodes. The results of these simulations are shown in Figures 2a and 2b. The results in Figure 2a were generated for a 1 K temperature difference between the cell air and the guarded zone. High heat fluxes were seen at the sealing of the door and at the sealing between cell and removable external wall. Figure 2c shows an image of the test cell taken by an infrared of the thermal bridges at the door. This picture was taken for a 20 K temperature difference between the cell air and the guarded zone. Bright areas represent regions with higher surface temperatures.

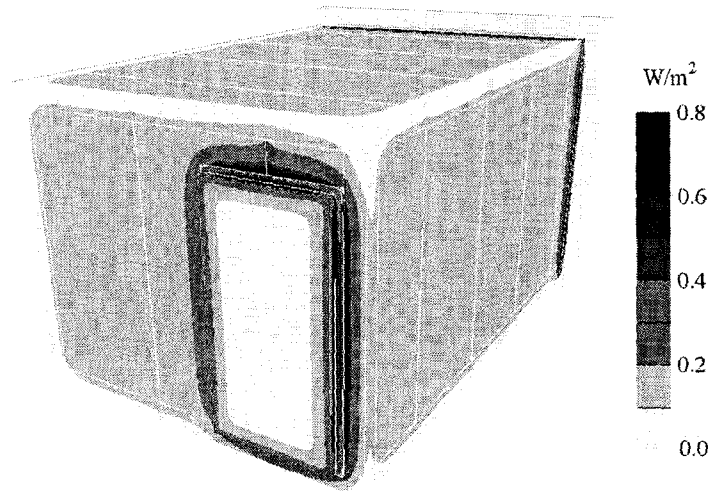


Figure 2a Computed heat fluxes at the outer surfaces of the test cell.

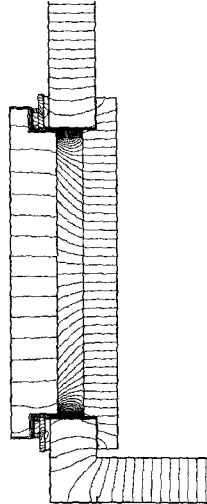


Figure 2b Computed heat fluxes for a horizontal cross-section of the door.



Figure 2c Infrared picture of the test cell door.

The internal mass of the technical equipment positioned in the cell, which consisted of metallic ducts, grills, fans, a heat exchanger apparatus inside a metal casing, an electrical cabinet, etc., was estimated to be 200 KJ/K. Because the steel sheets are a major component in the thermal mass, the thermal response was assumed to be fast compared to the cell envelope. The impact of this mass on the overall transient thermal behavior of the cell is rather small.

Tables 7a and 7b contain the total steady-state properties at 20°C for the thermal conductance. This parameter refers to the heat flow between the cell air and the outer surface of the cell envelope.

Table 7a Heat transfer characteristics of the guarded zone.

	Area $m^2$	Thermal conductance W/K
Ceiling, north (incl. door), east and west wall	41.745	6.478
Floor	13.184	1.941
Thermal bridges guarded zone	-	4.526
Total		12.945

Table 7b Heat transfer characteristics of the exterior wall.

	Area A $m^2$	Thermal conductance W/K
External wall	6.726	1.736
Thermal bridges outside	-	0.040
Total		1.776

The thermal conductance from a TRISCO software simulation of the entire cell envelop (from inside the cell to the outer surface, including thermal bridges) at 0°C and 20°C were calculated to be 13.539 W/K and 14.721 W/K, respectively.

The thermal conductance,  $H$ , as a function of mean wall temperature,  $\theta$  in °C, for the guarded zone and the exterior wall are given in Equations 1 and 2.

$$\text{Guarded zone: } H_{GZ}(\theta) = 11.877 + 0.0534 \cdot \theta \quad (\text{W/K}) \quad (1)$$

$$\text{Exterior wall: } H_{EW}(\theta) = 1.662 + 0.0057 \cdot \theta \quad (\text{W/K}) \quad (2)$$

Prior to running this experiment, a steady-state experiment was performed and results were used to calculate the thermal conductance. These calculations were performed for mean wall temperatures for the exterior wall and guarded zone of 36.6°C and 31.6°C, respectively. The calculated thermal conductance for the exterior wall was  $2.12 \pm 0.59$  W/K and  $12.23 \pm 0.53$  W/K for the guarded zone.

To ensure the test cell was airtight, gaps between the steel sheets used for cell construction were sealed with silicon. Two stage rubber seals were installed and the door and the external walls to eliminate air leads. Cell infiltration was tested using the blower door method. When the test cell was pressurized to 50 Pa, the air exchange rate was found to be  $0.2 \text{ h}^{-1}$ . It was therefore assumed that zone infiltration was negligible.

## Experimental Setup

For this experiment, an external chamber was mounted on the exterior wall for climate control for the exterior wall. The temperature in the guarded zone and the external chamber were maintained near 23°C, and the air inside the guarded cell was re-circulated and stirred to reduce thermal stratification. During the tests the re-circulating fans operated constantly and added an internal heat load of 77 W. After an initial preconditioning phase of 50 hours, a pseudo-random heat source of 196 W was turned on and off to provide an additional internal load. The heat source was located inside the cell recirculation/conditioning apparatus and can therefore be considered purely convective.

Hourly averaged values (where 1 corresponds to a time from 0:00 to 1:00) for the measured mean surface temperatures (boundary conditions), cell air temperatures and internal loads are given in an Excel file accompanying this document entitled “Experiment 2.xls”. This file contains all the input data that are required to perform the simulation. Figure 3 shows the locations of the temperature sensors in cell and described in this file.

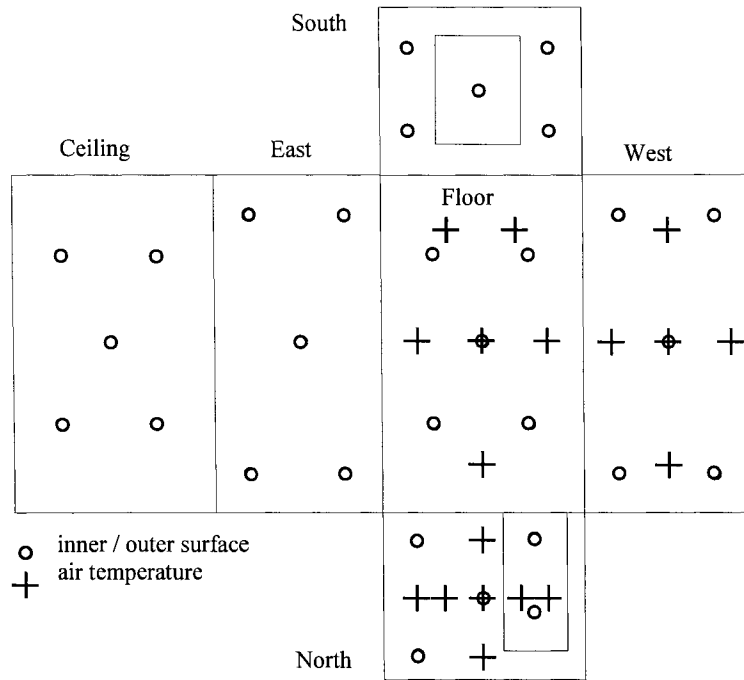


Figure 4. contains a plot of the results for the experiment. Included in the plot are the mean cell temperature, mean surface temperatures, and the additional internal load introduced into the space.

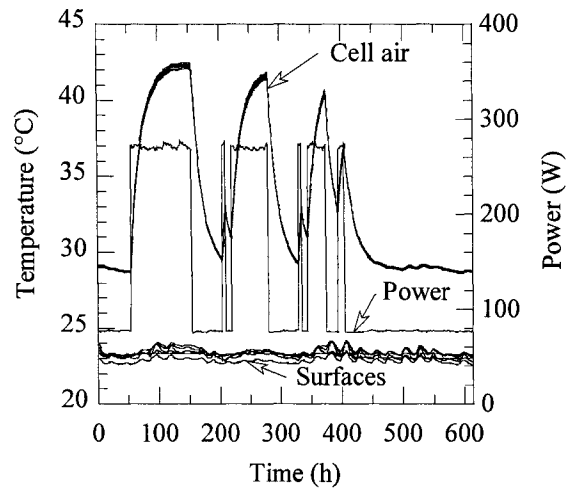


Figure 5. Comparison plots for zone temperature.

## Output Report

A report describing the following output for each hour the experiment was run should be submitted. The output will be used to compare the results for the various models and the experiment. The headers for the output file and a description of their meaning are described in Table 8.

Table 8 List of output headers.

Hour	Zn-Temp <sup>1)</sup>	South-IST <sup>2)</sup>	West-IST <sup>3)</sup>	North-IST <sup>4)</sup>	East-IST <sup>5)</sup>	Ceil-IST <sup>6)</sup>	Floor-IST <sup>7)</sup>
	1) is the average cell air temperature in °C.						
	2) is the inside cell surface temperature of the south wall in °C.						
	3) is the inside cell surface temperature of the west wall in °C.						
	4) is the inside cell surface temperature of the north wall in °C.						
	5) is the inside cell surface temperature of the east wall in °C.						
	6) is the inside cell surface temperature of the ceiling in °C.						
	7) is the inside cell surface temperature of the floor in °C.						

## Input Report

Reports describing the thermophysical properties that were used for the simulation should be submitted. Table 6a lists the format for the input file that contains material properties. Also a brief written summary of how the thermal bridges and thermal mass were simulated would prove useful when comparing the results. Tables 9b and 9c lists the headers for the convective heat transfer coefficient and the radiative heat transfer coefficient (if an available output) for and hourly output from the simulations. If constant values were used, please just provide one row of values.

Table 9a Material inputs.

Material	Thermal conductivity W/(m K)	Density kg/m <sup>3</sup>	Specific heat J/(kg K)
Sheet steel <sup>1)</sup>			
PU foam <sup>2)</sup>			
PU foam (higher density) <sup>1)</sup>			
Sheet steel with surface structure <sup>1)</sup>			
Plywood <sup>1)</sup>			
EPS foam <sup>2)</sup>			

1) Please provide a value if an alternate property was used in lieu of the one provided.

2) If the values change as a function of time, please provide hour-by-hour output of the thermophysical properties.

Table 9b Convective heat transfer coefficients.

Hour	South- CHTC <sup>1)</sup>	West- CHTC <sup>2)</sup>	North- CHTC <sup>3)</sup>	East- CHTC <sup>4)</sup>	Ceil- CHTC <sup>5)</sup>	Floor- CHTC <sup>6)</sup>	TBridge- CHTC <sup>7)</sup>
------	------------------------------	-----------------------------	------------------------------	-----------------------------	-----------------------------	------------------------------	--------------------------------

1) is the convective heat transfer coefficient for the south wall in W/m<sup>2</sup>-K.

2) is the convective heat transfer coefficient for the west wall in W/m<sup>2</sup>-K.

3) is the convective heat transfer coefficient for the north wall in W/m<sup>2</sup>-K.

4) is the convective heat transfer coefficient for the east wall in W/m<sup>2</sup>-K.

5) is the convective heat transfer coefficient for the ceiling in W/m<sup>2</sup>-K.

6) is the convective heat transfer coefficient for the floor in W/m<sup>2</sup>-K.

7) is the convective heat transfer coefficient for the thermal bridge in W/m<sup>2</sup>-K.

Table 9c Radiative heat transfer coefficients.

Hour	South-RHTC <sup>1)</sup>	West-RHTC <sup>2)</sup>	North-RHTC <sup>3)</sup>	East-RHTC <sup>4)</sup>	Ceil-RHTC <sup>5)</sup>	Floor-RHTC <sup>6)</sup>	TBridge-CHTC <sup>7)</sup>
------	--------------------------	-------------------------	--------------------------	-------------------------	-------------------------	--------------------------	----------------------------

1) is the radiative heat transfer coefficient for the south wall in  $W/m^2 \cdot K$ .

2) is the radiative heat transfer coefficient for the west wall in  $W/m^2 \cdot K$ .

3) is the radiative heat transfer coefficient for the north wall in  $W/m^2 \cdot K$ .

4) is the radiative heat transfer coefficient for the east wall in  $W/m^2 \cdot K$ .

5) is the radiative heat transfer coefficient for the ceiling in  $W/m^2 \cdot K$ .

6) is the radiative heat transfer coefficient for the floor in  $W/m^2 \cdot K$ .

7) is the radiative heat transfer coefficient for the thermal bridge in  $W/m^2 \cdot K$ .

## References

- [1] European Standard EN 410. Glass in building – Determination of luminous and solar characteristics of glazing. European Committee for Standardization, Brussels, Belgium, 1998
- [2] GLAD Software. Swiss Federal Laboratories for Materials Testing and Research (EMPA), Duebendorf, Switzerland, 2002
- [3] TRISCO Version 10.0w, A computer program to calculate 3D steady-state heat transfer, Physibel, Heirweg 21, B-9990 Maldegem, Belgium
- [4] prEN ISO 10077 - 2 Thermal performance of windows, doors and shutters - Calculation of thermal transmittance - Part 2: Numerical method for frames (Final Draft), European Committee for Standardization, Brussels, 2003

**Appendix B: Evaluation of Building Energy Simulation Codes' Irradiance Models**

**IEA Task 34/Annex 43 Subtask C  
Empirical Validation of Building Energy Simulation Tools  
Shading / Daylighting / Load Interaction**

**Evaluation of Building Energy Simulation Codes' Irradiance  
Models**

Written by  
Peter Loutzenhiser  
Heinrich Manz  
Thomas Frank

April 18, 2006

## Introduction

In preparation for the solar gain experiments, a description of a preliminary exercise designed to validate incident radiation models from each building energy simulation is provided in this document. The experiment was performed from October 2 to October 26, 2004 at the EMPA outdoor test facility in Duebendorf, Switzerland. The purpose of this exercise is to take two of three radiation measurement (direct-normal irradiance, diffuse irradiance, or global horizontal irradiance) along with the measured ground reflectance and predict the incident radiation (or total vertical irradiance) on the southwest façade. Weather data that were measured for this experiment are contained in an associated Excel file entitled “Experiment 3 Weather Data.xls”. This exercise is not intended to be a blind exercise; therefore the measured incident radiation on the façade is also provided in the weather file. Because these weather data will also be used for the first solar gain experiment, data for all the weather parameters measured are provided. Information about the location, orientation, and dimensions of the test cell is contained in two previous documents<sup>1,2</sup> and can be made available upon request.

---

<sup>2</sup> *Results from the Test Cell Transient Characteristic Exercise Round 1* sent out to participants October 26, 2004

## Weather Data

The weather data for the experiment were measured at the test site. Additional weather data measured near the facility (i.e. cloud cover modifier) can be provided if necessary. The parameters and equipment used to perform the measurements are shown in Table 1. A photograph of the equipment is shown in Figure 1.

Table 1 Weather data parameters and equipment.

Parameter	Unit	Type of sensor / measurement	Number of sensors	Accuracy
Solar global irradiance, façade plane (29° W)	W/m <sup>2</sup>	Pyranometer (Kipp & Zonen CM 21)	1	± 2 %
Solar global horizontal irradiance	W/m <sup>2</sup>	Pyranometer (Kipp & Zonen CM 21)	1	± 2 %
Solar diffuse horizontal irradiance	W/m <sup>2</sup>	Pyranometer, mounted under the shading ball of a tracker (Kipp & Zonen CM 11)	1	± 3 %
Direct-normal irradiance	W/m <sup>2</sup>	Pyrheliometer, mounted in an automatic sun-following tracker (Kipp & Zonen CH 1)	1	± 2 %
Infrared irradiance, façade plane	W/m <sup>2</sup>	Pyrgeometers (Kipp & Zonen CG 4)	1	± 2 %
Outside air temperature, in front of façade	°C	Radiation shielded, mechanically ventilated thermocouples	2	± 0.5 K
Wind speed, in front of façade	m/s	Ultrasonic anemometer (WindMaster )	1	± 1.5 %
Horizontal illuminance	Lx	Luxmeter (Kipp & Zonen LuxLite, Minolta T-10W)	2	± 3 %
Pressure	hPa	Barometric Pressure Measuring Device (Vaisala PTA 427)	1	± 0.5 hPa
Relative humidity	%	Humidity Transmitter (Vaisala HMP 130Y Series)	1	± 1% (0-90%) ± 2% (90-100%)

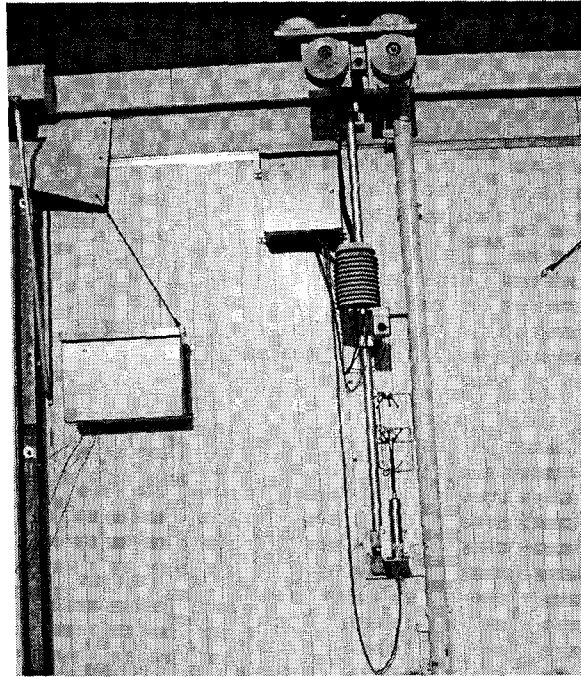


Figure 1 Weather station instruments.

## Ground Reflectance Measurement

Artificial green turf was installed in front of the test cell to represent a typical outdoor surface. Hemispherical-hemispherical reflectance at each wavelength were determined by using angular dependent model for absorptance,  $\alpha(\theta)$ , [1] for incident angles between  $0^\circ$  and  $80^\circ$ , and the a linear model between  $80^\circ$  and  $90^\circ$ . This piecewise function is shown in Equation 1. Equation 2 was used to calculate the hemispherical-hemispherical reflectance,  $\rho_{hem}$  [2]. This integral was evaluated numerically using Engineering Equation Solver [3]. Directional-hemispherical reflectance at a normal incident angle, which were measured at Basel University by Professor Peter Oelhafen and his research group, and are contained in the associated Excel file entitled “Experiment 3 Weather Data.xls”. Integral values for reflectance were determined according to EN 410 [4] by means of GLAD software [5] and the directional-hemispherical reflectance at a normal angle of incidence is provided in Table 2. A photograph of the artificial turf is shown in Figure 2. The specular components of the reflectance were measured at incident angles of  $20^\circ$ ,  $40^\circ$ , and  $60^\circ$  and found to be less than 1%; therefore the surface was considered a Lambert surface [3].

$$\frac{\alpha(\theta)}{\alpha_n} = \begin{cases} 1 + 2.0345 \times 10^{-3} \theta - 1.99 \times 10^{-4} \theta^2 + 5.324 \times 10^{-6} \theta^3 - 4.799 \times 10^{-8} \theta^4 & 0^\circ \leq \theta \leq 80^\circ \\ -0.064\theta + 5.76 & 80^\circ \leq \theta \leq 90^\circ \end{cases} \quad [1]$$

where

$\theta$  is the angle of incidence, °

$\alpha_n$  is the normal absorptance

$$\rho_{hem} = 2 \int_0^{90} (1 - \alpha(\theta)) \sin(\theta) \cos(\theta) d\theta \quad [2]$$

Table 2 Ground reflectance.

	Hemispherical Reflectance, %	Normal Incident Reflectance, %
Solar	14.8	8.8
Visible	8.1	14.2

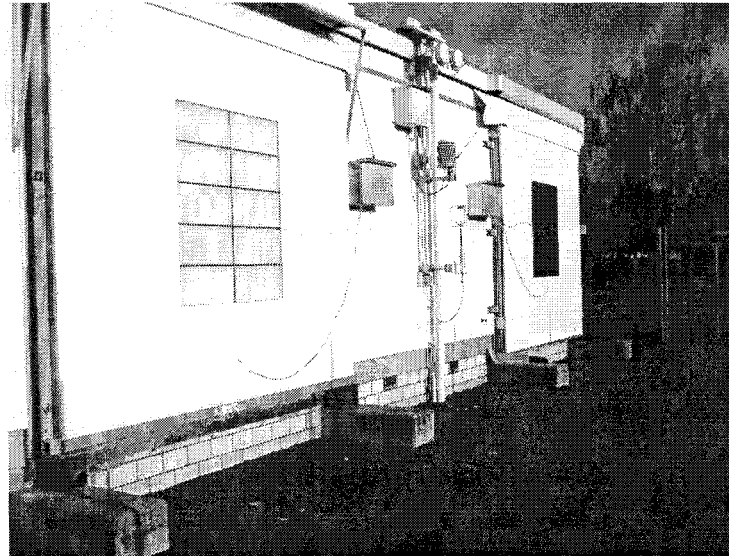


Figure 2 A photograph of the test cell.

## Output Report

The output variables will be divided up into two components which include: 1) output that can be compared to measured data at the test facility--empirical validations, and 2) code-to-code comparisons of output parameters that are not measured at the facility. The code-to-code comparison may prove useful in identifying discrepancies in the results.

A report describing the following output for each hour the experiment was run should be submitted. The headers for the data file and a description of their meaning are described in Table 3. Please provide all results from the simulations in an Excel file, if

possible, using this format. In addition to the parameters requested in Table 3, please provide a description of the model used in the building energy simulation software to calculate the incident radiation on the exterior surface. Please direct any questions regarding the exercise to Peter Loutzenhiser ([peter.loutzenhiser@empa.ch](mailto:peter.loutzenhiser@empa.ch)).

Table 3 List of headers for data file.

Hour <sup>1)</sup>	Input Parameters			Output Parameters			
	Bn <sup>2,a)</sup>	Dh <sup>3,a)</sup>	Gh <sup>4,a)</sup>	IIR <sup>5,b)</sup>	Bn-IIR <sup>6,c)</sup>	Dv-IIR <sup>7,c)</sup>	RF-IIR <sup>8,c)</sup>

\* Please provide the two parameters used for the exercise.

1) is the time in Western European Standard time (GMT +1).

2) is the direct-normal irradiance in  $W/m^2$ .

3) is the diffuse horizontal irradiance in  $W/m^2$ .

4) is the global horizontal irradiance in  $W/m^2$ .

5) is incident radiation (total vertical irradiance) on the southwest façade in  $W/m^2$ .

6) is the direct component of the incident radiation on the southwest façade in  $W/m^2$ .

7) is the diffuse component of the incident irradiance on the southwest façade in  $W/m^2$ .

8) is the reflected component of the incident irradiance on the southwest façade in  $W/m^2$ .

a) is an empirical validation where the parameter is measured on site.

b) is a code-to-code comparisons where the parameters are not measured on site.

## References

- [1] Duffie, JA, and Beckman, WA, Solar Engineering and Thermal Processes 2<sup>nd</sup> Edition, John Wiley and Sons Inc., New York, Chichester, Brisbane, Toronto, Singapore, 1991
- [2] Klein, SA, Engineering Equation Solver (EES) Software, Department of Mechanical Engineering, University of Wisconsin—Madison, 2004
- [3] Modest, M., Radiative Heat Transfer 2<sup>nd</sup> Edition, Academic Press, Amsterdam, Boston, London, New York, Oxford, Paris, San Diego, San Francisco, Singapore, Sydney, Tokyo, 2003
- [4] European Standard EN 410. Glass in building – Determination of luminous and solar characteristics of glazing. European Committee for Standardization, Brussels, Belgium, 1998
- [5] GLAD Software. Swiss Federal Laboratories for Materials Testing and Research (EMPA), Duebendorf, Switzerland, 2002

**Appendix C: Constant Temperature Experiment with Glazing Only**

**IEA Task 34/Annex 43 Subtask C  
Empirical Validation Project of Building Energy  
Simulation Tools  
Shading / Daylighting / Load Interaction**

**Constant Temperature Experiment with Glazing Only**

Written by  
Peter Loutzenhiser  
Heinrich Manz  
Thomas Frank

June 6, 2005  
Revised June 20, 2005  
Revised October 21, 2005

## Introduction

This document contains information regarding the parameters and conditions used for an experiment performed at the Swiss Federal Laboratories for Material Testing and Research (EMPA) in Applied Building Physics Laboratory outdoor test cell facility in Duebendorf, Switzerland from October 2 to October 26, 2004. The experiment was designed to evaluate the impact of solar gains through a glazing and was done in conjunction with the International Energy Agency (IEA) Task 34/Annex 43 Subtask C. The purpose of this exercise is to use the boundary conditions, weather data, and glazing properties to predict—in each respective building energy simulation code—the required heating and cooling heating to maintain a relatively constant temperature (average hourly space temperatures are provided as a code input). The first round of simulations will be a blind exercise; therefore information regarding the measured heating and cooling power requirements was not included in this document. Information about the glazing, thermophysical properties evaluated at mean envelope temperatures, and the linear thermal transmittance are provided in this document. An associated Excel document entitled “Experiment 3.xls” contains measured hourly weather data, exterior surface temperatures adjacent to the guarded zone, space temperatures, internal load, and glazing properties (inside and outside reflectance, and transmittance) as a function of wavelength. Information concerning the test cell location, geometrical and temperature dependent thermophysical properties, thermal bridge, and outside ground reflectance calculations are contained in previous IEA Task 34/Annex 43 Subtask C documents<sup>3,4,3</sup> that can be made available upon request.

---

<sup>3</sup> *Test Cell Transient Characteristic Exercise*, August 25, 2004

<sup>4</sup> *Results from the Test Cell Transient Characteristic Exercise Round 1*, sent out to participants on October 26, 2004

<sup>3</sup> *Evaluation of Building Energy Simulation Codes' Irradiance Models*, February 9, 2005

## Description of the Experiment

This section contains specific information about the experiment, which includes the following information.

- Test configuration.
- The placement and properties of the glazing.
- A two-dimensional steady-state heat transfer simulation and calorimetric measurements used to calculate the linear thermal transmittance of the frame and the space.
- A description of the equipment used to measure the weather data.
- Thermophysical and surface properties of the cell.

Prior to running the experiment, green turf was installed in front of the cell to simulate grass. A photograph of the test cell is shown in Figure 1. A hemispherical-hemispherical reflectance was calculated and is described in a previous document entitled *Evaluation of Building Energy Simulation Codes' Irradiance Models*.

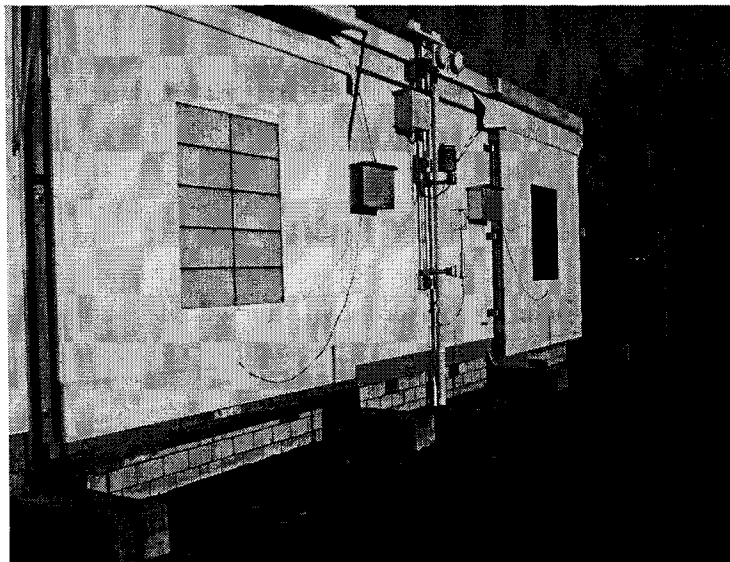


Figure 1 A photograph of the test cell.

## Test Configuration

This test was configured to maintain a near-constant temperature by adjusting heating and cooling power in the cell. Air temperatures in the cell were measured during the experiment with 18 double-shielded thermocouples. During the experiment, air was distributed throughout the cell using two fans near the floor through textile ducts and extracted through return ducts mounted near the ceiling. Photographs taken from inside of the test cell at the front (exterior wall) and back (north wall) are shown in Figures 2a and 2b, respectively. A plot of the volume-weighted average cell air temperature is

shown in Figure 3 and a plot of maximum temperature difference for any given thermocouples at a given hour is shown in Figure 4.



Figure 2a Photograph of the equipment taken from the front of the test cell.

Figure 2b Photograph of the equipment taken from the back of the test cell.

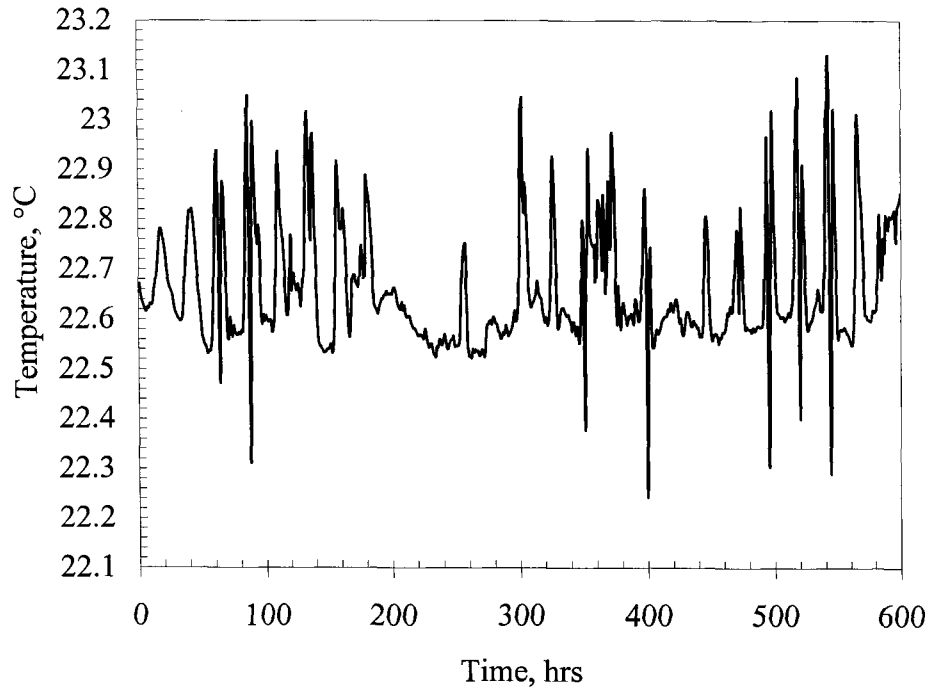


Figure 3 Volume-weighted average hourly cell temperatures for the experiment.

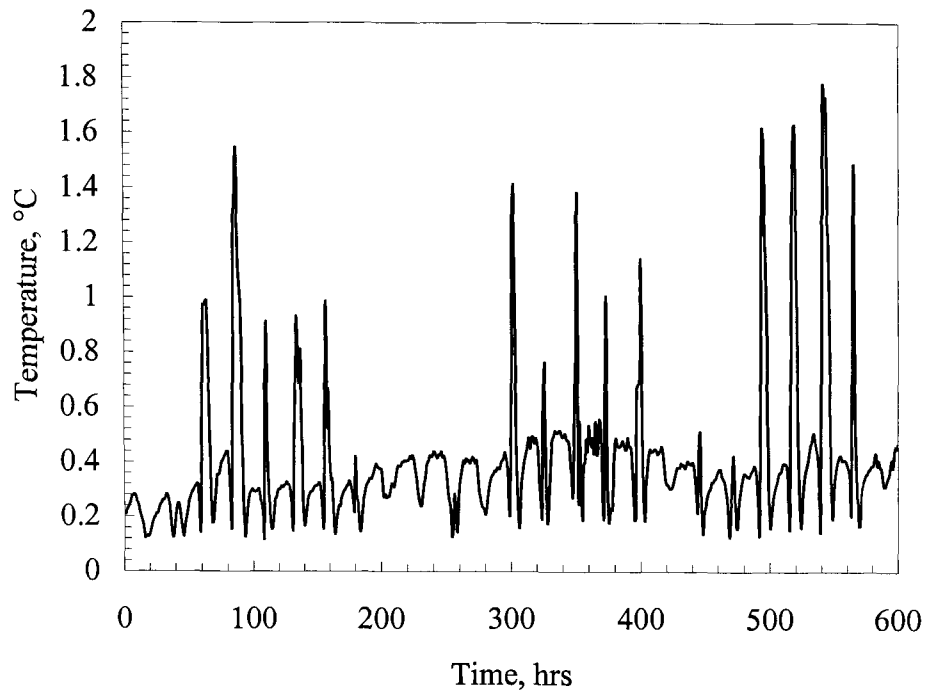


Figure 2 Maximum hourly temperature differences.

The exterior surface temperatures of the interior surfaces were measured during the experiment and are provided in an associated Excel file to be used as boundary

conditions. Despite large air changes in the cell, measurements taken near the walls, floor, and ceiling with a hot wire anemometer revealed negligible velocities. The two fans generated nearly constant load of  $\sim 160$  W; the hourly measured values are reported in the associated Excel file. If modelers want to account for the radiative heat transfer that may take place due to the duct work and textile ducts, Table 1 provides surface areas and emissivities. The inlet and outlet temperatures to the HVAC equipment were measured during the experiment and are contained in associated Excel file.

Table 1 Properties of the inlet and outlet ducts.

Equipment	Surface Area
Outlet Textile Duct	8 m <sup>2</sup>
Inlet Duct	10 m <sup>2</sup>
Stainless Steel HVAC Cabinet	5 m <sup>2</sup>

The first 56 hours of the experiment were setup as a preconditioning phase where glazing was covered with a highly reflective material shown in Figure 5. This was accounted for in the weather data by setting the solar irradiation to zero during this time.

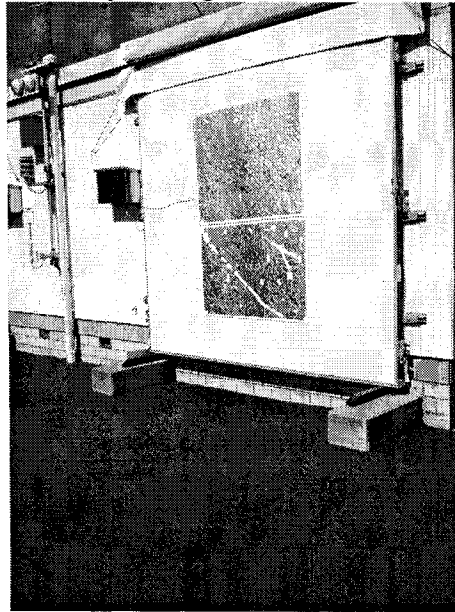


Figure 5 Photograph of the test cell during the preconditioning phase.

### Glazing Properties

The glazing for this experiment was mounted in the south exterior wall of the test cell. The glazing properties from measured data are listed in Table 2. Additional measurements for the individual panes of glass as a function of wavelength are provided in the associated Excel file. Properties of the individual panes are described in Table 3. The inside and outside reflectance and transmittance were calculated using European Standard EN 410 [1] in GLAD software [2] and the u-value was calculated from simulation and a calorimetric experiment described in a later section. For the individual panes of glass, the emissivity was measured using a hemispherical method. A

dimensioned drawing of the exterior wall as seen from this inside of the test cell showing the position of the glazing is presented in Figure 6. The dimensions in meters of the glazing in the figure correspond to the aperture height and width.

Table 2 Glazing properties.

Parameter	Quantity
Normal Solar Transmittance	42.9%
Normal Solar Exterior Reflectance	25.2%
Normal Solar Interior Reflectance	21.4%
Center-pane U-value	1.144 W/m <sup>2</sup> -K
Aperture Glazing Width	1.17 m
Aperture Glazing Height	1.42 m
Aperture Glazing Area	1.66 m <sup>2</sup>
Aperture Perimeter Length	5.18 m

Table 3a Optical properties for the outer pane of glass (solar control Low-E).

Parameter	Quantity
Normal Solar Transmittance	50.9%
Normal Solar Exterior Reflectance	28.5%
Normal Solar Interior Reflectance	29.6%
Outer Emmissivity	0.894
Inner Emmissivity	0.097

Table 3b Optical properties for the inner pane of glass (clear float glass).

Parameter	Quantity
Normal Solar Transmittance	80.8%
Normal Solar Exterior Reflectance	7.6%
Normal Solar Interior Reflectance	7.6%
Outer Emmissivity	0.878
Inner Emmissivity	0.887

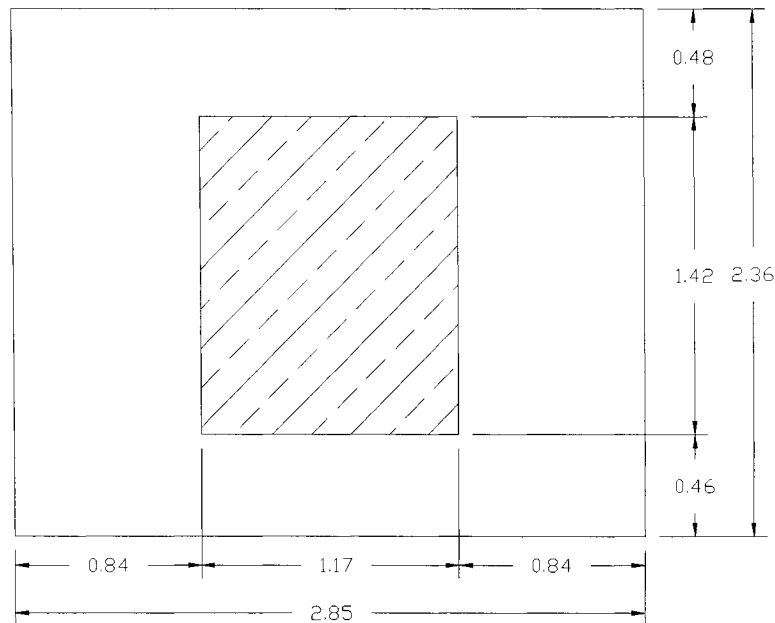


Figure 6 Position of the glazing in the exterior wall in meters.

In addition to normal optical properties, angular dependent front reflectance, back reflectance, and transmittance were measured at various angles of incidents for the glazing (both panes and the argon cavity) were calculated using European Standard EN 410 [1] in GLAD software [2]. The solar properties were computed used Glad Software and are shown in Tables 4. The individual measurements as a function of wavelength are contained in the associated Excel file.

Table 4 Transmittance and as a function of incident angle.

Incident Angle, °	0	15	30	45	50	55	60	65	67.5	70	72.5	75
Solar Transmittance, %	42.1	41.7	40.9	38.9	37.6	35.8	33.2	29.5	27.2	24.6	21.6	18.4
Solar Reflectance (Front), %	-	26.7	26.6	27.6	28.4	30.0	32.3	35.9	38.5	41.6	45.0	49.4
Solar Reflectance (Back), %	-	24.6	24.7	26.2	27.3	29.3	32.2	36.7	39.7	43.4	47.4	52.6

### Linear Thermal Transmittance

The impact of the window spacer and construction used to mount the glazing in the test cell was simulated using a two-dimensional steady-state heat transfer software package called BISCO [3]. To simulate the aluminum spacer, a dimensioned cross-section of the aluminum spacer provided by the manufacturer was used. Figure 7 shows a dimensioned AutoCAD drawing in millimeters of the spacer, the mounting construction and a portion of the exterior window and wall. BISCO simulation results coupled with calorimetric measurements [4] were used to quantify the impact of the spacer and the frame. From these calculations, the linear thermal transmittance was then computed.

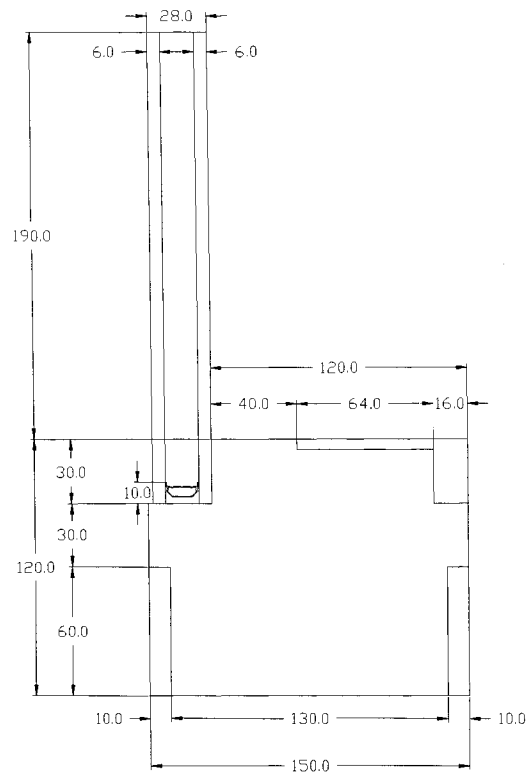


Figure 7 AutoCAD drawing of the spacer and frame in millimeters.

The thermal conductivities of the construction materials were required to perform the simulation. These properties were taken from literature, calculation, and in-house measurements. For temperature dependent properties, the thermal conductivity was evaluated at a mean envelope temperature of 10°C. Table 5 provides a list of the quantities and color-coding of the materials and their respective thermal conductivities. An iterative procedure using the simulation results and the calorimetric measurements was employed to calculate the equivalent thermal conductivity for the Argon cavity space—which factored in the impact of conduction, radiation, and convection—simulate the spacer calculate the linear thermal transmittance, and then recalculate a center-pane U-value.

Table 5 List of materials and their respective thermal conductivities.

Material	Thermal Conductivity, W/m-K	Color-coding
Desiccant	0.130	
Aluminum	220.0	
Polyisobutylene	0.220	
Polysulfid	0.400	
Argon 90%/Air 10%	0.02313	
Glass	1.0	
Plywood	0.1381	
Wood	0.110	
EPS Foam	0.03483	

The specified properties for the boundary conditions included the temperature and the heat transfer coefficients for the outside and inside of the frame; these values were taken from prEN ISO 10077-2 [5]. These results, as well as the color-codings, are presented in Table 6.

Table 6 Boundary condition properties.

Boundary Condition	Temperature, °C	Heat Transfer Coefficient, W/m <sup>2</sup> -K	Color-coding
Inside Air	20	7.7	
Outside Air	0	25.0	

The two-dimensional bitmap drawings used for the BISCO simulation of the frame and glazing construction and the spacer are shown in Figures 8a and 8b.

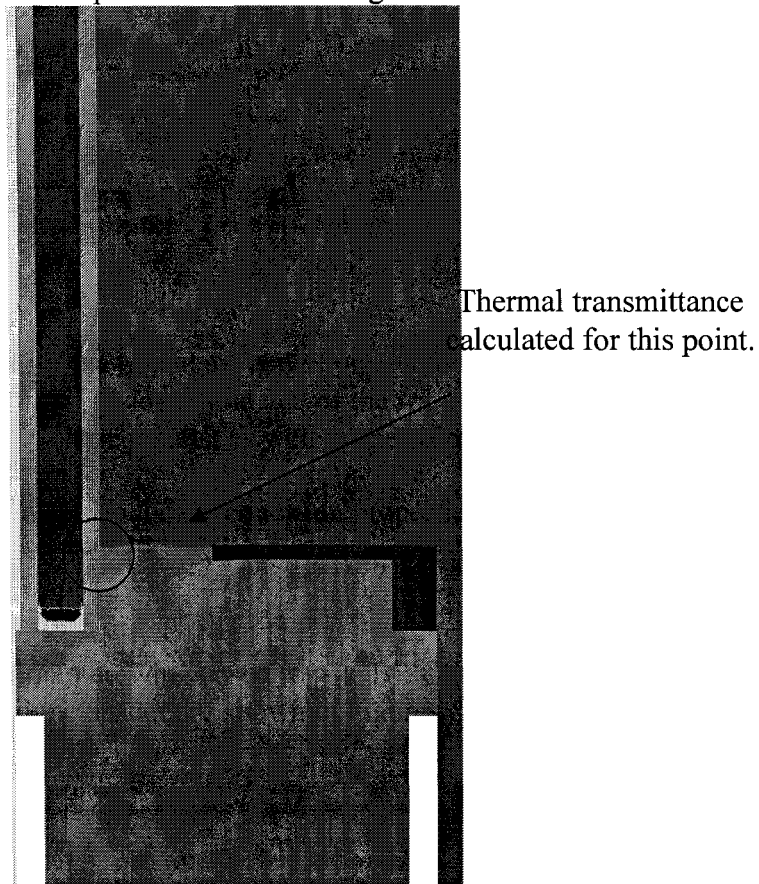


Figure 8a Two-dimensional bitmap of the glazing and frame.

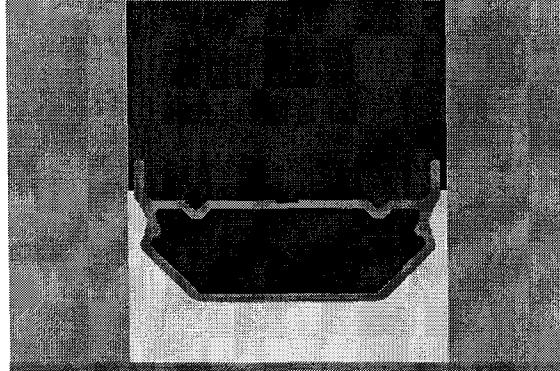


Figure 8b Two-dimensional bitmap of the aluminum spacer.

For the BISCO simulation, the bitmap was divided up into 243,205 nodes and the heat transfer through the element was calculated as 6.72 W/m. Isotherm and heat flow line illustrations are shown in Figures 9a and 9b to help visualize the two-dimensional heat flow path.

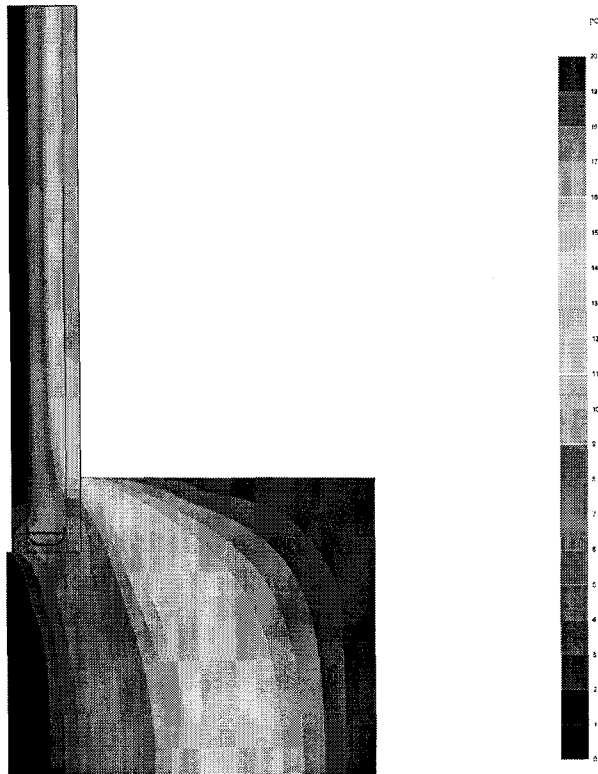


Figure 9a Isotherm illustration from the BISCO simulation.

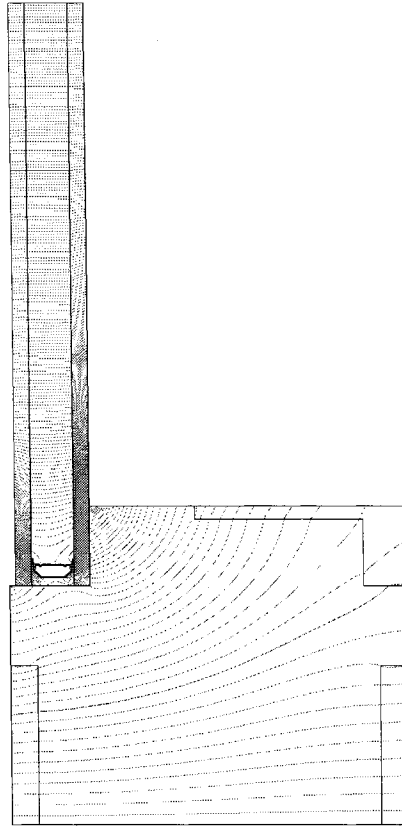


Figure 9b Heat flow line illustration from the BISCO simulation.

One-dimensional heat transfer was calculated using Equation 1. A list of the additional parameters used for this calculation is shown in Table 7.

$$Q'_{I-D} = \left\{ L_g U_g + \frac{L_w}{\left( \frac{1}{h_i} + \frac{2d_{ply}}{\lambda_{ply}} + \frac{d_{eps}}{\lambda_{eps}} + \frac{1}{h_o} \right)} \right\} (\theta_i - \theta_o) \quad (1)$$

where

$L_g$  is the length of the glazing used from the simulation,

$U_g$  is the center pane u-value of the glazing,

$L_w$  is the length of the wall from the simulation,

$h_i$  is the inside heat transfer coefficient,

$d_{ply}$  is the width of the plywood,

$\lambda_{ply}$  is the thermal conductivity of the plywood,

$d_{eps}$  is the width of the eps foam,

$\lambda_{eps}$  is the thermal conductivity of the eps foam,

$h_o$  is the outside heat transfer coefficient,  
 $\theta_i$  is the inside temperature, and  
 $\theta_o$  is the outside temperature.

Table 7 Values of the variables used for the 1-D heat transfer calculation.

Parameter	Quantity
$L_g$	0.190 m
$U_g$	1.144 W/m <sup>2</sup> -K
$L_w$	0.120 m
$d_{ply}$	0.01 m
$d_{eps}$	0.130 m

Using the simulation conditions, the one-dimensional heat transfer was calculated to be 4.94 W/m. The linear thermal transmittance,  $\psi$ , was calculated using Equation 2 to be 0.08899 W/m-K.

$$\psi = \frac{Q'_{BISCO} - Q'_{1-D}}{\theta_i - \theta_o} \quad (2)$$

where

$Q'_{BISCO}$  is the heat transfer from the BISCO simulation.

### Thermophysical Properties

The thermophysical properties of the cell were determined from literature and in-house measurements. The properties obtained from in-house measurement were found to be temperature dependent. These parameters are available in an earlier document entitled *Test Cell Transient Characteristic Exercise Round 1* and can be made available upon request. Most building energy simulation codes cannot account for temperature dependent thermophysical properties. Therefore the thermophysical properties evaluated at the mean envelope temperature for the test for the ceiling, interior walls, floor, and exterior wall. The mean temperature for the ceiling and interior walls was area weighted, and, because the exterior surface of the south wall was not measured, the mean envelope temperature was calculated using hourly inside and outside air measurements. The mean envelope temperatures are shown in Table 8. The thermophysical properties evaluated at these mean envelope temperatures are contained in Tables 9a to 9c.

Table 8 Mean envelope temperatures for experiment.

Element	Mean temperature, °C
Ceiling, East, West, and North Walls	22.78
Floor	22.72
South Wall	17.49

Table 9a Ceiling, North, East and West wall construction evaluate at 22.78°C.

Layer Number	Material	Thickness mm	Thermal conductivity W/m-K	Density kg/m <sup>3</sup>	Specific heat J/kg-K
1	Sheet steel	0.7	53.62	7837	460.8
2	PU foam	139	0.02233	30	1800
3	Sheet steel	0.7	53.62	7837	460.8

Table 9b Floor construction evaluated at 22.72°C.

Layer Number	Material	Thickness mm	Thermal conductivity W/m-K	Density kg/m <sup>3</sup>	Specific heat J/kg-K
1	Sheet steel	0.7	53.62	7837	460.8
2	PU foam	140	0.02232	30	1800
3	PU foam (higher density)	20	0.070	45	1800
4	Sheet steel with surface structure	2.5	53.62	7837	460.8

Table 9c South wall construction evaluated at 17.49°C.

Layer Number	Material	Thickness mm	Thermal conductivity W/m-K	Density kg/m <sup>3</sup>	Specific heat J/kg-K
1	Plywood	10	0.1394	850	1605
2	EPS foam	130	0.03578	28	1460
3	Plywood	10	0.1394	850	1605

The surface properties of the cell were also measured with sample from material inside the cell. Quantities for emissivity, solar reflectance, and ultra-violet reflectance are presented in Table 10; surfaces inside the test cell were either painted or coated which is reflected in these calculations. The reflectance were measured at normal incidents and were calculated using GLAD software [2] and emissivities were measured using an integral method.

Table 10 Surface properties of the cell.

	Emissivity	Solar Reflectance
Plywood	0.93	0.77
Steel sheet	0.92	0.76
Sheet steel with surface structure	0.96	0.25

## Output Report

The output reports will be divided up into two sections which include 1) output that can be compared to measured data at the test facility—empirical validations, and 2) code-to-code comparisons of code output parameters that are not measured at the facility. The code-to-code comparison reports may prove useful in identifying discrepancies and differences in the results. An Excel file with headers and appropriate worksheets entitled “XXXXXX Experiment 3 Results Revision1.xls” was created to expedite processing the results. Please change the XXXXXX to an appropriate name and complete the spreadsheet.

## Empirical Validations

A report describing the following output for each hour the experiment was run should be submitted. The output will be used to compare the results for the various models and the experiment. The headers for the output file and a description of their meaning are described in Table 11.

Table 11 Power and temperature of outputs.

Hour <sup>1)</sup>	HC-Power <sup>2)</sup>	Glaz-OST <sup>3)</sup>	Glaz-IST <sup>4)</sup>	West-IST <sup>5)</sup>	North-IST <sup>6)</sup>	East-IST <sup>7)</sup>	Ceil-IST <sup>8)</sup>	Floor-IST <sup>9)</sup>
--------------------	------------------------	------------------------	------------------------	------------------------	-------------------------	------------------------	------------------------	-------------------------

- 9) is the time in West European Standard time( GMT+1)  
 10) is the heating/cooling power required to maintain the space in W.  
 11) is the exterior surface temperature of the glazing in °C  
 12) is the interior surface temperature of the glazing in °C.  
 13) is the inside cell surface temperature of the west wall in °C.  
 14) is the inside cell surface temperature of the north wall in °C.  
 15) is the inside surface temperature of the east wall in °C.  
 16) is the inside surface temperature of the ceiling in °C.  
 17) is the inside surface temperature of the floor in °C.

## Code-to-Code Comparisons

A report describing the following outputs, which are often user inputs or algorithms in the codes used for the respective simulations, should be submitted if possible. The headers for the output file and a description of their meanings are contained in Tables 12 and 14.

Table 12 Inside convective heat transfer coefficients.

Hour <sup>1)</sup>	South-ICHTC <sup>2)</sup>	Glaz-ICHTC <sup>3)</sup>	West-ICHTC <sup>4)</sup>	North-ICHTC <sup>5)</sup>	East-ICHTC <sup>6)</sup>	Ceil-ICHTC <sup>7)</sup>	Floor-ICHTC <sup>8)</sup>	South-OCHTC <sup>9)</sup>	Glaz-OCHTC <sup>10)</sup>
--------------------	---------------------------	--------------------------	--------------------------	---------------------------	--------------------------	--------------------------	---------------------------	---------------------------	---------------------------

- 1) is the time in West European Standard time (GMT+1).  
 2) is the convective heat transfer coefficient for the south wall in  $W/m^2-K$ .  
 3) is the convective heat transfer coefficient for the glazing in  $W/m^2-K$ .  
 4) is the convective heat transfer coefficient for the west wall in  $W/m^2-K$ .  
 5) is the convective heat transfer coefficient for the north wall in  $W/m^2-K$ .  
 6) is the convective heat transfer coefficient for the east wall in  $W/m^2-K$ .  
 7) is the convective heat transfer coefficient for the ceiling in  $W/m^2-K$ .  
 8) is the convective heat transfer coefficient for the floor in  $W/m^2-K$ .  
 9) is the outside convective heat transfer coefficient for the south wall in  $W/m^2-K$   
 10) is the outside convective heat transfer coefficient for the glazing in  $W/m^2-K$

Table 13 Inside radiative heat transfer coefficients.

Hour <sup>1)</sup>	South-IRHTC <sup>2)</sup>	Glaz-IRHTC <sup>3)</sup>	West-IRHTC <sup>4)</sup>	North-IRHTC <sup>5)</sup>	East-IRHTC <sup>6)</sup>	Ceil-IRHTC <sup>7)</sup>	Floor-IRHTC <sup>8)</sup>	South-ORHTC <sup>9)</sup>	Glaz-ORHTC <sup>10)</sup>
--------------------	---------------------------	--------------------------	--------------------------	---------------------------	--------------------------	--------------------------	---------------------------	---------------------------	---------------------------

- 1) is the time in West European Standard time (GMT+1)
- 2) is the inside radiative heat transfer coefficient for the south wall in  $W/m^2-K$ .
- 3) is the inside radiative heat transfer coefficient for the glazing in  $W/m^2-K$ .
- 4) is the inside radiative heat transfer coefficient for the west wall in  $W/m^2-K$ .
- 5) is the inside radiative heat transfer coefficient for the north wall in  $W/m^2-K$ .
- 6) is the inside radiative heat transfer coefficient for the east wall in  $W/m^2-K$ .
- 7) is the inside radiative heat transfer coefficient for the ceiling in  $W/m^2-K$ .
- 8) is the inside radiative heat transfer coefficient for the floor in  $W/m^2-K$ .
- 9) is the outside radiative heat transfer coefficient for the south wall in  $W/m^2-K$ .
- 10) is the outside radiative heat transfer coefficient for the glazing in  $W/m^2-K$ .

Table 14 Solar gain calculations.

Hour <sup>1)</sup>	Solar Gain <sup>2)</sup>
--------------------	--------------------------

- 1) is the time in West European Standard time (GMT+1)
- 2) is the solar gain through the window in  $W$ .

## Simulation Report

In addition to simulation results, please provide a report that documents the following information:

- How the thermal transmittance was simulated.
- How and what properties, standards, and/or software were used to simulate window properties.
- Problems encountered and/or additional information that may be useful in describing how the simulation was performed.

## Simulation Ground Rules

In order to maintain model consistency between the experiments, only the following modifications can be made in the models from the finalized model used for the transient characterization experiment (obviously the models will be changed to reflect the insertion of a glazing and changing of the south wall from an interior to an exterior surface).

- Thermophysical properties for temperature dependent quantities of thermal conductivity.
- Changes to the radiative heat transfer to account for solar gains.

An email hotline will be used to clarifying information contained in this document, information not provided in the document but useful for simulation, and/or general questions concerning the experiment. Please direct all email questions to Peter Loutzenhiser ([peter.loutzenhiser@empa.ch](mailto:peter.loutzenhiser@empa.ch)). Responses to the emails will be directed to all participants in the simulation exercise.

## References

- [1] European Standard EN 410. Glass in building – Determination of luminous and solar characteristics of glazing. European Committee for Standardization, Brussels, Belgium, 1998
- [2] GLAD Software. Swiss Federal Laboratories for Materials Testing and Research (EMPA), Duebendorf, Switzerland, 2002
- [3] BISCO Version 7.0w, A computer program to calculate 2D steady-state heat transfer, Physibel, Heirweg 21, B-9990 Maldegem, Belgium
- [4] T. Nussbaumer, and T. Frank, Bestimmung des Wärmedurchgangskoeffizienten  $U_g$  einer 2-fach Isolierverglasung, Nr. 880'097, STS-Nr. 086, EMPA, Duebendorf, Switzerland, Nov. 30, 2004, (In German)
- [5] prEN ISO 10077 - 2 Thermal performance of windows, doors and shutters - Calculation of thermal transmittance - Part 2: Numerical method for frames (Final Draft), European Committee for Standardization, Brussels, 2003

**Appendix D: Constant Temperature Experiment with Glazing and External Shade**

**IEA Task 34/Annex 43 Subtask C  
Empirical Validation Project of Building Energy  
Simulation Tools  
Shading / Daylighting / Load Interaction**

**Constant Temperature Experiment with Glazing and External  
Shade**

Written by  
Peter Loutzenhiser  
Heinrich Manz  
Thomas Frank

June 6, 2005  
Revised June 20, 2005  
Revised again on July 19, 2005

## Introduction

This document contains information regarding the parameters and conditions used for an experiment performed at the Swiss Federal Laboratories for Material Testing and Research (EMPA) in Applied Building Physics Laboratory test facility in Duebendorf, Switzerland from March 23 to April 16, 2005. The experiment was designed to evaluate the impact of solar gains through a glazing with an exterior shade and was done in conjunction with the International Energy Agency (IEA) Task 34/Annex 43 Subtask C. The purpose of this exercise is to use the boundary conditions, weather data, glazing properties, and properties of the external shade to predict—in each respective building energy simulation code—the required heating and cooling heating to maintain a relatively constant temperature (average hourly space temperatures are provided as a code input). The first round of simulations will be a blind exercise; therefore information regarding the measured heating and cooling power requirements was not included in this document. However, information about how the exterior shade was mounted and desired output from this exercise are provided in this document. An associated Excel document entitled “Experiment 4.xls” contains measured hourly weather data, exterior surface temperatures adjacent to the guarded zone, external shade properties as a function of wavelength, space temperatures, and internal load. Information concerning the test cell location, geometrical and temperature dependent thermophysical properties, thermal bridge, outside ground reflectance calculations, and glazing properties are contained in previous IEA Task 34/Annex 43 Subtask C documents<sup>5,6,3,4</sup> that can be made available upon request.

---

<sup>5</sup> *Test Cell Transient Characteristic Exercise*, August 25, 2004

<sup>6</sup> *Results from the Test Cell Transient Characteristic Exercise Round 1*, sent out to participants on October 26, 2004

<sup>3</sup> *Evaluation of Building Energy Simulation Codes' Irradiance Models*, February 9, 2005

<sup>4</sup> *Constant Temperature Experiment with Glazing Only*, June 6, 2005

## Description of the Experiment

This section contains specific information about the experiment, which includes the following information.

- Exterior shade.
- Test configuration.
- Thermophysical properties.

### Exterior Shade

For this experiment, an exterior shade was installed 0.10 m from the glazing and is pictured in Figure 1. The shade was mounted to allow air to flow between gap of the external shade and the glazing; a dimensioned drawing of the shade position relative to the glazing is shown in Figure 2.

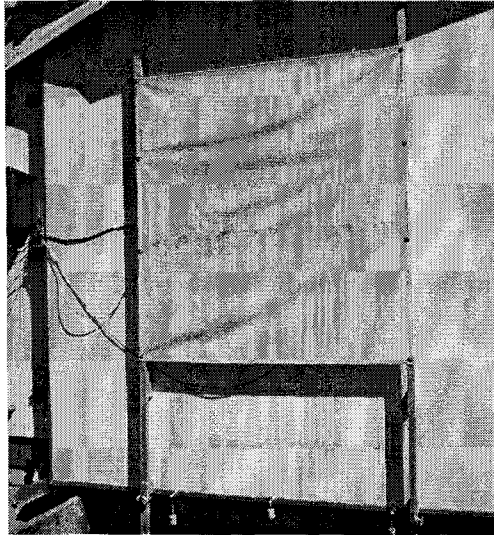


Figure 1 Photograph of the exterior shade mounted on the test cell.

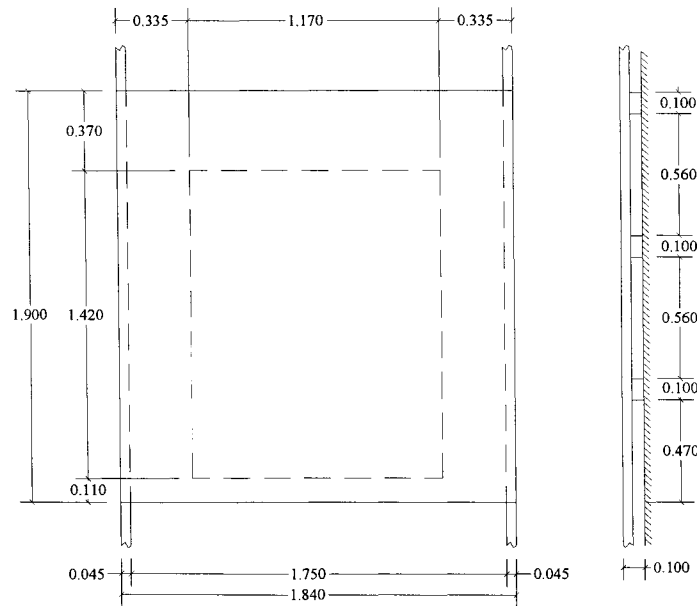


Figure 2 Dimensioned drawing of the external shade in meters relative to the glazing.

The optical properties of the shade were measured at normal incident angles using a spectrometer. The transmittance and reflectance as a function of wavelength from 250 nm to 2500 nm can be found in an associated Excel file entitled “Experiment 4.xls”. The optical properties for the shade were also computed according to EN 410 [1] using GLAD software [2] and are shown in Table 1.

Table 1 Optical properties of the exterior shade.

Property	Quantity
Normal Solar Transmittance, %	21.5
Normal Solar Reflectance, %	59.6

### Test Configuration

This test was configured to maintain a near-constant temperature by adjusting heating and cooling power in the test cell. The first 37 hours of the data were designed for preconditioning and the glazing was covered by highly reflective material (there was additional preconditioning that ran prior to the experiment); this was accounted for in the weather file by setting solar irradiance to zero during this time. Air temperatures in the test cell were measured during the experiment with 18 double-shielded thermocouples. During the experiment, air was distributed throughout the cell using two fans near the floor through textile ducts and extracted through return ducts mounted near the ceiling. A plot of the volume-weighted average cell air temperature is shown in Figure 3 and a plot of maximum temperature difference for any given thermocouples at a given hour is shown in Figure 4. For this experiment, the average maximum hourly temperature difference was 0.36 K.

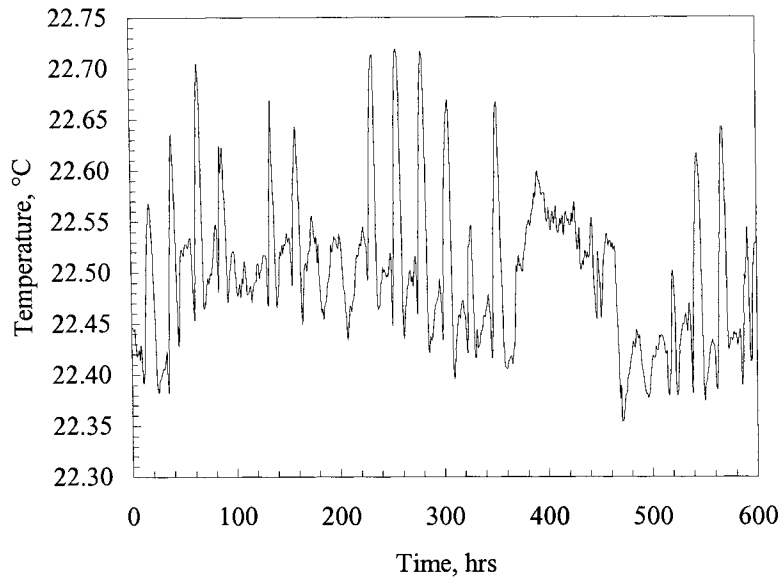


Figure 3 Volume-weighted average hourly cell temperatures for the experiment.

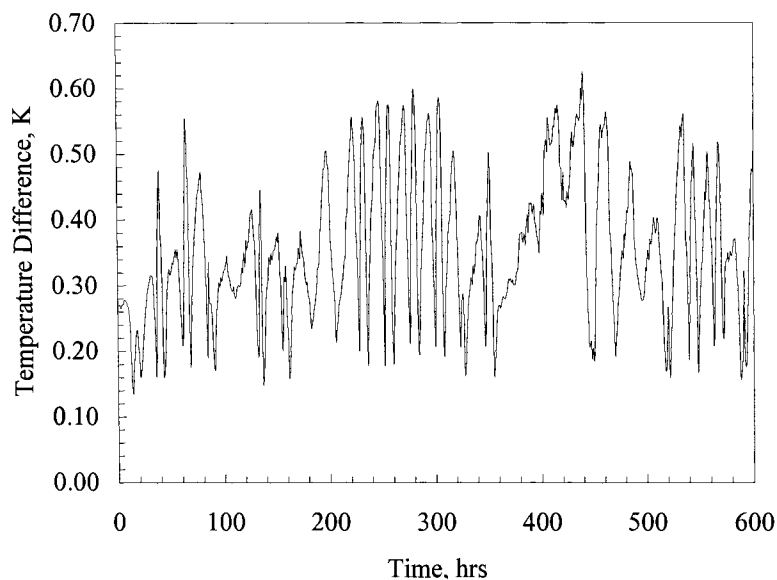


Figure 4 Maximum hourly temperature differences.

The exterior surface temperatures of the surfaces adjacent to the guarded zone were measured during the experiment and are provided in an associated Excel file to be used as boundary conditions. Despite large air changes in the cell, measurements taken near the walls, floor, and ceiling with a hot wire anemometer revealed negligible velocities. The two fans generated nearly constant load of  $\sim 160$  W (measured internal loads for each hour are provided for the building energy simulation codes in the associated Excel file entitled "Experiment 4.xls").

## Thermophysical and Surface Properties

The thermophysical properties of the cell were determined from literature and in-house measurements. The properties obtained from in-house measurement were found to be temperature dependent. These parameters are available in an earlier document entitled *Test Cell Transient Characteristic Exercise Round 1* and can be made available upon request. Most building energy simulation codes cannot account for temperature dependent thermophysical properties. Therefore the thermophysical properties evaluated at the mean envelope temperature for the test for the ceiling, interior walls, floor, and exterior wall. The mean temperature for the ceiling and interior walls was area weighted, and, because the exterior surface of the south wall was not measured, the mean envelope temperature was calculated using hourly inside and outside air temperature measurements. The mean envelope temperatures are shown in Table 2. The thermophysical properties evaluated at these mean envelope temperatures are contained in Tables 3a to 3c.

Table 2 Mean envelope temperatures for experiment.

Element	Mean temperature, °C
Ceiling, East, West, and North Walls	22.58
Floor	22.34
South Wall	16.34

Table 3a Ceiling, North, East and West wall construction evaluate at 22.58°C.

Layer number	Material	Thickness mm	Thermal conductivity W/m-K	Density Kg/m <sup>3</sup>	Specific heat J/kg-K
1	Sheet steel	0.7	53.62	7837	460.8
2	PU foam	139	0.02230	30	1800
3	Sheet steel	0.7	53.62	7837	460.8

Table 3b Floor construction evaluated at 22.34°C.

Layer Number	Material	Thickness mm	Thermal conductivity W/m-K	Density Kg/m <sup>3</sup>	Specific heat J/kg-K
1	Sheet steel	0.7	53.62	7837	460.8
2	PU foam	140	0.02227	30	1800
3	PU foam (higher density)	20	0.070	45	1800
4	Sheet steel with surface structure	2.5	53.62	7837	460.8

Table 3c South wall construction evaluated at 16.34°C.

Layer Number	Material	Thickness mm	Thermal conductivity W/m-K	Density Kg/m <sup>3</sup>	Specific heat J/kg-K
1	Plywood	10	0.1384	850	1605
2	EPS foam	130	0.03564	28	1460
3	Plywood	10	0.1384	850	1605

## Output Report

The output reports will be divided up into three sections which include 1) irradiance output on the vertical façade of the exterior wall and associated components, 2) output from the test cell that can be compared to measured data at the test facility—empirical validations, and 3) code-to-code comparisons from the test cell of code output parameters that are not measured at the facility. The code-to-code comparison reports may prove useful in identifying discrepancies and differences in the results. An Excel file with headers and appropriate worksheets entitled “XXXXXX Experiment 4 Results Revision 1.xls” was created to expedite processing the results. Please change the XXXXXX to an appropriate name and complete the spreadsheet.

## Irradiance Output

Table 4 contains headers for the requested output that pertains to the hourly irradiance output of the exterior wall of the test cell. A description of the headers is provided below the table.

Table 4 List of headers for data file.

Hour <sup>1)</sup>	Input Parameters			Output Parameters			
	Bn <sup>2,a)</sup>	Dh <sup>3,a)</sup>	Gh <sup>4,a)</sup>	IIR <sup>5,b)</sup>	Bn-IIR <sup>6,c)</sup>	Dv-IIR <sup>7,c)</sup>	RF-IIR <sup>8,c)</sup>

\* Please provide the two parameters used for the exercise.

18) is the time in Western European Standard time (GMT +1).

19) is the direct-normal irradiance in W/m<sup>2</sup>.

20) is the diffuse horizontal irradiance in W/m<sup>2</sup>.

21) is the global horizontal irradiance in W/m<sup>2</sup>.

22) is incident radiation (total vertical irradiance) on the southwest façade in W/m<sup>2</sup>.

23) is the direct component of the incident radiation on the southwest façade in W/m<sup>2</sup>.

24) is the diffuse component of the incident irradiance on the southwest façade in W/m<sup>2</sup>.

25) is the reflected component of the incident irradiance on the southwest façade in W/m<sup>2</sup>.

c) is useful for ensuring the correct input.

d) is an empirical validation where the parameter is measured on site.

e) is a code-to-code comparisons where the parameters are not measured on site.

## Empirical Validations

A report describing the following output for each hour the experiment was run should be submitted. The output will be used to compare the results for the various models and the experiment. The headers for the output file and a description of their meaning are described in Table 5.

Table 5 List of output headers.

Hour <sup>1)</sup>	HC-Power <sup>2)</sup>	Glaz-OST <sup>3)</sup>	Glaz-IST <sup>4)</sup>	West-IST <sup>5)</sup>	North-IST <sup>6)</sup>	East-IST <sup>7)</sup>	Ceil-IST <sup>8)</sup>	Floor-IST <sup>9)</sup>
--------------------	------------------------	------------------------	------------------------	------------------------	-------------------------	------------------------	------------------------	-------------------------

- 1) is the time in West European Standard time (GMT+1).
- 2) is the heating/cooling power required to maintain the space in W.
- 3) is the exterior surface temperature of the glazing in °C.
- 4) is the interior surface temperature of the glazing in °C.
- 5) is the inside cell surface temperature of the west wall in °C.
- 6) is the inside cell surface temperature of the north wall in °C.
- 7) is the inside surface temperature of the east wall in °C.
- 8) is the inside surface temperature of the ceiling in °C.
- 9) is the inside surface temperature of the floor in °C.

## Code-to-Code Comparisons

A report describing the following outputs, which are often user inputs or algorithms in the codes used for the respective simulations, should be submitted if possible. The headers for the output file and a description of their meanings are contained in Tables 6 and 8.

Table 6 Inside convective heat transfer coefficients.

Hour <sup>1)</sup>	South-ICHTC <sup>2)</sup>	Glaz-ICHTC <sup>3)</sup>	West-ICHTC <sup>4)</sup>	North-ICHTC <sup>5)</sup>	East-ICHTC <sup>6)</sup>	Ceil-ICHTC <sup>7)</sup>	Floor-ICHTC <sup>8)</sup>	South-OCHTC <sup>9)</sup>	Glaz-OCHTC <sup>10)</sup>
--------------------	---------------------------	--------------------------	--------------------------	---------------------------	--------------------------	--------------------------	---------------------------	---------------------------	---------------------------

- 1) is the time in West European Standard time (GMT+1).
- 2) is the convective heat transfer coefficient for the south wall in  $W/m^2-K$ .
- 3) is the convective heat transfer coefficient for the glazing in  $W/m^2-K$ .
- 4) is the convective heat transfer coefficient for the west wall in  $W/m^2-K$ .
- 5) is the convective heat transfer coefficient for the north wall in  $W/m^2-K$ .
- 6) is the convective heat transfer coefficient for the east wall in  $W/m^2-K$ .
- 7) is the convective heat transfer coefficient for the ceiling in  $W/m^2-K$ .
- 8) is the convective heat transfer coefficient for the floor in  $W/m^2-K$ .
- 9) is the outside convective heat transfer coefficient for the south wall in  $W/m^2-K$ .
- 10) is the outside convective heat transfer coefficient for the glazing in  $W/m^2-K$ .

Table 7 Inside radiative heat transfer coefficients.

Hour <sup>1)</sup>	South-IRHTC <sup>2)</sup>	Glaz-IRHTC <sup>3)</sup>	West-IRHTC <sup>4)</sup>	North-IRHTC <sup>5)</sup>	East-IRHTC <sup>6)</sup>	Ceil-IRHTC <sup>7)</sup>	Floor-IRHTC <sup>8)</sup>	South-ORHTC <sup>9)</sup>	Glaz-ORHTC <sup>10)</sup>
--------------------	---------------------------	--------------------------	--------------------------	---------------------------	--------------------------	--------------------------	---------------------------	---------------------------	---------------------------

- 1) is the time in West European Standard time (GMT+1).
- 2) is the inside radiative heat transfer coefficient for the south wall in  $W/m^2-K$ .
- 3) is the inside radiative heat transfer coefficient for the glazing in  $W/m^2-K$ .
- 4) is the inside radiative heat transfer coefficient for the west wall in  $W/m^2-K$ .
- 5) is the inside radiative heat transfer coefficient for the north wall in  $W/m^2-K$ .
- 6) is the inside radiative heat transfer coefficient for the east wall in  $W/m^2-K$ .
- 7) is the inside radiative heat transfer coefficient for the ceiling in  $W/m^2-K$ .
- 8) is the inside radiative heat transfer coefficient for the floor in  $W/m^2-K$ .
- 9) is the outside radiative heat transfer coefficient for the south wall in  $W/m^2-K$ .
- 10) is the outside radiative heat transfer coefficient for the glazing in  $W/m^2-K$ .

Table 8 Solar gain calculations.

Hour <sup>1)</sup>	Solar Gain <sup>2)</sup>
--------------------	--------------------------

- 1) is the time in West European Standard time (GMT+1)
- 2) is the solar gain through the window in W.

## Simulation Report

In addition to simulation results, please provide a description of the additional assumptions that were made when simulating the external shade.

## **Simulation Ground Rules**

In order to maintain model consistency between the experiments, only the following modifications can be made in the models from the finalized model from the glazing only experiment.

- Addition of the external shade and associated properties to the building energy simulation codes.
- Thermophysical properties for temperature dependent quantities of thermal conductivity.

An email hotline will be used to clarifying information contained in this document, information not provided in the document but useful for simulation, and/or general questions concerning the experiment. Please direct all email questions to Peter Loutzenhiser ([peter.loutzenhiser@empa.ch](mailto:peter.loutzenhiser@empa.ch)). Responses to the emails will be directed to all participants in the simulation exercise.

**Appendix E: Constant Temperature Experiment with Glazing and Interior Shade**

IEA Task 34/Annex 43 Subtask C  
Empirical Validation Project of Building Energy  
Simulation Tools  
Shading / Daylighting / Load Interaction

Constant Temperature Experiment with Glazing and Interior Shade

Written by  
Peter Loutzenhiser  
Heinrich Manz  
Thomas Frank

October 25, 2005

## Introduction

This document contains information regarding the parameters and conditions used for an experiment performed at the Swiss Federal Laboratories for Material Testing and Research (EMPA) in the Applied Building Physics Laboratory test facility in Duebendorf, Switzerland from June 8 to July 2, 2005. The experiment was designed to evaluate the impact of solar gains through a glazing with a diffuse interior shade and was done in conjunction with the International Energy Agency's (IEA) Task 34/Annex 43 Subtask C. The purpose of this exercise is to use the boundary conditions, weather data, glazing properties, and properties of the interior shade to predict—in each respective building energy simulation code—the required heating/cooling power to maintain a relatively constant temperature (average hourly space temperatures are provided as a code input). The first round of simulations will be a blind exercise; therefore information regarding the measured heating and cooling power requirements was not included in this document. However, information about how the interior shade was mounted and desired output from this exercise are provided in this document. An associated Excel document entitled “Experiment 5.xls” contains measured hourly weather data, exterior surface temperatures adjacent to the guarded zone, interior shade properties as a function of wavelength, space temperatures, and internal load. Information concerning the test cell location, geometrical and temperature dependent thermophysical properties, thermal bridge, outside ground reflectance calculations, and glazing properties are contained in previous IEA Task 34/Annex 43 Subtask C documents<sup>7,8,3,4</sup> that can be made available upon request.

---

<sup>7</sup> *Test Cell Transient Characteristic Exercise*, August 25, 2004

<sup>8</sup> *Results from the Test Cell Transient Characteristic Exercise Round 1*, sent out to participants on October 26, 2004

<sup>3</sup> *Evaluation of Building Energy Simulation Codes' Irradiance Models*, February 9, 2005

<sup>4</sup> *Constant Temperature Experiment with Glazing Only*, Revised on October 21, 2005

## Description of the Experiment

This section contains specific information about the experiment, which includes the following information.

- Interior shade.
- Test configuration.
- Thermophysical properties.

### Interior Shade

For this experiment, an interior shade was installed 16 cm from the glazing and is pictured in Figure 1. The shade was mounted to allow air to flow between gap of the interior shade and the glazing; a dimensioned drawing of the shade position relative to the glazing is shown in Figure 2.

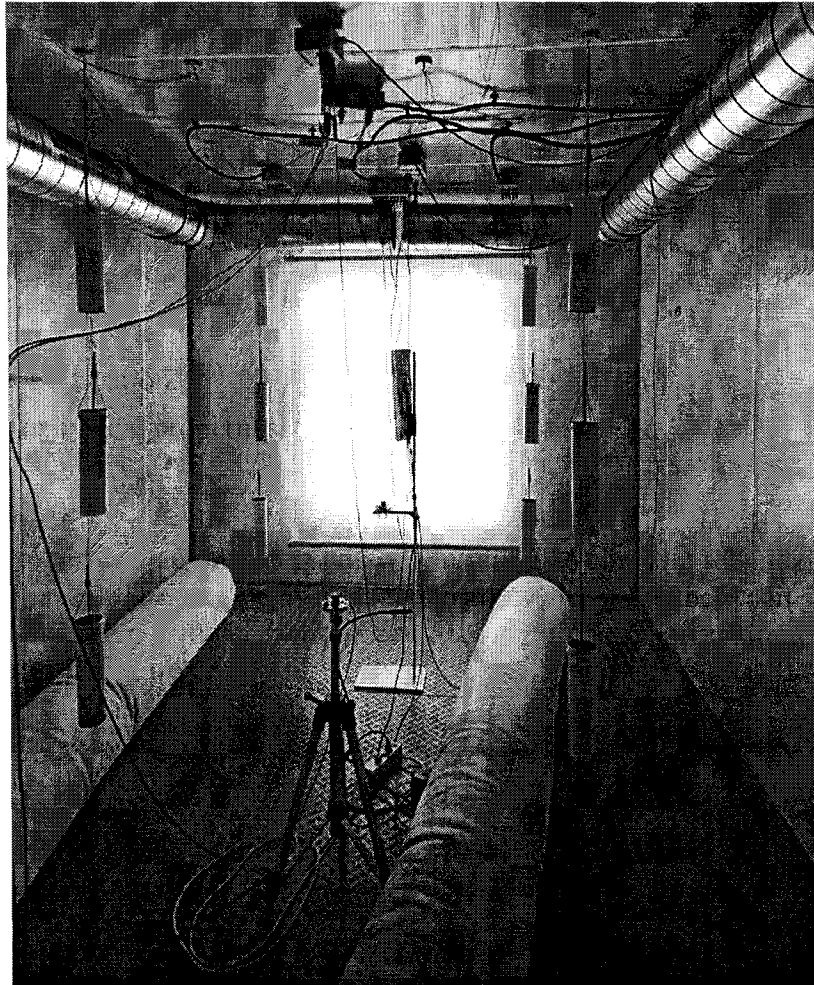


Figure 1. Photograph of the exterior shade mounted on the test cell.

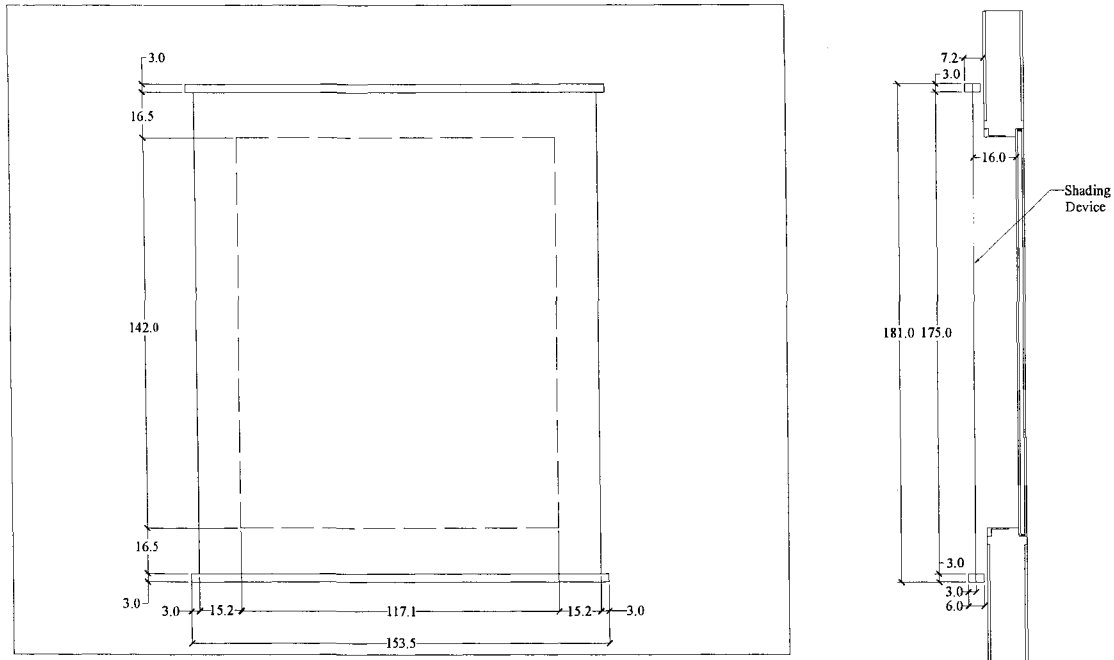


Figure 2. Dimensioned drawing of the interior shade in centimeters relative to the glazing.

The optical properties of the shade were measured at normal incident angles using a spectrometer. The transmittance and reflectance as a function of wavelength from 250 nm to 2500 nm can be found in an associated Excel file entitled “Experiment 5.xls”. The optical properties for the shade were also computed according to EN 410 [1] using GLAD software [2] and are shown in Table 1.

Table 1. Optical properties of the interior shade.

Property	Quantity
Normal Solar Transmittance, %	30.4
Normal Solar Reflectance, %	59.4

### Test Configuration

This test was configured to maintain a near-constant temperature by adjusting heating and cooling power in the test cell. The first 35 hours of the data were designed for preconditioning and the glazing was covered by highly reflective material (there was additional preconditioning that ran prior to the experiment); this was accounted for in the weather file by setting solar irradiance to zero during this time. Air temperatures in the test cell were measured during the experiment with 18 double-shielded thermocouples. During the experiment, air was distributed throughout the cell using two fans near the floor through textile ducts and extracted through return ducts mounted near the ceiling. A plot of the volume-weighted average cell air temperature is shown in Figure 3 and a plot of maximum temperature difference for any given thermocouples at a given hour is

shown in Figure 4. For this experiment, the average maximum hourly temperature difference was 0.31 K.

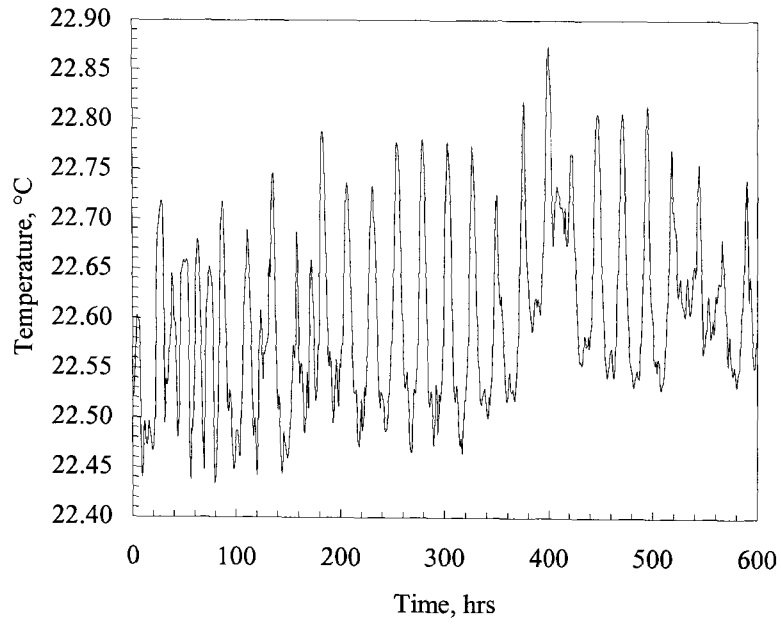


Figure 3. Volume-weighted average hourly cell temperatures for the experiment.

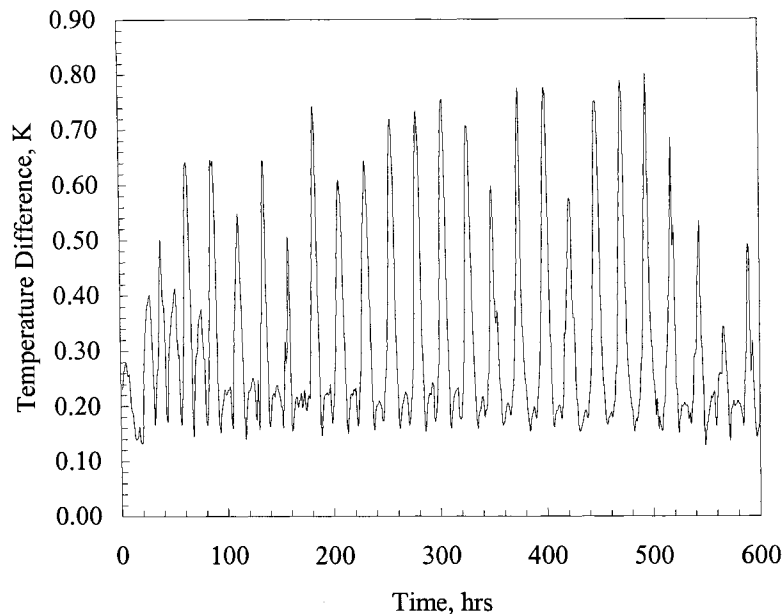


Figure 4. Maximum hourly temperature differences.

The exterior surface temperatures of the surfaces adjacent to the guarded zone were measured during the experiment and are provided in an associated Excel file to be used as boundary conditions. Despite large air changes in the cell, measurements taken near the walls, floor, and ceiling with a hot wire anemometer revealed negligible velocities. The two fans generated nearly constant load of  $\sim 160$  W (measured internal loads for each hour are provided for the building energy simulation codes in the associated Excel file entitled “Experiment 5.xls”).

### Thermophysical Properties

The thermophysical properties of the cell were determined from literature and in-house measurements. The properties obtained from in-house measurement were found to be temperature dependent. These parameters are available in an earlier document entitled *Test Cell Transient Characteristic Exercise Round 1* and can be made available upon request. Most building energy simulation codes cannot account for temperature dependent thermophysical properties. Therefore the thermophysical properties evaluated at the mean envelope temperature for the test for the ceiling, interior walls, floor, and exterior wall. The mean temperature for the ceiling and interior walls was area weighted, and, because the exterior surface of the south wall was not measured, the mean envelope temperature was calculated using hourly inside and outside air temperature measurements. The mean envelope temperatures are shown in Table 2. The thermophysical properties evaluated at these mean envelope temperatures are contained in Tables 3a to 3c.

Table 2. Mean envelope temperatures for experiment.

Element	Mean temperature, °C
Ceiling, East, West, and North Walls	22.83
Floor	22.75
South Wall	20.91

Table 3a. Ceiling, North, East and West wall construction evaluate at 22.83°C.

Layer Number	Material	Thickness mm	Thermal conductivity W/m-K	Density Kg/m <sup>3</sup>	Specific heat J/kg-K
1	Sheet steel	0.7	53.62	7837	460.8
2	PU foam	139	0.02234	30	1800
3	Sheet steel	0.7	53.62	7837	460.8

Table 3b. Floor construction evaluated at 22.75°C.

Layer Number	Material	Thickness mm	Thermal conductivity W/m-K	Density Kg/m <sup>3</sup>	Specific heat J/kg-K
1	Sheet steel	0.7	53.62	7837	460.8
2	PU foam	140	0.02233	30	1800
3	PU foam (higher density)	20	0.070	45	1800
4	Sheet steel with surface structure	2.5	53.62	7837	460.8

Table 3c. South wall construction evaluated at 20.91°C.

Layer Number	Material	Thickness mm	Thermal conductivity W/m-K	Density Kg/m <sup>3</sup>	Specific heat J/kg-K
1	Plywood	10	0.1404	850	1605
2	EPS foam	130	0.03622	28	1460
3	Plywood	10	0.1404	850	1605

## Output Report

The output reports will be divided up into three sections which include: 1) irradiance output on the vertical façade of the exterior wall and associated components, 2) output from the test cell that can be compared to measured data at the test facility—empirical validations, and 3) code-to-code comparisons from the test cell of code output parameters that are not measured at the facility. The code-to-code comparison reports may prove useful in identifying discrepancies and differences in the results. An Excel file with headers and appropriate worksheets entitled “XXXXXX Experiment 5 Results.xls” was created to expedite processing the results. Please change the XXXXXX to an appropriate name and complete the spreadsheet.

## Irradiance Output

Table 4 contains headers for the requested output that pertains to the hourly irradiance output of the exterior wall of the test cell. A description of the headers is provided below the table.

Table 4. List of headers for data file.

Hour <sup>1)</sup>	Input Parameters			Output Parameters			
	Bn <sup>2,a)</sup>	Dh <sup>3,a)</sup>	Gh <sup>4,a)</sup>	IIR <sup>5,b)</sup>	Bn-IIR <sup>6,c)</sup>	Dv-IIR <sup>7,c)</sup>	RF-IIR <sup>8,c)</sup>

- \* Please provide the two parameters used for the exercise.
- 26) is the time in Western European Standard time (GMT +1).
- 27) is the direct-normal irradiance in W/m<sup>2</sup>.
- 28) is the diffuse horizontal irradiance in W/m<sup>2</sup>.
- 29) is the global horizontal irradiance in W/m<sup>2</sup>.
- 30) is incident radiation (total vertical irradiance) on the southwest façade in W/m<sup>2</sup>.
- 31) is the direct component of the incident radiation on the southwest façade in W/m<sup>2</sup>.
- 32) is the diffuse component of the incident irradiance on the southwest façade in W/m<sup>2</sup>.
- 33) is the reflected component of the incident irradiance on the southwest façade in W/m<sup>2</sup>.
- f) is useful for ensuring the correct input.
- g) is an empirical validation where the parameter is measured on site.
- h) is a code-to-code comparisons where the parameters are not measured on site.

## Empirical Validations

A report describing the following output for each hour the experiment was run should be submitted. The output will be used to compare the results for the various models and the experiment. The headers for the output file and a description of their meaning are described in Table 5.

Table 5. List of output headers.

Hour <sup>1)</sup>	HC-Power <sup>2)</sup>	Glaz-OST <sup>3)</sup>	Glaz-IST <sup>4)</sup>	West-IST <sup>5)</sup>	North-IST <sup>6)</sup>	East-IST <sup>7)</sup>	Ceil-IST <sup>8)</sup>	Floor-IST <sup>9)</sup>
--------------------	------------------------	------------------------	------------------------	------------------------	-------------------------	------------------------	------------------------	-------------------------

- 10) is the time in Western European Standard time(GMT +1).
- 11) is the heating/cooling power required to maintain the space in W.
- 12) is the exterior surface temperature of the glazing in °C.
- 13) is the interior surface temperature of the glazing in °C.
- 14) is the inside cell surface temperature of the west wall in °C.
- 15) is the inside cell surface temperature of the north wall in °C.
- 16) is the inside surface temperature of the east wall in °C.
- 17) is the inside surface temperature of the ceiling in °C.
- 18) is the inside surface temperature of the floor in °C.

## Code-to-Code Comparisons

A report describing the following outputs, which are often user inputs or algorithms in the codes used for the respective simulations, should be submitted if possible. The headers for the output file and a description of their meanings are contained in Tables 6 and 8.

Table 6. Inside convective heat transfer coefficients.

Hour <sup>1)</sup>	South-ICHTC <sup>2)</sup>	Glaz-ICHTC <sup>3)</sup>	West-ICHTC <sup>4)</sup>	North-ICHTC <sup>5)</sup>	East-ICHTC <sup>6)</sup>	Ceil-ICHTC <sup>7)</sup>	Floor-ICHTC <sup>8)</sup>	South-OCHTC <sup>9)</sup>	Glaz-OCHTC <sup>10)</sup>
--------------------	---------------------------	--------------------------	--------------------------	---------------------------	--------------------------	--------------------------	---------------------------	---------------------------	---------------------------

- 1) is the time in Western European Standard time (GMT+1).
- 2) is the convective heat transfer coefficient for the south wall in  $W/m^2-K$ .
- 3) is the convective heat transfer coefficient for the glazing in  $W/m^2-K$ .
- 4) is the convective heat transfer coefficient for the west wall in  $W/m^2-K$ .
- 5) is the convective heat transfer coefficient for the north wall in  $W/m^2-K$ .
- 6) is the convective heat transfer coefficient for the east wall in  $W/m^2-K$ .
- 7) is the convective heat transfer coefficient for the ceiling in  $W/m^2-K$ .
- 8) is the convective heat transfer coefficient for the floor in  $W/m^2-K$ .
- 9) is the outside convective heat transfer coefficient for the south wall in  $W/m^2-K$ .
- 10) is the outside convective heat transfer coefficient for the glazing in  $W/m^2-K$ .

Table 7. Inside radiative heat transfer coefficients.

Hour <sup>1)</sup>	South-IRHTC <sup>2)</sup>	Glaz-IRHTC <sup>3)</sup>	West-IRHTC <sup>4)</sup>	North-IRHTC <sup>5)</sup>	East-IRHTC <sup>6)</sup>	Ceil-IRHTC <sup>7)</sup>	Floor-IRHTC <sup>8)</sup>	South-ORHTC <sup>9)</sup>	Glaz-ORHTC <sup>10)</sup>
--------------------	---------------------------	--------------------------	--------------------------	---------------------------	--------------------------	--------------------------	---------------------------	---------------------------	---------------------------

- 1) is the time in West European Standard time (GMT+1)
- 2) is the inside radiative heat transfer coefficient for the south wall in  $W/m^2-K$ .
- 3) is the inside radiative heat transfer coefficient for the glazing in  $W/m^2-K$ .
- 4) is the inside radiative heat transfer coefficient for the west wall in  $W/m^2-K$ .
- 5) is the inside radiative heat transfer coefficient for the north wall in  $W/m^2-K$ .
- 6) is the inside radiative heat transfer coefficient for the east wall in  $W/m^2-K$ .
- 7) is the inside radiative heat transfer coefficient for the ceiling in  $W/m^2-K$ .
- 8) is the inside radiative heat transfer coefficient for the floor in  $W/m^2-K$ .
- 9) is the outside radiative heat transfer coefficient for the south wall in  $W/m^2-K$ .
- 10) is the outside radiative heat transfer coefficient for the glazing in  $W/m^2-K$ .

After reviewing the output of various codes, the solar gain parameter was redefined as the transmitted solar power given by Equation 1 (note: in most codes this relationship is a

sum of the direct and diffuse components factoring in angular dependent properties of the glazing units).

$$TSP = \tau_s I_s A_w \quad [1]$$

where

$I_s$  is the incident solar radiation, in  $\text{W}/\text{m}^2$   
 $\tau_s$  is the transmitted solar energy ratio, no units  
 $A_w$  is the window area, in  $\text{m}^2$

Table 8. Transmitted solar power.

Hour <sup>1)</sup>	Transmitted Solar Power <sup>1)</sup>
--------------------	---------------------------------------

*1) is the time in West European Standard time (GMT+1)*

*2) is the solar gain through the window in W.*

## Simulation Report

In addition to simulation results, please provide a description of the additional assumptions that were made when simulating the interior shade.

## Simulation Ground Rules

In order to maintain model consistency between the experiments, only the following modifications can be made in the models from the finalized model from the glazing only experiment.

- Addition of the interior shade and associated properties to the building energy simulation codes.
- Thermophysical properties for temperature dependent quantities of thermal conductivity.

An email hotline will be used to clarifying information contained in this document, information not provided in the document but useful for simulation, and/or general questions concerning the experiment. Please direct all email questions to Peter Loutzenhiser ([peter.loutzenhiser@empa.ch](mailto:peter.loutzenhiser@empa.ch)). Responses to the emails will be directed to all participants in the simulation exercise.

## References

- [1] European Standard EN 410. Glass in building – Determination of luminous and solar characteristics of glazing. European Committee for Standardization, Brussels, Belgium, 1998
- [2] GLAD Software. Swiss Federal Laboratories for Materials Testing and Research (EMPA), Duebendorf, Switzerland, 2002

**Appendix F: Constant Temperature Experiment with Glazing and Exterior Blind**

IEA Task 34/Annex 43 Subtask C  
Empirical Validation Project of Building Energy  
Simulation Tools  
Shading / Daylighting / Load Interaction

Constant Temperature Experiment with Glazing and Exterior Blind

Written by  
Peter Loutzenhiser  
Heinrich Manz  
Thomas Frank

January 31, 2006

## Introduction

This document contains information regarding the parameters and conditions used for an experiment performed at the Swiss Federal Laboratories for Material Testing and Research (EMPA) in the Laboratory for Building Technologies test facility in Duebendorf, Switzerland from July 16 to September 5, 2005. The experiment was designed to evaluate the impact of solar gains through a glazing unit with an exterior blind and was done in conjunction with the International Energy Agency's (IEA) Task 34/Annex 43 Subtask C. The purpose of this exercise is to use the boundary conditions, weather data, glazing properties, and properties of the exterior blind properties to predict—in each respective building energy simulation code—the required heating/cooling power to maintain a relatively constant temperature (average hourly space temperatures are provided as a code input); the first part of the experiment was performed with the slats in the horizontal position and the second with the blind slats tilted downward at a 45° angle. The first round of simulations will be a blind exercise; therefore information regarding the measured heating and cooling power requirements was not included in this document. Information about how exterior blind was mounted and desired output from this exercise are provided in this document. An associated Excel document entitled “Experiment 6.xls” contains measured hourly weather data, exterior surface temperatures adjacent to the guarded zone, exterior blind properties as a function of wavelength, space temperatures, and internal load. Information concerning the test cell location, geometrical and temperature dependent thermophysical properties, thermal bridge, outside ground reflectance calculations, and glazing properties are contained in previous IEA Task 34/Annex 43 Subtask C documents<sup>9,10,3,4</sup> that can be made available upon request.

---

<sup>9</sup> *Test Cell Transient Characteristic Exercise*, August 25, 2004

<sup>10</sup> *Results from the Test Cell Transient Characteristic Exercise Round 1*, sent out to participants on October 26, 2004

<sup>3</sup> *Evaluation of Building Energy Simulation Codes' Irradiance Models*, February 9, 2005

<sup>4</sup> *Constant Temperature Experiment with Glazing Only*, Revised on October 21, 2005

## Description of the Experiment

This section contains specific information about the experiment, which includes the following information.

- Exterior blind.
- Test configuration.
- Thermophysical properties.

### Exterior Blind

For this experiment, an exterior blind assembly was installed 1.0 cm from the exterior glazing surface and is pictured in Figure 1. A dimensioned drawing of the blind position relative to the glazing and the shape of the blind are shown in Figures 2 and 3, respectively.

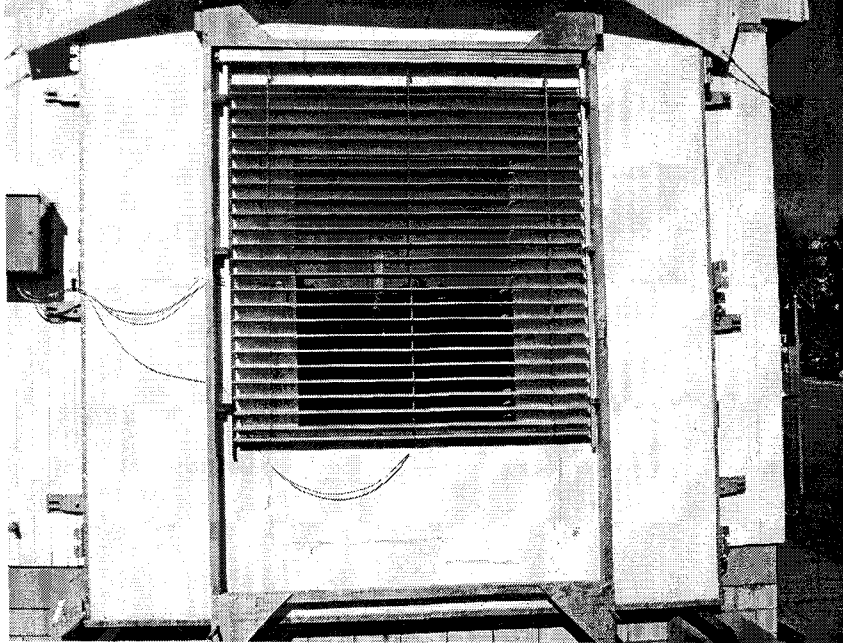


Figure 1. Photograph of the exterior blind mounted in front of the test cell.

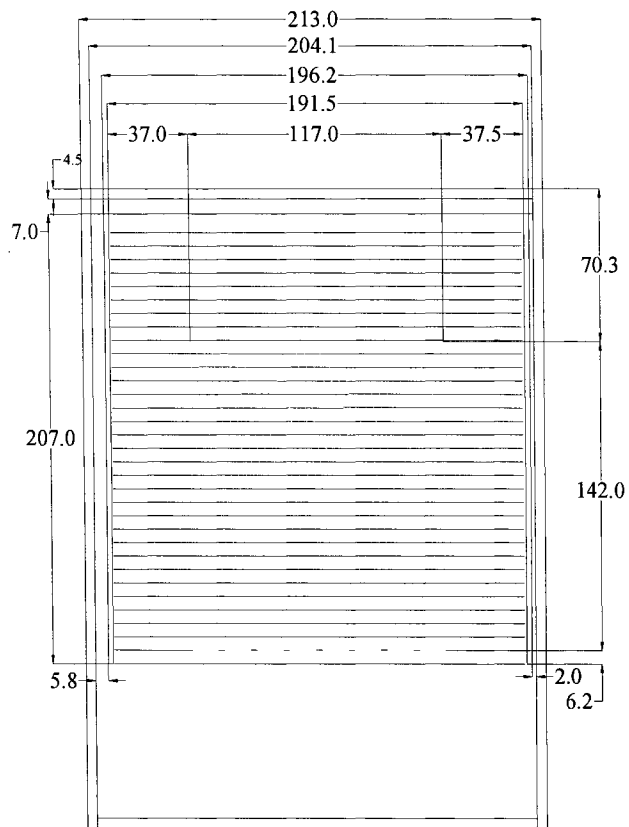


Figure 2. Dimensioned drawing of the exterior Venetian blind in centimeters relative to the glazing.

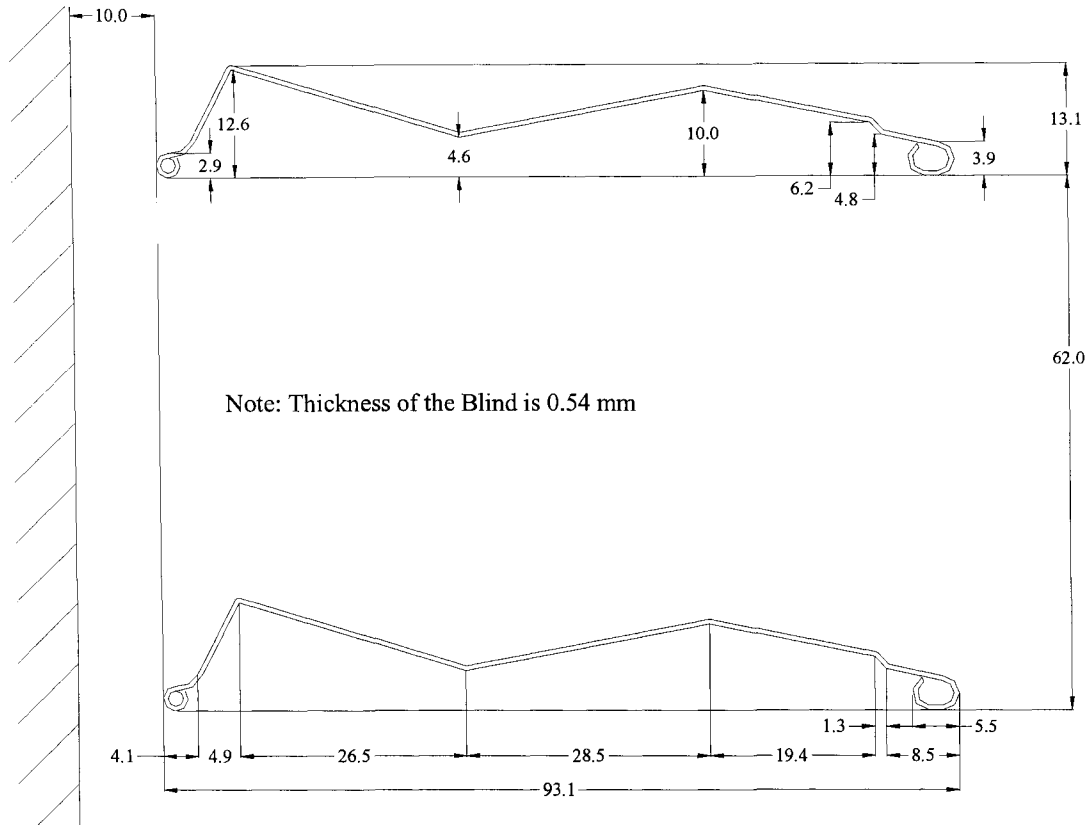


Figure 3. Dimension blind relative to the glazing in millimeters.

The optical properties of the exterior blind were measured at normal incident angles using a spectrometer. The transmittance and reflectance as a function of wavelength from 250 nm to 2500 nm can be found in an associated Excel file entitled “Experiment 6.xls”. The optical properties for the slat surfaces were also computed according to EN 410 [1] using GLAD software [2] and are shown in Table 1.

Table 1. Optical properties of the slat surfaces.

Property	Quantity
Normal Solar Reflectance, %	44.1
Hemispherical Emittance, %	86.2

### Test Configuration

This test was configured to maintain a near-constant temperature by adjusting heating and cooling power in the test cell. The first 103 hours of the provided data were designed for preconditioning and the glazing was covered by a foil with a highly reflective surface for solar radiation (there was additional preconditioning that ran prior to the experiment); this was accounted for in the weather file by setting solar irradiance to zero during this time. The slat angle was changed from a horizontal position to a 45° angle (downward to the outside) on August 16, 2005 at 7:00 AM. Air temperatures in the test cell were measured during the experiment with 18 double-shielded thermocouples. During the experiment, air

was distributed throughout the cell using two fans near the floor through textile ducts and extracted through return ducts mounted near the ceiling. A plot of the volume-weighted average cell air temperature is shown in Figure 4 and a plot of maximum temperature difference for any given thermocouples at a given hour is shown in Figure 5. For this experiment, the average maximum hourly temperature difference was 0.23 K.

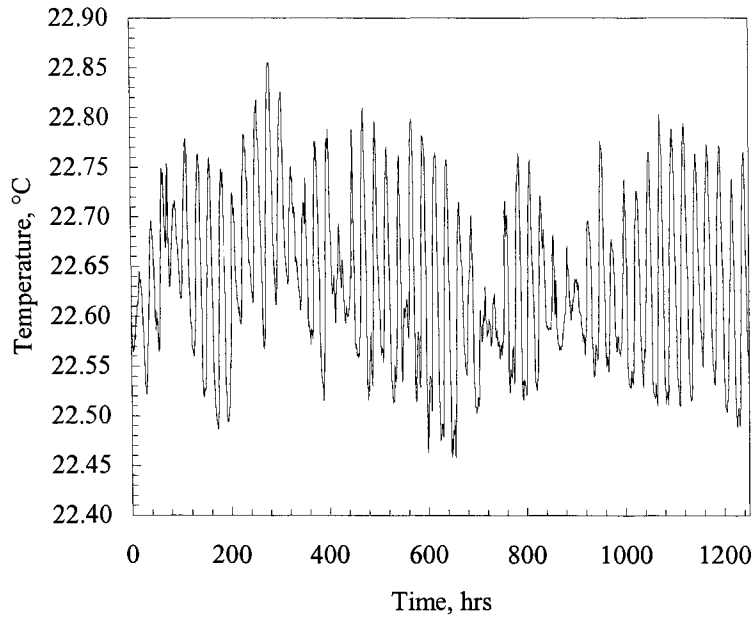


Figure 4. Volume-weighted average hourly cell temperatures for the experiment.

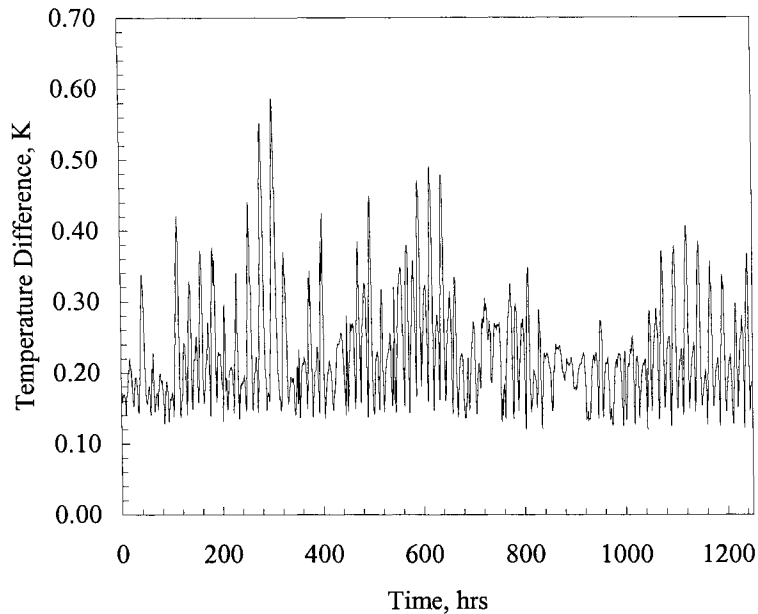


Figure 5. Maximum hourly temperature differences.

The temperatures of the cell exterior surfaces adjacent to the guarded zone were measured during the experiment and are provided in an associated Excel file to be used as boundary conditions. Despite large air changes in the cell, measurements taken near the walls, floor, and ceiling with a hot wire anemometer revealed very small velocities. The two fans generated nearly constant load of  $\sim 160$  W (measured internal loads for each hour are provided for the building energy simulation codes in the associated Excel file entitled “Experiment 6.xls”).

### Thermophysical Properties

The thermophysical properties of the cell were determined from literature and in-house measurements. The properties obtained from in-house measurement were found to be temperature dependent. These parameters are available in an earlier document entitled *Test Cell Transient Characteristic Exercise Round 1* and can be made available upon request. Most building energy simulation codes cannot account for temperature dependent thermophysical properties. Therefore the thermophysical properties evaluated at the mean envelope temperature for the test for the ceiling, interior walls, floor, and exterior wall. The mean temperature for the ceiling and interior walls was area weighted, and, because the exterior surface of the south wall was not measured, the mean envelope temperature was calculated using hourly inside and outside air temperature measurements. The mean envelope temperatures for both experiments are shown in Table 2. The thermophysical properties evaluated at these mean envelope temperatures

are contained in Tables 3a to 3c for the Venetian blinds horizontally positioned and Tables 4a to 4c when tilted downward 45°.

Table 2. Mean envelope temperatures for the experiments.

Element	Mean temperature, °C	
	Horizontal	45° Downward
Ceiling, East, West, and North Walls	22.72	20.83
Floor	22.72	20.83
South Wall	20.82	20.90

Table 3a. Ceiling, North, East and West wall construction evaluate at 22.72°C.

Layer number	Material	Thickness mm	Thermal conductivity W/m-K	Density Kg/m <sup>3</sup>	Specific heat J/kg-K
1	Sheet steel	0.7	53.62	7837	460.8
2	PU foam	139	0.02232	30	1800
3	Sheet steel	0.7	53.62	7837	460.8

Table 3b. Floor construction evaluated at 22.72°C.

Layer number	Material	Thickness mm	Thermal Conductivity W/m-K	Density Kg/m <sup>3</sup>	Specific heat J/kg-K
1	Sheet steel	0.7	53.62	7837	460.8
2	PU foam	140	0.02232	30	1800
3	PU foam (higher density)	20	0.070	45	1800
4	Sheet steel with surface structure	2.5	53.62	7837	460.8

Table 3c. South wall construction evaluated at 20.82°C.

Layer number	Material	Thickness mm	Thermal Conductivity W/m-K	Density Kg/m <sup>3</sup>	Specific heat J/kg-K
1	Plywood	10	0.1400	850	1605
2	EPS foam	130	0.03620	28	1460
3	Plywood	10	0.1400	850	1605

Table 4a. Ceiling, North, East and West wall construction evaluate at 22.83°C.

Layer number	Material	Thickness mm	Thermal Conductivity W/m-K	Density Kg/m <sup>3</sup>	Specific heat J/kg-K
1	Sheet steel	0.7	53.62	7837	460.8
2	PU foam	139	0.02234	30	1800
3	Sheet steel	0.7	53.62	7837	460.8

Table 4b. Floor construction evaluated at 22.83°C.

Layer number	Material	Thickness mm	Thermal Conductivity W/m-K	Density Kg/m <sup>3</sup>	Specific heat J/kg-K
1	Sheet steel	0.7	53.62	7837	460.8
2	PU foam	140	0.02232	30	1800
3	PU foam (higher density)	20	0.070	45	1800
4	Sheet steel with surface structure	2.5	53.62	7837	460.8

Table 4c. South wall construction evaluated at 20.90°C.

Layer number	Material	Thickness mm	Thermal Conductivity W/m-K	Density Kg/m <sup>3</sup>	Specific heat J/kg-K
1	Plywood	10	0.1400	850	1605
2	EPS foam	130	0.03621	28	1460
3	Plywood	10	0.1400	850	1605

## Output Report

The output reports will be divided up into three sections which include: 1) irradiance output on the vertical façade of the exterior wall and associated components, 2) output from the test cell that can be compared to measured data at the test facility—empirical validations, and 3) code-to-code comparisons from the test cell of code output parameters that are not measured at the facility. The code-to-code comparison reports may prove useful in identifying discrepancies and differences in the results. An Excel file with headers and appropriate worksheets entitled “XXXXXX Experiment 6 Results.xls” was created to expedite processing the results. Please change the XXXXXX to an appropriate name and complete the spreadsheet.

## Irradiance Output

Table 5 contains headers for the requested output that pertains to the hourly irradiance output of the exterior wall of the test cell. A description of the headers is provided below the table.

Table 5. List of headers for data file.

Hour <sup>j)</sup>	Input Parameters			Output Parameters			
	Bn <sup>2,a)</sup>	Dh <sup>3,a)</sup>	Gh <sup>4,a)</sup>	IIR <sup>5,b)</sup>	Bn-IIR <sup>6,c)</sup>	Dv-IIR <sup>7,c)</sup>	RF-IIR <sup>8,c)</sup>

\* Please provide the two parameters used for the exercise.

34) is the time in Western European Standard time (GMT +1).

35) is the direct-normal irradiance in  $W/m^2$ .

36) is the diffuse horizontal irradiance in  $W/m^2$ .

37) is the global horizontal irradiance in  $W/m^2$ .

38) is incident radiation (total vertical irradiance) on the southwest façade in  $W/m^2$ .

39) is the direct component of the incident radiation on the southwest façade in  $W/m^2$ .

40) is the diffuse component of the incident irradiance on the southwest façade in  $W/m^2$ .

41) is the reflected component of the incident irradiance on the southwest façade in  $W/m^2$ .

i) is useful for ensuring the correct input.

j) is an empirical validation where the parameter is measured on site.

k) is a code-to-code comparisons where the parameters are not measured on site.

## Empirical Validations

A report describing the following output for each hour the experiment was run should be submitted. The output will be used to compare the results for the various models and the experiment. The headers for the output file and a description of their meaning are described in Table 6.

Table 6. List of output headers.

Hour <sup>1)</sup>	HC-Power <sup>2)</sup>	Glaz-OST <sup>3)</sup>	Glaz-IST <sup>4)</sup>	West-IST <sup>5)</sup>	North-IST <sup>6)</sup>	East-IST <sup>7)</sup>	Ceil-IST <sup>8)</sup>	Floor-IST <sup>9)</sup>
--------------------	------------------------	------------------------	------------------------	------------------------	-------------------------	------------------------	------------------------	-------------------------

19) is the time in Western European Standard time(GMT+1).

20) is the heating/cooling power required to maintain the space in  $W$ .

21) is the exterior surface temperature of the glazing in  $^{\circ}C$ .

22) is the interior surface temperature of the glazing in  $^{\circ}C$ .

23) is the inside cell surface temperature of the west wall in  $^{\circ}C$ .

24) is the inside cell surface temperature of the north wall in  $^{\circ}C$ .

25) is the inside surface temperature of the east wall in  $^{\circ}C$ .

26) is the inside surface temperature of the ceiling in  $^{\circ}C$ .

27) is the inside surface temperature of the floor in  $^{\circ}C$ .

## Code-to-Code Comparisons

A report describing the following outputs, which are often user inputs or algorithms in the codes used for the respective simulations, should be submitted if possible. The headers for the output file and a description of their meanings are contained in Tables 7 and 9.

Table 7. Inside convective heat transfer coefficients.

Hour <sup>1)</sup>	South-ICHTC <sup>2)</sup>	Glaz-ICHTC <sup>3)</sup>	West-ICHTC <sup>4)</sup>	North-ICHTC <sup>5)</sup>	East-ICHTC <sup>6)</sup>	Ceil-ICHTC <sup>7)</sup>	Floor-ICHTC <sup>8)</sup>	South-OCHTC <sup>9)</sup>	Glaz-OCHTC <sup>10)</sup>
--------------------	---------------------------	--------------------------	--------------------------	---------------------------	--------------------------	--------------------------	---------------------------	---------------------------	---------------------------

1) is the time in Western European Standard time (GMT+1).

2) is the convective heat transfer coefficient for the south wall in  $W/m^2-K$ .

3) is the convective heat transfer coefficient for the glazing in  $W/m^2-K$ .

4) is the convective heat transfer coefficient for the west wall in  $W/m^2-K$ .

5) is the convective heat transfer coefficient for the north wall in  $W/m^2-K$ .

6) is the convective heat transfer coefficient for the east wall in  $W/m^2-K$ .

7) is the convective heat transfer coefficient for the ceiling in  $W/m^2-K$ .

8) is the convective heat transfer coefficient for the floor in  $W/m^2-K$ .

9) is the outside convective heat transfer coefficient for the south wall in  $W/m^2-K$ .

10) is the outside convective heat transfer coefficient for the glazing in  $W/m^2-K$ .

Table 8. Inside radiative heat transfer coefficients.

Hour <sup>1)</sup>	South-IRHTC <sup>2)</sup>	Glaz-IRHTC <sup>3)</sup>	West-IRHTC <sup>4)</sup>	North-IRHTC <sup>5)</sup>	East-IRHTC <sup>6)</sup>	Ceil-IRHTC <sup>7)</sup>	Floor-IRHTC <sup>8)</sup>	South-ORHTC <sup>9)</sup>	Glaz-ORHTC <sup>10)</sup>
--------------------	---------------------------	--------------------------	--------------------------	---------------------------	--------------------------	--------------------------	---------------------------	---------------------------	---------------------------

- 1) is the time in West European Standard time (GMT+1)  
 2) is the inside radiative heat transfer coefficient for the south wall in  $W/m^2-K$ .  
 3) is the inside radiative heat transfer coefficient for the glazing in  $W/m^2-K$ .  
 4) is the inside radiative heat transfer coefficient for the west wall in  $W/m^2-K$ .  
 5) is the inside radiative heat transfer coefficient for the north wall in  $W/m^2-K$ .  
 6) is the inside radiative heat transfer coefficient for the east wall in  $W/m^2-K$ .  
 7) is the inside radiative heat transfer coefficient for the ceiling in  $W/m^2-K$ .  
 8) is the inside radiative heat transfer coefficient for the floor in  $W/m^2-K$ .  
 9) is the outside radiative heat transfer coefficient for the south wall in  $W/m^2-K$ .  
 10) is the outside radiative heat transfer coefficient for the glazing in  $W/m^2-K$ .

After reviewing the output of various codes, the solar gain parameter was redefined as the transmitted solar power given by Equation 1 (note: in most codes this relationship is a sum of the direct and diffuse components factoring in angular dependent properties of the glazing units).

$$TSP = \tau_s I_s A_w \quad [1]$$

where

- $I_s$  is the incident solar radiation, in  $W/m^2$   
 $\tau_s$  is the transmitted solar energy ratio, no units  
 $A_w$  is the window area, in  $m^2$

Table 9. Transmitted solar power.

Hour <sup>1)</sup>	Transmitted Solar Power <sup>1)</sup>
--------------------	---------------------------------------

- 1) is the time in West European Standard time (GMT+1)  
 2) is the solar gain through the window in  $W$ .

## Simulation Report

In addition to simulation results, please provide a description of the additional assumptions that were made when simulating the exterior Venetian blind.

## Simulation Ground Rules

In order to maintain model consistency between the experiments, only the following modifications can be made in the models from the finalized model from the glazing only experiment.

- Addition of the interior shade and associated properties to the building energy simulation codes.

- Thermophysical properties for temperature dependent quantities of thermal conductivity.

An email hotline will be used to clarifying information contained in this document, information not provided in the document but useful for simulation, and/or general questions concerning the experiment. Please direct all email questions to Peter Loutzenhiser ([peter.loutzenhiser@empa.ch](mailto:peter.loutzenhiser@empa.ch)). Responses to the emails will be directed to all participants in the simulation exercise.

## References

- [1] European Standard EN 410. Glass in building – Determination of luminous and solar characteristics of glazing. European Committee for Standardization, Brussels, Belgium, 1998
- [2] GLAD Software. Swiss Federal Laboratories for Materials Testing and Research (EMPA), Duebendorf, Switzerland, 2002

**Appendix G: ERS Daylighting Experiment Setup Sheet**

IEA Daylight Test Case 1  
Task 34/43 Subtask C  
Conducted at the ERS  
From July 1 to July 7, 2005

Peter Loutzenhiser  
Gregory Maxwell  
Curtis Klaassen

Energy Resource Station  
Ankeny, IA

Iowa Energy Center

February 11, 2006  
Revised: February 20, 2006

## Chapter 1: Introduction

This document contains information regarding the parameters and conditions used for a daylighting test performed at the Iowa Energy Resource Station as part of the empirical validation study for International Energy Agency Task 34/43 Subtask C. The experiment was conducted over a seven-day period from July 1 to July 7, 2005. The test is referred to as IEA Daylight Test, Case 1<sup>1</sup>.

For this test, the A and B Rooms were operated using Variable-Air-Volume Reheat (VAVRH) with electric reheat. Two stages of electric coils were used to provide terminal heating. Chilled water was used when the system required cooling. During the experiment, 100% re-circulated air was used. The supply air temperature (temperature after the supply fan) was set at 13 °C (55.4 °F).

Various windows, window treatments, and exterior shading devices were used in the test rooms for this experiment. Dimmable ballasts were used in the exterior test rooms to reduce the illuminance in rooms based on available daylight and maintain illuminances of 645 lux (60 foot-candles) in the East and West Test Rooms and 700 lux (65 foot-candles) in the South Test Rooms. A control scheme was implemented that turned off the lamps when the illuminance at the reference point was at minimum capacity and the light level exceeded the setpoint; the lights were turned back on when the light level was 108 lux (10 foot-candles) below the setpoint. Internal loads were used for both sets of test rooms. Also included in this test specification are optical properties of interior surfaces of the test rooms that are not included in the building specifications used to construct models.

---

<sup>1</sup> This test corresponds to ERS test Daylighting 17.

## **Chapter 2: Input for load calculations**

### **2.1 Run-period**

The run period for the experiment, including initial and final dates of the desired simulation period, was from July 1 to July 7, 2005.

### **2.2 Weather data**

The test weather data for Ankeny, Iowa are located in an associated Excel file entitled “Daylight 17.xls”. Global illuminance on the west, south, and east vertical façade and in the horizontal plane are provided in this file.

### **2.3 Building location**

The location of the building and information concerning the time are listed as follows:

- LATITUDE: 41.71 degrees North
- LONGITUDE: 93.61 degrees West
- ALTITUDE: 285.9 m (or 938.0 ft)
- TIME-ZONE: GMT -6, Central Time Zone in the United States
- DAYLIGHT-SAVING TIME: NO

### **2.4 Test room operation**

The following conditions apply to all test rooms. These conditions do not apply to the rest of the building where occupants may be present and different lighting and shading devices may be used.

- Base board heating was scheduled to provide a sensible internal load (see Section 3.6).
- Light Schedule (see Section 3.7)
- Different windows were used for the A and B Test Rooms (see Section 3.8).
- Different window treatments were used for the A and B Test Rooms (see Section 3.8).
- Exterior shades were constructed for the West Test Rooms (see Section 3.8).
- Optical properties of the test rooms (see Section 3.8).
- No infiltration.

### Chapter 3: Input for system model

The information contained in this section pertains to the operating parameters used to control the HVAC systems for the A and B Test Rooms. During the tests, the A and B Air-Handling Units operated in a nearly identical manner. The test used a variable-air-volume (VAV) system with three stages of electrical reheat. The air-handling units both used chilled water to provide cooling. During the test, the both systems used 100% re-circulated air. The HVAC system which serves the remaining spaces in the ERS (i.e. computer room, classroom, etc.) was operated to provide nearly constant temperatures to these spaces. Adjacent space temperatures are provided in an associated Excel file entitled "Daylight 17.xls".

#### 3.1 Zone control

Each test room is equipped with its own thermostat and the set point values are the same for all rooms. These set point values for this test were as follows:

- Heating thermostat set point: 22 °C (71.6 °F)
- Cooling thermostat set point: 23 °C (73.4 °F)

#### 3.2 Zone airflow rates

The air flow rates for each test room were specified as follows:

- Exterior test rooms (East, South, and West):
  - maximum 1,000 m<sup>3</sup>/hr (588.6 cfm)
  - minimum 800 m<sup>3</sup>/hr (470.8 cfm)
- Interior test rooms:
  - maximum 700 m<sup>3</sup>/hr (412 cfm)
  - minimum 424.8 m<sup>3</sup>/hr (250 cfm)

#### 3.3 System controls

The air-handling system was specified as follows:

- Heating schedule: always available
- Cooling schedule: always available
- Cooling control supply air temperature set point after the fan: 13 °C (or 55.4 °F)
- Preheat: NOT available
- Humidity control: NOT available
- Economizer: disabled
- Outside air control: disabled (100% re-circulated)

### 3.4 System air

The system air flow rates were specified as follows:

- Return air path: plenum
- Outside airflow rate: none (100% re-circulated)
- Duct air loss: none
- Duct heat gain: 0.6 °C (1.0 °F)

### 3.5 System fan

The air-handling unit fans are specified as follows:

- Supply air static pressure: 348.4 Pa (1.4 inch H<sub>2</sub>O)
- Fan schedule: always on
- Supply fan power operated at a nearly constant power for the A and B Systems were 1,143 W and 1,096 W, respectively.
- Supply fan control: 348.4 Pa (1.4 inch H<sub>2</sub>O)
- Return fan control differential: No offset
- Motor placement: In-air flow
- Fan placement: Draw-through

### 3.6 Heat source

The source of the heating was specified as follows:

- System heat source: not available
- Zone heat source:
  - a) For the exterior rooms: 2 stages of electric maximum 3.34 kW (1.67 kW/stage)
  - b) For the interior rooms: 2 stages of electric maximum 2.0 kW (1.0 kW/stage)
  - c) Sensible internal loads: 890 W of baseboard heat always scheduled on for all test rooms and 125 W of boxfan heat for the exterior test rooms.

### 3.7 Light source

The source of lights for the rooms was specified as follows:

- Total installed total lighting capacity: see Table 3.1 (Note: the maximum power during the experiment may not correspond to the maximum capacity of the lights due to dimming to maintain light levels when no daylight entered the space).
- Light schedule: see Table 3.2
- Illuminance: see Tables 3.3a and 3.3b
- Table light sensor location: see Figure 3.1
- Reference point Illuminance setpoints:
  - 700 lux (65 foot-candles) in the South Test Rooms
  - 645 lux (60 foot-candles) in the East and West Test Rooms

Table 3.1 Maximum light power for each test room and minimum light power for the exterior test rooms during the experiment.

Test Room	Maximum Light Power, W	Minimum Light Power, W
East A	356	86.1
East B	362	89.3
South A	364	88.1
South B	362	89.3
West A	362	88.4
West B	348	86.9
Interior A	359	-
Interior B	358	-

Table 3.2 Test room lighting schedule used during the test.

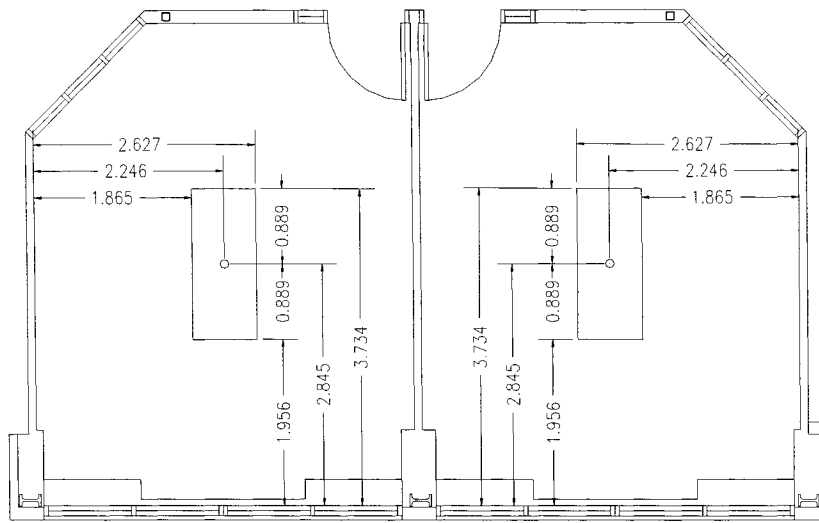
Time, h	Report Schedule (Midnight to 1 AM = Hour 1)	Lights, On/Off
0:00	1	Off
1:00	2	Off
2:00	3	Off
3:00	4	Off
4:00	5	On
5:00	6	On
6:00	7	On
7:00	8	On
8:00	9	On
9:00	10	On
10:00	11	On
11:00	12	On
12:00	13	On
13:00	14	On
14:00	15	On
15:00	16	On
16:00	17	On
17:00	18	On
18:00	19	On
19:00	20	On
20:00	21	On
21:00	22	Off
22:00	23	Off
23:00	24	Off
24:00		Off

Table 3.3a Reference point illuminance values and light power for the A Test Rooms.

East A Test Room		South A Test Room		West A Test Room	
Light Power W	Illuminance Lux	Light Power W	Illuminance Lux	Light Power W	Illuminance Lux
353.8	679.2	353.3	702.8	352.5	692.0
349.3	676.5	350.5	692.0	349.0	684.3
325.5	619.4	326.0	636.5	325.3	627.8
287.8	527.6	288.3	545.7	289.0	541.4
249.6	430.7	248.8	441.8	250.3	441.5
210.9	321.8	209.3	335.4	211.1	339.4
128.5	114.5	168.8	229.0	170.4	231.7
87.8	27.3	122.5	130.3	128.1	123.9
86.9	21.8	88.1	31.9	88.4	32.3

Table 3.3b Reference point illuminance values and light power for the B Test Rooms.

East A Test Room		South A Test Room		West A Test Room	
Light Power W	Illuminance Lux	Light Power W	Illuminance Lux	Light Power W	Illuminance Lux
350.8	662.4	357.3	666.1	357.5	687.6
346.5	654.3	352.0	657.7	351.8	674.2
323.3	604.6	329.5	606.3	328.0	618.0
288.5	519.8	292.0	519.2	292.0	532.6
250.9	427.4	251.9	424.0	252.8	436.1
212.4	327.2	212.4	320.8	213.4	331.7
172.0	224.1	171.6	217.4	172.3	224.6
129.6	121.4	129.5	119.5	129.1	123.0
89.3	36.9	89.3	32.6	86.9	32.1



Typical Exterior Test  
Room B

Typical Exterior Test  
Room A

Figure 3.1 Light sensor reference point (the sensor height is 0.7239 m from the floor).

### 3.8 Window glazing, shading, blind, and optical surface Properties

Various configurations were used in the test rooms to examine various facets of shading and various types of windows. Table 3.4 contains a matrix describing the configurations and the rooms. Detailed information about the windows, exterior fins, shading devices, and test room surface optical properties are provided in this section. For this experiment, all optical properties were computed according to EN 410 [1] using Glad software [2].

Table 3.4 Test rooms shading and window configurations for the experiment.

Test Room	Window Type	Interior Window Treatment	Exterior Window Treatment
East A	1" Low-E#3 Glazing System	Motorized Mini-blinds	none
East B	1" Low-E#3 Glazing System	Fixed Angle (0°) Mini-blinds	none
South A	1" Clear Glass Glazing System	Nysan Roller Shades	none
South B	1" Clear Glass Glazing System	Fixed Angle (0°) Mini-blinds	none
West A	1" Low-E#2 Glazing System	Nysan Roller Shades	Exterior Fins
West B	1" Low-E#2 Glazing System	none	Exterior Fins

### Windows

The windows used during the experiment for the exterior test rooms were 1"OA (25.2 mm) LOW-E #3 INSULATING, 1"OA (25.2 mm) LOW-E #2 INSULATING, and 1" (25.2 mm) OA clear glass glazing. The properties and construction of the glass are shown in Table 3.5.

Table 3.5 Test room window properties.

Type	1"OA (25.2 mm) LOW-E #3	1"OA (25.2 mm) LOW-E #2	1" OA (25.2 mm) Clear Glass
Makeup	1/4" (6 mm) Clear (103) <sup>11</sup> 1/2" (13.2 mm) airspace 1/4" (6 mm) Lof Pyro Low-E #3 (9924) <sup>2</sup>	1/4" (6 mm) VE3-55 #2 (6059) <sup>2</sup> 1/2" (13.2 mm) airspace 1/4" (6 mm) Clear (103) <sup>2</sup>	1/4" (6 mm) Clear (103) <sup>2</sup> 1/2" (13.2 mm) airspace 1/4" (6 mm) Clear (103) <sup>2</sup>
Visible Transmittance	73%	23%	79%
Solar Transmittance	52%	14%	61%
Visible Light-Exterior Reflectance	17%	6%	14%
Visible Light-Interior Reflectance	16%	15%	14%
Solar Exterior Reflectance	15%	10%	11%
ASHRAE U-Value Winter Nighttime	0.33 Btu/(hr-ft <sup>2</sup> -°F) (1.87 W/(m <sup>2</sup> -K))	0.31 Btu/(hr-ft <sup>2</sup> -°F) (1.76 W/(m <sup>2</sup> -K))	0.47 Btu/(hr-ft <sup>2</sup> -°F) (2.68 W/(m <sup>2</sup> -K))
ASHRAE U-Value Summer Daytime	0.35 Btu/(hr-ft <sup>2</sup> -°F) (2.0 W/(m <sup>2</sup> -K))	0.33 Btu/(hr-ft <sup>2</sup> -°F) (1.87 W/(m <sup>2</sup> -K))	0.49 Btu/(hr-ft <sup>2</sup> -°F) (2.81 W/(m <sup>2</sup> -K))
Shading Coefficient	0.79	0.26	0.81
Solar Factor (SHGC)	0.66	0.22	0.70
Relative Heat Gain	158 Btu/(hr-ft <sup>2</sup> ) (497.7 W/m <sup>2</sup> )	56 Btu/(hr-ft <sup>2</sup> ) (176.4 W/m <sup>2</sup> )	169 Btu/(hr-ft <sup>2</sup> ) (533 W/m <sup>2</sup> )

Note: All properties are centerpane values.

<sup>11</sup> ID number from the Window 5.2 Glazing System Library.

### Interior Shading

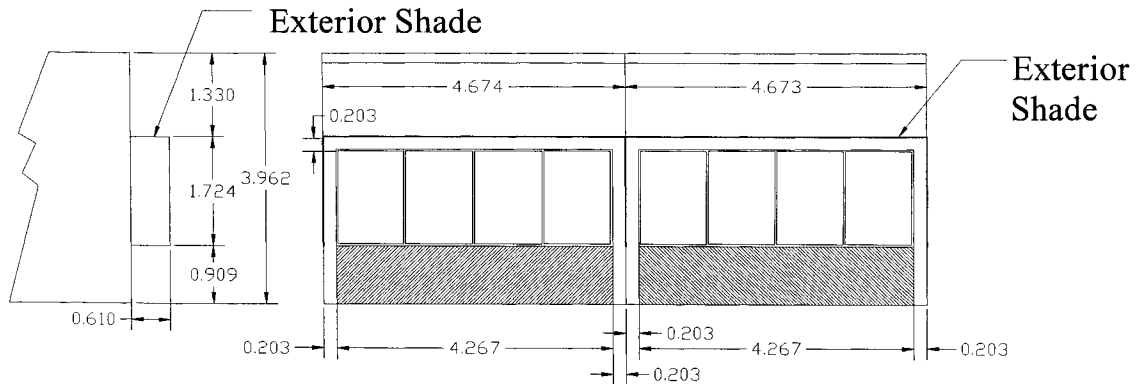
Diffuse interior window shades were used for this test. The shades installed South A and West A test rooms were Nysan Superweave 1000 (10% open) white fabric and white muslin cloth. These shades were mounted 108.0 mm (4.25 inches) from the glazing. The optical and solar properties measured at EMPA are shown in Table 3.6.

Table 3.6 Test room interior shade properties.

Type	Nysan Superweave 1000 (10% open) White Fabric
Visible Transmittance	30.5%
Solar Transmittance	30.4%
Visible Reflectance	67.3%
Solar Energy Reflectance	59.4%

### Exterior Fins

Opaque exterior shades were installed for the west test rooms. The dimensions of these exterior shades are shown in Figure 3.2.

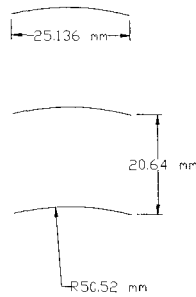


**Note: Dimensions in meters**

Figure 3.2 Drawing and dimensions of the exterior shades for west test rooms.

### Interior Blinds

Interior blinds were mounted inside the east test rooms for this experiment configured in two different ways. Figure 3.3 gives the dimension of the blind blades and the spacing. The blind units in the East A test room were setup to adjust to block out beam irradiance entering the space. The blind units in the South B and East B test rooms were set in a horizontal position. The fixed-angle and motorized mini-blinds were mounted 3 inches (76.2 mm) and 1.5 inches (38.1 mm), respectively, from the tip of the blade nearest the inner pane to the window when in the horizontal position. Optical measurements were taken on a blade from a blind unit similar to the one installed in the east test rooms and are reported in Table 3.7



Mini blinds are nominal 1-inch (25.4 mm) wide aluminum sheet metal which are formed to produce a curved blade with a 50.52 mm (2 inch) radius. The cord length of the blade is 25.136 mm (0.99 inch). The aluminum sheet thickness is 0.248 mm (0.0098 inch). Blades are spaced 20.64 mm (0.813 inch) apart.

Figure 3.3 Dimensioned drawing of the blades.

Table 3.7 Optical properties of the blind blades.

Property	Quantity
Solar Reflectance, %	63.9
Visible Reflectance, %	73.1
Hemispherical Emittance, %	72.1

**Test Room Optical Properties**

Optical measurements were taken on the interior walls, ceiling, and floor of the test rooms. The integral properties were computed for the visible and solar properties of the test rooms and are shown in Table 3.8.

Table 3.8 Optical properties for the interior surfaces.

Surface	Solar Reflectance, %	Visible Reflectance, %
Ceiling	49.8	55.7
Walls	78.8	83.6
Floor	26.4	10.3

## **Chapter 4: Output reports**

This section describes the output desired for each model. This output will be used to compare the results from the various models to each other as well as to compare the model results to the actual data collected at the ERS during the test period. ERS test data are only available for the systems and spaces associated with the test rooms.

### **4.1 Input verification report**

This report will be used to verify the building information that modelers used for the ERS building. The report should include the following information.

#### **General**

- Latitude
- Longitude
- Altitude
- Time Zone

#### **Summary of spaces occurring in the model**

- Number of spaces
- Number of exterior walls
- Space information: name, height, and area

#### **Details of exterior surfaces occurring in the model**

- Number of exterior surfaces
- Surface information: name, height, width, azimuth, angle, tilt angle, and U-value

#### **Details of interior surfaces occurring in the model**

- Number of interior surfaces
- Surface information: name, area, and U-value

#### **Details of windows occurring in the model**

- Number of windows
- Window information: name, height, width, shading coefficient, and U-value

## 4.2 Summary report

This report will be used to compare simulation results from the models. Results should be reported on an hourly basis where Hour 1 represents the time interval from midnight to 1 AM central daylight time. The report should include the following information:

### Weather Report

- Month, day, and hour
- Outside air dry-bulb temperature and wet-bulb temperature
- Solar irradiation (direct normal and total horizontal)

### Zone Report

- Month, day, and hour
- Zone temperature<sup>12</sup>
- Zone air flow rate<sup>3</sup>
- Supply air flow rate<sup>3</sup>
- Reheat Power<sup>3</sup>
- Illuminance level on the work plane<sup>3</sup>
- Lighting input power<sup>3</sup>

### System Report

- Month, day, and hour
- Supply air flow rate<sup>3</sup>
- Temperature of the air entering the cooling coil<sup>3</sup>
- Temperature of the air leaving the cooling coil<sup>3</sup>
- Temperature of the return air<sup>3</sup>
- Cooling coil heat transfer rate<sup>3</sup>

Table 4.1 depicts the headers for the weather report. Table 4.2 shows the headers for the test room reports, and Table 4.3 shows the system headers.

---

<sup>12</sup> These values can be directly measured or calculated at the ERS.

Table 4.1 Output weather report headers.

Month	Day	Hour <sup>a</sup>	DB-temp <sup>b</sup>	WB-temp <sup>c</sup>	Dir-solar <sup>d</sup>	Hor-solar <sup>e</sup>
-------	-----	-------------------	----------------------	----------------------	------------------------	------------------------

- Note (a) Hour is local standard time (GMT-6).  
 (b) DB-temp is the dry bulb temperature in °C.  
 (c) WB-temp is the wet bulb temperature in °C.  
 (d) Dir-solar is the direct normal solar radiation in W/m<sup>2</sup>.  
 (e) Hor-solar is the horizontal solar radiation in W/m<sup>2</sup>.

Table 4.2 Output zone report headers.

Month	Day	Hour <sup>a</sup>	Zn-temp <sup>b</sup>	Zn-flow <sup>c</sup>	Htg-power <sup>d</sup>	Lt-elec <sup>e</sup>	Dayl-ill <sup>f</sup>
-------	-----	-------------------	----------------------	----------------------	------------------------	----------------------	-----------------------

- Note (a) Hour is local standard time (GMT-6).  
 (b) Zn-temp is the dry bulb temperature for the zone in °C.  
 (c) Zn-flow is the discharge is the discharge airflow rate from the VAV box in m<sup>3</sup>/hr.  
 (d) Htg-power is the zone heating coil power in Watts.  
 (e) Lt-elec is the total room light power in Watts.  
 (f) Dayl-ill is the illuminance at the reference point due to daylighting in lux.

Table 4.3 Output system report headers.

Month	Day	Hour <sup>a</sup>	SA-flow <sup>b</sup>	Clg-eat <sup>d</sup>	Clg-lat <sup>e</sup>	RA-temp <sup>f</sup>	Clg-htr <sup>g</sup>
-------	-----	-------------------	----------------------	----------------------	----------------------	----------------------	----------------------

- Note (a) Hour is local standard time (GMT-6).  
 (b) SA-flow is the system supply airflow rate in m<sup>3</sup>/hr.  
 (c) OA-flow is the system outside airflow rate in m<sup>3</sup>/hr.  
 (d) Clg-eat is the entering air temperature to the cooling coil in °C.  
 (e) Clg-lat is the leaving air temperature from the cooling coil in °C.  
 (f) RA-temp is the return air temperature in °C.  
 (g) Clg-htr is the heat transfer rate required to cool the air in W.

**References**

- [1] European Standard EN 410. Glass in building—Determination of luminous and solar characteristics of glazing. European Committee for Standardization, Brussels, Belgium, 1998
- [2] GLAD Software. Swiss Federal Laboratories for Material Testing and Research (EMPA), Duebendorf, Switzerland, 2002